DOE/JPL/1060-84
(DE85014502)

PARABOLIC DISH TEST SITE: HISTORY AND OPERATING EXPERIENCE

By
M. K. Selcuk

February 15, 1985

Work Performed Under Contract No. AM04-80AL13137

Jet Propulsion Laboratory
Pasadena, California

Technical Information Center
Office of Scientific and Technical Information
United States Department of Energy

DOE/JPL/1060-84
(DE85014502)
Distribution Category UC-62

Parabolic Dish Test Site: History and Operating Experience

Compiled by:
M.K. Selçuk

February 15, 1985

Prepared for
U.S. Department of Energy
Through an Agreement with
National Aeronautics and Space Administration
by
Jet Propulsion Laboratory
California Institute of Technology
Pasadena, California

JPL Publication 85-18

DISCLAIMER

ABSTRACT

The Parabolic Dish Test Site (PDTS), located at the JPL Edwards Test Station on Edwards Air Force Base in California, was established in 1978 for the U.S. Department of Energy for testing point-focusing solar concentrator systems operating at temperatures approaching 1650°C (3000°F). Among tests run were evaluation and performance characterization of parabolic dish concentrators, receivers, power conversion units, and solar/fossil-fuel hybrid systems. The PDTS was fully operational until its closure in June 1984.

This report presents the evolution of the test program, a chronological listing of the experiments run, and data summaries for most of the tests conducted.

ACKNOWLEDGMENTS

The author wishes to thank V. Truscello, Thermal Power Systems (TPS) Project Manager; J. Lucas , A. Marriott, and J. Becker, Assistant Project Managers; D. Ross, PDTS Task Manager, who contributed significantly to the preparation of this report; PDTS staff: T. Hagen, J. Woodbury, and their personnel; TPS Task Managers and Cognizant Engineers: M. Argoud, H. Bank, W. Carley, E. Dennison, E. Hanseth, H. Holbeck, L. Jaffe, T. Kiceniuk, F. Livingston, C. Miyazono, B. Nesmith, W. Owen, J. Patzold, J. Roschke, J. Schredder, D. Starkey, J. Stearns, and T. Thostesen; and for text editing and composition: H. Hill, P. Panda, and M. Rice.

The work described herein was conducted by the Jet Propulsion Laboratory, California Institute of Technology, for the U.S. Department of Energy through an agreement with the National Aeronautics and Space Administration (NASA Task RE-152, Amendment 327; DOE/ALO/NASA Interagency Agreement No. DE-AM04-80AL13137).

ACRONYMS AND INITIALISMS

ABSR	air Brayton solar receiver
CPC	compound parabolic concentrator
CRT	cathode ray tube
CWCC	cold-water cavity calorimeter
DGAP	data gathering and processing
DOE	U.S. Department of Energy
DSSE	Dish/Stirling System Experiment
DSSR	dish/Stirling solar (hybrid) receiver
DTV	digital television
ESOR	experimental solar-only receiver
ETS	Edwards Test Station
FACC	Ford Aerospace and Communications Corporation
FOV	field of view
GE	General Electric Company
ID	inner diameter
JPL	Jet Propulsion Laboratory
LBL	Lawrence Berkeley Laboratory
NASA	National Aeronautics and Space Administration
OD	outer diameter
OG	Omnium-G Company
ORC	organic Rankine cycle
PCA	power conversion assembly (receiver plus PCU)
PCU	power conversion unit (engine plus alternator)
PDC-1	Parabolic Dish Concentrator No. 1
PDTS	Parabolic Dish Test Site

RMS	root mean square
SNLA	Sandia National Laboratories-Albuquerque
SRSR	steam Rankine solar receiver
TBC	test bed concentrator
TC	thermocouple
UPS	uninterruptible power supply
USAB	United Stirling AB of Sweden

CONTENTS

EXECUTIVE SUMMARY

The Parabolic Dish Test Site (PDTS) was established in 1978 to test point-focusing solar collector systems. The following is a brief description of the test equipment that was developed for that purpose and a listing of the power conversion assemblies that were subsequently tested.

Two identical test bed concentrators (TBCs) built by E-Systems, having back-silvered thin clear-glass mirrors bonded on a foam glass substrate[1] were built, characterized, and used for evaluation of several solar components and power assemblies. A third concentrator built by Omnium-G Company and a fourth (PDC-1) by Ford Aerospace and Communications Corporation (FACC), based on a design developed by General Electric, were also tested.

A cold-water cavity calorimeter and a JPL-developed flux mapper were used to characterize the concentrators. Optical tests devised by JPL were also run for mirror alignment purposes. A steam generating cavity-type receiver, a plate-fin design metallic high-temperature air heater, a ceramic design air heater with quartz window, and two steam engines using solar steam were major components tested individually. Among other component tests conducted at the PDTS were receiver face-plate material tests, compound parabolic concentrator (CPC) type secondary concentrator tests, and Pyrex window transmittance tests.

Also established in 1978 was the PDTS weather station wherein solar radiation and environmental data were continually monitored, recorded, processed, and distributed to experimenters. Data were collected, though not evaluated, using the Lawrence Berkeley Laboratory's circumsolar telescope.

Complete power conversion assemblies were also tested and evaluated:

(1) Organic (toluene) Rankine-cycle power conversion assembly built by FACC and Barber-Nichols.

(2) Hybrid (natural gas plus solar) receiver coupled with a United Stirling of Sweden (USAB) 4-95 Stirling engine.

(3) Experimental solar-only receivers (ESORs) coupled with 4-95 Stirling engines. Five varieties of receivers were evaluated during tests run by USAB from 1982 to early 1984. Quartz window, focal plane radiator, and infrared camera tests for recording of flux distribution were run on Stirling power modules.

The scientific testing programs conducted at the Parabolic Dish Test Site provided (1) a means of verifying predicted subsystem performance, (2) a baseline for parametric analyses of how each variable affects performance, and (3) a facility for developing rapid optical testing techniques. Generally,

---

[1]The TBC mirror facets were fabricated by JPL.

the test site's principal contribution to the Parabolic Dish Program, its contractors, and industry was the gathering of test data that showed how specific dish-electric components, including pre-prototype hardware, performed under various solar operating conditions and that also provided early information indicating expected operational characteristics in a user environment.

The PDTS was closed down in June 1984, and the equipment was transferred to Sandia National Laboratories in Albuquerque, New Mexico.

SECTION I

PDTS SITE AND GENERAL INFORMATION

The Parabolic Dish Test Site (PDTS), managed and operated for the U.S. Department of Energy (DOE) by the Jet Propulsion Laboratory (JPL), was a high-temperature, point-focusing solar thermal test facility. The PDTS was located approximately 70 airline miles north of Los Angeles, in the California high desert (elevation of 2300 ft) with an average rainfall of 4 in. per year. The site occupied approximately 10 acres of the 600-acre JPL Edwards Test Station (ETS)(Reference 1). Testing was possible on a near year-round basis.

A. OBJECTIVES

The primary objectives of the Parabolic Dish Test Site were to provide experimental support for DOE's Solar Thermal Parabolic Dish Technology Development Program (managed by JPL) through the testing, evaluation, and performance characterization of parabolic dish concentrators, high flux receivers, power conversion systems, thermal (300 to 1427°C, 572 to 2600°F) transport subsystems, dish modules, solar/fossil hybrid systems, and instrumentation. A secondary objective was to provide a site for the test and evaluation of hardware developed independently by industry. A chronology of activities at the PDTS is contained in Appendix A.

B. DESCRIPTION OF BASIC EQUIPMENT

1. Concentrators

Concentrators installed at the PDTS for the Parabolic Dish Program are described briefly below.

a. Precursor Concentrator. The precursor concentrator consisted of a backing structure simulating a portion of a parabolic concentrator together with an hour angle declination mount. Six mirror facets (24 by 28 in.), similar to those used subsequently on the test bed concentrators, were mounted on the structure. The precursor was used primarily as a tool to measure mirror performance and to evaluate alignment techniques.

b. Omnium-G Module. An Omnium-G (Heliodyne model MTC-25) solar-powered electric generating plant, an early product of industry, was purchased from the Omnium-G Company (OG) and installed at the PDTS. Its characteristics were as follows:

(1) Concentrator: 6-m diameter (19.7 ft), 18 petals (mirrors) 25.9-m^2 usable reflective area, electro-polished aluminum mirror surface (trade name Alzac, made by Alcoa), reflectance 81 to 85%, 4-m focal length (13.1 ft).

(2) Tracker: 2-axis sun tracker, 1.9-deg/s slew rate (down to up) at 24 V, 0.45-deg/s slew rate in azimuth at 24 V.

c. Test Bed Concentrator (TBC). Two 11-m-diameter TBCs were built by E-Systems, Incorporated, of Dallas, Texas, and installed at the PDTS. Based on a JPL development effort, the mirror facets for the TBCs were fabricated by bonding a second-surface mirror to a spherically contoured block of Foamglas (from Pittsburgh Corning Corporation) and by coating the substrate with a protective sealer and painting it white. Supports for the facets are bonded to the edges. Characteristics of the TBCs are as follows:

(1) Nominal 11-m diameter reflector.

(2) 70 kW_t at 800 W/m^2 insolation.

(3) 224 facets: second-surface silvered glass; 24 by 28 in. nominal size; 3 regions of nominally different radii of curvature: 510, 610, and 634 in.; initial reflectance, 95% maximum; slope error 1 mrad.

(4) 6.6-m focal length.

(5) Paraboloidal mounting structure with f/D = 0.6.

(6) Design weight at focus = 1100 lb.

(7) Tracking error, 1 mrad.

(8) Slew rates: azimuth 2000 deg/h, elevation 200 deg/h.

(9) 8-in.-diameter concentrated beam at the focal plane.

(10) 1858 W/cm^2 peak flux.

(11) 3600°K peak equilibrium temperature.

d. Parabolic Dish Concentrator-1. Parabolic Dish Concentrator-1 (PDC-1), designed by the General Electric Company (GE) and fabricated by the Ford Aerospace and Communications Corporation (FACC), was installed at the PDTS in 1982. Formerly known as the General Electric Low-Cost Concentrator, this is the first dish concentrator designed for mass-production under the JPL Parabolic Dish Program. PDC-1 characteristics are listed below.

(1) Mirror diameter, 12 m.

(2) Focal length, 6 m.

(3) Concentration ratio, 1500.

(4) Thermal energy to engine, 58.5 kW_t.

(5) Reflective surface, aluminized plastic film, Llumar.

(6) Gore design, balsa wood with molded reinforced plastic sandwich, 36 panels, 34 ft^2 each.

(7) Tracking, azimuth/elevation drive, cable/drum.

(8) Reinforcement, internal corrugated ribs.

(9) Stow position, horizontal, facing down.

(10) Structure, aluminum tubing.

C. EXPERIMENTS AND EXPERIMENTATION EQUIPMENT

1. Types of Tests

The test and evaluation phase of systems and subsystems at the PDTS included the following tests:

(1) Tracker mechanical checkout.

(2) Concentrator mechanical checkout.

(3) Mirror segment alignment.

(4) Solar tracking error.

(5) Reflectance of mirror surface.

(6) Moonlight focal point location.

(7) Flux mapping in the focal zone.

(8) Cold-water calorimeter tests.

(9) Receiver thermal performance.

(10) System proof and leak test.

(11) Power conversion performance.

Dish-Stirling solar experiments were run on both TBCs to test the feasibility of the advanced receiver and Stirling engine/alternator subsystem designed by Fairchild Stratos Division of Fairchild Industries, Inc., and United Stirling AB (USAB) of Sweden. When mounted on the TBC, the test module showed a capability of generating 20 kW_e. Tests of the hybrid Stirling engine were later abandoned due to thermal stress problems that occurred at tube braze joints; however, the solar-only Stirling engine tests were quite successful (References 2 and 19).

Organic Rankine-cycle (ORC) power module tests were also run on TBC-1. The receiver was designed and built by FACC of Newport Beach, California. The

ORC engine, which uses toluene as the working fluid, was developed by the Barber-Nichols Company of Arvada, Colorado. Extensive data were collected for limited runs. (Evaluation of the test data is contained in Reference 3.) Tests could not be concluded due to bearing problems, which were later corrected by Barber-Nichols; however, testing on TBC-1 was not resumed.

2. Test Equipment

Three different cold-water calorimeters were designed and built by JPL: coil tubing calorimeter, flat-plate calorimeter, and cavity calorimeter. These calorimeters were used to measure the integrated thermal flux at and near the concentrator's focal plane. The coil tubing calorimeter used on the precursor concentrator is capable of accepting thermal loads up to 2 kW_t. The flat-plate calorimeter was used on the Omnium-G unit for thermal loads up to 25 kW_t. The cavity calorimeter, for use on the TBCs, had a capacity for thermal loads up to 95 kW_t.

A flux mapper was developed and fabricated for use in characterizing concentrator flux pattern and intensity. The flux mapper is a radiometer on a three-axis scan system for measurement of high radiant flux levels expected near the focal plane of a solar concentrator having a high concentration ratio.

The flux mapper has three modes of operation: (1) PIN diode relative, (2) cone radiometer relative, and (3) cone radiometer absolute. In the PIN diode relative mode, a PIN diode probe scans through the concentrated sunbeam while a reference diode is pointed at the sun. The two readings are combined to arrive at a concentration ratio. Similarly, a cone radiometer probe can be used in conjunction with the reference diode for a concentration ratio. The cone radiometer probe may also be used alone to measure flux by calibrating the probe with a small electrical resistive-type heater that is built into the probe.

D. CAPABILITIES

The JPL Edwards Test Station was selected as the location to perform testing and evaluation of point-focusing distributed receivers at the subsystem and system level at temperatures between 320 and 1650°C (600 and 3000°F) for the following reasons:

(1) ETS-based personnel had previous experience in working with high-temperature, high-pressure fluids because ETS is JPL's rocket engine test facility. This experience was directly applicable to thermal power system projects.

(2) A high insolation level exists at ETS and is considered one of the best in the United States.

(3) Excellent meteorological conditions exist at ETS; thus, there was minimal downtime because of bad weather.

(4) Supporting services included: instrumentation and calibration laboratories; electric, machine, and weld shops with personnel; office space; and a cafeteria.

(5) All required utilities were readily available.

(6) Security as well as easy access for visitors was provided at all times.

(7) An emergency rescue crew and vehicle was available to provide emergency medical treatment.

E. DATA ACQUISITION AND REDUCTION

To obtain the required data formatted for efficient analysis during performance testing of the subsystem and system tests, a computer-automated data gathering and processing (DGAP) system was designed and implemented at the PDTS. DGAP equipment was required to make parametric measurements, display the data in real time, and monitor and record data on mass storage. The necessity of a computer processing system is dictated by the large volume of data to be processed, the need for real-time analysis of critical parameters, the requirement for graphical representation and off-line data analysis with higher mathematical functions, and the requirement for efficient system flexibility to support a wide range of testing. Operational experience to date has shown the value of real-time printout of data as well as real-time displays of critical parameters.

The computerized data acquisition system at the PDTS included a Digital Equipment Corporation PDP-11/34A minicomputer with two RK05 disk drives, a mass storage unit, 0.5-in. nine-track magnetic tape transport, high-speed multiplexers, A/D converters, three Acurex Auto Data Nine data loggers, CRT terminals, alphanumeric and graphic video monitor, and a printer-plotter. The interface between the computer and its peripherals was provided by RS-232C serial data lines.

Each of the three data loggers had the capability of accepting up to 1000 channels of data. Input cards were provided for type "K" and "T" thermocouples, voltages up to 120 Vdc, 4-10 and 10-50 mA current transmitters, and RTDs. Programming of the data loggers could be accomplished manually or by the computer. The data loggers scanned up to 24 channels per second with resolution to 0.01% of full scale. Resolution to 0.001% was available at reduced scan rates. A data logger with high common mode rejection was essential because signals being measured were in the millivolt range.

F. SAFETY

Safety of PDTS operating personnel received primary attention. The key points of the PDTS safety practices are listed below:

(1) Written test procedures were required prior to the start of any testing activity.

(2) Safe operating limits of critical parameters (temperature, pressure, etc.) were remotely monitored during subsystem and system testing, and displayed in the control room. Upper and lower limits were predetermined and set into the data logger so that an alarm could alert the operator in the control room.

(3) An emergency override procedure was implemented if a safe operating limit was exceeded or anticipated.

(4) Safety glasses (gas welding goggles) and hard hats were required for operating personnel in the test area during "on sun" operation of solar concentrators.

(5) Operating personnel were not permitted to work closer than two focal lengths from the concentrator while it was tracking the sun.

(6) The "buddy system" was used by personnel in the test area during operation of the solar concentrators.

G. OTHER SUPPORT

Utilities available at the PDTS included 60-Hz single and three-phase electrical power, water, natural gas, demineralized water, and compressed air or nitrogen.

Supporting facilities available at the PDTS included the Instrumentation Laboratory, Calibration Laboratory, Photography Laboratory, Electrical Shop, Machine Shop, Welding Shop, and a Motor Pool including crane, forklift, and a two-man self-propelled aerial lift.

A photograph of the facility is presented in Figure 1-1.

H. WEATHER STATION

Insolation measurements were initiated in October 1977 at ETS, Building E-22. This facility is approximately 500 ft from the PDTS. The following measurements were taken and recorded:

(1) Direct component of radiation, using two pyrheliometers.

(2) Total sky radiation, using a pyranometer.

(3) Wind speed and direction.

(4) Temperature and dew point.

(5) Barometric pressure.

(6) Circumsolar telescope data.

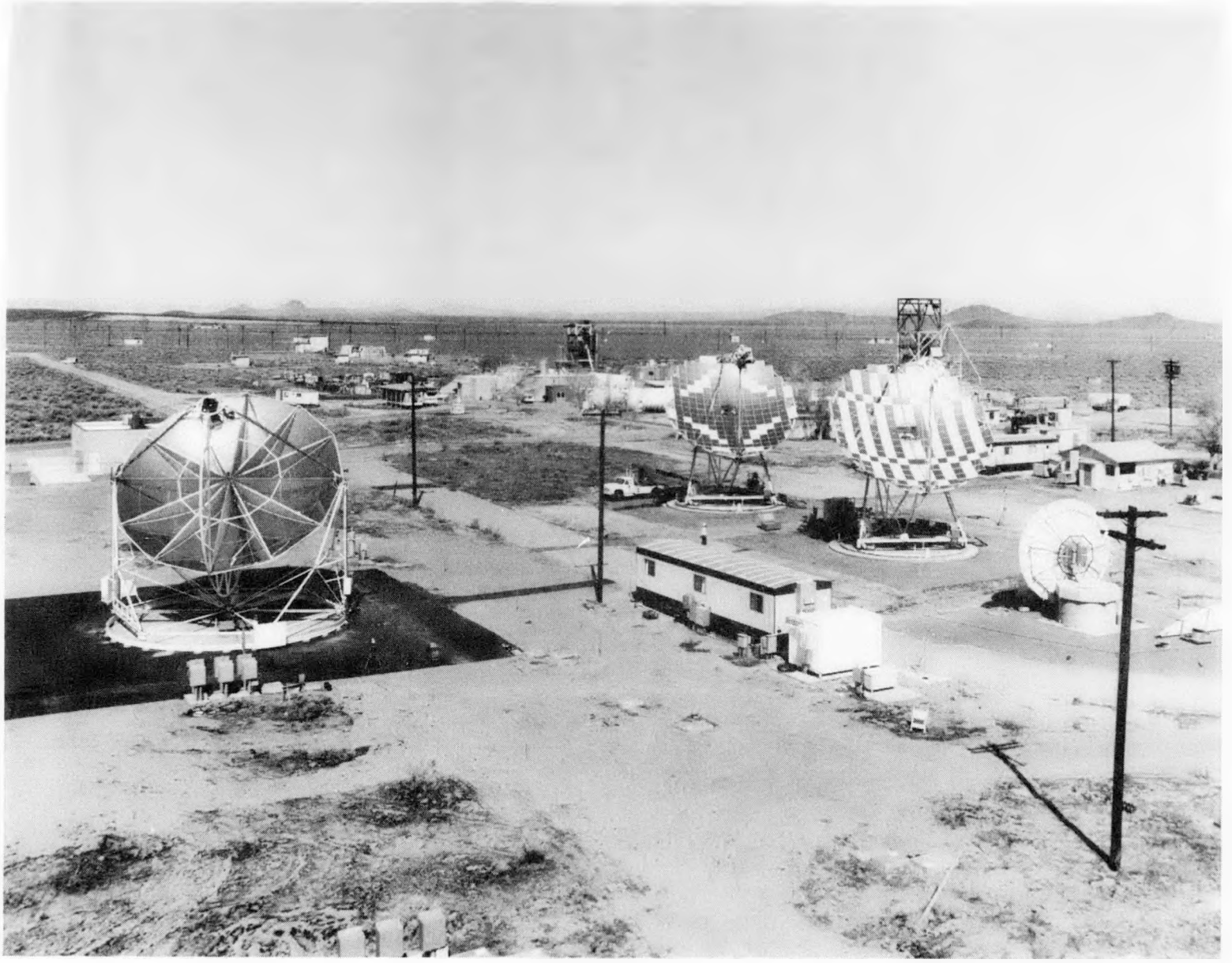

Figure 1-1. Parabolic Dish Test Site

The pyrheliometers and the pyranometer, Kendall models Mark III and VII, respectively, were developed by JPL utilizing the absolute radiometer concept. These instruments have a range of 0 to well over 1000 W/m^2.

The wind speed instrument, model 1022S, was manufactured by Meteorology Research, Incorporated. This instrument has a range of 0 to 120 km/h (0 to 75 mi/h). The wind direction instrument, model 1022D, also was manufactured by Meteorology Research, Incorporated. This instrument has a range of 0 to 540 deg.

The ambient temperature and dew point measuring instruments were each designated as model 892-1, manufactured by Meteorology Research, Incorporated. These instruments each have a range of -30 to +50°C. Humidity is derived from these instruments.

The barometric pressure measuring instrument, model 751, was manufactured by Meteorology Research, Incorporated. This instrument has a range of 24.6 to 31.5 in.-Hg.

The circumsolar telescope was developed by Lawrence Berkeley Laboratory to obtain solar radiation measurements for accurate prediction of performance of solar thermal systems utilizing focusing collectors. The instrument measures the effects of atmospheric conditions on the direct and circumsolar components of solar flux. In operation, the solar guider aligns the instrument platform at the center of the sun. The telescope body scans back and forth across the image of the sun and circumsolar region to an angle of $\pm$3 deg (the solar diameter is about 32 minutes of arc). A small aperture located in the image plane restricts the angular view of the telescope to solar disk. The light passing through this aperture is chopped, filtered, detected, digitized, and written on a magnetic tape as a function of the angular position.

Weather Station data were recorded at 1-minute intervals, 24 hours a day. One month's worth of data could be acquired on a single reel of magnetic tape. Original tapes were retained by JPL. A small uninterruptible power system was included to prevent data dropouts during commercial power outages.

I. 1984 ACTIVITIES AND CLOSURE

The most important activity at the PDTS in fiscal year 1984 was the testing of the solar-only Stirling power conversion assembly. A new type of receiver, ESOR-IV, was tested. Tests to select face-plate materials for the Stirling module also were run.

Activities leading to closure of the PDTS are listed below:

(1) Radiation and other environmental data acquisition was discontinued in August 1983.

(2) USAB test equipment was returned to their facility in Sweden.

(3) TBC-1 and TBC-2 were dismantled and sent to Sandia National Laboratories in Albuquerque, New Mexico (SNLA).

(4) PDC-1 characterization tests continued until closure of the PDTS, at which time PDC-1 was dismantled and shipped to SNLA.

(5) The cold-water cavity calorimeter was provided to Advanco Corporation for their testing of the Vanguard Stirling module at Rancho Mirage, California.

(6) A stand-alone data acquisition system utilizing a data logger was also provided to Advanco.

By June 1984 all activities at the PDTS were concluded. Equipment and instrumentation were returned to the JPL loan pool or transferred to SNLA.

SECTION II

DATA ACQUISITION AND EVALUATION

A. TESTING OF BASIC EQUIPMENT

1. Data Acquisition System

During the conceptual phase of the system design, it was decided that digitizing the analog signals would be accomplished by commercial data loggers; the Acurex Auto Data Nine data logger was selected, which enabled operation in a stand-alone mode, or control by a minicomputer.

There were several design approaches that were considered necessary to establish a flexible, noise-tolerant, simple system as listed in Table 2-1.

A block diagram (Figure 2-1) shows two data acquisition systems; one system that gathered data from solar thermal experiments and another dedicated to gathering data on meteorological conditions.

2. System Description

a. Data Logging for Solar Thermal Experiments. This portion of the data system consists of a data logger, a remote scanner (or scanners), and electronic conditioning equipment. Each of the data loggers, which were located within the PDTS control center, can digitize any of 40 channels independent of outside influences. The remote scanner, as commanded by a related data logger, can select any of 100 channels per scanner, and up to 1000 channels maximum (in blocks of 10 channels).

Typically, most of the analog signals from an experiment were routed through a remote scanner that was mounted on or near the concentrator structure. However, some signals required conditioning before being selected by the scanner. These conditioners could not tolerate the harsh desert environment at the PDTS and, therefore, were housed in the PDTS control center. The outputs of these conditioners were sent directly to the related data logger.

In Figure 2-1, the block labeled "ancillary electronics" consists of analog apparatus that are not part of the data system. These might be some or all of the following:

(1) A collection of digital displays of functions that are critical to a solar thermal system and thus need to be displayed at all times.

(2) Strip chart recorder.

(3) Insolation amplifiers.

(4) Buffer amplifiers (instrumentation amplifiers).

(5) Other, as required.

Table 2-1. Data Logger Requirements List

(1) Fully operational in stand-alone mode.

(2) All major functions remotely controllable by a computer via an RS-232C interface.

(3) Multiplexer shall use Reed relays with less than 1-V offset, three-wire switching, expected lifetime of 10^9 closures[a], and 250 Vdc or ac peak standoff between any two input leads.

(4) A/D converter shall exhibit the following features:

  (a) Input impedence not less than 100 megohm.

  (b) Dynamic range not less than 40,000 counts.

  (c) 1-V resolution on 40 mV range.

  (d) Automatic zeroing.

  (e) Common mode rejection not less than 140 dB at 60 Hz.

  (f) Normal mode rejection not less than 70 db.

(5) Alarm option shall provide a minimum of two alarms per channel and 30 individually programmable limits with dedicated outputs from each.

(6) Capability to display one channel while scanning all channels.

(7) All functions programmable from front panel.

(8) Crystal-controlled clock available as option to "keep-alive" battery.

(9) Front panel controls shall be inhibited by front panel keylock switch or hidden switch.

(10) Averaging option available to calculate arithmetic mean value digitally, averaging period selectable from 1 minute to 24 hours, averaging assignable to 50 channels minimum.

(11) Mainframe shall be able to support growth to 1000 channels with additional extender chassis assemblies.

(12) Program protection battery shall have an operating life of one year minimum.

(13) Operation with remote scanner located up to 1500 ft from mainframe.

[a]Six years at one closure per second, 12 h/day.

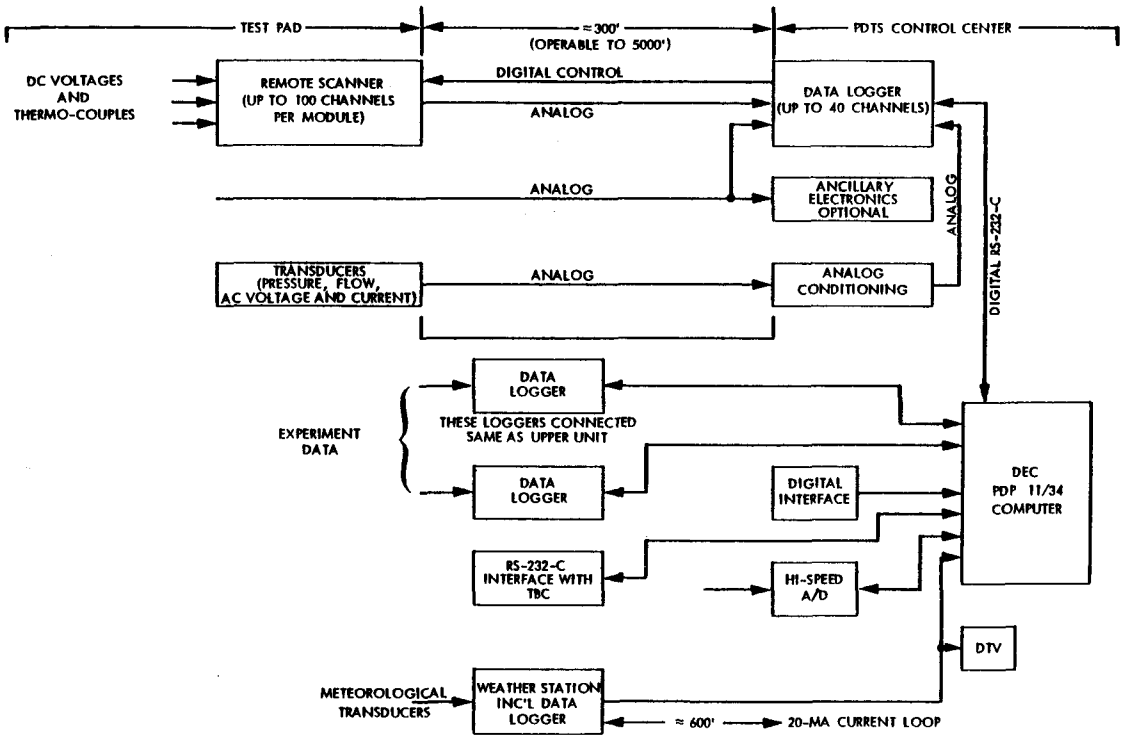

Figure 2-1. Data Acquisition and Processing System

b. Data Logging for Meteorological Data. This system (Figure 2-2) is dedicated to recording the outputs of nine meteorological transducers. Outputs from these transducers are fed into conditioning electronics where they are put into a standard 0-5 volt output level, and then routed into the data logger.

The data logger scans these inputs once every minute, 24 hours per day. Within the logger, the signals are digitized into two serial data streams. One of these is an RS-232C port, and the other is a 20-mA current loop. The RS-232C port feeds a serial-to-parallel data converter, the output of which feeds the digital tape recorder.

Once a month, the meteorological data tape was removed and sent to the JPL Pasadena facility for analysis. Monthly summaries of daily insolation and daily total solar energy received were plotted and distributed to the engineering staff, along with minimum/maximum values for wind speed, relative humidity, ambient temperature, and barometric pressure (refer to Figures 2-3, 2-4, and 2-5). Earlier, meteorological data were only available at the end of the month. However, after modifications to the data gathering software, weather station data were added to the test run data, giving this weather information to the experimenter at the conclusion of the test run.

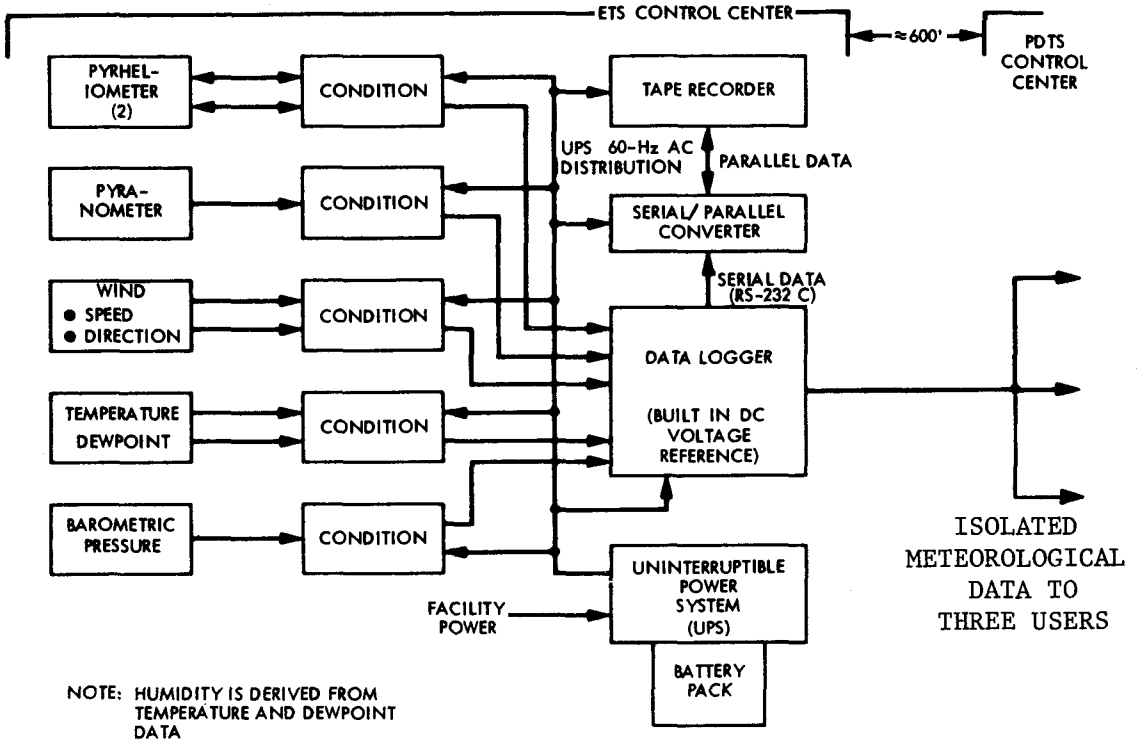

Figure 2-2. Meteorological Conditions Data Acquisition Block Diagram

Originally, the current loop output from the data logger was routed to the PDTS control center, about 600 ft away, with only one user. However, because of a requirement for a larger distribution of these data and the need to transport the data over extended distances, the system was changed to transmit the data to the control center via an RS-422 circuit. The RS-422 data were then converted into three isolated current loop outputs, one for each of three different users (Figure 2-6).

In the control center, the raw meteorological data were viewed on a digital TV (DTV). The other users were the solar thermal experimenters, some 450 ft away, where the data were recorded on digital tape along with the experiment data. Each user then had his own dedicated, isolated source of meteorological data.

To minimize the loss of meteorological data, this system was powered from an uninterruptible power supply (UPS). The UPS contained a battery pack that kept the system operating for 10 to 15 minutes if ac power was interrupted. This length of time was adequate to allow a backup engine/ generator to come on line.

3. Typical Data Logger Interfaces

Figure 2-7 is representative of typical interfaces that were encountered in the PDTS computer "front-end." All dc signals were converted

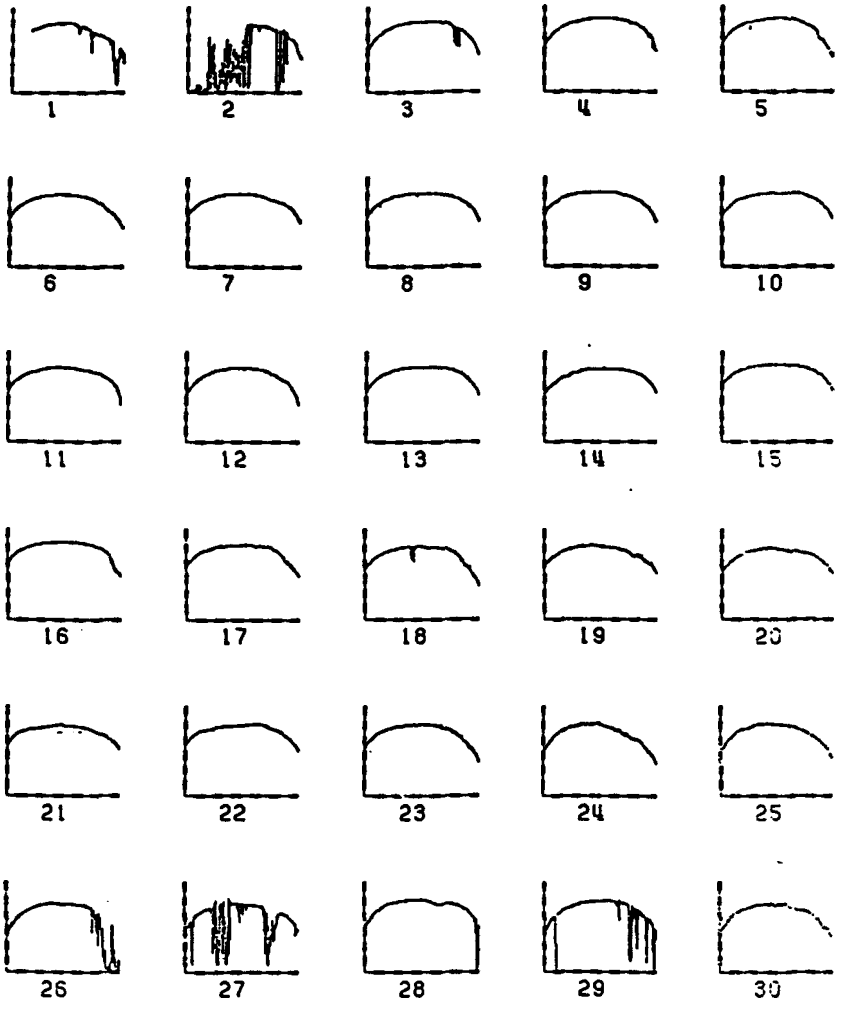

Figure 2-3. PDTS Normal Incidence Pyrheliometer No. 1, Insolation for June 1981

within the data logger; all ac signals had to be converted to dc by conditioners or transducers.

The following is a list of interfaces, other than analog, that were used within the data system:

Digital Signal	Typical Use
RS-232C	Data logger output
RS-422	Meteorological data
20-mA current loop	Meteorological data

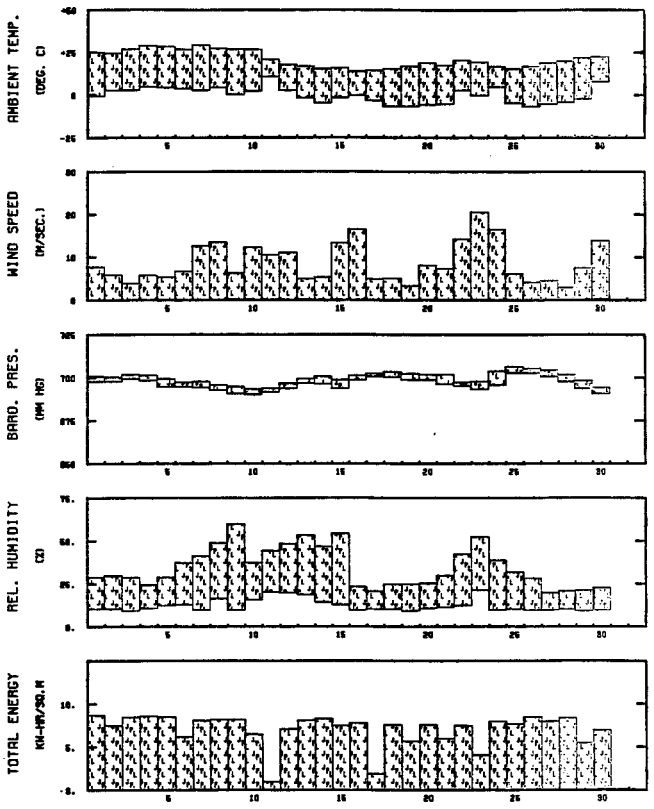

Figure 2-4. Minimum/Maximum Values for June 1981

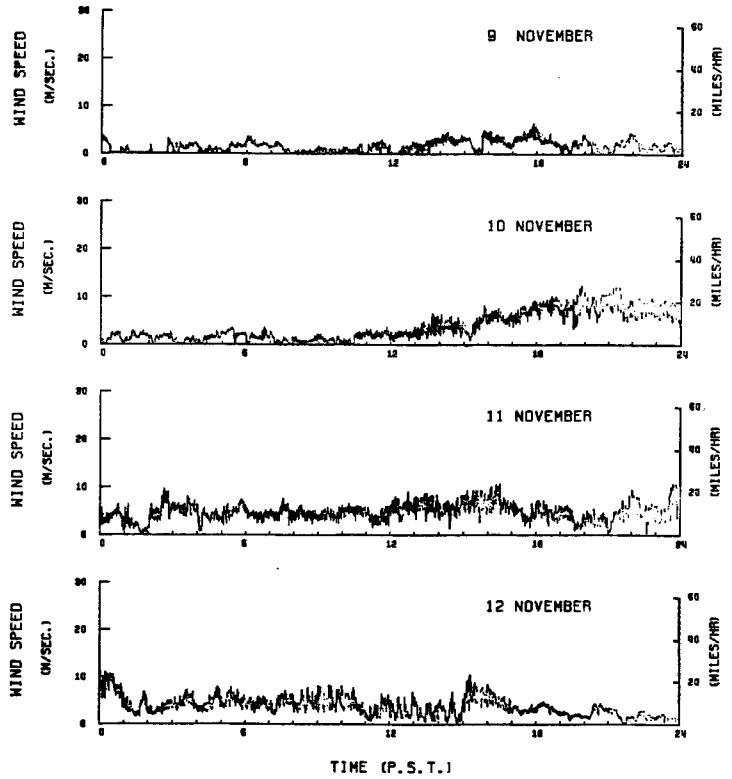

Figure 2-5. PDTS Wind Speed Data

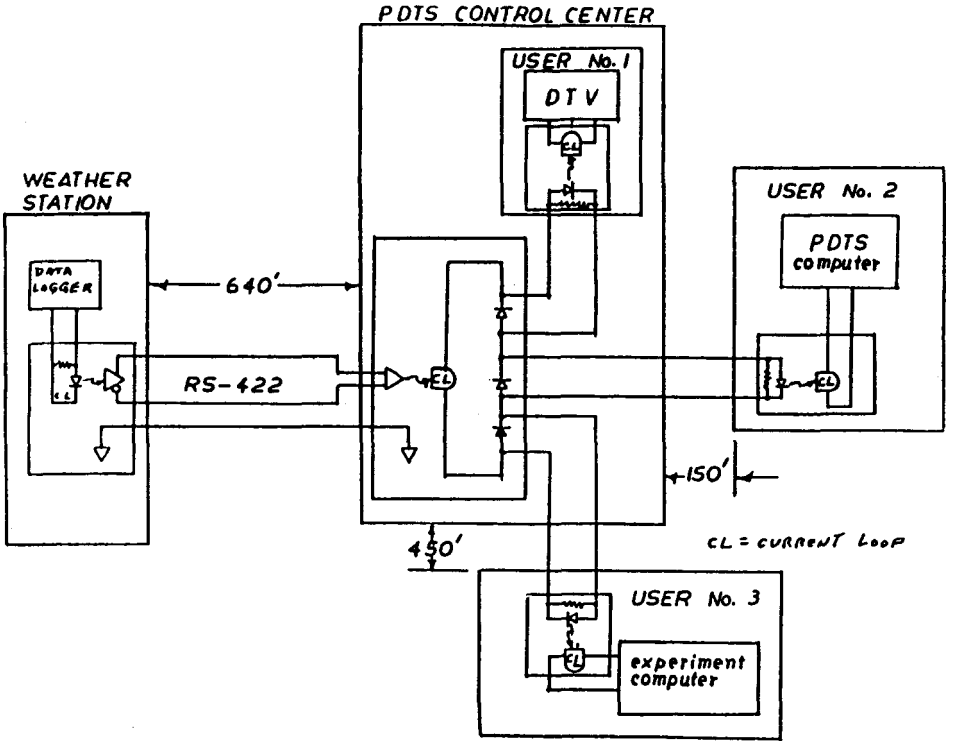

Figure 2-6. Meteorological Data Interface Block Diagram

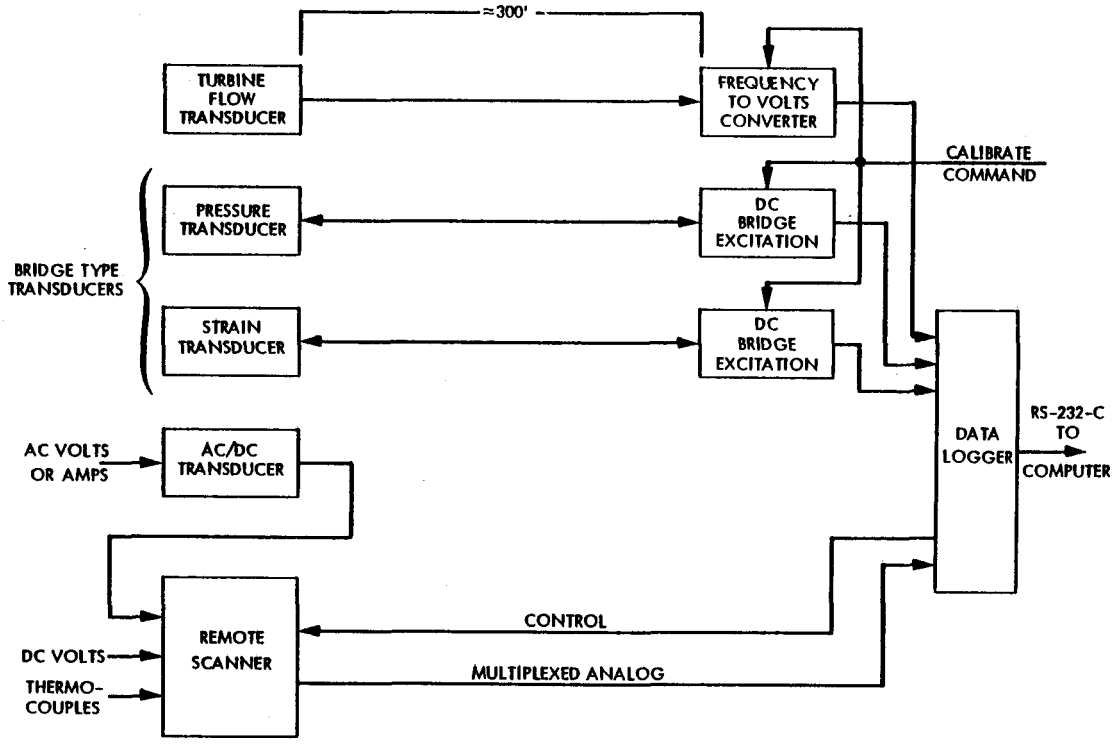

Figure 2-7. Typical Data Logger Interfaces

4. System Operation

When it was necessary to measure dc voltages higher than 10 V, dedicated voltage dividers were used. This allowed individual scale factoring when desired and allowed the measurement of voltages that were greater than 100 V.

Problems from electrical interference (noise) during system operation were negligible. Characteristics of the data logger are presented in Table 2-2. The output of the differential temperature probes is low-level, requiring the most sensitive range of the data logger. Observations showed that the least significant digit (1 μV) was steady during operation.

The major portion of data were taken during periods of steady-state operation, or when the rate of operation was changing slowly. Accordingly, there was no need for sample and hold circuits or anti-aliasing filters; thus, a simpler system. If the need arose to analyze transients, a high-speed analog-to-digital converter was used.

5. The Computer System

The computer portion of the data acquisition system used at the PDTS included a Digital Equipment Corporation (DEC) PDP-11/34A minicomputer (Figure 2-8). In support of this computer, the system also included two RK05 hard disk drives with a capacity of 2.5 megabytes of information each, a Kennedy 1.27-cm nine-track digital magnetic tape drive, a Versatec line printer/plotter, a Control Data Corporation CDC-9766 disk drive with a capacity of 300 megabytes of information, and other assorted hardware. The minicomputer and support equipment, with the exception of the computer terminals, were located in a controlled environment trailer near the test site. High winds with blowing sand and excessive daytime temperatures, common occurrences at the site, would have been detrimental to the computer system.

The software used with the data acquisition system was the DEC-supplied RSX-11M multi-user, multi-task operating system. This operating system was chosen to allow the data acquisition system to perform multiple tasks during an experimental run, such as data gathering, data display, and data conversion. The task software programs that actually performed the data gathering and recording function were written using DEC FORTRAN and DEC assembly languages.

The capabilities of software in use at the PDTS included data logging and storage on disk of 150 separate data channels from the data logger, concurrent data logging from more than one data logger, screen display of alarm limits exceeded during a scan, screen display of selected data channels during the test run, conversion of the data logger output from frequency, voltage, or current to engineering units, plotting of engineering unit values for selected data channels versus time at the conclusion of a test run, the display of selected calculations during a test, printouts of selected channels of engineering data for selected time intervals, the inclusion of comments in the test run data, and transferring the data from disk to magnetic tape for archival storage. Programming was also available to set up the data logger

Table 2-2. PDTS Data Acquisition System Data Logger Features

(1)	180 dB CMRR
(2)	Resolution: 0.001% of full scale (1 V for 100 mV scale)
(3)	Speed: 24 readings/second with standard resolution, 2.4/second with high resolution
(4)	dc voltage ranges: ±100 mV, ±1.99 V, ±10.0 V, ±100 V with option
(5)	Overrange: greater than 120%, less than 130%
(6)	Input impedance: greater than 1000 megohms/V, potentiometric
(7)	Thermocouple inputs: ice point compensated; options: Type - J, K, T, E, R, S; linearized; direct readout in ^{o}C
(8)	40 input channels in mainframe
(9)	100 channels in each remote scanner (1000 channels maximum)
(10)	Blocks of 10 input channels with same function (e.g., volts, temperature)
(11)	RS-232C digital interface
(12)	Current loop interface (20 mA)
(13)	Stand-alone operation or under computer control
(14)	Remote scanner operable up to 5000 ft from data logger
(15)	Manufacturer and model of data logger: Acurex Auto Data Nine

for a test, and programming was available to interact with the solar concentrator control units.

The data acquisition system began operation in February 1979. At that time, a DEC PDP-11/10 minicomputer was used instead of the larger PDP-11/34A that replaced it, and the operating system was the DEC RT-11 real-time, single-user operating system. The originally configured acquisition system could handle a single logger during a test, provide a dump of raw data at the conclusion of a test, and provide a printout of selected channels converted to engineering units. This original data acquisition system was adequate until testing at the PDTS increased dramatically, at which time the PDP-11/34A minicomputer was installed.

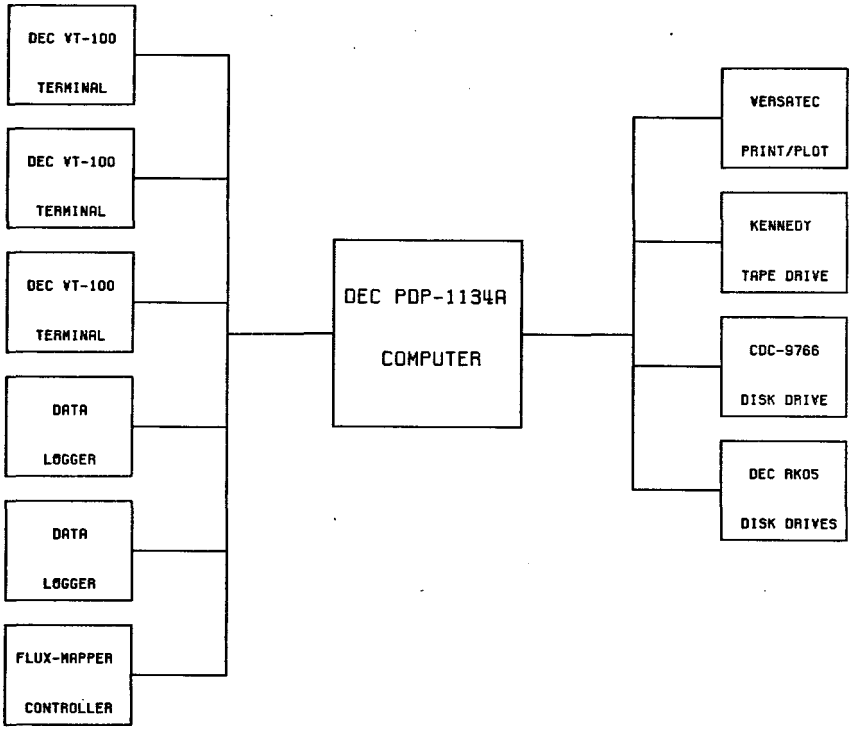

Figure 2-8. PDTS Computer System

In addition to the data acquisition from the data loggers, a special set of programs was developed to interface with the JPL-designed flux mapper. (These computer programs are discussed in Reference 5.) The flux mapper is a three-axis scan system for measurement of high radiation flux levels that might be expected near the focal point of a solar concentrator. In normal operation, the flux mapper scans an X-Y plane in a boustrophedonic manner for a single Z value, measuring the flux at points along its motion. The flux mapper is microprocessor-controlled, with the data transmitted to the PDP-11/34A minicomputer upon the completion of an X-Y scan. Special data acquisition programming was developed to store these data on magnetic tape for archival storage and to provide three-dimensional plots of the flux intensity over the X-Y plane (see Figure 2-14). Some custom programming was provided for the analysis of flux mapper data. The JPL flux mapper is discussed in more detail below.

6. The Flux Mapper[1]

a. Purpose. JPL designed and built a flux mapper to gather empirical data about the concentrated energy at the focal zone of a solar concentrator. These data provide an understanding of optimal solar receiver

[1]For further details see Reference 4. Computer programs used for processing flux mapper data are discussed in Reference 5.

design, help characterize solar concentrators, provide a means for comparing analysis with actual hardware, and are a tool for comparing various systems in the field.

b. System. The principal components of the flux mapper system (Figure 2-9) are a radiometer probe, a mechanical locating device, a data and control processor, and a data acquisition system.

c. Probes. Two radiometer probes were tested. The first was a high-speed probe (Figure 2-10), which consists of a highly reflective, water-cooled body and heat shield. A 0.006-in.-diameter aperture limits the amount of energy falling on the PIN diode detector, whose voltage output provides a signal proportional to the incoming energy. This system has an extremely short time constant (nanoseconds), and when carefully calibrated can provide data with about ±10% accuracy. The second probe (Figure 2-11) is a water-cooled Kendall absolute cavity radiometer. This probe is a more rugged version of the absolute standard laboratory instrument. Where the longer time constant of 4 to 6 seconds can be tolerated, this instrument can provide accuracies of better than ±2%.

d. Mechanism. The traversing mechanism (Figure 2-12) consists of a mounting frame from which the probe mounting carriage travels in an X-Y plane. This carriage contains a stepping motor that allows the probe to be indexed in the Z direction. The normal scanning sequence is horizontally (X) from the lower left corner, stepping upward (Y) at the end of each line until an entire X-Y plane is measured. The probe then moves to a new plane (Z) and the X-Y process is repeated. Scanning rates are variable, but a typical 1250 data point plane takes about 90 seconds to scan.

e. Data Acquisition. Data are acquired simultaneously on both a hard copy "quick-look" printout and on magnetic tape. For "quick-look" needs, an X-Y-Z plotter is utilized to give an intensity trace as a function of position, with system parameters displayed or printed from the CRT. These same data can also be stored on magnetic tape for later computer reduction.

f. Data Reduction. Data display can be either full digital or in a variety of graphical displays, such as contour plots of each plane (Figure 2-13) or isometric displays for visual examination (Figure 2-14).

7. Cold-Water Cavity Calorimeters

Two types of cold-water cavity calorimeters (CWCCs) were designed and constructed for the evaluation of thermal performance of parabolic dish concentrators.

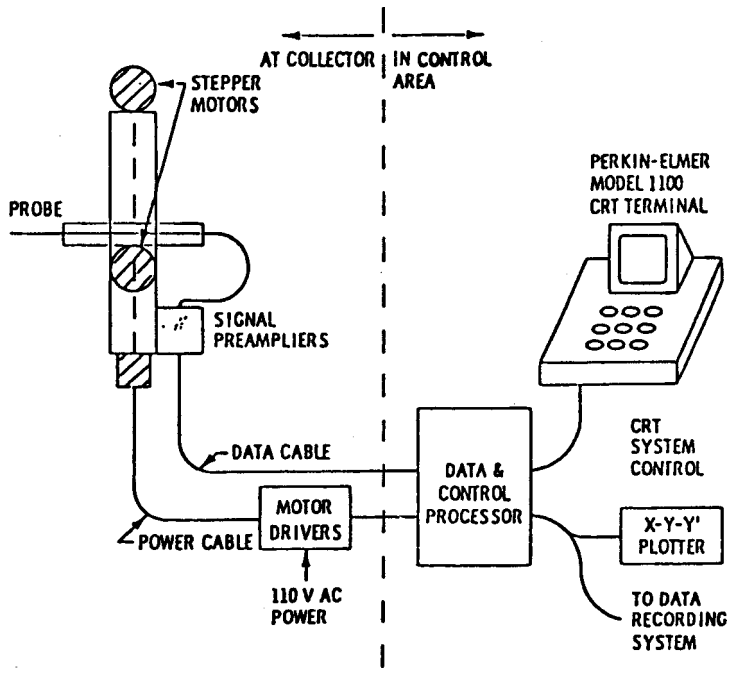

Figure 2-9. Flux Mapper Layout

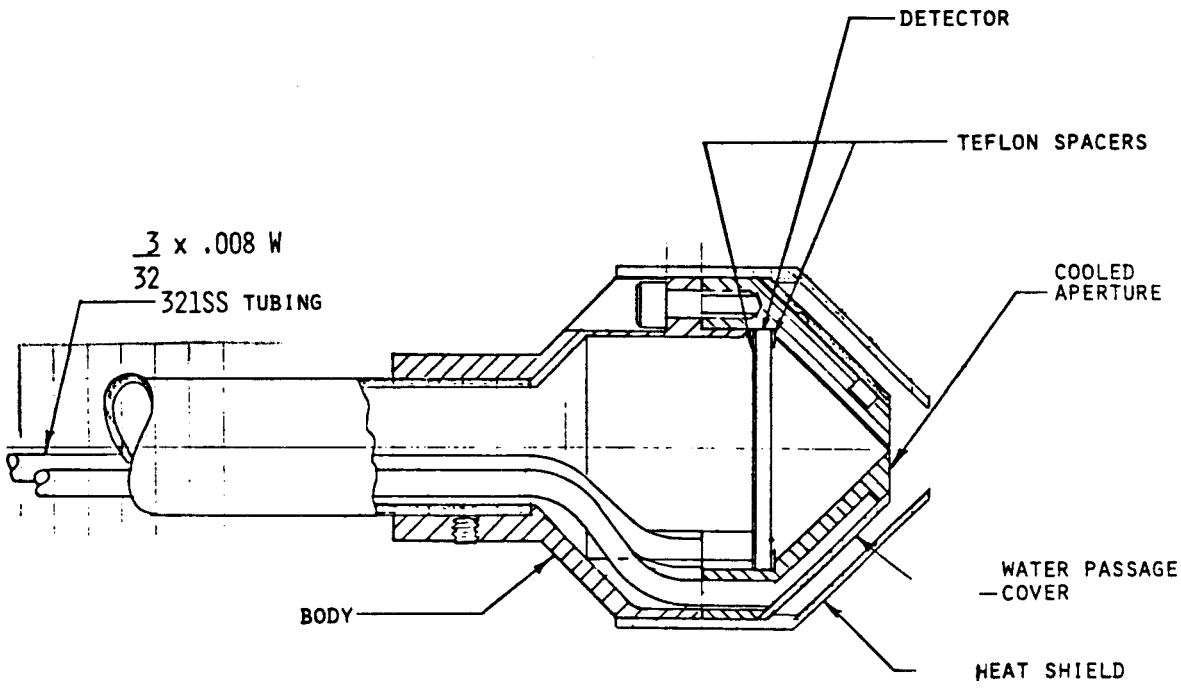

Figure 2-10. High-Intensity PIN Sensor

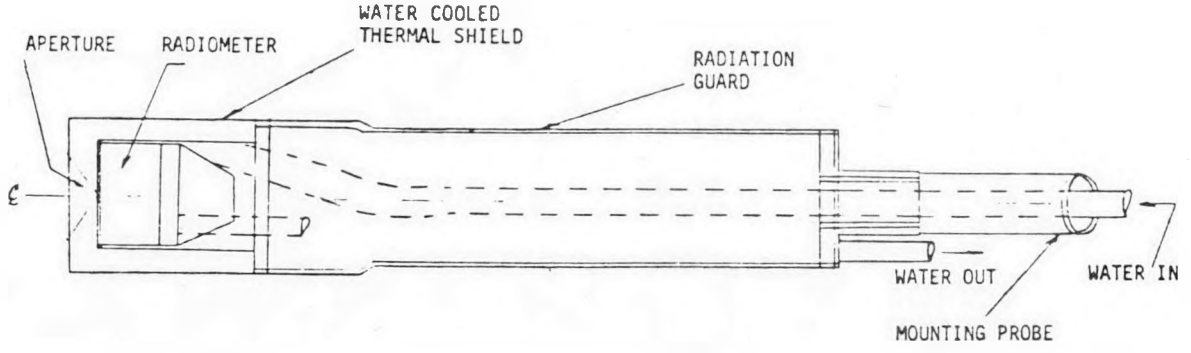

Figure 2-11. Absolute Cavity Radiometer

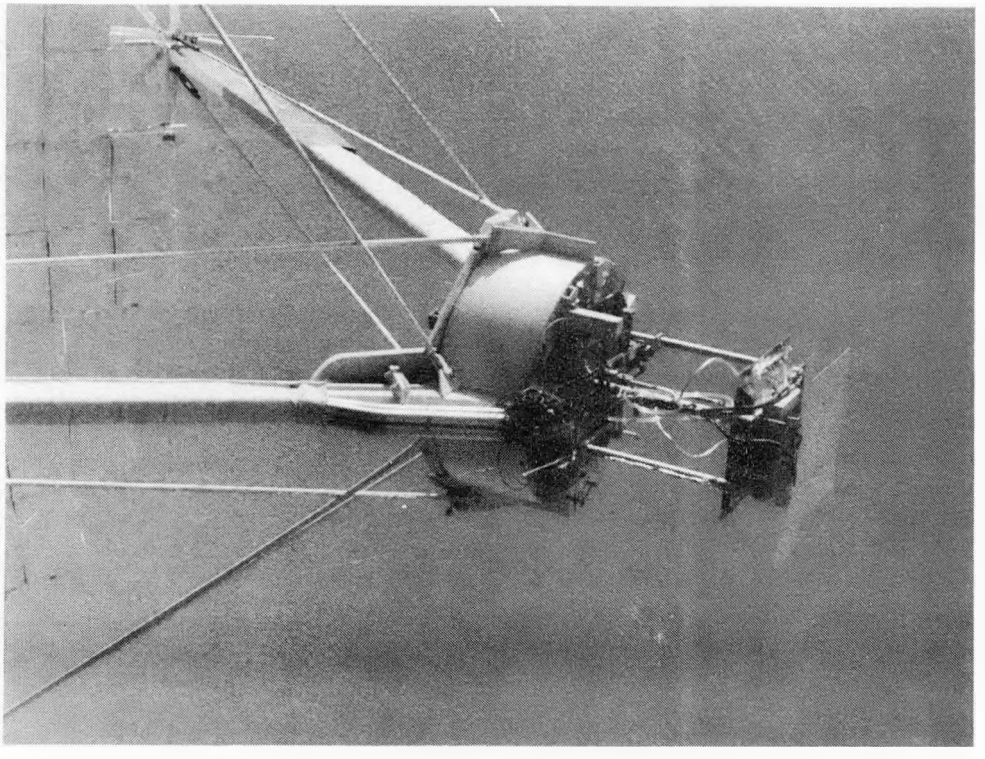

Figure 2-12. Flux Mapper Mechanism

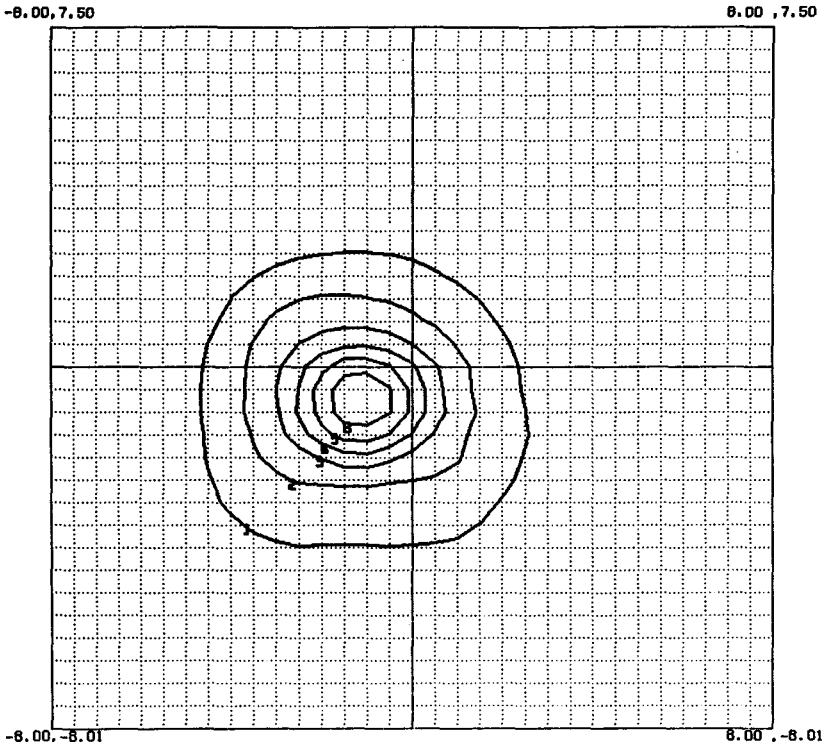

Figure 2-13. Flux Mapper Contour Plot Display

a. Omnium-G CWCC.[2] A cold-water calorimeter was designed and fabricated for use in evaluating the thermal performance of the 6-m-diameter Omnium-G Heliodyne dish concentrator.

A calorimeter is a device that, when placed in the focal area (3 to 6 in. behind the focal plane) and run with known flow rate and temperature rise of fluid, results in empirically determined energy flux onto the calorimeter using a given heat capacity of the fluid being used. Water is used as the fluid for its high heat capacity, safety, and convenience of operation. Copper is chosen for the calorimeter material for its high heat transfer coefficient that allows a low operating temperature. In order to obtain adequate flow across the heat transfer area with the least possible operating pressure, a parallel flow across the area is implemented.

A flat-plate design was selected for ease of fabrication and thermal characteristics. Two plates of copper were furnace-brazed by MCI after JPL personnel had milled channels in one plate. The channels provide the parallel flow necessary for adequate heat removal from the focal area. The plate assembly is manifolded by two 1.275-in. inside diameter (ID) brass tubing brazed (by JPL) to the inlet and outlet sides of the copper plate assembly. A 10-in.-diameter mixer extension was added to the exit header to ensure proper

[2]Computer programs used for processing these test data are described in Appendix B.

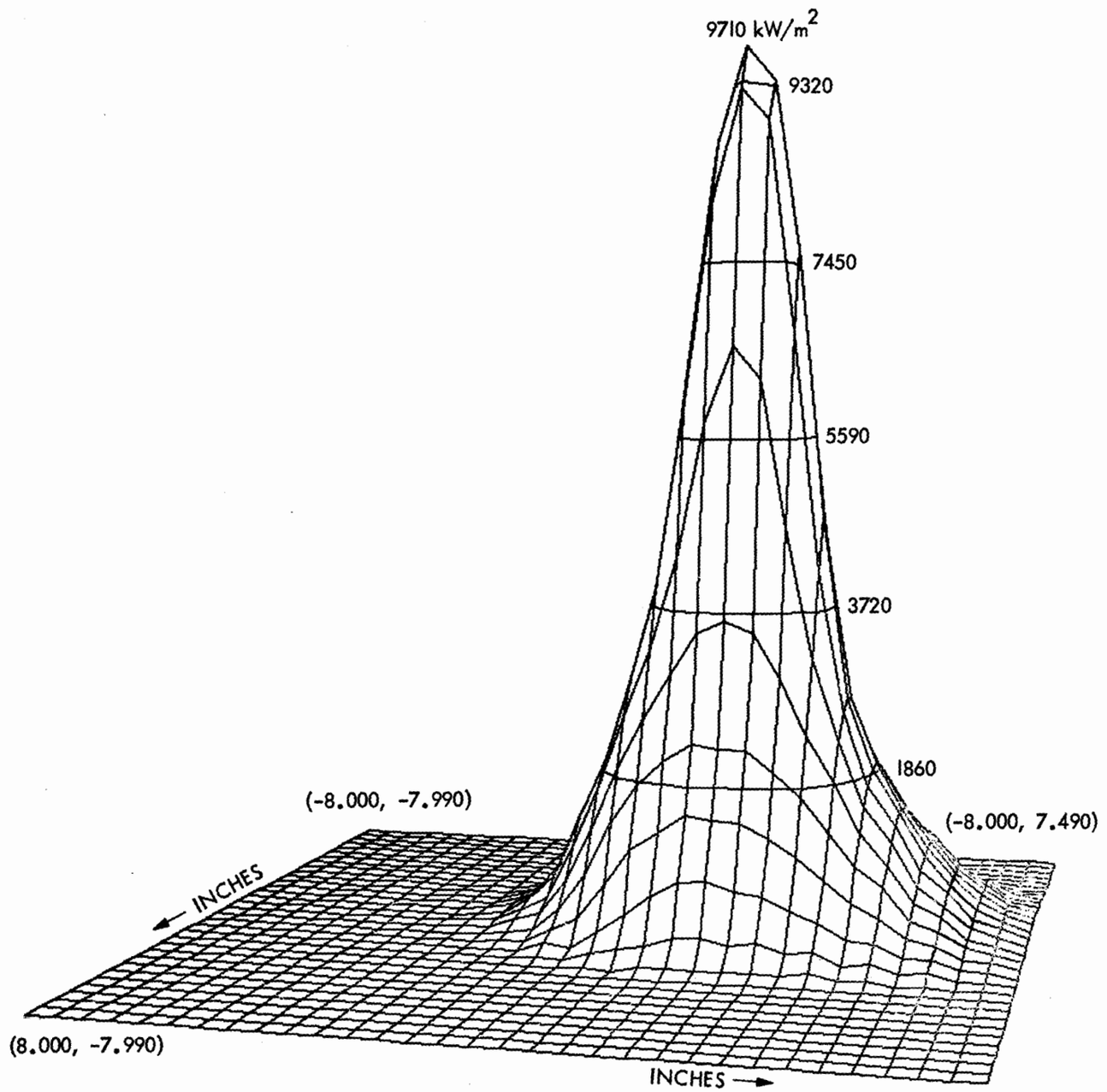

Figure 2-14. Flux Mapper Isometric Data Display

mixing of the thermal fluid. The front surface of the calorimeter is painted with 3M Velvet Black spray paint for an accurately known absorptance of 0.97.

Other than the measurement of the total reflected energy of the concentrator, the calorimeter had the capability of measuring the amount of energy passing through different sizes of concentric areas of the focal plane. A geometric computer program (SPOT) was developed to ensure proper placement of the calorimeter. The calorimeter is positioned so that all the flux passing through an aperture diameter at the focal plane is intercepted by the flat-plate heat exchanger. Convective and radiation heat losses were calculated to be less than 0.5%.

b. TBC CWCC.[3] Another calorimeter was designed and built to provide thermal power measurements of the TBCs. This was a cold-water cavity calorimeter capable of measuring up to 90 kW thermal through an aperture up to 50 cm (20 in.) in diameter. The mass flow rate is 50 gal/min with a fluid temperature rise of up to 6.7°C (12°F).

Such flow rates through the calorimeter and aperture plates are sufficiently high to maintain near ambient temperatures throughout the hardware. This minimizes error due to heat transfer with the ambient environment.

The TBC CWCC was developed to characterize the power available in and around the focal plane for several aperture sizes for point-focusing parabolic dish solar collectors. Water-cooled aperture plates screen the calorimeter cavity from solar input except for the desired aperture size.

Hardware Description. A cavity design was chosen to simulate the known and unknown optical properties of thermal conversion in the high-temperature receiver cavities to be tested on these concentrators. The CWCC is a closely packed cylindrical coil of copper tubing mounted to an aluminum shell that is attached to the concentrator's mounting ring near the focal plane as seen in Figures 2-15 and 2-16. The copper tubing is 1-in. ID with a 1/16-in. wall (1.125-in. OD) and is coiled at an inside diameter of 20.7 in. This 20.7-in. coil is left open on one end (aperture side) and a cone shaped coil of the same tubing forms part of the closed end, which is completed by a 7-in. diameter solid copper plate. The total depth of the CWCC is 28 in. from the open end to the copper plate closed end. The coil assembly is bound by four aluminum c-channels between aluminum end rings and is bolted to the outer shell through fixed nuts on the c-channels. Flow through the coil starts at the open end by way of a downcomer from the back of the CWCC shell and flows through the cavity coil and out the back or closed end.

---

[3]Computer programs used for processing these test data are described in Appendix B.

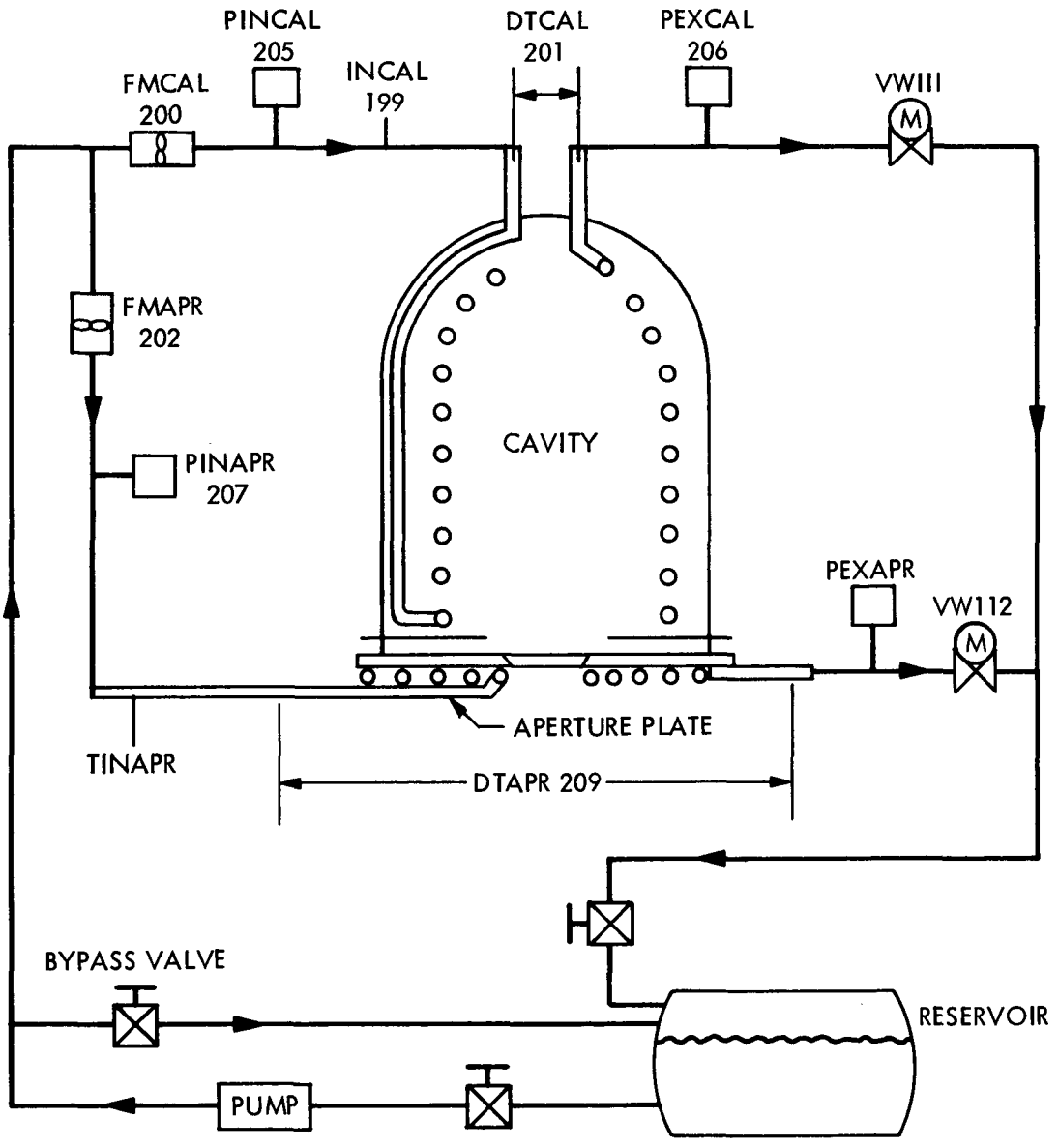

Figure 2-15. CWCC Flow Instrumentation Diagram

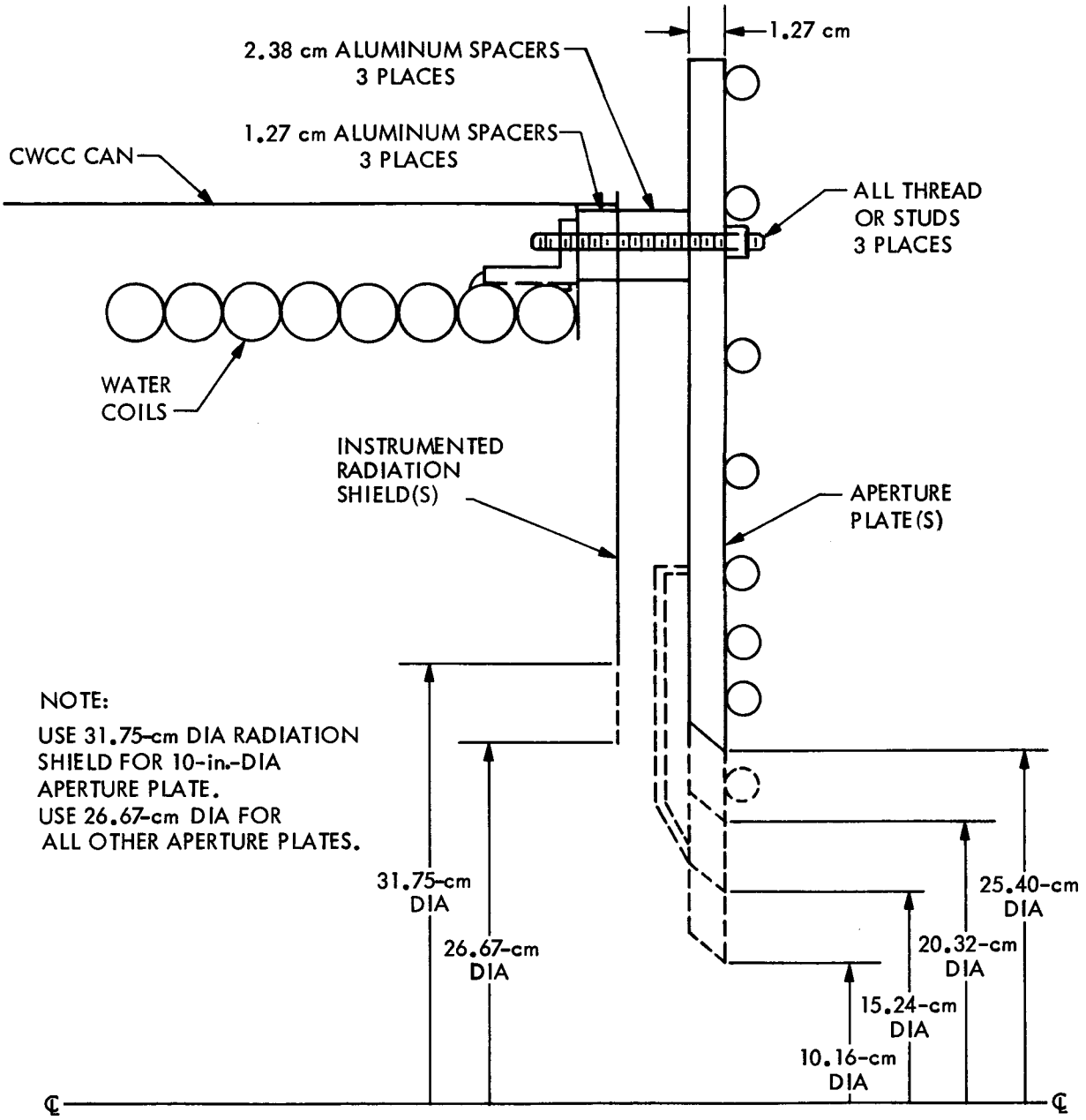

Figure 2-16. CWCC Radiation Shield and Aperture Mounting Assembly

Calibration. CWCC calibration tests were performed at the PDTS. It was concluded that the device with its associated instrumentation is accurate to within ±2.5%. Thermal input for calibration was an array of quartz-iodine light tubes and the power into them was accurately measured to better than +1%. The light power was then transferred to the CWCC, which measured from 24 to 42 kW within +2.5% of the known input. The 2.5% uncertainty is believed to come from 1% in the flow meter and 1.5% from the delta-T thermopile.

Friction Heating. When the full exposed TBC was operated at about 50 gal/min, the temperature rise of the water was about 11°F, and a static pressure drop of about 100 psi was measured as predicted from analysis. The dynamic pressure is a constant for an incompressible flow assumption. Loss of static pressure is due to friction in the flow, and this friction requires energy that heats the copper walls at start-up and heats the water when the copper comes to equilibrium in steady-flow, steady-state conditions. The friction power is energy that has been added to the water measured in temperature rise as the water flows through the CWCC heat exchanger. Heat loss or pressure drop of the fluid's potential energy is transformed via friction to thermal energy. Static pressure is measured at the inlet and outlet of the CWCC and the energy is calculated using a conversion constant and the known flow rate.

$$Q_{friction} = \Delta p \; k \; m \tag{1}$$

The net energy input in kW from the concentrator is then:

$$Q_{net} = (Q_{gross} - Q_{friction}) \tag{2}$$

Q_{net}, the net energy input measured, corresponds to the insolation level measured during the instant in which the flow and delta-T measurements are taken. The output of the concentrator is normalized to 1000 W/m^2. Thus corrected (normalized), the CWCC measurement becomes

$$Q_{net,corr} = Q_{net} * \frac{1000}{I_b} \tag{3}$$

where I_b = beam insolation intensity in W/m^2.

An Eppley radiometer (5-deg view angle) was used during the test for insolation measurements.

After the original calibration of the CWCC, it was used several times to characterize parabolic dish concentrators TBC-1, TBC-2, and PDC-1. Results of calorimetric testing of these concentrators will be examined further in the following section entitled "Characterization of Concentrators."

B. CHARACTERIZATION OF CONCENTRATORS

1. Omnium-G Concentrator Characterization Tests

JPL conducted a performance evaluation on a commercially available point-focusing solar concentrator manufactured by the Omnium-G Company of Anaheim, California. In summary, thermal power test results indicated that slightly more than 6 kW_t is available from this concentrator using a 10-cm aperture under the conditions outlined below.

Tests were conducted to determine the thermal performance of an Omnium-G Heliodyne model HTC-25S tracker/concentrator. (The concentrator is part of the OG-7500 module purchased by JPL in 1978.) The test setup is shown in Figure 2-17, and the characteristics of the system and components are listed in Table 2-3.

The system consisted of a two-axis, sun-tracking parabolic dish concentrator 6-m in diameter with a 4-m focal length. The dish structure has 18 pie-shaped elements, or petals, surfaced with anodized aluminum (Alzak).

All tests were conducted with petals that were new, clean, and in an "as received" condition. Sun-tracking was done in the manual override mode, i.e., automatic sun-tracking was not employed. Only results for the "C"-mold petals are presented.

The system checkout testing was conducted to determine an operational ready state and to establish remote control capability of the system at the PDTS.

a. Optical Tests (Reference 6). The concentrator was positioned in the azimuth and elevation axes by a null-seeking sun-tracker system consisting of a sun-sensor photocell box and tracker electronics module. The sun-sensor photocell determines the error, and the tracker electronics module controls the tracker dc drive motors. The diagram shown in Figure 2-18 illustrates the concentrator with the converter (receiver) mounted at the focal plane. A hemispherical reflectance test series was performed before the first set of concentrator petals was installed. In this test, a light source was used to illuminate a small area of a concentrator petal, and the reflected light intensity was measured. Twenty-two concentrator petals were measured at nine locations; the average reflectance was 84%.

The concentrator petals were aligned at night to assure that all reflected images were superimposed at the focal plane. Three different alignment methods were used. Figure 2-19 illustrates the method used for the "C"-type petal concentrator installation. After positioning the concentrator toward the light source, an observer viewed the reflecting surface through the wire-hoop eyepiece. Technicians then adjusted each individual petal manually until full illumination of the reflective surface was observed. The manufacturer selected the mirror elements for installation prior to delivery, and no further provision was made to refocus the petals after delivery to the test site.

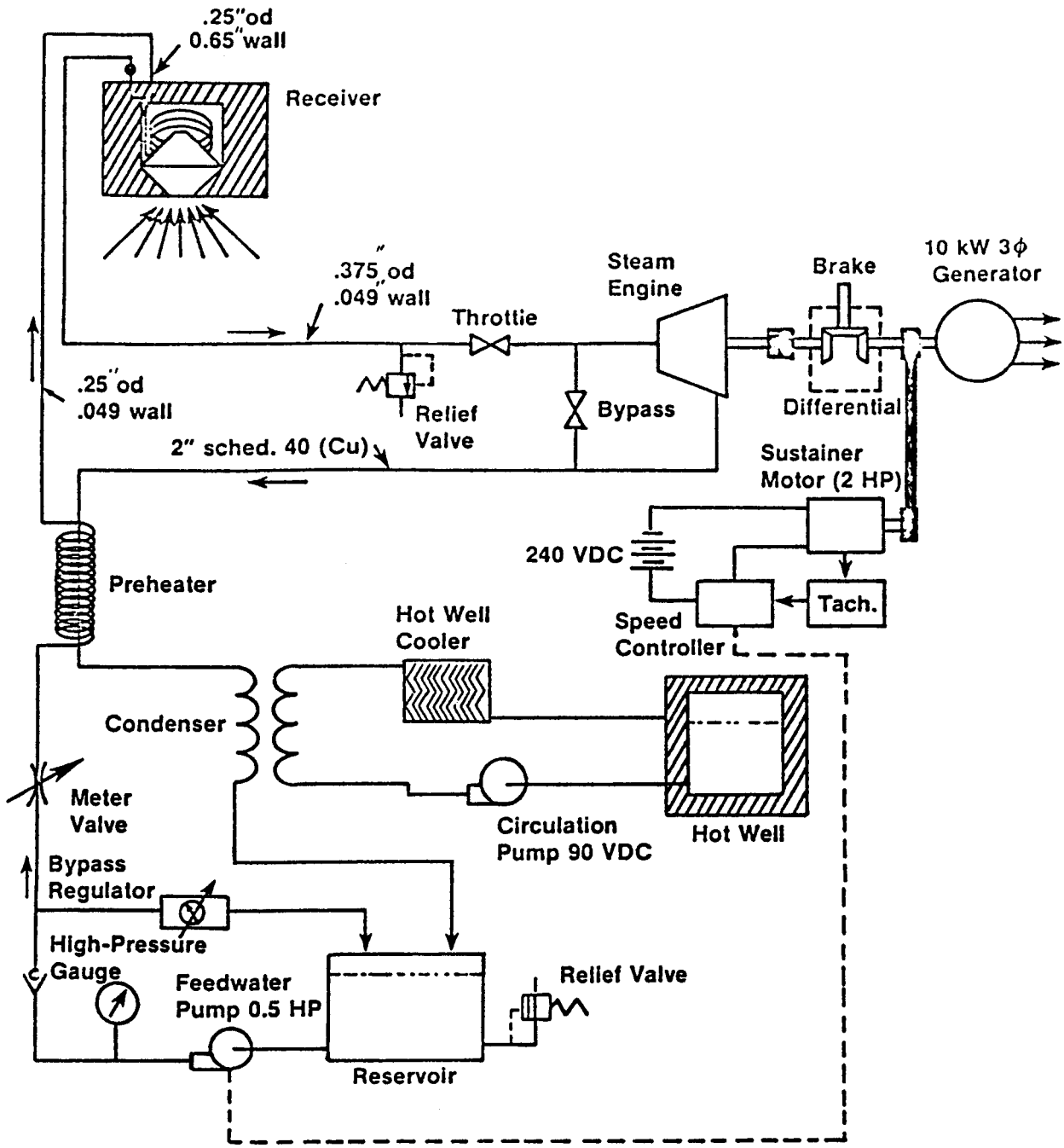

Figure 2-17. Omnium-G Electric Power Generating Loop

Table 2-3. Omnium-G Tracking Concentrator Equipment

Concentrator:

- 6-m diameter (19.7 ft)
- 18 petals (mirrors)
- 25.9 m^2 of usable reflective area
- Electro-polished aluminum mirror surface: trade name Alzac (made by Alcoa)
- Reflectivity: 81 to 85%
- 4-m focal length (13.1 ft)

Receiver:

- 34.02 kg (75 lb) of aluminum in an Inconel container
- Steam passage is through coiled stainless steel tubing embedded in the aluminum
- 20-cm (8-in.) aperture

Tracker:

- 2-axes sun tracker
- Azimuth and elevation limit switches
- 0.12-deg/s slew rate (down to up) at 24 V
- 0.45-deg/s slew rate in azimuth at 24 V
- Automotive-type batteries used
- Self-sustaining system (requires no facility power)
- JPL modification provides remote, manual tracking

Boresighting, the final alignment operation, requires the manual repositioning of the sun-sensor photocell box relative to the concentrator support structure. Repositioning assures that the aggregate group of solar images is centered on the receiver aperture. This operation, or its verification, must take place following each changeout of an experiment to compensate for mass changes at the focal-point end of the support structure.

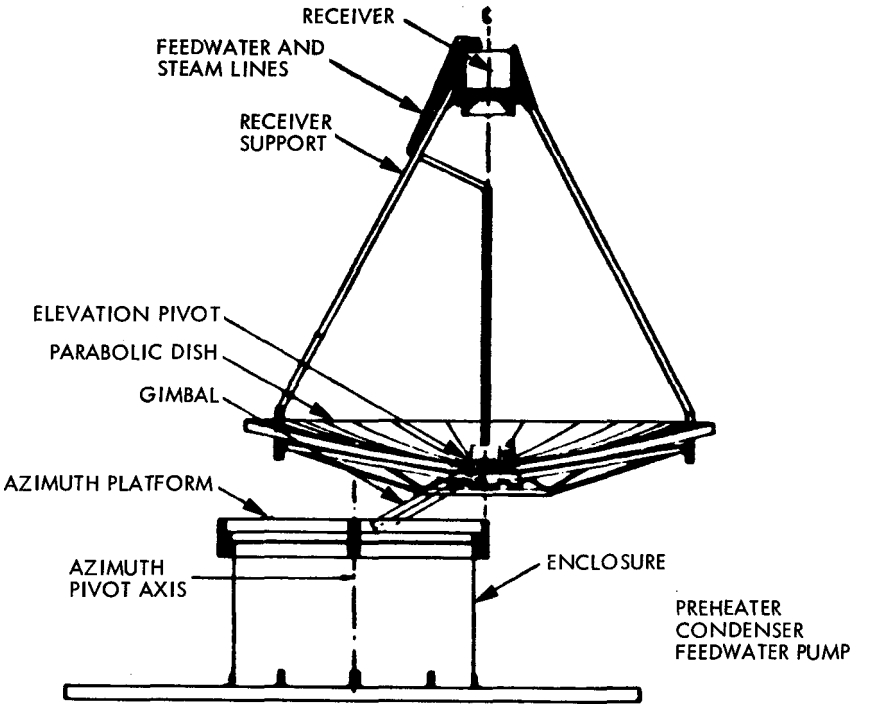

Figure 2-18. Omnium-G Heliodyne Tracking Concentrator/Collector

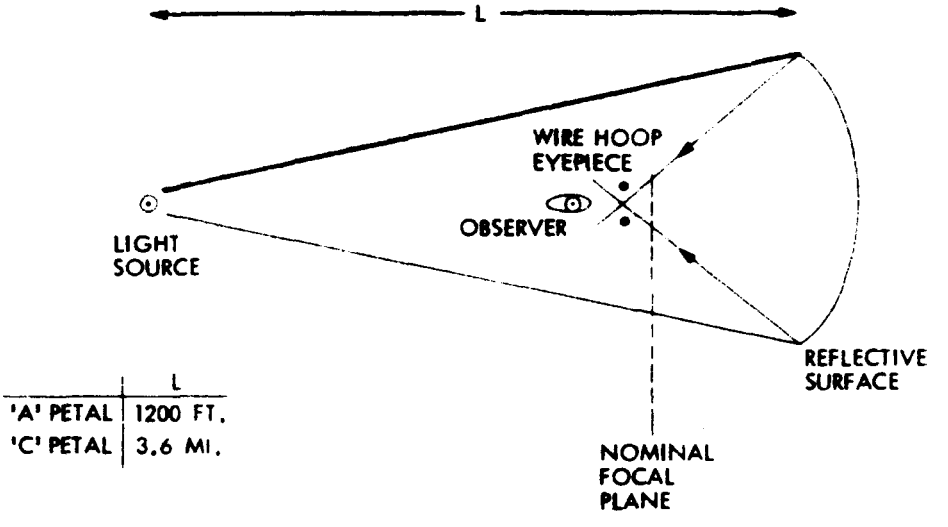

	L
'A' PETAL	1200 FT.
'C' PETAL	3.6 MI.

Figure 2-19. Nighttime Alignment Technique

b. Thermal Tests. The thermal performance output of the concentrator was determined by three different tests. The flat-plate cold-water calorimeter, the flux mapper, and the Omnium-G receiver were the devices used for testing. The flat-plate calorimeter and the flux mapper provided data as a function of aperture diameter. There was special interest in the results of the 10-cm (4-in.)-diameter aperture because it was the cavity entrance diameter for the receiver supplied by Omnium-G.

Flat-Plate Calorimeter Tests. The flat-plate calorimeter was fabricated from two 36-by-36-cm square copper plates. The plates were furnace brazed together after cooling-water passages were machined into one of them. These parallel passages were connected to inlet and outlet passages forming manifolds. The calorimeter was designed to permit a low-water temperature rise and a hot-side surface temperature of less than 38°C. The front surface of the calorimeter was painted with 3M Velvet Black spray paint providing a 0.97 solar absorptivity.

The water temperature rise across the calorimeter was controlled from 3 to 6°C by adjusting the flow rate. If the temperature rise is too low, there will be a high degree of uncertainty in the measurement results; if the temperature rise is too high, it will cause an excessive calorimeter operating temperature.

The calorimeter water flow rate was measured using a turbine-type flow meter. The absolute inlet temperature of the feedwater was measured with a thermocouple probe near the flow meter. The rise in water temperature was measured with thermocouples arranged in series (a thermopile) so that a larger output voltage for the small temperature difference could be measured. Nominal water flow rate was 28 liters/minute.

The calorimeter was mounted approximately 10 cm behind the focal plane location supplied by the Omnium-G Company. Separate aperture plates (with various size apertures) were mounted at the focal plane. These plates were fabricated from 1.9-cm-thick sheets of transite (asbestos), and had a lifetime of about two hours, sufficient to acquire test information. Aperture size (diameter) was varied in the range of approximately 8 to 18 cm.

Initial calorimetric data indicated that a problem existed in the original concentrator petals. As a result of these data, the concentrator system was realigned so that thermal performance could be improved. Some improvement was noted, but further information was required to evaluate the optical image near the focal plane.

Visual evaluation of focal length and focusing quality of each concentrator petal was accomplished by using the moon as a light source and viewing the reflected lunar image on a moveable target located at and near the focal plane. Representatives of the Omnium-G Company, present for these tests, determined that the concentrator petals were not properly focused individually or collectively. The recommendation of the manufacturer was to terminate the evaluation of the original "A"-type petals and replace them with "C"-type petals. After the concentrator petals were replaced, final alignment was performed by Omnium-G personnel.

Flux Mapper Tests. The flux-mapper was then installed, and the first thermal performance data were obtained for the "C"-type concentrator assembly. All controls for the flux mapper were programmed into a microprocessor that was also used to gather, store, and process the data acquired by the probe. Output from the processor was displayed on an X-Y plotter or line printer for real-time evaluation of concentrator focal plane shape and flux intensity.

Omnium-G Receiver Tests (Reference 6). The third device used to determine thermal performance of the concentrator was the converter (receiver) manufactured by the Omnium-G Company. This receiver, an early design, incorporated a 10-cm-diameter aperture and a steam coil buried in an aluminum block. Originally, this aluminum was to have been heated to a molten state, but the present design limits the aluminum mass temperature to 638°C (1180°F) due to the extremely corrosive action of molten aluminum on the case and heating coil.

The receiver was tested at two temperature levels: 93°C (200°C), which is a "cold" test, and at 104°C (400°F), which is a "hot" test. In the first test series, facility tap water was used and no steam was produced. The second series utilized the arrangement shown in Figure 2-20; sufficient back pressure was applied to maintain a saturated water condition at the receiver exit. Steam that formed across the expansion valve was condensed and returned to the feed-water reservoir. During this test, the receiver outlet water temperature was maintained for an hour to allow the receiver to achieve thermal equilibrium.

c. Remarks on Testing Conditions. The flat-plate calorimeter data and the flux-mapper data were obtained with new, clean petals. Some of the receiver data were obtained with petals that were dirty. In all cases, a manual override tracking mode was employed to assure a continuous on-sun condition; automatic tracking was not utilized because of occasional tracker drift.

Data were recovered continuously for each test run, but only data taken at insolation levels greater than 800 W/m^2 were analyzed. All data were normalized to a solar insolation value of 1000 W/m^2. Solar insolation data were acquired with three Kendell Mark III pyrheliometers and one Eppley pyrheliometer. Wind speed and direction also were recorded.

Omnium-G personnel were invited and encouraged to observe all tests at the PDTS. In addition, JPL furnished the Omnium-G Company with various test data and other results.

d. Thermal Performance Test Results (Reference 6). A typical flux contour plot obtained for the "C"-type petals is shown in Figure 2-21. Superimposed is a hypothetical aperture diameter of 10 cm (4 in.). The peak flux near the center of 700 $W/in.^2$ corresponds approximately to 110 W/cm^2.

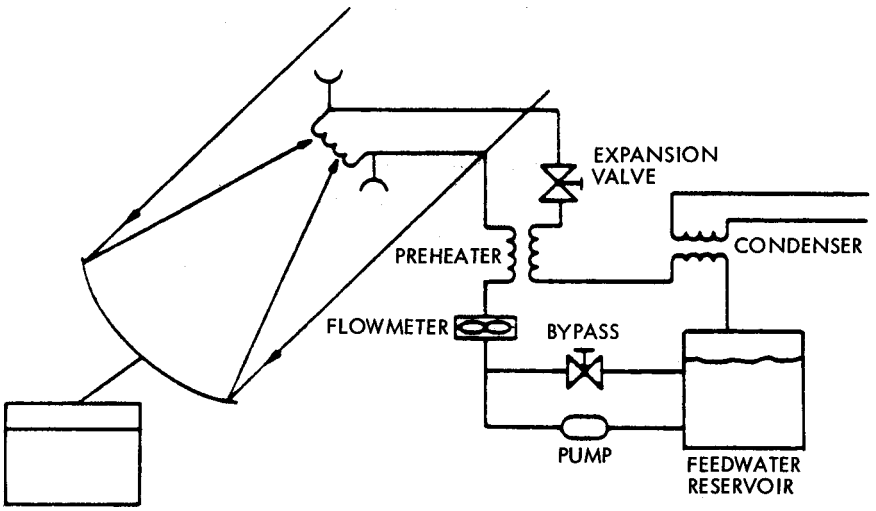

Figure 2-20. Omnium-G Receiver Thermal Performance Test Schematic Diagram

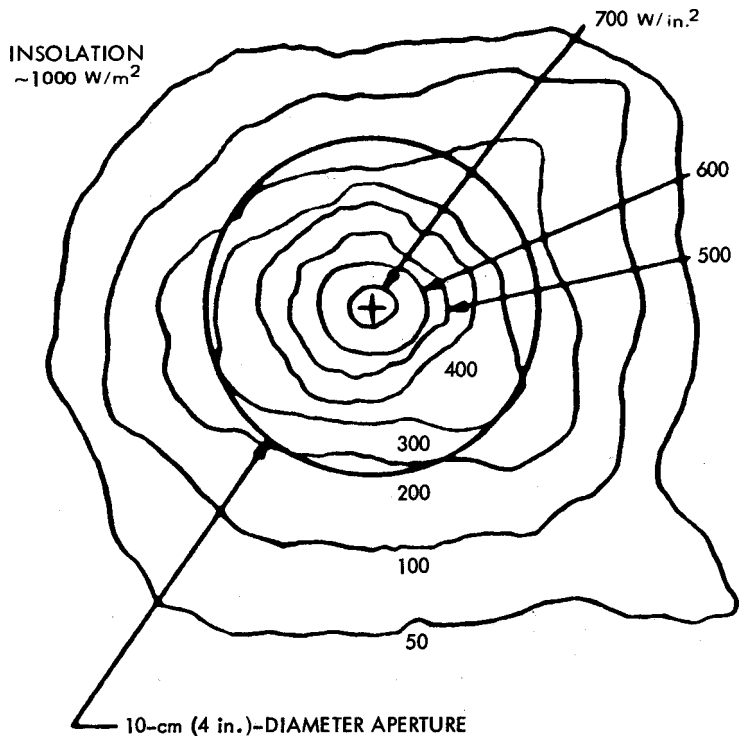

Figure 2-21. Typical Flux Map at the Omnium-G Concentrator Focal Plane

Flux-mapper data corresponding to various aperture sizes as well as flat-plate, cold-water calorimeter data are shown in Figure 2-22. Flat-plate and cold-water calorimeter data have an uncertainty of ±400 W, which is indicated by bound-bars in the figure. Agreement between flux-mapper data and calorimetric data was excellent.

Cold and hot receiver test data, shown in Figure 2-23 relative to the previous data, are represented by the cross-hatched region. Of course, the receiver test results apply only for a 10-cm aperture. The cold receiver test data agree well with the previous data.

For the cold receiver tests, the receiver outlet temperature was maintained at less than 93°C (200°F) to prevent two-phase flow. A comparison series of tests was performed during the cold-water receiver series to determine the effect of dirt and dust accumulation on the concentrator. A 16% improvement in thermal performance was obtained following a mirror cleaning operation recommended by the Omnium-G Company.

The data plotted for the hot receiver test series were obtained while the petals were dirty. Assuming the same 16% improvement could be achieved, thermal performance close to the calorimetric, flux-mapper, and cold converter data might be expected. However, the difference in the cold and hot receiver data (Figure 2-23, dirty petals) cannot be explained solely on the basis of differences in thermal reradiation.

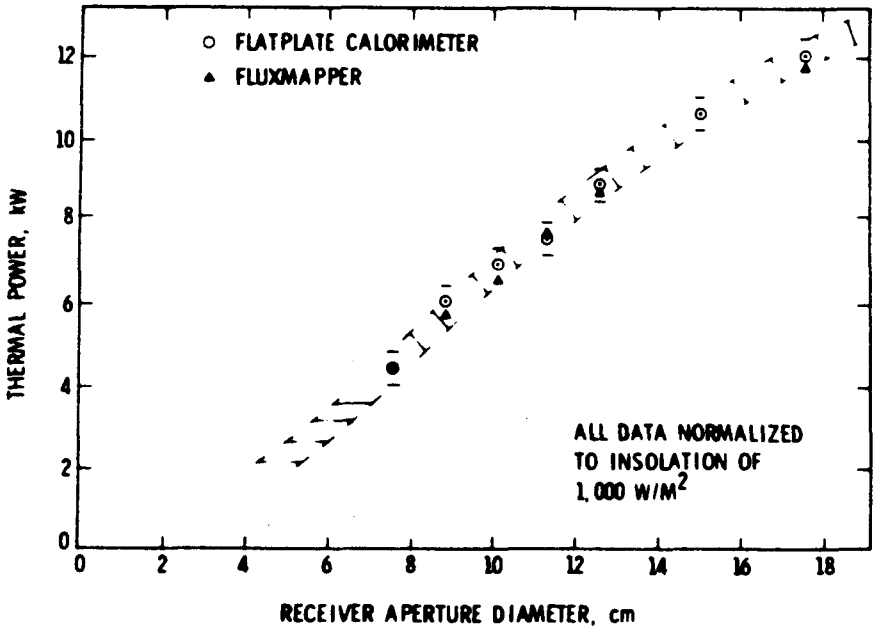

Figure 2-22. Preliminary Thermal Power Test Results for Omnium-G Collector

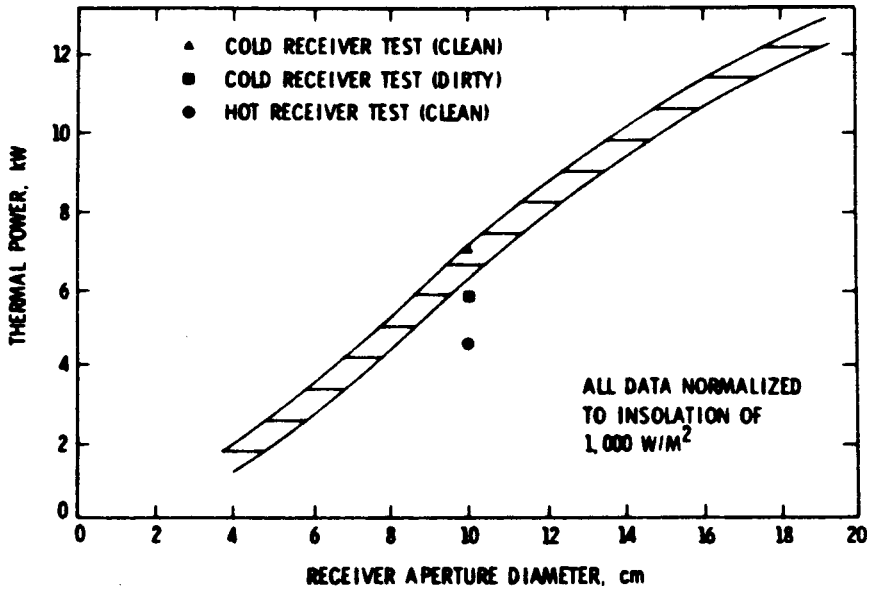

Figure 2-23. Omnium-G Receiver (Converter) Test Results

Uncertainty in data, including a statistical variation of calorimetric data of ±400 W (approximately 6% of the energy through a 10-cm-diameter aperture), has been estimated. Thermal reradiation received by the flat-plate calorimeter from the heated aperture plates was estimated to be about 420 W for an aperture plate temperature of 325°C. This effect, investigated experimentally, is expected to decrease with increasing aperture size. Estimates of thermal losses from forced convection, due to winds of the magnitude seen during test data acquisition (10 mi/h), indicate about 1 to 2% wind effect.

e. Conclusions. Thermal power test results on an Omnium-G tracking concentrator, purchased by JPL in the fall of 1978, included cold-water calorimeter and flux-mapper data and some preliminary data using the early Omnium-G receiver design. The measured thermal power was in the range of 6 to 7 kW_t for new, clean petals and a 10-cm-diameter aperture. Design changes to increase the receiver aperture diameter to 20 cm were completed by the Omnium-G Company.

f. Other Tests. In late 1979, the Southern New England Telephone Company (SNETCO) received a grant from the U.S. Department of Energy to share in funding a solar energy system at SNETCO's Bethany, Connecticut, central office. The system was to produce electricity and steam for use in the central office building. The contractor selected was Omnium-G of Anaheim,

California. During January and February of 1980, Omnium-G installed the parabolic dish system, but due to a number of technical problems, the system did not meet its performance goals. To assist in correcting this problem and to ensure that the SNETCO system was using the latest technology available, DOE requested that JPL monitor the SNETCO project.

To do this, JPL retrofitted its Omnium-G system at the PDTS to the latest system configuration. Among the improvements made to the system since the original system was installed at the PDTS over two-and-a-half years before were (1) a new solar energy converter (receiver) with high-temperature copper-zinc buffer storage in place of the original aluminum, which extends the useful operating range of the receiver upwards to over 816°C (1500°F), (2) a completely redesigned elevation drive utilizing a screw jack power system to replace the existing gear box to stabilize the dish against gusty winds, (3) an improved tracking electronics system which, in addition to being much less weather sensitive due to complete repackaging, incorporates advanced features (e.g., a new sun tracker, sensitive thermal sensing network, and electromagnetic interference resistant circuitry) to enhance reliable operation, and (4) an improved steam engine/generator "power cart" to increase efficiency during continuous operation.

Testing began in late August 1981 to prove the new tracking system and elevation drive. After a few adjustments, the system was operating reliably in a completely "hands-off" mode, i.e., no operator intervention required during a normal diurnal cycle. Thermal tests were performed in parallel to the tracking tests. Early results showed low collection efficiency ($\sim$10 kW_t). This was improved, however, by a careful refocusing of the mirror petals and adding insulation to the steam lines.

Installation of the steam engine/generator was completed early in September 1981. Early tests indicated a number of minor problems that had to be solved before electric power could be generated. These problems proved to be intractable, however, mainly due to frictional problems with the engine cylinder materials. In light of this, the dish components were shipped to SNETCO in October 1981, terminating JPL's involvement in the SNETCO OG unit testing.

It was JPL's intention to replace the new components sent to SNETCO to allow use of the JPL OG dish for thermal testing. However, Omnium-G ceased operation before these plans could be executed, and the Omnium-G system was dismantled and surplused in 1984.

2. TBC Characterization Tests (Reference 7)

Two TBCs[4] were designed, fabricated, and assembled by E-Systems, Inc., at the PDTS (see Figure 1-1). JPL retained responsibility for the optical design and mirror alignment of the TBCs. Electrospace, Inc., the

---

[4]For a more detailed description of the TBCs, see Reference 2.

control system subcontractor to E-Systems, Inc., instructed JPL test personnel in the operation, circuitry, maintenance, and troubleshooting of the control unit.

a. Control System Operational Characteristics. The final design of the TBC control system provided one axis of fast slew capability so that either the sun acquisition or emergency off-sun mode could be obtained in minimum time. The slew velocities of the two axes are 2028 deg/h (0.56 deg/s) for azimuth and 168 deg/h (0.05 deg/s) for elevation. These rates are achieved with 48 km/h (30 mi/h) wind loadings; calm day velocities are slightly higher.

The procedure for slewing on and off sun is to run the elevation axis up to the approximate elevation of the sun for the particular time of acquisition and then slew the concentrator on sun in azimuth. This prevents the sun spot from crossing the bipods or guy rods. Fiberfrax insulation material 5-cm (2-in.) thick was installed on the ring structure and over the bipod joints. The remaining upper half of the bipods and guy rods was covered with 3-mm (1/8-in.)-thick Fiberfrax.

The TBC base, or alidade, has the capability of rotating 178 deg from south due to its wheel and track design. Therefore, during maintenance or malfunction, the concentrator dish can be pointed toward the north. The dish can be moved about the elevation axis between the zenith position and the horizon or 0 to 90 deg.

The automatic sun-acquisition system is controlled by two sun sensors, one for each axis. Each of the sun sensors has a $\pm$2-deg acquisition cone angle within which the concentrators are programmed to point. Pointing within $\pm$2 deg is accomplished through a memory track system. The memory track consists of a computer memory bank device that stores ephemeris data for the day of interest. The stored data are used to point the concentrator dish to within a few hundredths of a degree of the sun.

As the sun sensor system views the edge of the sun disk, it reduces the slew velocity rate of the drive motor. This in turn makes the sun spot track across the receiver ring support structure at a very slow rate. The early slow slew speed can be changed by a keyboard input from the control unit in order to insert a time lag between the first acquired sun signal and the speed reduction in the motor. This time lag allows the sun spot to track at full speed across the ring and not slow down until it reaches the receiver.

The control unit can also be used to roughly determine the sun sensor mechanical misalignment through the use of the sensor sun presence signal (sun intensity) and the axis angle readout dial. If the sensor mechanical misalignment is 1 deg or less, it can be corrected electrically by inputting data through the keyboard.

b. Mirror Alignment. TBC mirrors (Figure 2-24) were aligned to provide the desired flux pattern and intensity at the focal plane. Light sources considered for mirror alignment were moon, sun, and an incandescent

Figure 2-24. TBC Mirror Facet

lamp. The technique chosen utilized a semi-distant incandescent light source that produced a reflected image on the focal point target. The target surface is composed of a series of concentric rings 2.54 cm (1 in.) apart. The moon was not selected because of its cyclic appearance and potential occlusion by clouds. The sun was not used because of weather and safety considerations.

Only one TBC mirror facet could be aligned at a time. Opaque plastic covers with Velcro fasteners, which could be removed and reinstalled easily, were used. The alignment of one entire concentrator (224 mirrors) took about two weeks of night work.

The light source was located at a NASA facility atop a hill 5.8 km (3.6 mi) southwest of the test site. The light was aimed toward the concentrators until maximum brightness could be observed at the TBC site, then the TBC was boresighted to it. This was done using two sets of cross hairs and two disks that were replaced by a series of disks with successively smaller apertures. The final aperture size in the two disks was 1.27 cm (0.5 in.) in diameter, resulting in a maximum pointing error within $\theta = \tan^{-1} 0.5 \div 259.8$ or 0.11 deg. The cross hairs used in conjunction with the dish apertures and the light reduced the boresighting error by half, or $\theta = 0.05$ deg. The control system position repeatability for the concentrator system was designed to be ± 0.01 deg. When it was programmed to move the concentrator to the boresighted position of the light source, a visual alignment check was performed several times by physically sighting the light source along the cross hairs and through the two disks. This verified that the image was geometrically centered at the focal plane target location.

Mirror alignment was implemented by using a three-point adjustment system. Each mirror facet is attached to the concentrator structure with three flexures. The three flexure halves bonded to the mirror facet are bolted to a matching bracket on the concentrator structure. Both halves of the joint have slotted holes to allow for adjustment or movement. One at a time, each of the 224 mirror facets was loosened at the flexure joint and adjusted to center its image on the focal target. When the image was centered, the three flexure joints were tightened in place.

Additional alignment verification checks were made periodically by removing a cover from a previously aligned mirror and reverifying its light image position. No displacement was evident in these checks. After all mirrors were aligned, the opaque target at the focal plane was replaced with a translucent target and a picture was taken of each individual mirror image. Images of center and edge mirrors are presented in Figure 2-25. All mirror covers were then removed, and the resulting image was also recorded on film. A further alignment check was made by pointing the concentrator at the moon and imaging the moon on the target; this image was also recorded on film. The moon's image was approximately 20 cm (8 in.) in diameter. This matched the predicted image size and further verified that the mirrors were aligned satisfactorily. On several occasions one edge mirror was uncovered while the concentrator was pointing at the sun.

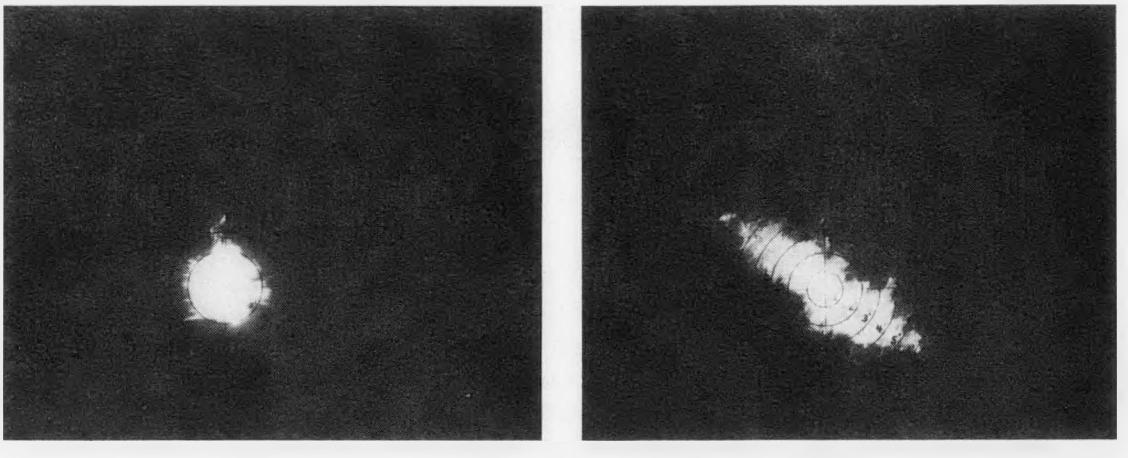

Center Edge

Figure 2-25. Mirror Alignment Images

This procedure provided increased confidence in the mirror alignment because the sun produced an elliptical image from these edge mirrors of approximately 20 cm (8 in.) maximum dimension, as determined by eye observation from the ground. The edge mirrors produced the maximum elliptical image size because they were the farthest off axis.

c. On-Sun Characterization of TBCs. The characterization process for the TBCs was conducted in discrete steps to minimize any thermal damage from the sun's image and to provide the test team with low-level solar operating experience. These steps consisted of uncovering the concentrator mirrors in five discrete groups. The process was additive in that the previously tested group of mirrors was not recovered when the next group was uncovered. A complete set of flux mapping data was recorded using a Kendall radiometer for each step in the mirror uncovering process. A set of data included a minimum of three rasters. Each raster consisted of 1056 discrete data points. For several of the mirror configurations, rasters were taken 1 in. in front of and behind the nominal focal plane and then every 2 in. along the Z direction thereafter (concentrator axis). Each raster took approximately 45 minutes to complete. If acquisition and normal operational sequence time is included, one complete raster consumed at least one and a half hours.

d. Insulation. To preclude damaging the receiver mounting structure of the TBCs during sun acquisition and deacquisition, this area was originally covered with an insulating material, Fiberfrax Hot Board, which has a melting point of 1260°C (2300°F). As more and more mirrors were uncovered, the Fiberfrax ablated rapidly on the front face of the ring. The Fiberfrax was supplemented in the high heat area with pure Zirconia held together with a Yttria binder. Although far more expensive (by an order of magnitude), it has a temperature of 2593°C (4700°F). The ablation rate of this material was much less. However, with the full 224 mirrors the rate was still a problem because the molten material was dropping on the concentrator mirrors and causing damage. An active water-cooled plate was installed in the area where the sun spot traverses the receiver ring structure. The plate was made of 1/4-in. aluminum with a single-pass water flow at a flow rate of 11 to 14 gal/min. This plate, in conjunction with the Fiberfrax used in the less critical heat areas, solved the thermal protection problem.

e. Results (Reference 8). The initial flux-mapping results indicated that the TBCs, with the initial mirror alignment where all the mirror facets were focused on the center of the target at the nominal focal plane, produced a peak flux of 1500 W/cm^2 when the insolation was normalized to 1000 W/m^2 (Figure 2-26).[5] Flux densities of this magnitude produce almost instantaneous temperatures in excess of 2760°C (5000°F), which would severely damage most passive receiver aperture materials. It should be noted from the figure that 98% of the energy is within a 20.3-cm

[5]A peak flux of 1750 W/cm^2 with an insolation of 1000 W/m^2 was obtained in other tests.

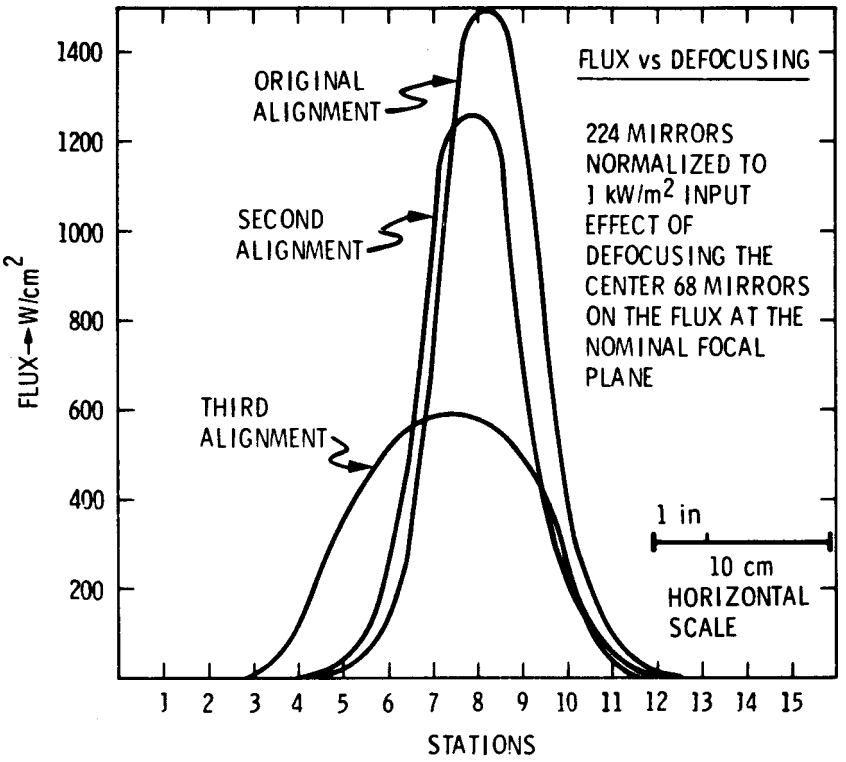

Figure 2-26. Solar Flux Measurements on TBCs, Flux versus Defocusing

(8-in.)-diameter aperture. Flux mapper results also indicated that the majority of the peak flux was being produced by the center mirror section, which totaled 68 facets. In addition to being nearly on-axis, these 68 mirror facets had focal lengths very close to their geometric nominal requirement. It was concluded that by readjusting these center mirror facets, the peak flux could be reduced, thereby reducing the possible thermal damage to the TBC structure and the receiver cavities.

During the second mirror alignment, all the images from the center 68 mirrors were centered on a 51-mm (2-in.)-diameter circle on the target at the nominal focal plane. This produced a slightly reduced peak flux of approximately 1250 W/cm^2 (Figure 2-26). This was still too high for initial testing requirements; therefore, a third mirror alignment was undertaken. The center mirrors were realigned so that their image was geometrically on the opposite side of the target as compared to their physical location on the dish. Their images were centered on a 102-mm (4-in.)-diameter circle but across the center of the target. This alignment change drastically reduced the peak flux to the 550-W/cm^2 range, but kept the total energy through the 20.3-cm (8-in.)-diameter aperture essentially constant (Figure 2-26).

After the third mirror alignment, the flux mapper was operated at several "Z" locations. The data from this test sequence indicated that the actual focal plane is closer to the dish surface than the nominal or geometric focal plane (Figure 2-27). This difference is primarily attributable to using a finite-distant light source to align the mirror facets. It is also obvious that with cross-focused mirrors, the sun's beam is highly converging/

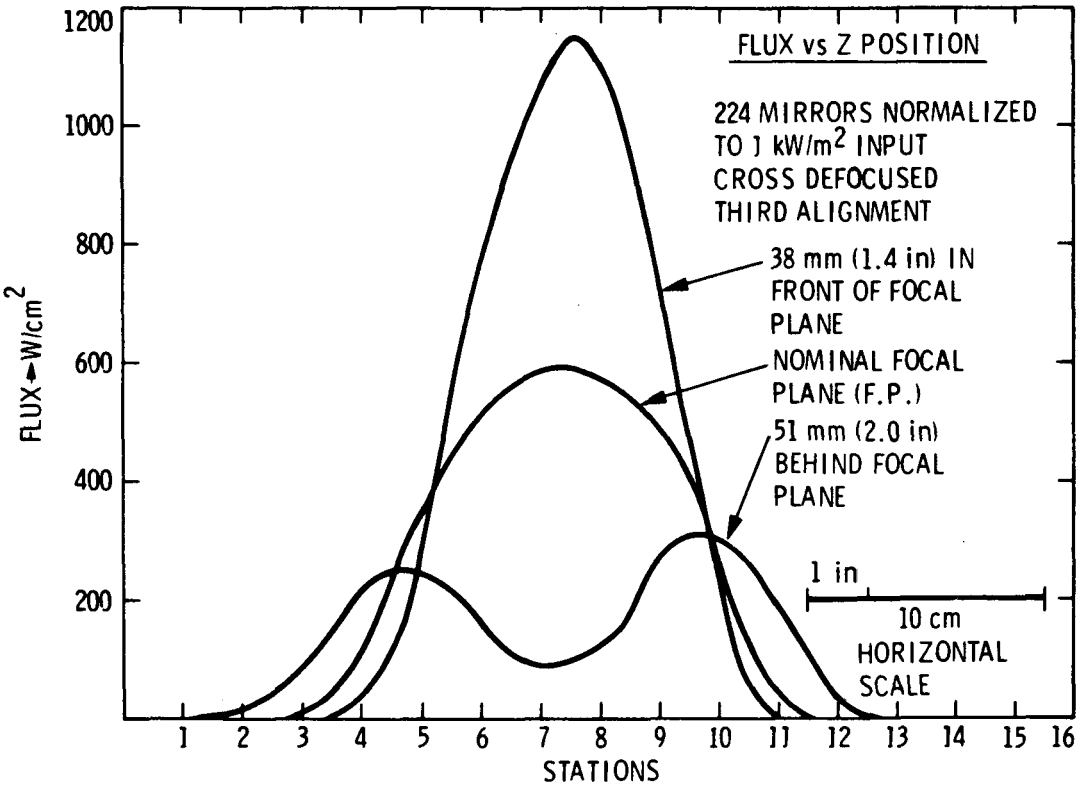

Figure 2-27. Solar Flux Measurements on TBCs for ESOR Tests, Flux versus Z Position

diverging. Currently, the technique for determining the flux on a receiver wall is to extrapolate the X-Y plane data from several Z positions of the flux mapper, plotting constant flux lines, and estimating where they will intersect a receiver. The development of a direct flux receiver wall measurement device was also evaluated. These techniques were used for ESOR testing.

The initial calorimeter results to date have established that each concentrator will produce a maximum of 82 kW_t with 1000 W/m^2 of insolation through a 56-cm (22-in.) and a 25.4-cm (10-in.)-diameter aperture. The energy measurement data from the calorimeter was measured as a function of the various aperture sizes in additional tests. The apertures ranged from the totally open sunlit end down to a 15.2-cm (6-in.)-diameter opening.

While TBC tests were run, some discrepancies were observed and further characterization tests were run. Results of these investigations are summarized below.

A series of CWCC measurements was made on TBC-1 during July and August of 1980. These measurements were made with the original receiver mounting ring and the center four mirrors in place. The Mk-III thermopile transducer was used to measure the difference between the inlet and outlet water temperature of the CWCC. Measurements were made with both dirty and freshly cleaned mirrors. It was concluded that the total thermal power into the CWCC varied between 76.0 and 81.2 kW_t, depending on the mirror cleanliness.

The second series of CWCC measurements was made on TBC-2 during July and August of 1981. The most significant instrumentation change was the use of a new temperature differential transducer using platinum sensing elements. The Eppley pyrheliometer provided inconsistent data for some of the measurements. All of the measurements were made within 8 days of mirror washing, and degradation from dust and dirt was not measured. The four center mirrors were not in place, and two mirrors may have been misaligned. It was concluded that TBC-2, with an 18-in. (25.5-cm) calorimeter aperture diameter, delivered 77.8 kW_t.

A third series of CWCC measurements was made on TBC-1 during November and December 1981. These measurements used the same instrumentation configuration that was used for the TBC-2 measurements (July and August 1981), but the Eppley pyrheliometer was consistent with the Kendall pyrheliometer. The larger organic Rankine-cycle (ORC) receiver ring was in place. The tentative conclusion of this measurement series was that the net power with a 15-in (38.1-cm) calorimeter aperture diameter is 75.7 kW_t.

The ORC mounting ring is 1.5 m^2 larger than the original TBC receiver ring. Correcting for this larger ring, the net power for TBC-1 from the 1980 measurements was reduced to 79.7 kW_t.

The reconciliation of all of these measurements was attempted during tests and analyses undertaken in 1982; i.e., algorithms for calculating the net thermal power, reexamination of the older data, and a search for the error sources. First, the algorithms used to evaluate the test data were modified. Final algorithms are presented in another report documenting the computer programs utilized at the PDTS (Reference 9).

The net and gross areas as measured are reproduced in Table 2-4. It appears that the net area uncertainty is accurate to better than 1 m^2.

During December 1981, a series of CWCC measurements of the thermal output of TBC-1 gave a final value of 75.7 kW_t (normalized) for 1 kW/m^2 insolation. During the following April, May, and June, 52 different measurements were made. The most reliable values ranged from 73.4 to 75.4 kW_t. These values appeared to be inconsistent with the calculated values of 77.6 to 79.3 kW_t (reflectance 0.92 to 0.94).

During July 1982, the temperature difference transducer was repaired by the manufacturer and given a complete recalibration at the JPL standards lab. Two sets of measurements were made in August and September. The resulting thermal output values for TBC-1 ranged from 77.5 to 78.7 kW_t. The new transducer constants account for less than 1 kW_t error in the previous measurements. The systematic errors that may result from the large field of view of the Eppley pyrheliometer have not been investigated.

It was anticipated that a series of measurements would be made during October 1982, but weather, equipment failures, and manpower limitations prevented a confirmation of these higher numbers. Until further TBC-1 measurements can be made, it is not unreasonable to use 78 kW_t as the thermal output of TBC-1, but the accuracy of this number is still in doubt.

Table 2-4. TBC Area Calculations

Item	Dimension, in.	Number	Area, in.^{2}	Area, m^2
Facets	27.75 by 23.75	220	144,993.8	93.54
Tabs	1 by 1	8 by 220	- 1,760.0	1.14
		Net Panel Area:	143,233.8	92.41
Correction: Paraboloid to Aperture (0.9595)			137,432.8	88.67
Rods	168 by 1	8	- 1,344.0	0.87
Pods	168 by 6	2	- 2,016.0	1.30
Open Shutter Plate	20 by 24	1	- 480.0	0.31
ORC Ring OD (71.25)	Less 4 panels	1	- 1,299.1	0.84
Junction Box	16 by 16	1	- 256.0	0.17
Speckles, etc.	36 by 36	1	- 1,296.0	0.84
		Net Area:	130,741.7	84.35

CWCC measurements of the thermal power in the TBC-2 focal plane were made on January 10, 11, and 12, 1983. The aperture plane was -11 in. from the reference mounting plane (measured toward the vertex from the receiver mounting pads on the sun side). This is the focal plane for the Stirling receiver aperture. Flux mapper data are also available for this focal plane. The TBC-2 mirrors were washed January 7. Table 2-5 summarizes the data from January 11 and 12 and includes the aperture diameter, the measured power (normalized to 1 kW/m^2), the intercept factor derived from the flux-mapper data, and the measured power divided by the intercept factor.

The January 10 data were not included because of sun tracker problems and large discrepancies in the insolation values. The tabulated data could be in error by as much as 2% because of uncertainties in the insolation values.

The insolation uncertainties are not the result of dirty windows, tracking errors, or calibration errors. The measured power values may be lower than anticipated because of shadowing due to the focal plane equipment and tie rod interference with the reflected light near the focal plane.

3. PDC-1 Characterization[6]

The 12-m-diameter parabolic dish concentrator planned for use with the Small Community Solar Thermal Power Experiment was developed by the

[6]For further details on the development and testing of PDC-1, see Reference 10.

Table 2-5. CWCC Test Results Summary

Aperture, in.	Measured Power (MP), kW_t	Intercept Factor (IF)	MP/IF, kW_t
20.5	76.2	1.000	76.2
8	75.2	0.994	75.6
6	71.8	0.945	76.0

General Electric Company and Ford Aerospace and Communications Corporation for JPL. The PDC-1 unit features a plastic reflector bonded to glass-reinforced plastic sandwich gores. An elevation-over-azimuth mount fabricated of structural steel and thin-walled tubing is driven by a cable and drum arrangement powered by a pair of variable speed motors. The PDC-1 unit is shown in Figure 2-28.

The optical properties of PDC-1, when first measured, were poorer than expected. The panels were attached to the ribs after the rework of the mounting system in temperatures of up to 40°C (108°F). The shrinkage of the panels relative to the steel ribs in cooler weather, combined with the gravity sag when the panels were installed face down, resulted in the panels' being flattened circumferentially between the ribs. The result was a broadening of the reflected beam. The dish was taken down from the base frame, and the panels were removed and reinstalled. The bolt holes were redrilled while the panels were constrained in the proper parabolic contour between the ribs in a target temperature range of 10 to 15.6°C (50 to 60°F). A dial indicator tool was used for positioning the panel contour. These efforts resulted in a three-fold reduction in the focal spot diameter.

The approach to optical performance measurement by JPL was to use a test configuration in which a perfect reflecting panel would form a point image from a point source of light. For a spherical surface, this configuration occurs with the source and image at the center curvature of the mirror. This method was successfully used for testing the JPL test bed concentrator mirrors. Parabolic surfaces only satisfy the ideal configuration requirement when the source is on the optical axis at infinity and the image is in the nominal focal plane. In practice, the source can be finite in size and the distance close enough for practical measurement.

For example, a perfect paraboloid with PDC-1 dimensions will form an image with a maximum diameter of 4.12 cm (1.6 in.) from a source of 32 cm (12.6 in.) diameter at a distance of 400 m (1310 ft) in a focal plane that is displaced 13 cm (5.1 in.) from the nominal focal plane. This test setup gives comparable results to those obtained if a point source at infinity were used.

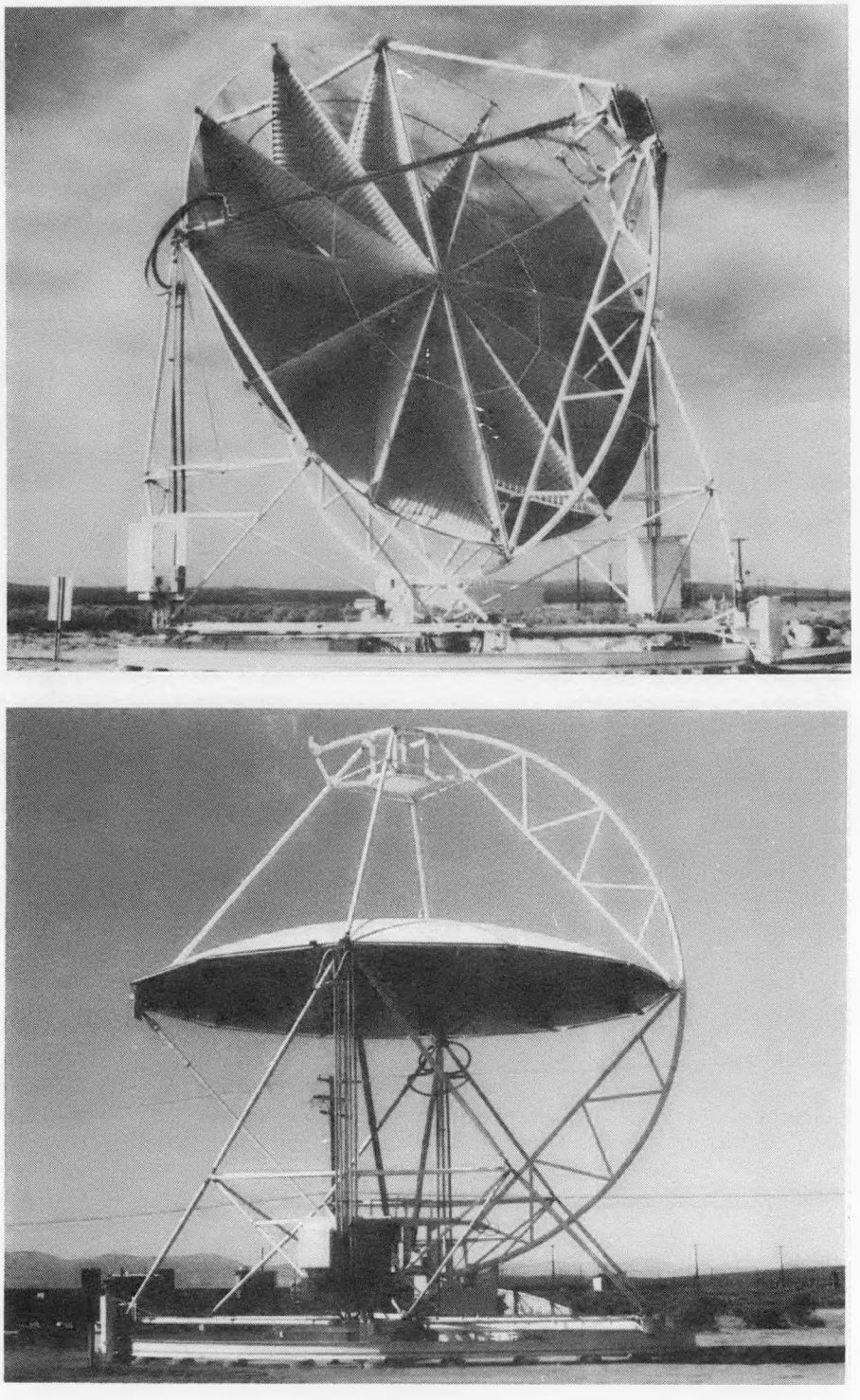

Figure 2-28. Complete PDC-1 Unit (above); PDC-1 in Stowed Position (below)

The point-source configuration was chosen because it provided unambiguous data about the reflecting surfaces. With point-source data it is possible to predict, with acceptable accuracy, the intensity distribution of a concentrator when it is pointed at the sun. However, the image formed from an extended source, such as the sun, cannot be easily used to determine the point-source image intensity distribution.

The measured data were reduced to a mathematical expression based on two Gaussian distribution terms. These equations represent the measured data with a root mean square (RMS) error of less than 1%. These distribution terms are the intercept factor distribution and the fraction of the focal plane power that passes through any specified receiver aperture.

a. Measurements (Reference 10). The first measurements of PDC-1 optical performance were made in the JPL 25-ft space simulator during the summer of 1981 because it was believed that the simulator would produce a collimated beam of light over one full concentrator gore (a 30-deg segment of the concentrator consisting of three panels). The tests were performed on the first-article prototype panels manufactured by Design Evolution 4 (DE-4) under a subcontract to the General Electric Company. During the Spring of 1982, DE-4 manufactured the PDC-1 panels and shipped them to JPL for testing.

PDC-1 testing started during the early Fall of 1982. The direct images were photographed through a telescope located at the vertex of the concentrator. The same telescope was used with a photo-detector to measure the intercept factor distribution. The aperture masks were white, and the photocell measured the amount of light that did not pass through the aperture. This technique was used because the large rim angle (52 deg) of the concentrator precluded the possibility of using any practical optical system behind the focal plane.

The unexpectedly large size of the focal plane image necessitated the use of a diagnostic technique to determine the source of the image errors. Because the optical panels had shown good imaging characteristics during the earlier tests, it appeared that the source of the problem must be the concentrator structure or the method of panel installation. The large rim angle also eliminated the possibility of any practical diagnostic optical system behind the focal plane. The most successful technique was to view a target of colored patterns mounted at the focal plane (Figure 2-29) from a distance of 600 to 900 m (2000 to 3000 ft) through a small telescope. Pictures were also taken through this telescope. The observed color of each part of the reflecting panels indicated the area on the target that would be illuminated by a distant point source reflected from the panels.

The diagnostic pictures (see Figure 2-30) demonstrated that the panels were distorted by excessive tension, that this tension could be removed, and that the image quality of the concentrator was substantially improved by reinstalling the panels. These pictures also indicated that the basic concentrator structure is very rigid and shows no significant deformation by gravity. This diagnostic procedure also demonstrated that the concentrator was less temperature-sensitive after the panels were reinstalled.

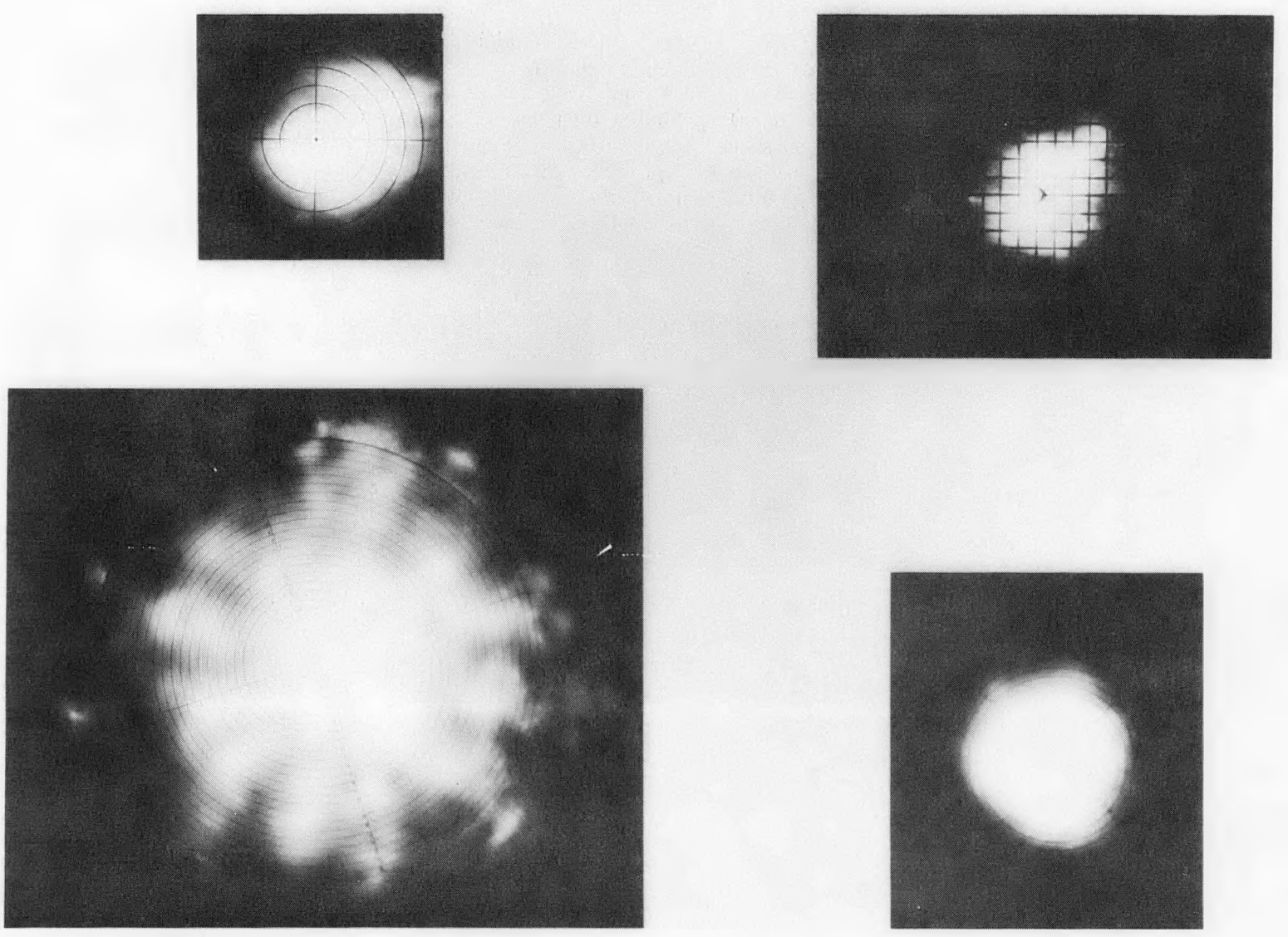

Figure 2-29. Direct Images of a Point-Source Formed by the PDC-1 Paraboloidal Reflecting Panels. The upper left image is from the prototype panels; the upper right image is from the production panels. The lower images are from the assembled concentrator before (left) and after (right) reinstallation of the panels.

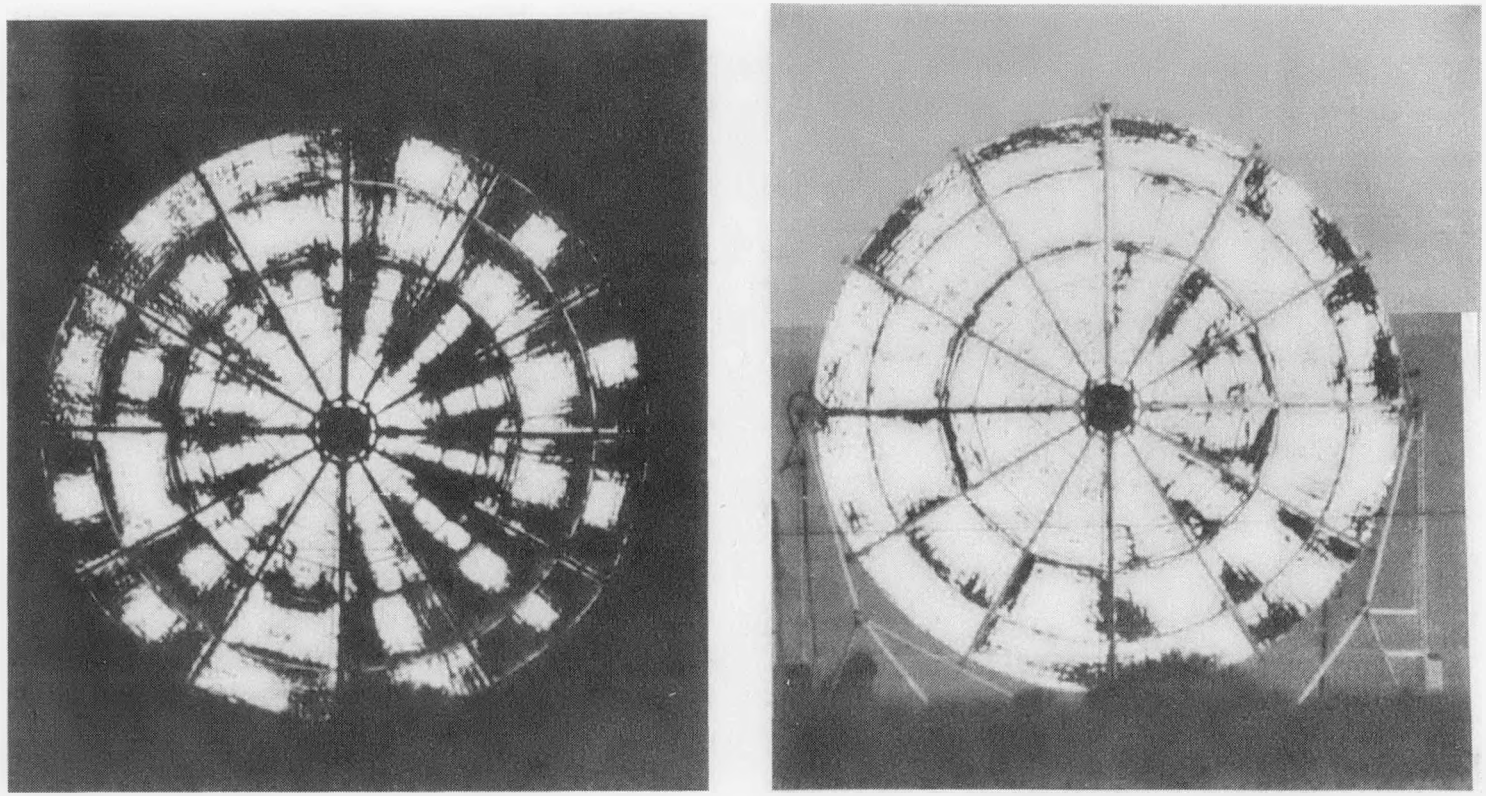

Figure 2-30. Diagnostic Photographs Taken of the Assembled Concentrator. The left image is at an ambient temperature of 1.67°C (35°F) and the right image at 18.3°C (65°F). The white areas indicate regions of the reflecting panels forming an image smaller than 15 cm (6 in.) in diameter. The dark areas indicate panel areas forming images up to 38 cm (15 in.) in diameter from the colored parts of the focal plane target.

b. Conclusion. The final concentrator performance evaluation should come from cold-water cavity calorimeter measurements. However, the point-source optical testing techniques have proven effective for determining the performance characteristics of a solar concentrator during initial development and production as well as being a valuable tool for diagnosing optical problems. The diagnostic pictures and the intercept factor distribution (Figure 2-31) indicated that PDC-1 would give satisfactory performance with the organic Rankine-cycle power conversion unit. Future improvements in the panel construction and installation techniques may permit the use of this concentrator with higher temperature power conversion systems.

C. TESTING OF SOLAR COMPONENTS

1. Testing of 85-kW_t Steam Rankine Solar Receiver[7]

The Garrett AiResearch Manufacturing Company of California, under contract to JPL, manufactured a prototype steam Rankine solar receiver (SRSR). The SRSR was sized for a steam/electric application with provisions for dual-mode operation (with or without reheat) and is adaptable to industrial process steam applications.

The design conditions for both applications are summarized in Table 2-6. The peak input is 85 kW_t, and the receiver must accept irregularities in solar flux input caused by mirror slope errors, reduced power (10%) from one-half of the concentrator, and an asymmetric flux profile resulting from a $\pm$2.54-cm (1.0-in.) offset of the receiver axis from the optical axis.

a. Description of the SRSR (Reference 11). A cutaway drawing of the SRSR is shown in Figure 2-32. The SRSR is a once-through monotube boiler designed for steam/electric and process steam applications at pressures up to 17.24 MPa (2500 psia) and temperatures up to 704°C (1300°F).

The major components are the outer shell assembly, 15.2 cm (6 in.) of Cerablanket insulation, an Inconel 625 tube-coil heat exchanger assembly, a rear plate that can be moved axially 7.6 cm (3 in.), and an aperture assembly that can be adjusted from 20.3 to 25.4 cm (8 to 10 in.). The rear plate and aperture assembly were made of NC405 silicon carbide, but, as a result of test experience, it was changed to a rear plate of chromium nickel steel (RA 330) although an aperture assembly of graphite is recommended. The unit is 76.2 cm (30.0 in.) in diameter and 95.8 cm (37.7 in.) in length; it weighs 220 kg (485 lb). Its heat transfer surface, which is 45.7 cm (18 in.) in diameter by 57 cm (22.4 in.) long, is an Inconel 625, cylindrical, tube-coil assembly composed of primary and reheat sections.

---

[7]Computer programs used for processing these test data are described in Appendix B.

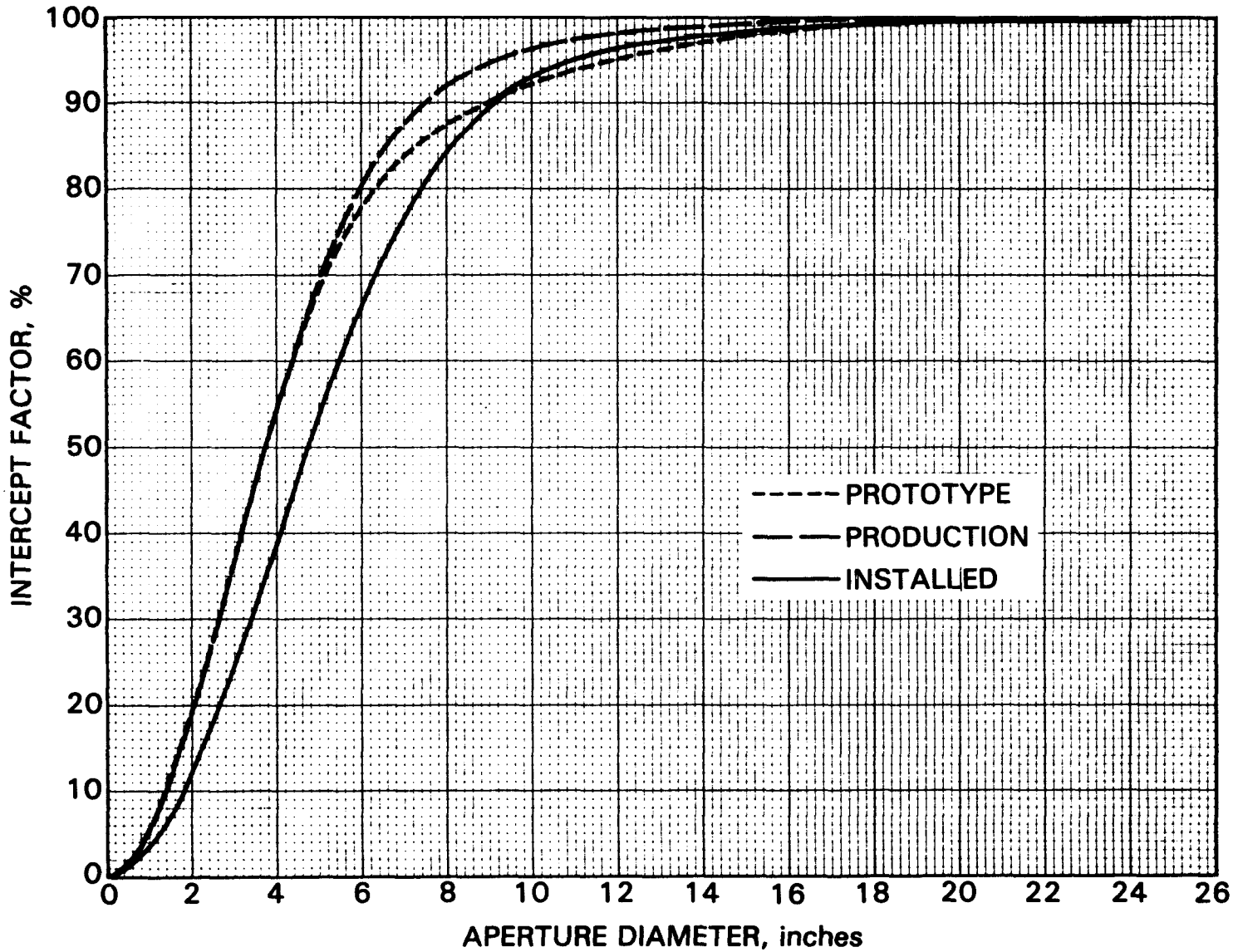

Figure 2-31. The Intercept Factor Distribution Curves from the Prototype, Production, and Assembled Concentrator (After Reinstallation)

Table 2-6. SRSR Design Conditions
(Peak Power Input: 85 kW_t)

	Process Steam (up to)	Steam/ Electric
Primary Section:		
Inlet feedwater temperature, °C (°F)	149 (300)	93 to 149 (200 to 300)
Outlet steam		
Temperature, °C (°F)	704 (1300)	704 (1300)
Pressure, MPa (psia)	17.24 (2500)	17.24 (2500)
Reheat Section:		
Outlet steam temperature, °C (°F)	704 (1300)	704 (1300)
Inlet steam		
Temperature, °C (°F)	704 (1300)	343 (650)
Pressure, MPa (psia)	17.24 (2500)	
Flow rate:	Determine from energy balance; same in both sections	
Pressure drop:	$\Delta P/P$ = 10%	

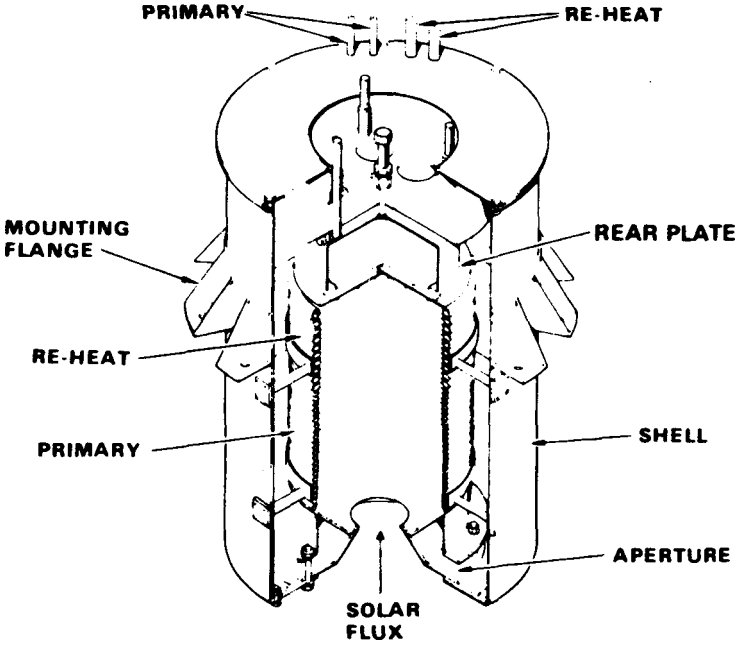

Figure 2-32. Steam Rankine Solar Receiver (Cutaway)

The active heat transfer portion consists of 34 turns of 11.11-mm OD (outer diameter) by 1.728-mm wall (7/16 by 0.070 in.) primary section tubing and 10 turns of 19.05-mm OD by 3.05-mm wall (3/4 by 0.120 in.) reheat section tubing. An additional turn of tubing at the ends of each section allows for thermal contraction and expansion of the assembly, and straight runs of tubing are used to route the water or steam to and from the coil. The inner surface of the coil is oxide-coated to produce a surface emissivity of about 0.8. Each section is a rigid, brazed unit, and the two sections are held together by three hinge-type joints. Eight radial post-type supports welded to the coil are used to attach the assembly to the outer case. These supports allow for radial and axial thermal expansion or contraction while preventing rigid body movement of the coil. The entire assembly is mounted to the concentrator boom structures so that the center of the receiver aperture is located at the focal point. The two coil sections can be connected in series for operation in primary mode only, or in parallel for operation in the primary plus reheat mode. In the latter case, the primary and reheat outlets are adjacent to each other.

b. Testing at Parabolic Dish Test Site. Preliminary testing was started at the PDTS in September 1980 using TBC-1, which has a total concentrated solar power output capability of 80 kW_t for an insolation level of 1000 W/m^2 (317 $Btu/hr\text{-}ft^2$).

The steam receiver was mounted on the TBC assembly ring, and water lines were hooked up as shown in Figures 2-33 and 2-34. Water pumping, storage, and GN_2 supply loops serving the needs of both TBCs are illustrated in Figure 2-35. The SRSR was instrumented to measure temperature distribution inside the cavity and across the insulation as seen in Figure 2-36. Specifications of the instrumentation are given in Table 2-7.

Initial testing was done with water heating at 25 and 50% mirrors at low pressures (about 1.1 MPa or 160 psia) and low temperatures (about 150°C or 300°F). The second series of tests was conducted at medium pressures and temperatures (about 4.8 MPa or 700 psia and 288°C or 500°F) using 50, 75, and 100% mirrors. Exploratory high-temperature, high-pressure tests have also been run. In all runs, the primary and reheat sections of the coil were connected in series. Also, for procurement reasons, originally selected material was changed to type 321 stainless steel, and the primary section tubing size was increased to 12.7-mm OD by 2.41-mm wall (1/2 by 0.095 in.), and the number of turns was reduced to 30.

The tests of the receiver indicated good thermal and flow performance. No major instabilities were detected, but some modifications to the receiver were required. The ceramic end plate and aperture cone were severely damaged (shattered) by solar heating during early tests. An end plate of RA 330 nickel chromium steel and a water-cooled aluminum aperture assembly were needed to continue testing.

Typical test results obtained by JPL during the exploratory high-temperature testing on October 17, 1980, is shown in Figure 2-37. This is a graph of the backside and heated-side tube-wall temperature versus axial distance along the coil. Also, the water inlet and steam outlet temperatures

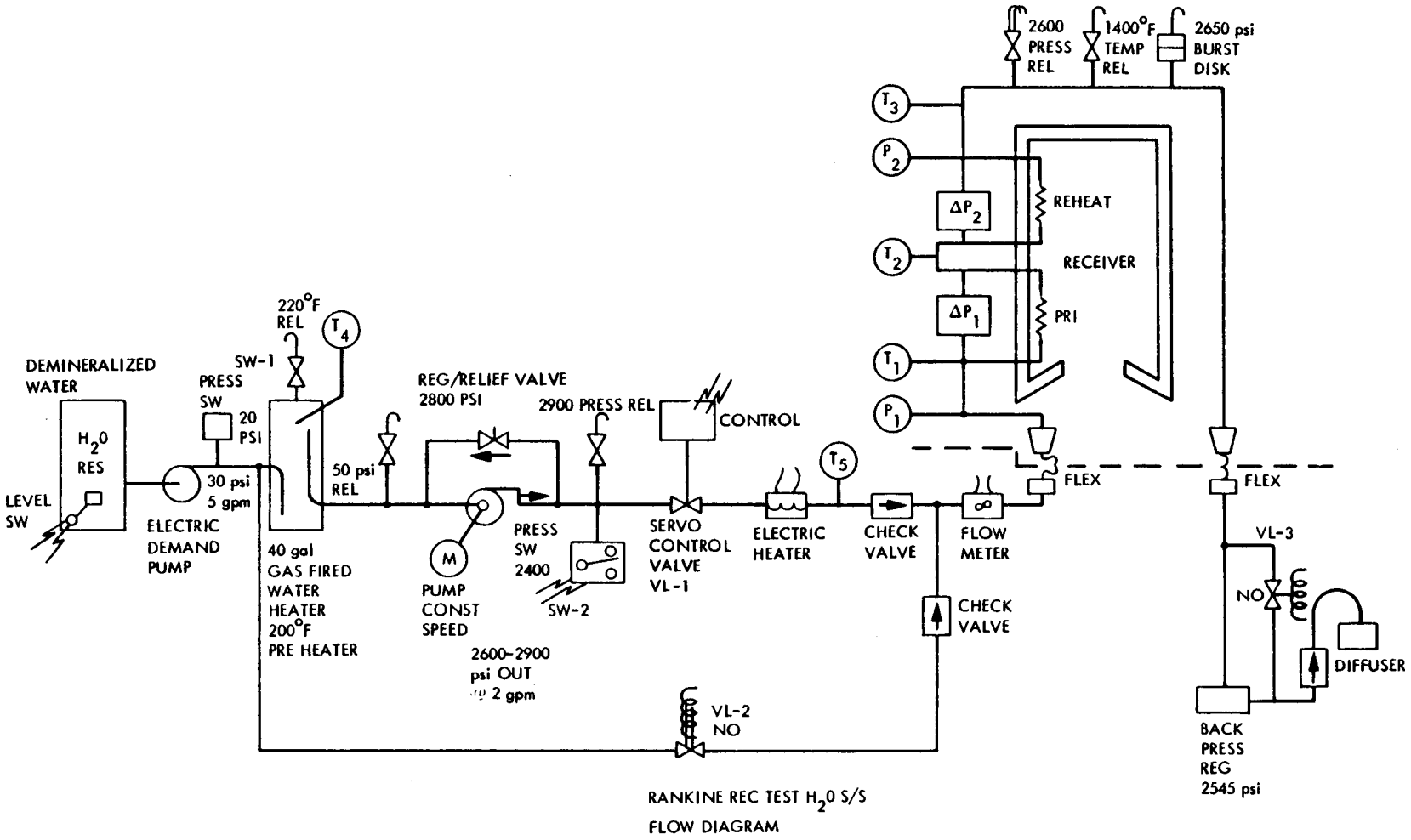

Figure 2-33. Performance Test Setup for SRSR. (Set for All-Primary Flow Configuration.)

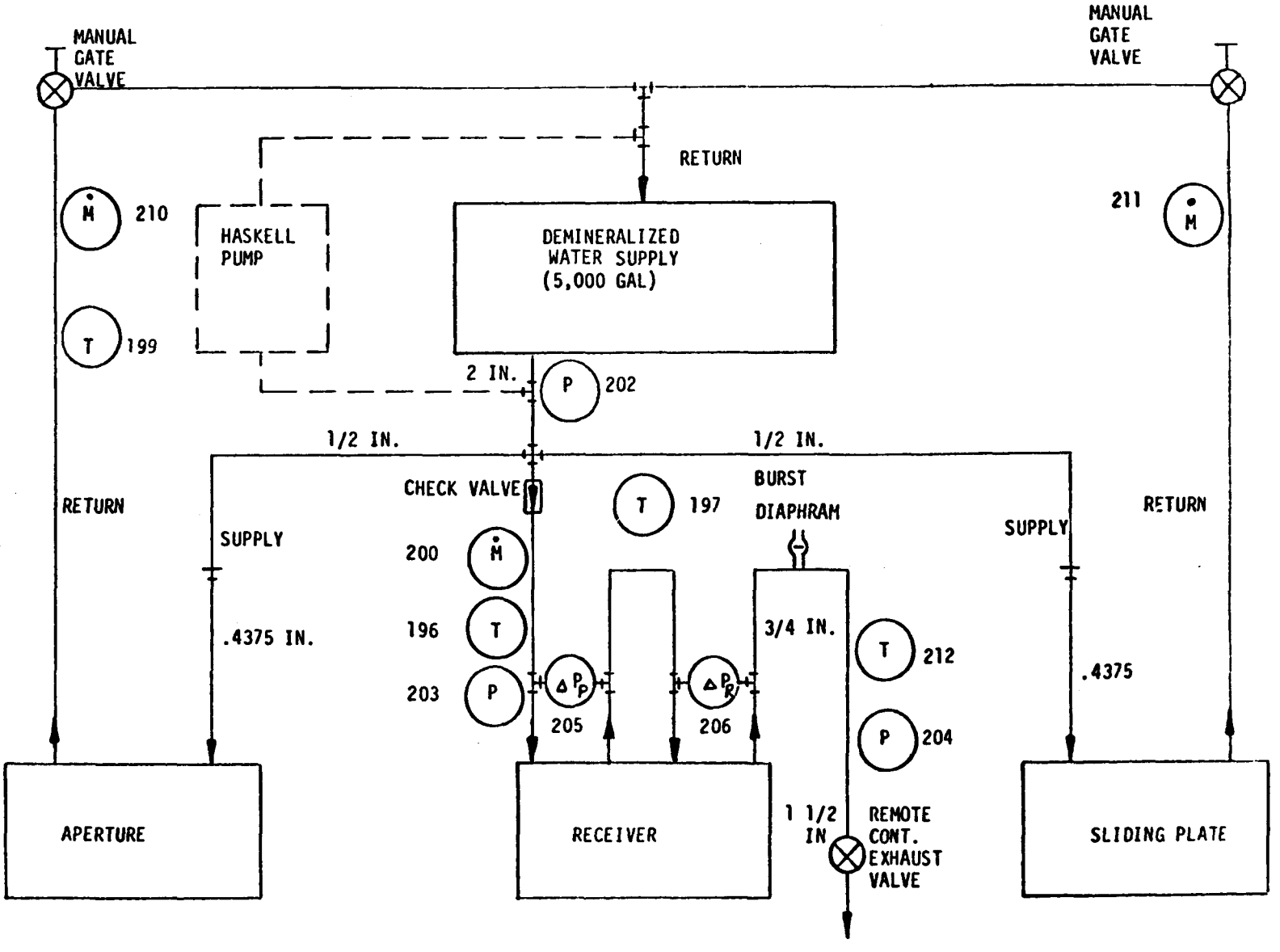

Figure 2-34. Line Diagram for SRSR Test Setup

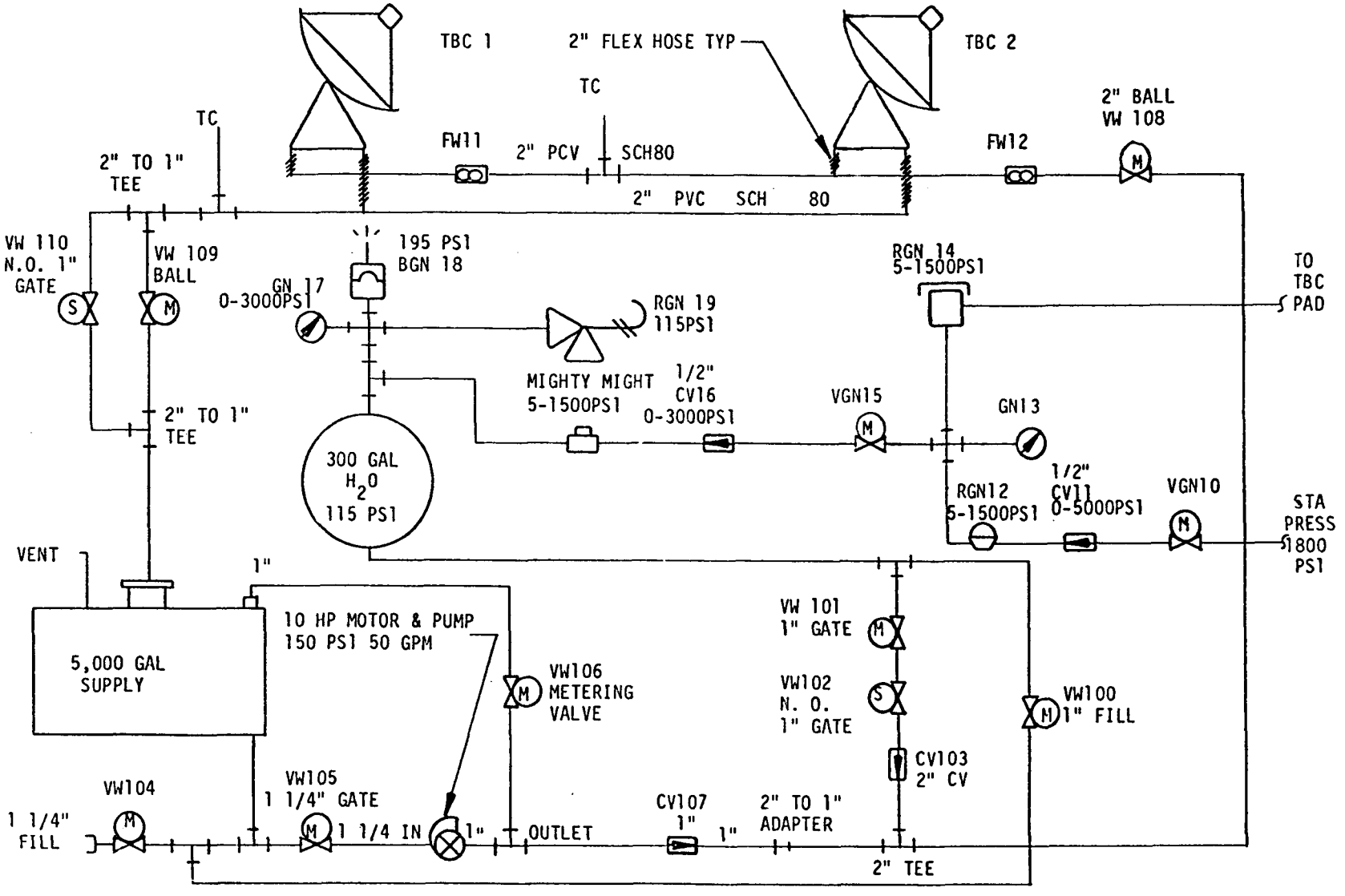

Figure 2-35. Water Pumping, Storage, and GN_2 Supply for SRSR Testing

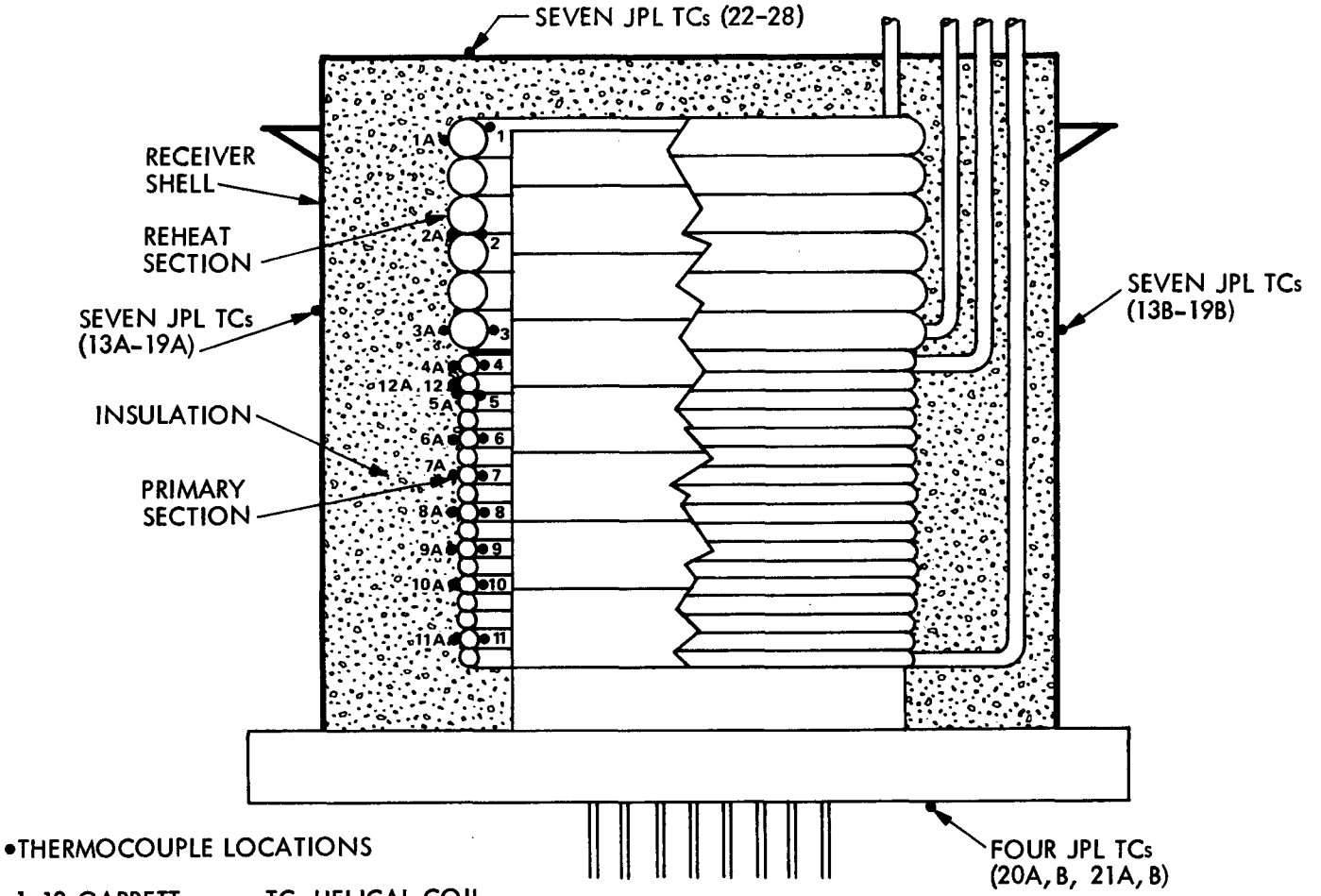

•THERMOCOUPLE LOCATIONS

1-12 GARRETT	TCs HELICAL COIL
1A - 12A JPL	TCs HELICAL COIL
13A-19A JPL	TCs OUTSIDE CASE
13B-19B JPL	TCs OUTSIDE CASE
20A,21A JPL	TCs APERTURE COVER
20B,21B JPL	TCs APERTURE COVER
22-28 JPL	TCs REAR CASE

Figure 2-36. SRSR Thermocouple Positions

Table 2-7. SRSR Instrumentation Specifications

Parameter	Approximate Test Range	Required Measurement Accuracy	Recommended Instrument Type
Water inlet pressure	100 to 700 psi	±1% reading	0 to 1000 psi pressure gauge accuracy: ±9.5% full scale
Water & steam inlet & outlet temperatures	70 to 650°F	±10°F	Chromel-Alumel thermocouples & direct-reading potentiometer
Water flow	0 to 5 gal/min	±3% reading	Turbine-type flowmeter
Water/steam pressure drop	0 to 20 psig	±1% reading	0 to 30 psid differential pressure gauge accuracy ±0.1 in. H_2O
Tube wall temperature	70 to 1400°F	±25°F	Chromel-Alumel thermocouple and direct reading potentiometer
Housing outside temperature	ambient to 500°F	±10°F	Chromel-Alumel thermocouple and direct reading potentiometer

are identified. The backside or unheated tube-wall temperature profile is as predicted, but the heated-side temperature profile shows a very high peak at the beginning of the boiling region. This may be due to a thermocouple error or to excessive local incident solar heat flux.

Interpretation of the test data is documented in Reference 12.

2. Air Brayton Solar Receiver Testing[8]

In June 1979, the Garrett AiResearch Manufacturing Company received a contract from JPL for the development of a metallic air Brayton solar receiver (ABSR). The ABSR is designed to receive 85-kW thermal energy at the focal plane of a parabolic dish concentrator and transfer that energy into the fluid stream of an open, regenerated, Brayton-cycle system (Reference 13).

[8]Computer programs used for processing these test data are described in Appendix B.

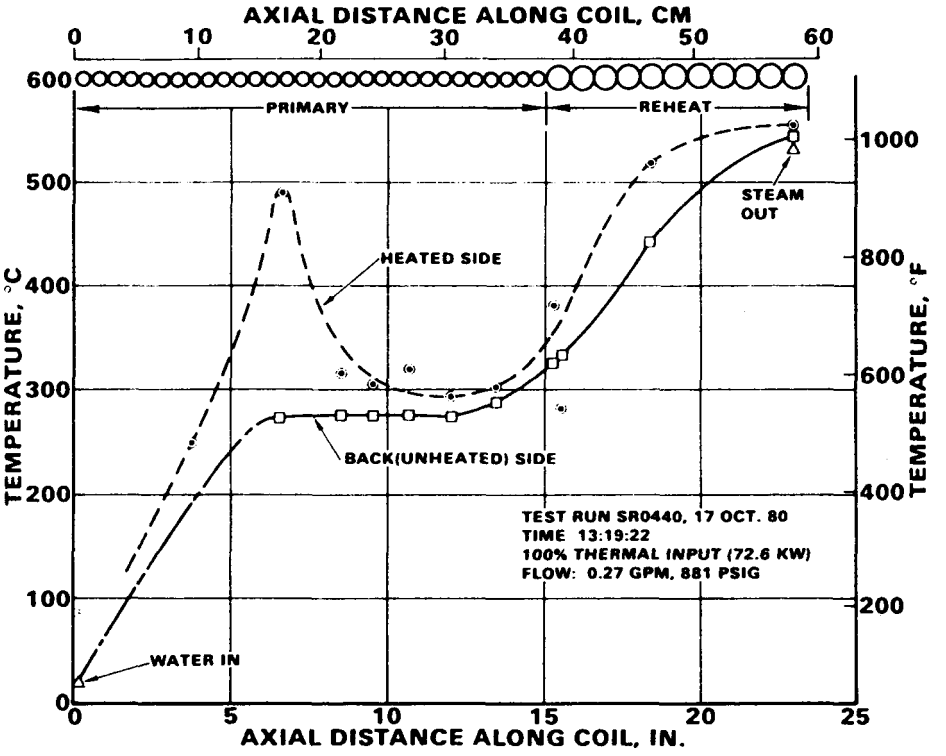

Figure 2-37. SRSR Typical Test Result, Tube-Wall Temperature Profile

a. Design Features. The ABSR operates as follows: Solar flux passes through an aperture located on the concentrator focal plane and falls upon the interior surfaces of a closed cylinder whose axis is located on the concentrator center line. The cylinder contains axial flow passages that bring the air discharging from the recuperator into contact with solar-heated surfaces. Heat transfer in the flow passages is enhanced by the use of an extended-fin surface. Neither the closed nor aperture ends of the receiver have airflow. These surfaces reradiate the impinging energy to the cooled heat-transfer cylinder.

The optimized design is shown in Figure 2-38. The single sandwich cylindrical panel with an offset fin matrix of 4.72 fins/cm (12 fins/in.) has a 1.27-cm (1/2-in.) high flow passage. The heat exchanger is supported by a series of slotted tubes and is insulated from the outer case. The heat exchanger is a brazed and welded structure fabricated from Inconel 625. The stainless steel mount system allows for both axial and radial expansion of the heat exchanger with respect to the external mild steel case. The ducts that bring the air discharging from the recuperator are stainless steel. The aperture plate and closed end plate were originally fabricated from silicon carbide but did not have adequate thermal shock resistance. The aperture plate was replaced by one made of CS-grade graphite and the back plate by stainless steel. Both the circular closed end plate and the aperture assembly are mounted to minimize heat loss to the relatively cold receiver case. The physical characteristics of the design are listed in Table 2-8. Figure 2-39 is a photograph of the assembled ABSR.

Table 2-8. Physical Characteristics of the ABSR

Materials		
Heat exchanger	Inconel 625	
Insulation	Cerablanket	
Case	Mild steel	
Aperture	Graphite	
Receiver		
Weight, kg (lb)	203	(447)
Length, cm (in.)	116.1	(45.7)
Diameter, cm (in.)	76.2	(30.0)
Heat exchanger		
Length, cm (in.)	80.3	(31.6)
Diameter, cm (in.)	50.8	(20.0)
Skin thickness, cm (in.)	0.02	(0.008)
Fin thickness, cm (in.)	0.01	(0.004)
Aperture		
Diameter, cm (in.)	25.4	(10)
Conical height, cm (in.)	8.6	(3.4)

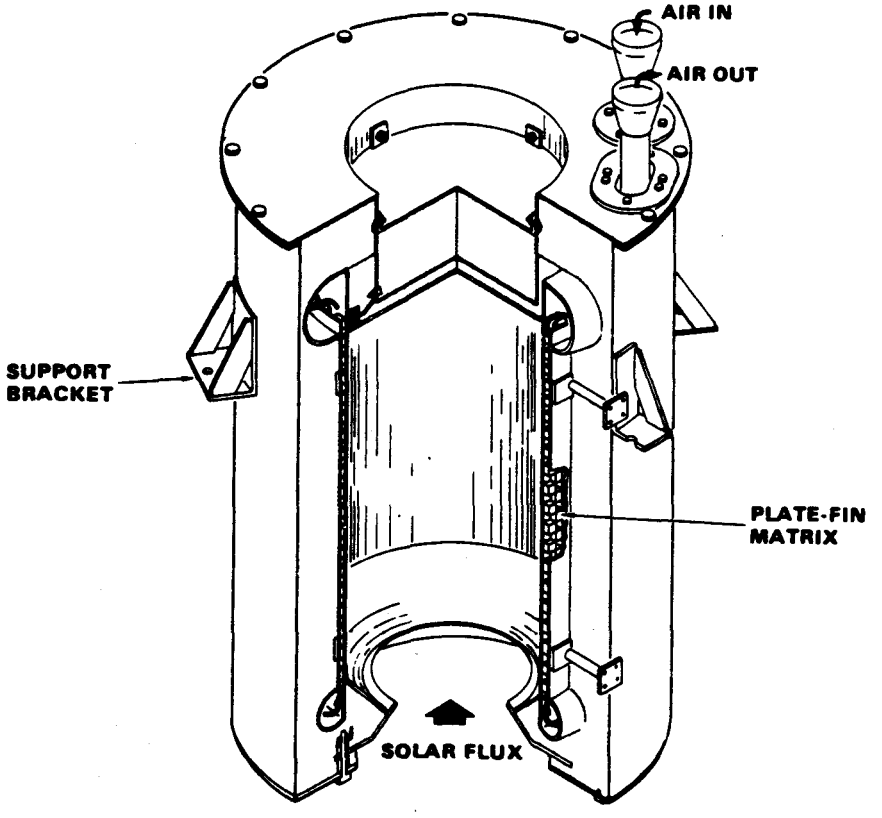

Figure 2-38. 85-kW_t Air Brayton Plate-Fin Solar Receiver

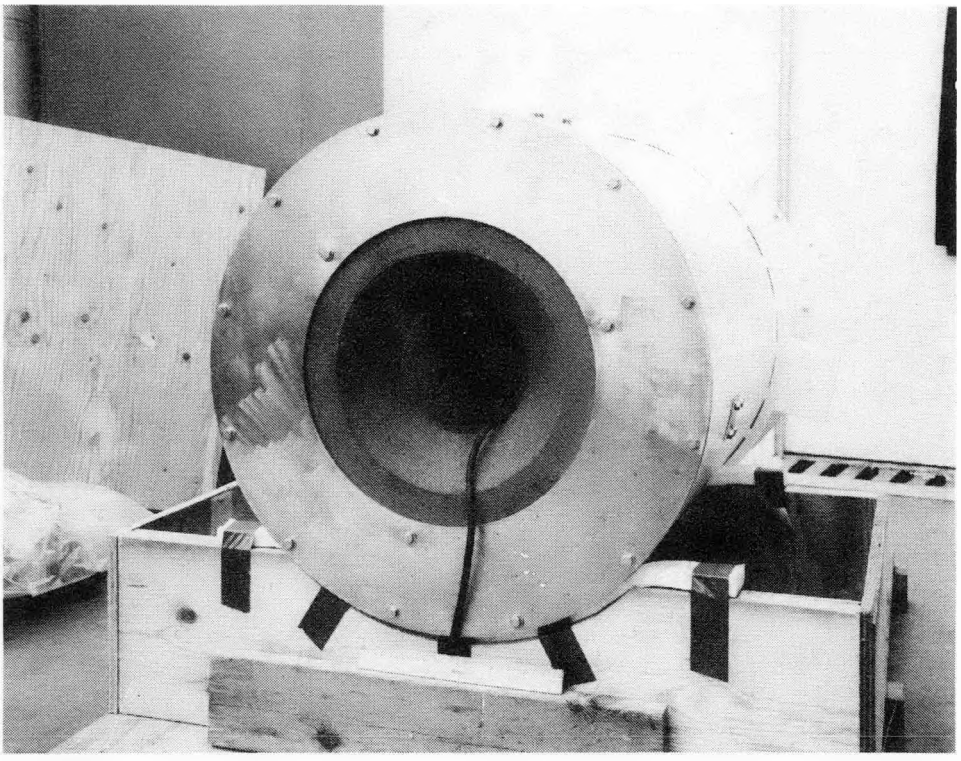

Figure 2-39. Completed Brayton Receiver

b. Performance Tests. Performance testing was planned and conducted at JPL's Parabolic Dish Test Site using one of the TBCs. Expected thermal input on a clear day was about 82 kW_t into a 20.3-cm (8-in.) diameter focal spot.

Airflow was provided by a 750-cfm diesel-powered air compressor. The air passes through an aftercooler, oil separator, dryer, and filter to ensure flow with only about 0.05-ppm contaminants. Flow rates between 0 and 0.43 kg/s (0.93 lb/s) can be produced, which brackets the 0.23 to 0.27 kg/s (0.5 to 0.6 lb/s) design flow of the ABSR. Inlet pressures to the receiver are in the 138 to 276 kPa (20 to 40 psia) range. Flow is controlled by a series of automatic valves; pressure in the ABSR is maintained by a ceramic orifice plate in the outlet piping.

The outlet temperature of the receiver was automatically maintained by the control system. Temperatures range from about 260°C (500°F) up to the design maximum of 816°C (1500°F). Inlet temperatures range from ambient to about 700°C (1300°F), the maximum design inlet temperature. In the 200 to 700°C (400 to 1300°F) range, heat is supplied by a propane-fired preheater.

The test matrix is a combination of three dynamic variables: mass flow, temperature, and pressure, plus a range of power inputs at 25, 50, and 75% as well as full power. Less than full power runs are made by masking off individual mirror facets in patterns devised to maintain the proper overall

flux distribution. Testing begins with the lowest temperatures and power levels and is increased in steps until full power at maximum temperature is attained.

The ABSR was installed at the focal plane of the TBC for testing, and connections to air and gas lines were made. The airflow was measured through an orifice meter. Both orifice meter and plate-fin receiver pressure drops were measured. Figure 2-40 is the test arrangement indicating pressure drop and air flow measuring gauges. In addition to air flow measurement, air inlet/outlet temperatures and several receiver surface temperatures were measured. A list of the instrumentation used for measuring air flow and surface and air temperatures is presented in Table 2-9.

A variety of tests were run on the ABSR to ensure its basic structural integrity as well as its thermal performance. Tests normally performed at the PDTS included (1) cold pressurization, (2) cold airflow and pressure drop, and (3) a variety of on-sun thermal performance tests. The latter were performed at various power levels by covering portions of the solar concentrator to achieve 25, 50, and 75% power levels in addition to full power tests. Flow rates from about 0.25 to 0.56 lb/s were utilized. Typical data taken included mass flow rate, pressure drop across the receiver, inlet and outlet air temperatures, and a variety of temperatures and pressures inside and outside the heat exchanger and case. Typical data are shown in Figure 2-41 and Table 2-10.[9]

3. Air Brayton Ceramic Receiver (Reference 14)[10]

a. Description of Receiver. The air Brayton ceramic receiver developed by Sanders Associates of Nashua, New Hampshire, was designed to operate on a test bed concentrator at the PDTS. In order to simulate the interface with an open-cycle recuperated gas turbine, a 950°C inlet temperature, a 1370°C outlet temperature, and a 113 g/s (0.25 lbm/s) flow rate with air as the working fluid were specified. The maximum allowable pressure drop was specified to be less than 4% $\Delta P/P$ (pressure loss divided by inlet pressure) for the 300 kPa absolute (3 atm) design inlet pressure. Nominal thermal output of the receiver was 60 kW_t.

A cross-sectional diagram of the receiver is shown in Figure 2-42. The flow path begins at the internally insulated inlet air duct and is quickly diverted to a duct located along the receiver axis. The flow continues along this central duct and enters the receiver cavity, which is sealed by the fused silica window. The General Electric 125 fused silica window is 21.6 cm (8.5 in.) in diameter, 1.0-cm (0.413-in.) thick, and is held in place by two 316 stainless steel flanges providing a 18.1-cm (7.1-in.) diameter aperture.

---

[9]Interpretation of the test data is documented in Reference 12.

[10]Computer programs used for processing these test data are described in Appendix B.

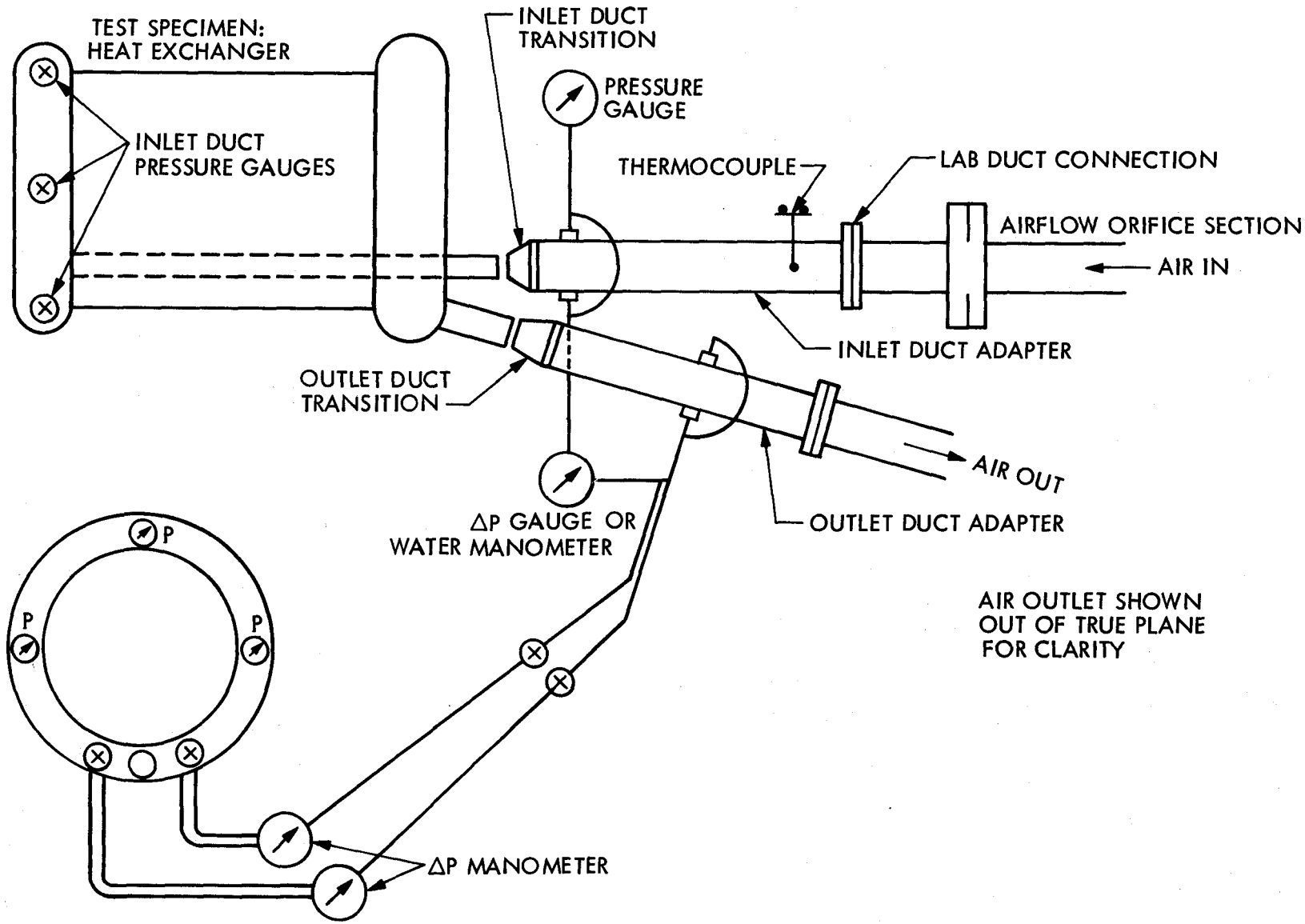

Figure 2-40. ABSR Airflow/Pressure Drop Test Setup

Table 2-9. ABSR Test Instrumentation

Parameter	Approximate Test Range	Required Measurement Accuracy	Recommended Instrument Type
Air inlet pressure	23.5 psig	± 1% reading	0 to 50 psig pressure gauge; accuracy: ±0.5% full scale
Air inlet & outlet temperatures	1050 to 1500°F	± 10°F	Chromel-Alumel thermocouples & direct-reading potentiometer
Air flow	12 to 36 lb/min	± 3% reading	(1) ASME sharp-edge orifice with flange tap duct section (2) Mercury manometer or pressure gauge (3) Water manometer or differential pressure gauge (4) Thermocouple with readout
Air pressure drop	0 to 4 psig	± 1% reading	Differential pressure gauge or water manometer; accuracy: ±0.1 in. H_2O
Inner wall temperatures	1500 to 2400°F	± 25°F	Chromel-Alumel thermocouples & direct-reading potentiometer
Outer wall temperatures	1000 to 2000°F	± 15°F	Chromel-Alumel thermocouples & direct-reading potentiometer
Housing outside temperature	Ambient to 400°F	± 10°F	Chromel-Constantan thermocouples & direct-heating potentiometer

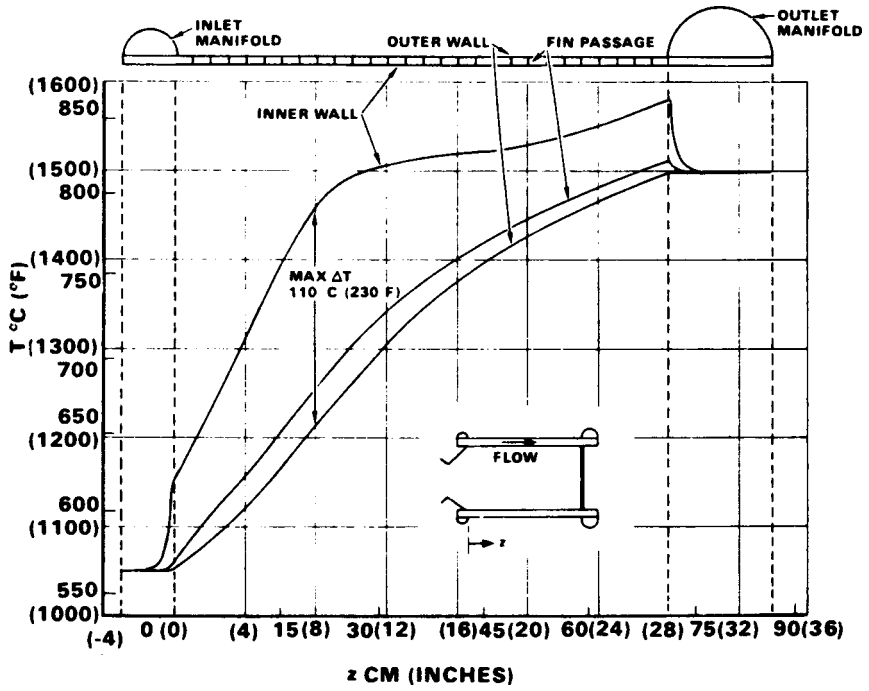

Figure 2-41. ABSR Typical Test Results

Radial jets of air were used to provide additional exterior window and flange cooling. Solar energy passing through the window impinges upon the twelve silicon carbide (SiC) square honeycomb (15 cells/cm^2) solar receiving panels (Figure 2-43) and is immediately transferred to the flowing air by convection.

The heated air then passes through fifteen mullite[11] sensible energy storage segments with 4 cells/cm^2 (Figure 2-44) before exiting the receiver via the larger insulated duct. Johns Manville Ceraform insulation boards, cut to shape and cemented together with Cera-Kote ceramic coating, hold the ceramic pieces in position and provide the thermal insulation for the receiver and ducting.

b. Test Apparatus. During 1980 and 1981, the receiver was tested on one of the test bed concentrators at the PDTS. The schematic of the test setup is illustrated in Figure 2-45. Major components of the test setup are

(1) The test bed concentrator.

(2) Receiver with auxiliary preheat propane burner (Figure 2-46).

---

[11]An aluminum silicate ceramic ($3Al_2O_3 \cdot 2SiO_2$)

Table 2-10. ABSR Test Data: Part I - Summary

Date (1981)	Time (PST)	Test	Input Temperature, °F	Output Temperature, °F	Mass Flow Rate, lbm/s	Average Temperature, °F	Azimuth, deg	Elevation, deg	Thermal Loss, kW_t	Wind Speed, m/s
4/27	10:14:11	Preheat	952	833	0.337	893	0	5	10.9	2.1
4/27	10:24:11	Preheat	941	824	0.337	883	0	5	10.8	2.6
4/27	13:55:57	Preheat	588	552	0.519	570	0	5	4.9	7.0
4/27	14:18:58	Preheat	959	862	0.451	911	0	5	12.1	8.4
4/29	12:02:00	Preheat	568	549	0.468	559	0	-	2.5	2.4
4/29	12:05:30	Preheat	572	556	0.467	564	0	71	2.2	2.0
4/30	11:34:05	Preheat	572	554	0.481	563	0	71	2.3	1.6
5/4	11:15:41	Preheat	576	554	0.586	565	0	69	3.4	3.6
5/4	13:34:27	Solar	1153	1511	0.458	1580	239	60	23.7	4.6
5/4	13:48:09	Solar	1174	1498	0.504	1581	724	58	23.7	5.6
5/7	8:26:55	Preheat	862	819	0.551	841	0	5	6.5	1.1
5/7	9:22:30	Preheat	871	844	0.544	858	-	-	4.0	1.0
5/7	10:39:00	Solar	1209	1513	0.604	1614	137	65	23.4	2.4
5/7	10:51:30	Solar	785	1260	0.467	1370	142	68	14.6	2.6
5/7	11:14:30	Solar	938	1507	0.348	1570	156	70	19.9	2.9
5/7	12:04:10	Solar	803	1356	0.382	1444	190	71	17.3	2.1

Table 2-10. ABSR Test Data: Part II - Test Condition Comparison

Date (1981)	Time (PST)	Test	Input Power, kW_t	Output Power, kW_t	Mass Flow Rate, lbm/s	Input Temperature, ^oF	Output Temperature, ^oF	Input Pressure, psia	Pressure Drop, %
-	-	Design	85	78.3	0.610	1050	1500	35	2.0
5/7	10:38:00	Case 1	74.4	53.0	0.604	1209	1513	51.8	4.7
5/7	9:59:30	Case 2	72.6	51.8	0.502	1143	1503	43.2	4.6
5/4	13:25:03	Case 3	69.3	47.9	0.411	1096	1503	34.7	4.4
5/7	11:15:30	Case 4	74.4	56.3	0.348	939	1508	31.2	3.8
5/7	11:33:30	Case 5	74.8	56.0	0.303	862	1517	27.7	3.7

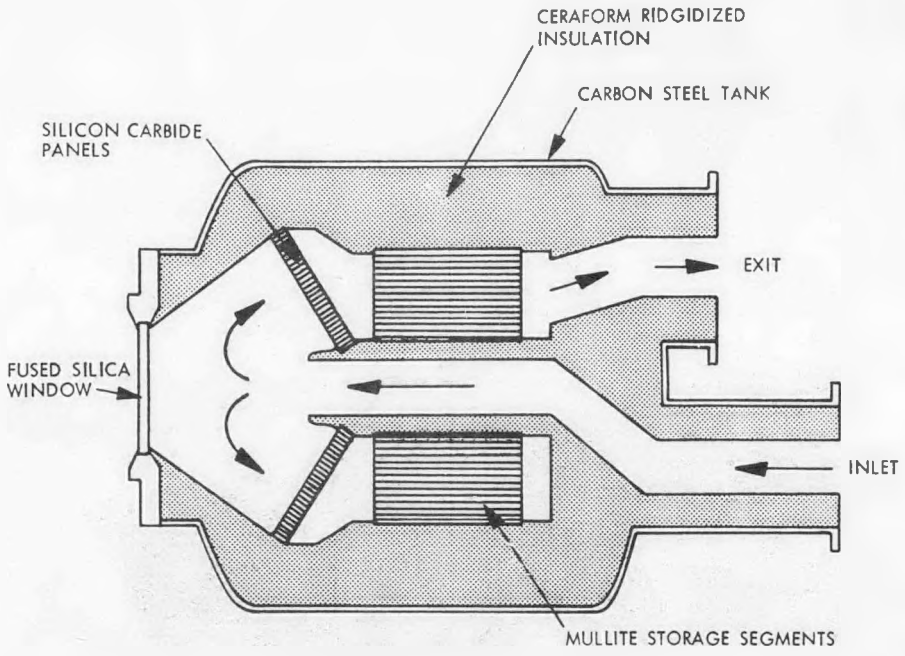

Figure 2-42. Brayton Ceramic Receiver Cross-Sectional Diagram

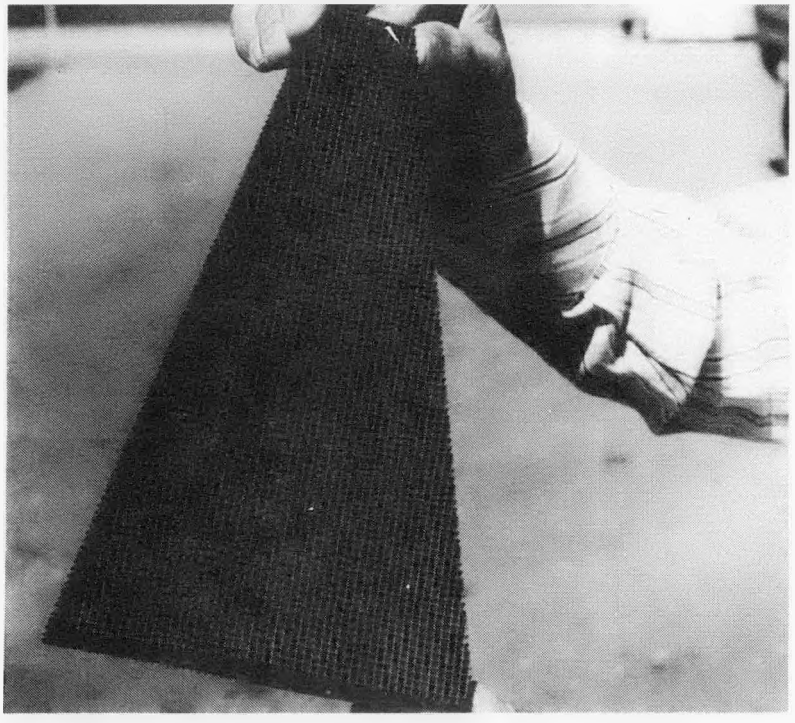

Figure 2-43. Silicon Carbide Solar Receiving Panel of the Ceramic Receiver

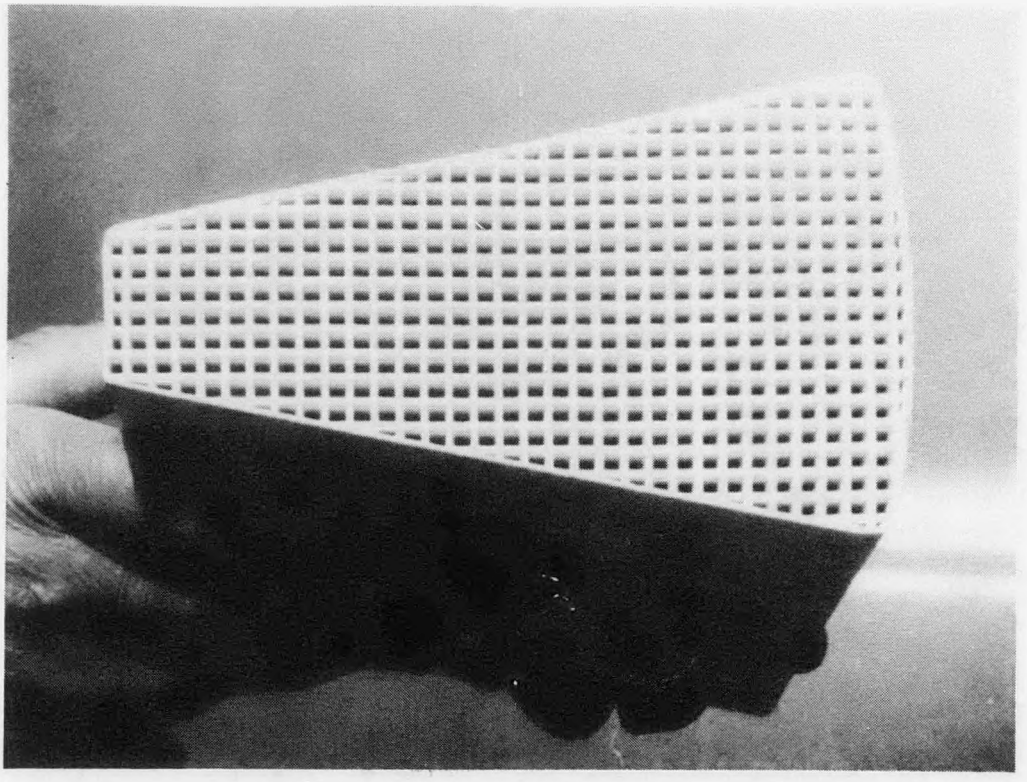

Figure 2-44. Ceramic Receiver Mullite Thermal Buffer Storage Segment

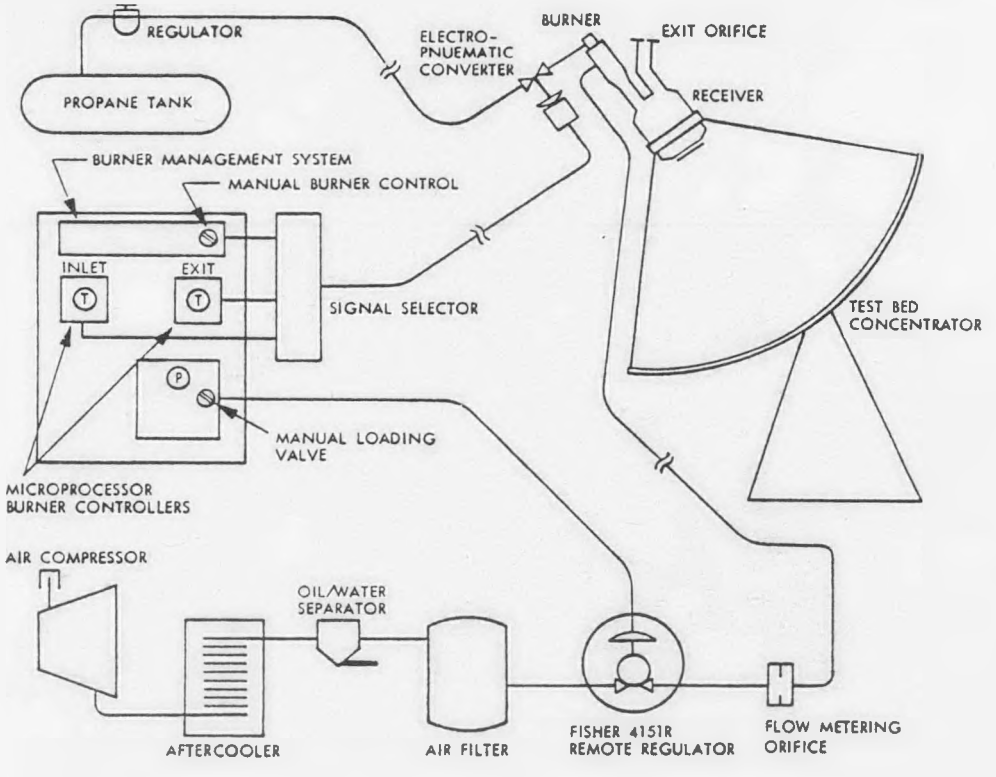

Figure 2-45. Ceramic Receiver Test Apparatus Schematic

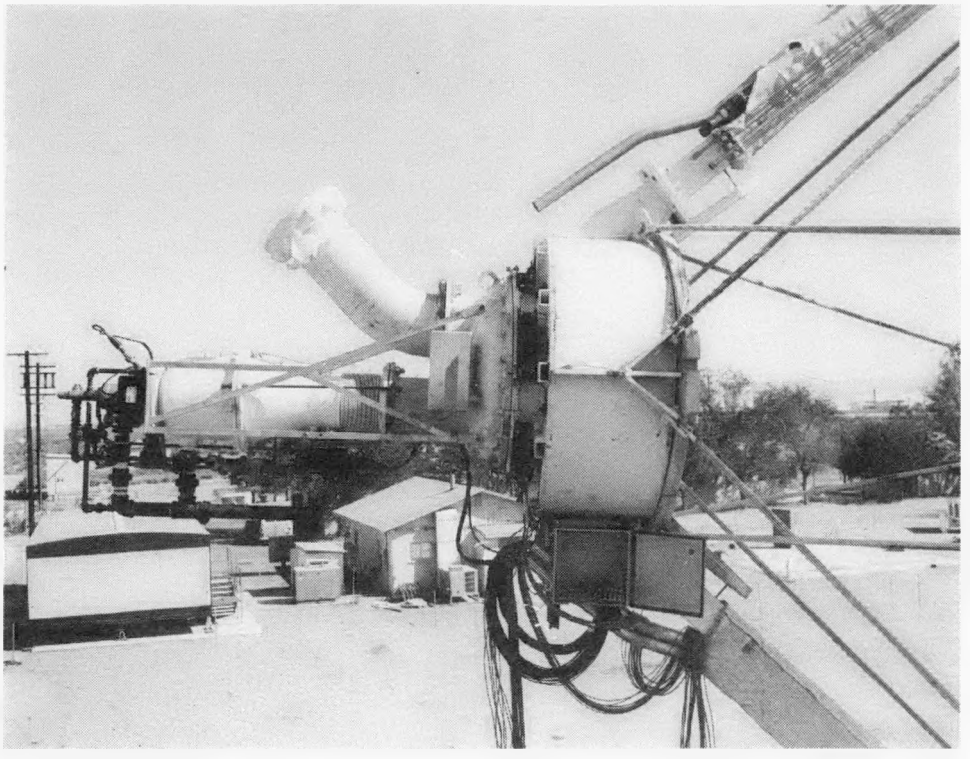

Figure 2-46. Preheat Burner for Ceramic Receiver Testing

(3) Propane tank, gas lines, flow metering orifice, and controls.

(4) Air compressor, filter, and flow metering orifice.

To test the receiver at or near its design conditions, a substantial effort was put into designing test auxiliary equipment. An Eclipse process heat burner attached to the rear of the receiver (as shown in Figure 2-46) was utilized to provide the desired receiver inlet temperature. As displayed by the schematic in Figure 2-47, air was supplied by a 750 cfm air compressor and was cooled and filtered before flowing to an air control system. Air flow was remotely controlled from a control console by adjusting control pressure to a Fisher 4151R regulator located near the concentrator. Burner temperature was controlled by a current signal to an electro-pneumatic converter, which in turn activated a pressure-controlled propane valve. Interchangeable silicon carbide orifices at the receiver exit provided the flow restriction for receiver operation at selected pressures above ambient. The test setup has an additional water loop that is used to cool the receiver face plate and aperture shutter. Schematics of the water pumping, storage, and GN_2 supply systems are identical to those shown in Figure 2-35.

c. Instrumentation. The setup was fully instrumented to obtain data required for monitoring the operation of the system and analyzing the performance of the receiver. The receiver, burner, and a sharp-edged orifice mass flow meter were instrumented for desired temperatures using Type K and Type R thermocouples; pressures were sensed using Microswitch transducers. The list of data points (in mnemonic representation) is presented in Table 2-11.

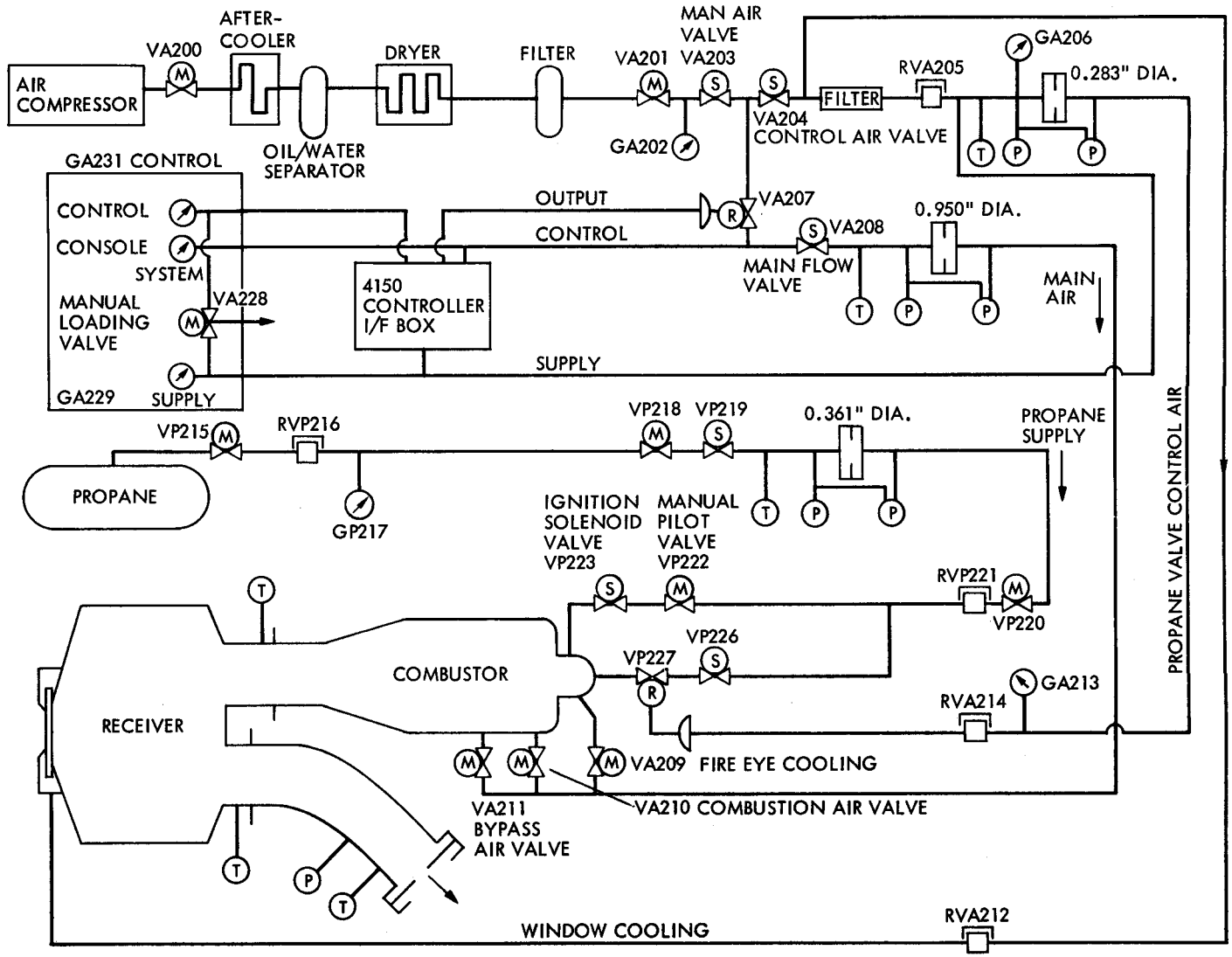

Figure 2-47. Air and Propane Flow Schematic for Ceramic Receiver Testing

Table 2-11. Sample List of Data Points, Ceramic Receiver Testing

Channel	Mnemonic	Units	Scale	Channel	Mnemonic	Units	Scale
0	REF	1000MV	100	157	VEFLAT	DEG. C	1400
108	PSOT	DEG. C	2000	158	OUNWT	DEG. C	1400
109	PEFT	DEG. C	1990	159	EXFLT	DEG. C	1400
110	CAVTY.WALL	DEG. C	1400	160	WICOAT	DEG. C	1400
111	R73,Z24	DEG. C	1400	178	BPRCT	DEG. C	1400
115	R116,Z87	DEG. C	1400	180	BOR75T	DEG. C	1400
116	R116,Z46	DEG. C	1400	182	BIRNT	DEG. C	1400
117	R114,Z06	DEG. C	1400	183	BIRT	DEG. C	1400
118	R130,Z-20	DEG. C	1400	184	BURIT	DEG. C	1400
119	R105,Z-17	DEG. C	1400	185	BVIST	DEG. C	1400
120	AMTEMP	DEG. C	50	186	BPEFT	DEG. C	1400
121	RXRLET	DEG. C	100	187	BPCFT	DEG. C	1400
122	RERET-1	DEG. C	100	188	BPIFT	DEG. C	1400
123	RERET-2	DEG. C	100	189	BPCFT	DEG. C	1400
124	RERET-3	DEG. C	100	190	BPI.FAR.T	DEG. C	1400
125	RERET-4	DEG. C	100	193	BCMFT	DEG. C	1400
126	BPTC-1	DEG. C	100	195	MAPT	DEG. C	1400
127	BPTC-3	DEG. C	100	196	BEFT	DEG. C	1400
128	BPTC-4	DEG. C	100	200	FP.FLOW	GPM	1
134	SIPMAT	DEG. C	1400	202	APFLO-1	GPM	1
135	SIPAT	DEG. C	1400	205	PYRHEL	W/SQ.M	1200
136	SIPMIT	DEG. C	1400	207	MFPSIG	PSID	5
137	SOPMAT	DEG. C	1400	208	CAPSID	PSID	5
139	SOPMIT	DEG. C	1400	209	MFPSID	PSIG	40
142	RIRT-1	DEG. C	1400	210	FUPSID	PSID	5
144	RIRT-2	DEG. C	1400	211	FUPSID	PSID	40
145	RIRCT	DEG. C	1400	212	REDPI-2	PSIG	5
146	RORT-1	DEG. C	1400	213	REDPI-3	PSID	5
148	RORT-2	DEG. C	1400	214	RECPSIG	PSIG	30
149	RORCT	DEG. C	1400	215	REDPI-5	PSID	5
154	WISFT	DEG. C	1400	216	IFVOS	VOLTS	12
155	VESNET	DEG. C	1400	217	REVOS	VOLTS	12
156	FOVEWT	DEG. C	1400	218	FLADET	VOLTS	12

Table 2-11. Sample List of Data Points, Ceramic Receiver Testing (Cont'd)

Channel	Mnemonic	Units	Scale	Channel	Mnemonic	Units	Scale
219	INSOLKEN	W/SQ.M	1000	225	GASPSIG	PSIG	100
220	INSOLEP	W/SQ.M	1200	229	100 MV REF	MV	120
221	INCONS	VOLTS	12	232	IFCAFT	DEG. C	100
222	EXCONS	VOLTS	12	233	IFCOFFT	DEG. C	100
223	MANCOS	VOLTS	12	234	IFMAFT	DEG. C	100
224	WINPSIG	PSIG	100				

The test control console consisted of the manual pneumatic loading valve to provide the pressure signal to the air regulator, the burner ignition and management system, and Barber Coleman process heat microprocessor controllers for control of both receiver inlet and exit temperatures. Microprocessor temperature controllers and a manual control provide current input signals to a signal selector, which selects the lowest signal to be sent to the burner propane valve actuating system. This system allows burner fuel control so that neither controller nor manual temperature set points are exceeded.

d. Test Objective. The objective of this test program was to investigate steady-state and start-up/shutdown transient performance of the advanced ceramic receiver in terms of thermal and materials considerations over a range of outlet temperatures from 38 to 1370°C (100 to 2500°F), pressures from 1 to 3 atm, and mass flows from 0.2 to 0.3 lb/s. The purpose of these tests was to fully characterize the performance of the ceramic receiver over a range of operating conditions simulating a multitude of potential applications.

The entire test sequence was divided into three phases: checkout phase, low-temperature phase, and high-temperature phase. The checkout phase consisted of the non-solar test and the 25, 50, and 75% power tests. The non-solar test brings the receiver up to a maximum inlet temperature of 955°C (1750°F) and a pressure of 3 atm to assure its performance and to check out operations and controls. The 25, 50, and 75% solar power tests check out these operations with actual solar input. Upon completion of these tests, the 100% power low-temperture and high-temperature test phases began.

The 100% power low-temperature and high-temperature test phases were performed as described below and in Table 2-12. In order to operate the receiver at pressures above ambient, a restricting orifice at the receiver exit is required. This orifice governs the mass flow rate of air for a given receiver exit pressure and temperature. To operate the receiver at the same exit pressures and temperatures, but at different air mass flow rates, different size orifices are used. Because outlet pressure and temperature can be governed from the control box, testing was approached by running the matrix of pressure and temperature appropriate for each orifice first and then by proceeding to the next orifice for each test phase. The matrix of outlet temperature and inlet pressure was run for only those conditions indicated and with two orifices (mass flows) for each condition.

e. Test Procedure. Testing was implemented by igniting the burner and preheating the receiver to the desired inlet temperature. The concentrator was commanded via its own micro-processor control and tracking system to acquire the sun. A water-cooled sliding plate was located in front of the aperture for thermal protection as shown in Figure 2-48.

After sun acquisition, the cold water plate was activated to "open," allowing solar input to the receiver. An additional water-cooled ring was

Table 2-12. Low- and High-Temperature Tests

Test Phase	Larger Orifice	Smaller Orifice
100% Power Low-Temperature Phase:		
Inlet Pressure, atm	2.0	3.0
Outlet Temperature, °F		
1200	X	X
1500	X	X
1800	X	X
100% Power High-Temperature Phase:		
Inlet Pressure, atm	2.0	3.0
Outlet Temperature, °F		
2000	X	X
2250	X	X
2500	X	X

located in front of the receiver to protect the receiver in case of concentrator tracking failure.

Data were recorded via multiplexed inputs to an Auto Data Nine data logger, and were in turn recorded on magnetic tape using the PDP 11 site computer. At the conclusion of each test sequence, computer algorithms were executed for preliminary data reduction and analysis. Further analysis was performed at a later date, again using a PDP 11 computer.

The test sequence was planned to cover 25, 50, and 100% solar input powers. Non-solar preheat tests were conducted to check out control and data acquisition systems. Solar tests were then conducted beginning with the lowest power level and working up to full power. Preheat tests were conducted by heating the receiver with the burner up to 927°C at 265 kPa absolute pressure and establishing steady-state conditions.

Subsequent to the 25% test, a cracked receiver window was discovered. It was found that the crack was caused by misalignment of the solar "spot" with respect to the aperture. The test was terminated, and window retaining

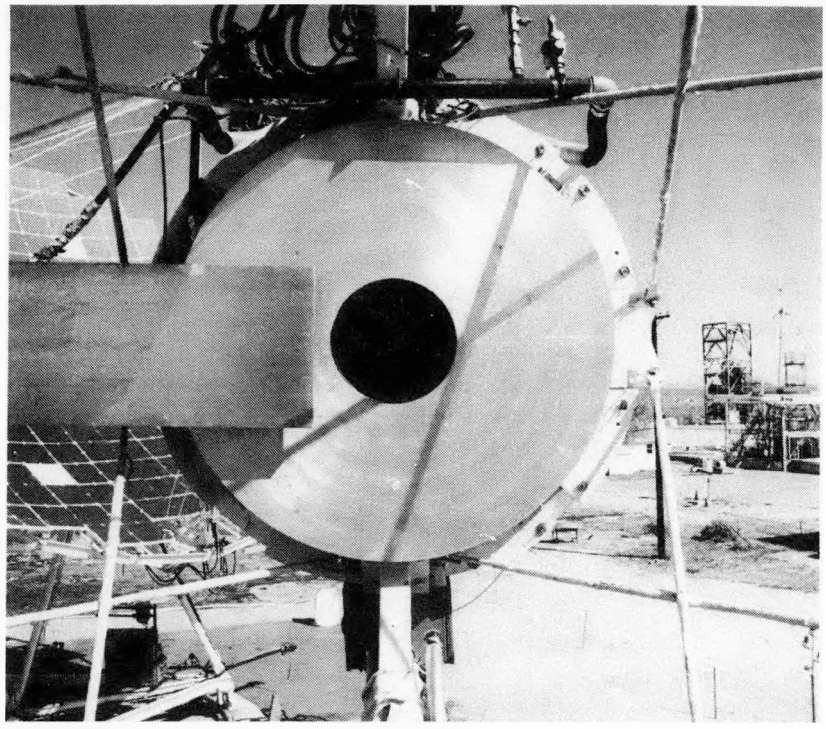

Figure 2-48. Water-Cooled Protective Plates (Receiver Not Installed)

flanges were inspected for trueness and clearance. It was determined that insufficient clearance combined with thermal distortion of the retaining flanges (caused by the solar tracking misalignment) overstressed the window. Window seal gasketing was changed to allow more seal compliance. The window was replaced and carefully installed, and a subsequent preheat checkout test was conducted without further difficulties.

Solar tracking was realigned, and an insulation ring of Saffil 3000 was placed in front of the retaining flange to intercept excess spillage energy. This insulation ring narrowed the aperture diameter down to 16.5 cm (6.5 in.). Successful 25 and 50% mirror tests were performed. An attempt at full power resulted in a cracked window 4-1/2 minutes after solar input. Alignment of the solar flux was fairly good (off by ~1 cm). Inspection of the hardware indicated that the retaining flange had coned inward and had then fractured the window over the edge of the support flange. The window retention scheme was altered to eliminate mechanical interference by providing the necessary clearance to accommodate thermal distortion of the window retainer flange without inducing window failure. Successful full power tests were conducted for 885, 1014, and 1104°C exit temperatures without further problems.

Subsequent testing was performed without the insulation ring in front of the retaining flange. With the improved window retaining system, few problems were encountered in the remaining tests. Steady-state operation of

the receiver was performed for 966, 1060, and 1120°C exit temperatures. Transient runs were performed for exit controller thermocouple readings up to 1427°C for a few minutes. During the last transient run, a tracking offset was again implemented to better align the solar spot into the aperture. This last tracking adjustment was very successful in that the spillage was apparently uniform around the aperture.

Table 2-13 contains a log of the tests performed in this program. Reduction of the data for steady-state runs is displayed in Table 2-14. Based upon the above methodology, the intercept factor for the cases with and without the insulation ring around the aperture were 85.7 and 91.9%, respectively. Because peak insolation during any test was 975 W/m^2, the peak flux endured by the fused silica window was 530 W/cm^2. Calculated overall receiver efficiency (ratio of the power into the working fluid to the power delivered by the concentrator) varied from, 69.1 to 51.2% as the temperature varied from 885 to 1120°C, when aperture spillage losses are considered as receiver losses. When aperture spillage losses are accounted for separately, corrected receiver efficiencies are 80.6 to 59.7%, respectively. Receiver performance was extremely good in view of the demanding requirements of the test.

Post test inspections showed that the receiver performed well up to the 1120°C exit temperature. At temperatures exceeding 1120°C, and prior to the solar tracking adjustment, solar flux impingement upon rigidized insulation around the aperture (caused by the solar aiming misalignment) melted the insulation, and molten insulation partially blocked flow passages through the SiC solar receiving panels. Also, shrinkage of the insulation allowed some loosening of these panels. Subsequent to the last test, cracks in two of the SiC panels were noted.

4. Steam Engine Testing at the PDTS

Three steam engines underwent testing at the PDTS, all during 1981. These engines were tested on the ground using solar powered steam supplied by TBC-1 and the Garrett steam Rankine receiver.

The first engine tested was a two-cylinder, 15-kW_e steam engine produced by Jay Carter Enterprises, Inc. This was the first engine to produce electricity from solar energy at the PDTS. Operating at 18% efficiency, it supplied 10 kW_e to the utility grid. The second engine, also developed by Jay Carter Enterprises, Inc., was a one-cylinder, 5-kW_e steam engine. Tests were run from July 3 to July 6, 1981. From 1.5 to 3.7 shaft hp was produced from this engine at efficiencies of 11 to 14%. The third engine was an Omnium-G steam engine designed specifically for that dish module. Up to 2.5 kW_e was produced at 11% efficiency. A minimum of 10 to 12 kW_t (34,000 to 41,000 Btu/h) was required to operate the engine at partial power.

Table 2-13. Ceramic Receiver Test Log

Test Date	Test Type	Receiver Conditions				Remarks
		Inlet Temperature, °C	Exit Temperature, °C	Pressure, kPa	Flow Rate, g/s	
11/19/80	Non-solar	927	832	265	93	window failed
11/20/80	Non-solar	---	---	---	---	checkout
11/25/80	25% solar	816	---	---	---	window failed
12/04/80	Non-solar	814	750	210	75	checkout
12/05/80	25% solar	542	651	199	75	steady-state conditions
12/08/80	50% solar	522	762	213	78	steady-state conditions
12/09/80	100% solar	---	---	---	---	water-cooled plate failed
12/10/80	100% solar	494	---	---	---	window failed
12/11/80	100% solar	478	885	193	105	steady-state conditions
12/16/80	100% solar	607	1014	192	101	steady-state conditions
12/16/80	100% solar	739	1104	194	98	steady-state conditions
01/08/81	100% solar	538	---	---	---	cloud cover
01/20/81	100% solar	520	966	181	89	steady-state conditions
01/20/81	100% solar	615	1060	179	85	steady-state conditions
01/20/81	100% solar	721	1120	179	84	steady-state conditions
02/02/81	100% solar	varying	up to 1427	varying	varying	varying conditions
02/06/81	100% solar	varying	up to 1371	varying	varying	varying conditions

Table 2-14. Ceramic Receiver Full Power Steady-State Performance

Test Date	Receiver Conditions						Efficiency	
	Inlet Temperature, °C	Exit Temperature, °C	Pressure, kPa	Flow Rate, g/s	Power Out of Receiver, kW_t	Power Delivered by Concentrator, kW_t	$\eta_{Overall}$ [a]	$\eta_{Receiver}$ [b]
12/11/80 [c]	478	885	193	105	48.4	70.1	0.691	0.806
12/16/80 [c]	607	1014	192	101	47.2	76.5	0.617	0.720
12/16/80 [c]	739	1104	194	98	42.1	76.3	0.552	0.644
01/20/81 [d]	520	966	181	89	45.3	75.6	0.600	0.653
01/20/81 [d]	615	1060	179	85	44.0	76.8	0.573	0.624
01/20/81 [d]	721	1120	179	84	39.5	77.2	0.512	0.597

[a] Receiver thermal output divided by concentrator thermal output (includes spillage).

[b] Receiver thermal output divided by energy into the receiver aperture.

[c] Insulation ring around aperture: Intercept factor = 0.857

[d] Insulation ring removed: Intercept factor = 0.919.

a. Testing of the J. Carter Two-Cylinder Steam Engine[12]

Description of Two-Cylinder Test Engine (Reference 15). The expander on the two-cylinder engine for a solar application, shown schematically in Figure 2-49, consists of two vertically mounted piston-cylinders operating in parallel. Each piston-cylinder has a spring return inlet valve opened by a spike attached to the piston. These valves are commonly referred to as "bash valves." This valve design is a fixed-cutoff type where a constant volume of steam is admitted into the cylinder at the top of each stroke. Power output from the engine is controlled by varying the boiler pressure which also changes the mass flow rate into the expander. This type of control system requires minimum throttle valve control; however, a positive displacement feed pump with solenoid valving is required to deliver controlled mass flow at variable pressures. Toward the end of each stroke, oil is injected directly onto the piston rings to minimize wear and leakage around the rings. The oil is a non-emulsifying oil that is allowed to freely mix with the steam at the expander exhaust. The expander is a uniflow design, i.e., at the end of each stroke the piston uncovers exhaust ports, allowing the oil/steam mixture to pass through the feedwater heater and on to the air-cooled condenser. After the steam is condensed, the oil and water are separated using a centrifuge that returns the oil to the expander and the water to an open-to-atmosphere water tank. The piston-type feed pump delivers the water from the water tank through the feedwater heater and back to the boiler.

Test Results. The two-cylinder engine was tested at expander inlet temperatures between 399 and 566°C (750 and 1050°F) and at power levels from 25 to 80 kW_t input. Efficiencies as high as 20% were measured, based on net electrical power delivered to the grid divided by the thermal input to the working fluid. All electric power parasitics were subtracted from the alternator output to obtain the net electric output. Preliminary data showing efficiency versus thermal input are plotted in Figure 2-50 at 538°C (1000°F) expander inlet temperatures for a 10:1 expansion ratio. These efficiencies could be improved by adding insulation and repairing leaks in the condenser, which created excessive expander back pressure. Testing at a 14 to 1 expansion ratio was initiated; however, these data are not available. Engine simulations predict improved efficiencies at this higher expansion ratio.

Engine Solar Applications. Several engine mounting configurations are possible with a Carter engine mounted on a parabolic dish collector. In Carter's approach, everything except the condenser and the oil/water separation storage tank would be mounted at the focal point of the dish. This configuration would result in a dish-mounted weight of 297 kg (654 lb) and a total weight of 601 kg (1323 lb). The condenser would be fitted with a chimney to minimize parasitic fan power. Other mounting configurations might include using the condenser as a counterweight for the

[12]Computer programs used for processing these test data are described in Appendix B.

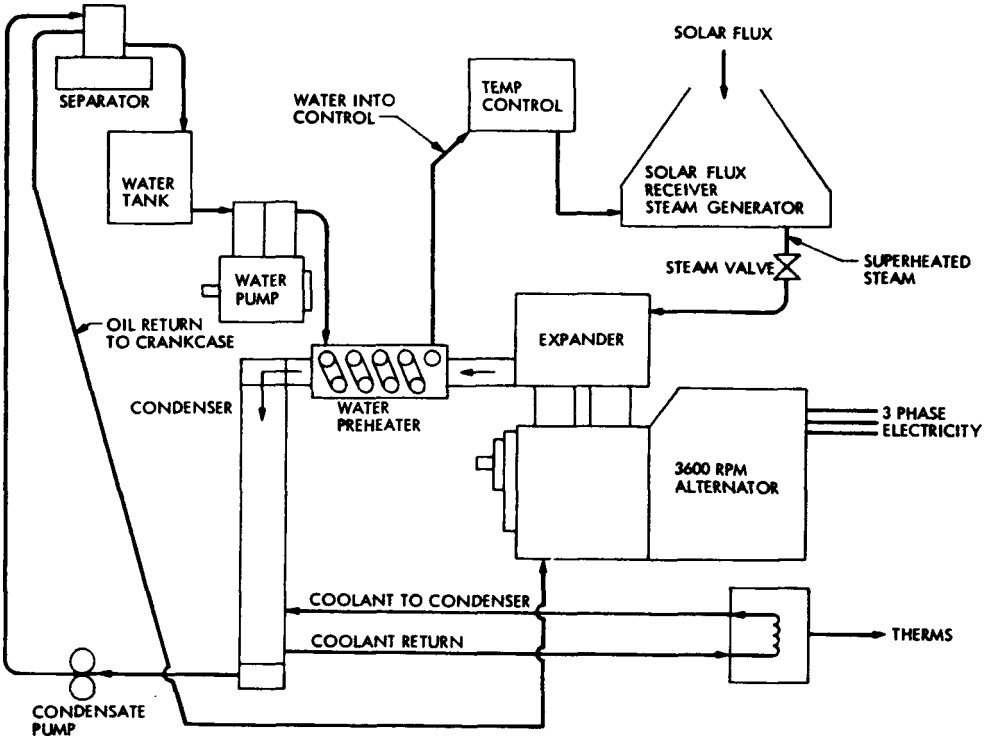

Figure 2-49. Power Module Schematic

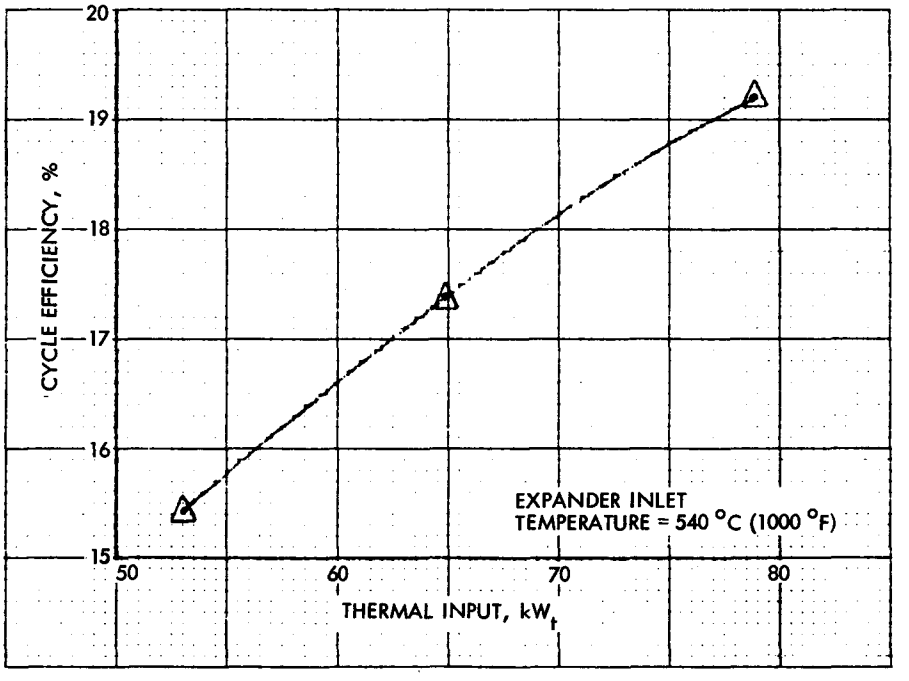

Figure 2-50. Preliminary Engine Data

concentrator or simply mounting everything at the focus. Freeze protection could be accomplished with flexible freeze tanks, resistance heaters, or a buried water storage tank.

Conclusion. The Carter two-cylinder steam engine demonstrated total power conversion efficiencies (thermal to electric) of approximately 20%. The engine test data correspond closely with the predicted data at several operating conditions, adding credibility to the model. Verification of the engine and model through testing indicates that predicted thermal-to-electric efficiencies of 26% for the simple cycle and 30% for the reheat cycle are achievable at 677°C (1250°F) for 15-kW_e power levels. The value of this engine in a solar application could be further enhanced by using 100°C (215°F) exhaust heat, thus increasing the total system efficiency to approximately 90%.

b. Testing of the Carter Single-Cylinder Steam Engine.[13] The single-cylinder steam engine from Carter Enterprises, Inc., was tested at the PDTS in June and July 1981 to establish its power output and thermal efficiency under various steam inlet conditions. TBC-1 was used as the source of steam. Although steam inlet temperatures in excess of 427°C (800°F) were reached on three occasions (with inconclusive results), the bulk of the data was generated at 410°C (770°F) or below. The experiments covered power levels of 1.5 to 3.7 shaft horsepower and two temperature ranges: 332 to 366 and 382 to 410°C (630 to 690 and 720 to 770°F). Twenty-two data points were run, totaling five hours of operation.

The test setup comprised a steam source, the engine ground-mounted on a rigid test bench, and a dynamometer to measure shaft power output. Figure 2-51 shows the engine and dynamometer test bench; Figure 2-52 is a schematic diagram of the system. Table 2-15 gives the engine specifications.

Steam Engine Repair Work. The engine was partially refurbished prior to testing. A new cylinder head, intake valve, and valve lifter were made. A portion of the journal bearing and the corresponding surface of the connecting rod had been gouged; these surfaces were built up with new material and remachined. A bronze bushing was pressed into place and used as a journal bearing.

Because of the pressing need to assemble the engine and begin operation, the overhaul was not completed: First, the engine originally used a caged roller bearing on the crankshaft journal, but a bronze bushing was used instead. Also, the cylinder wall was somewhat worn and scored. Given more time, the cylinder would have been honed or replaced, the porous chrome inner surface would have been replaced, and new piston rings would have been installed.

---

[13] Computer programs used for processing these test data are described in Appendix B.

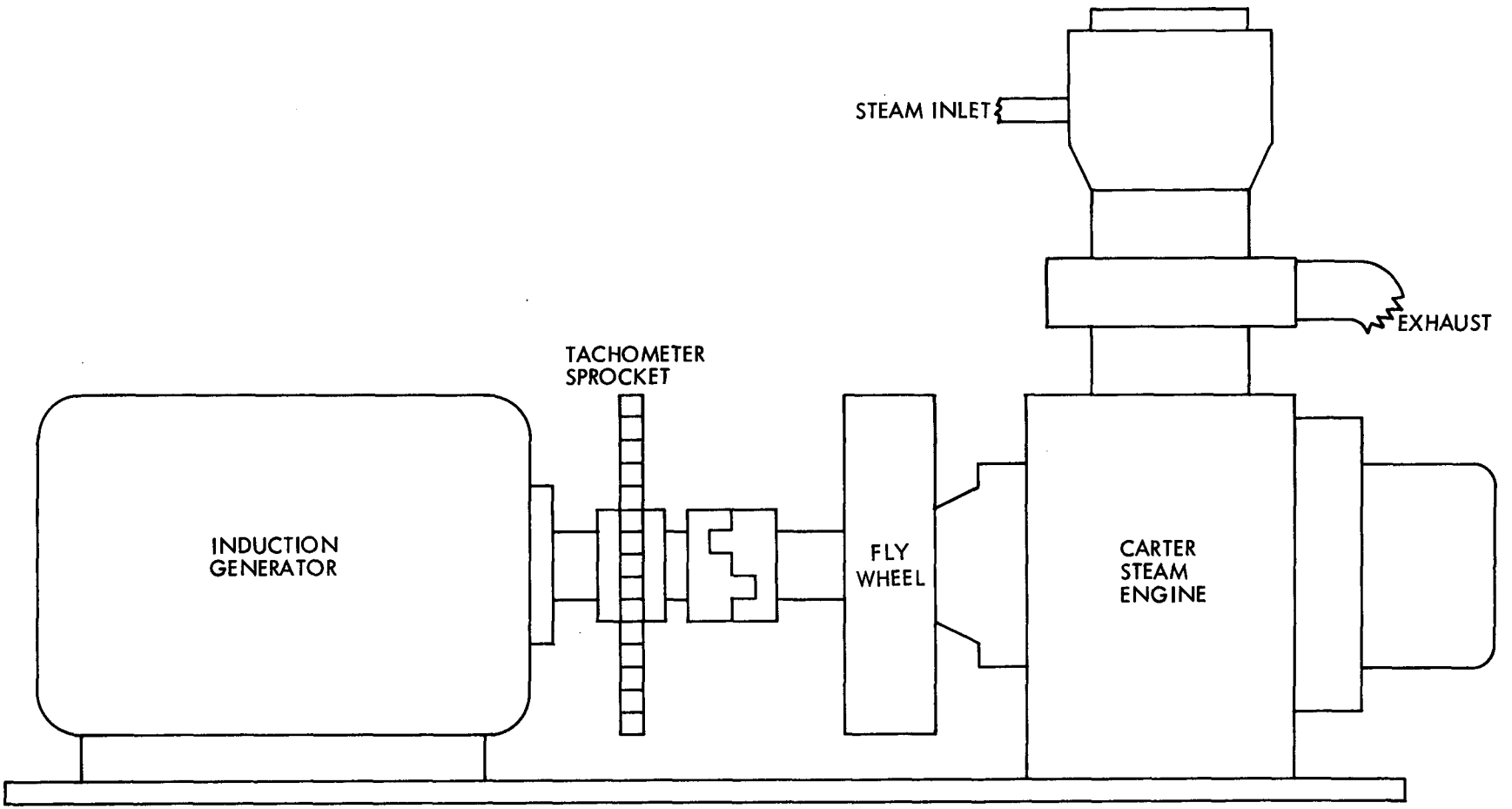

Figure 2-51. Carter Single-Cylinder Engine Test Bench

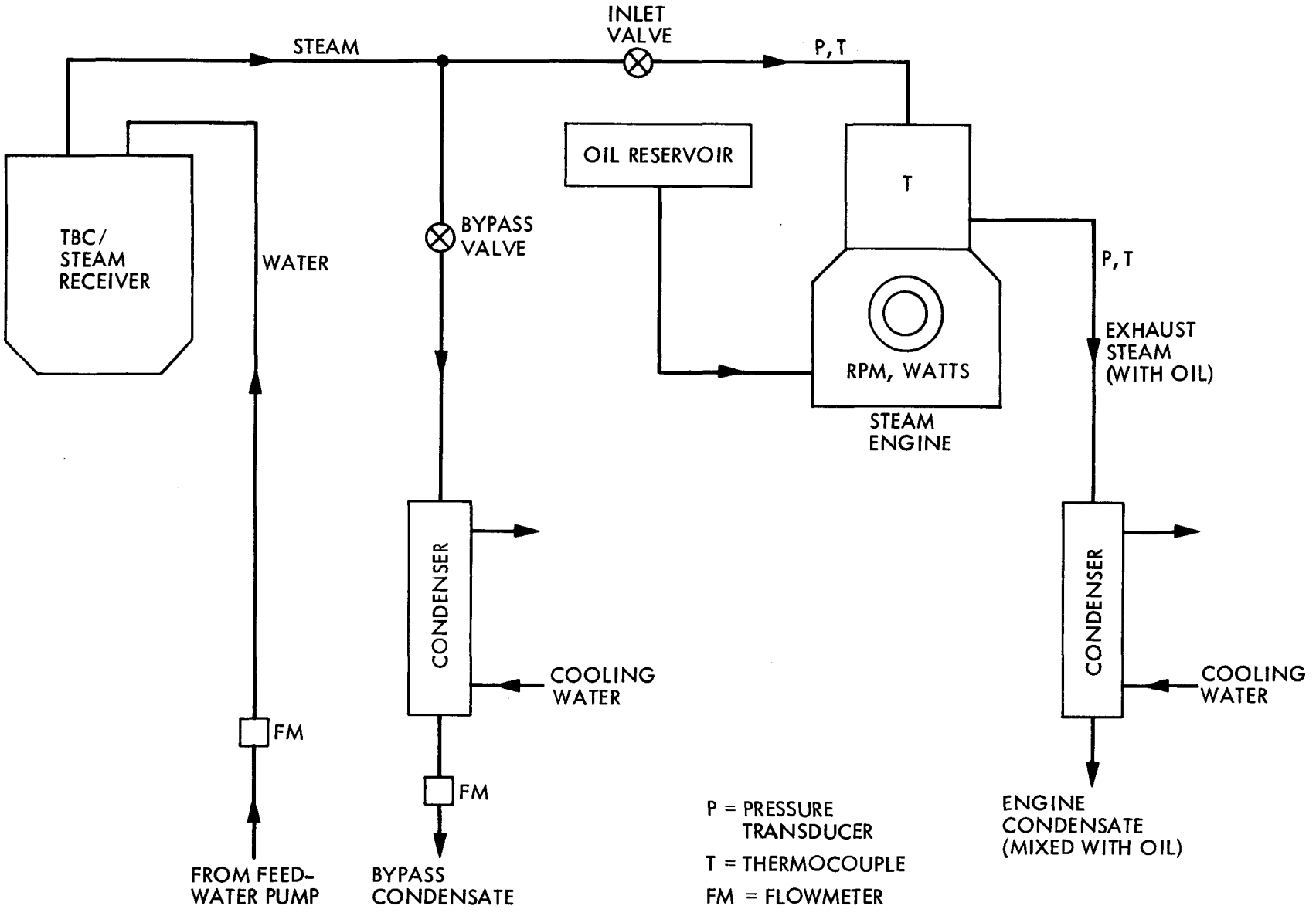

Figure 2-52. Carter Single-Cylinder Engine Test System Schematic

Table 2-15. Carter Steam Engine Specifications

Type:	Single-cylinder, single-acting uniflow
Bore:	2 in.
Stroke:	2.5 in.
Displacement:	7.85 $in.^3$
Expansion Ratio:	11.6 to 1
Speed:	1800 rev/min
Nominal Power Rating:	8 shaft horsepower

Steam Source. The steam source consisted of the TBC with the Garrett AiResearch steam Rankine receiver and downcomer line, a deionized water reservoir, feedwater pump, and bypass system. Deionized water was used for steam generation. The minimum feedwater flow rate required to prevent overheating of the receiver was three or four times the steam flow rate demanded by the Carter engine; therefore, it was necessary to bypass most of the steam. The condensate was then sent through two flowmeters in series (each with a different range). Subtracting the bypass condensate flow from the feedwater flow gave the flow to the engine.

A pressure sensor and a thermocouple were placed in the steam inlet line, immediately upstream of the engine (see Figure 2-52).

Dynamometer. The dynamometer consisted of a calibrated electric generator wired to an electronic power meter. The generator calibration curve allowed conversion of electrical power readings to mechanical power values.

The generator was a 3-phase, 5-hp, 4-pole induction motor, connected to 230-V utility power. When driven at speeds higher than its synchronous speed of 1800 rev/min, the motor becomes a generator and sends power to the utility. The generator was calibrated in an electric power laboratory at California State University, Los Angeles. The source of input shaft power was a large dc motor equipped with a controlled power supply and a tachometer plus a torque arm connected to a force gauge. The electrical output was measured using a Weston (secondary-standard) polyphase electrodynamometer-type wattmeter. Two curves were generated: electrical output versus shaft horsepower input (Figure 2-53) and efficiency versus electrical output (Figure 2-54).

The electronic power meter was made by EIL (Model WTM 020) and gives accurate power readings at any power factor. This feature was important to these engine tests because the generator made power at low power factors, usually below 50%.

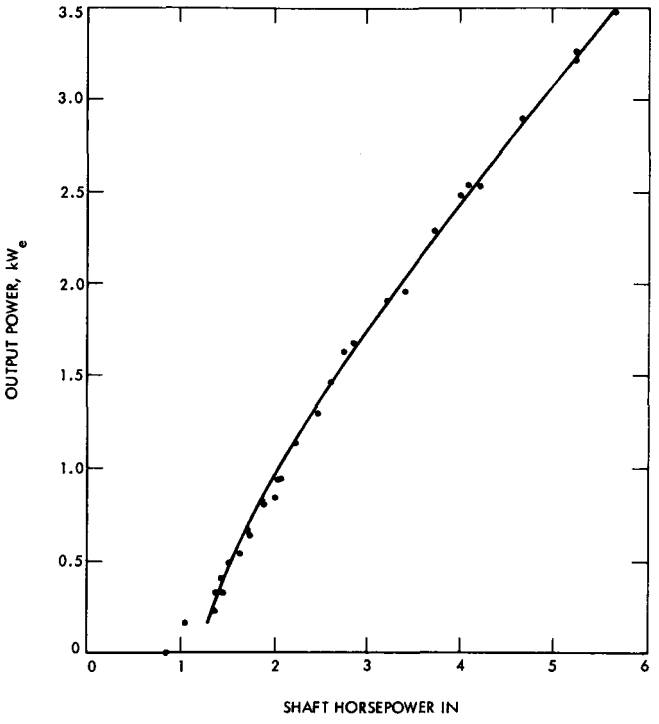

Figure 2-53. Carter Steam Engine Generator Calibration, Electrical Output versus Shaft Horsepower Input

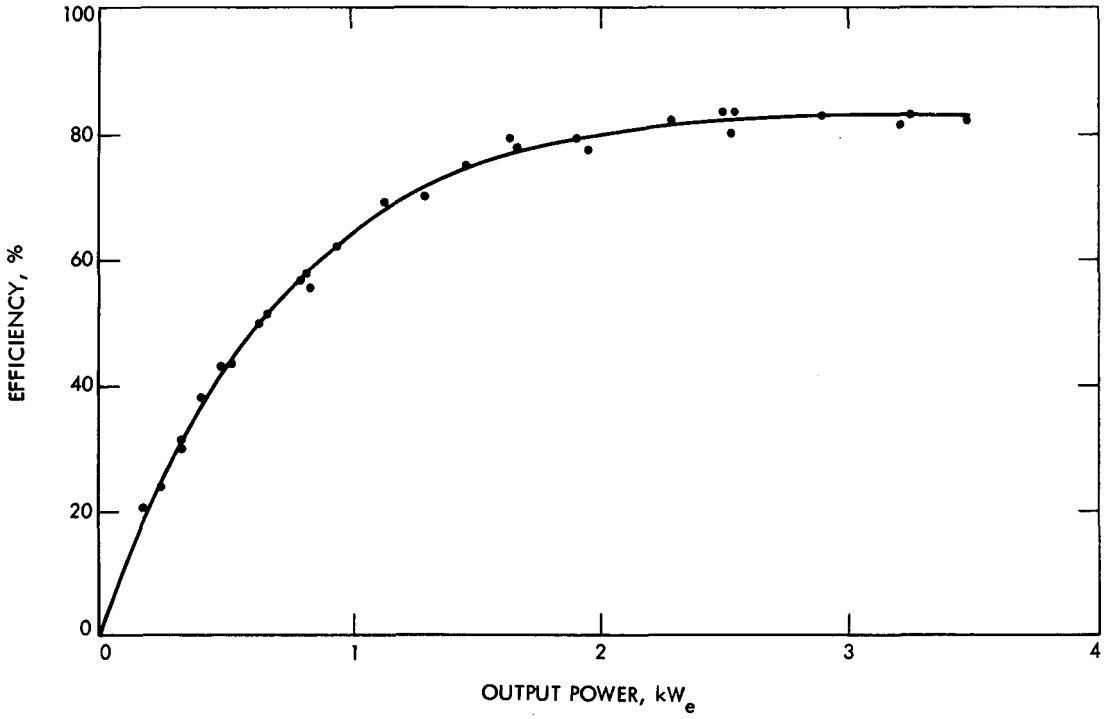

Figure 2-54. Carter Steam Engine Generator Calibration, Efficiency versus Electrical Output

Experimental Procedure. Figure 2-52 shows the schematic diagram of the test setup. The oil reservoir held sufficient oil to run the engine for 20 to 25 minutes, which was enough time for the engine to reach a steady operating temperature.

At the start of a typical test day, after acquiring the sun, all the generated steam was run through the bypass circuit for 2 to 3 hours. This served to heat up the downcomer and part of the steam inlet line. An engine run was performed in the following manner: The bypass valve was partially closed to increase the system pressure to the estimated operating value. Then the induction motor was started, causing the engine to turn. Opening the inlet valve fed steam to the engine and power generation commenced. After waiting several minutes for the engine to reach a stable temperature, the bypass valve was adjusted to give steady power generation at the desired level. At the end of a run (to replenish the oil supply or finish a day's testing) the bypass valve was opened, depressurizing the system. Then, the induction motor was shut off.

Steam inlet pressure and temperature, feedwater and bypass flow rates, and watts generated were all monitored by the automated data acquisition system at the PDTS. Also recorded were revolutions per minute, cylinder head temperature, and exhaust steam pressure and temperature. Values were sampled approximately every 20 seconds. Averaging several minutes' worth of data (during which time values were holding steady) resulted in one data point. All transducers were calibrated by PDTS personnel, using their standard procedures.

Results. It was not possible to control the steam temperature with much precision; therefore, operating inlet temperatures varied widely. However, the temperatures (with the exception of four data points) seemed to fall naturally into two ranges: 343 to 366°C and 382 to 410°C. The data are organized into these two ranges. The mean thermal-to-mechanical efficiency in the 343 to 366°C temperature range was 11.3%; it was 12.7% for 382 to 410°C. There is, however, a great deal of scatter in the data, precluding a firm conclusion that efficiency increases with temperature.

Tables 2-16, 2-17, and 2-18 show the individual data points. The 382 to 410°C data and the 427°C data seem to indicate that engine performance deteriorates with time. Also, linear regression plots were made of shaft horsepower against inlet pressure, steam flow rate, and thermal input. These plots are shown in Figures 2-55, 2-56 and 2-57.

No trend of increasing efficiency with increasing power level is seen, probably because all data points are on the "flat" region of the power-versus-efficiency curve. Data previously published by Carter show that this curve levels off at about 20% of rated power. If a rated power of 8 horsepower (shaft) is assumed for this engine, a leveling-off value of 1.6 horsepower (shaft) results, which is about the lowest power run. The generator must have at least 1-1/4 shaft horsepower input to overcome windage and friction in order to generate any power.

Table 2-16. Engine Performance in the Temperature Range 343 to 366°C (630 to 690°F)

Date (1981)	Output, kW_e	Input, kW_t	Inlet, psig	Steam, lb/h	lb/SHP-h[a]	Shaft Horsepower	Engine[b] Efficiency,	Inlet Temperature, °F
6-8	0.59	11.8	571	31.0	19.6	1.58	10.0	689
6-8	1.01	13.0	730	35.5	17.5	2.02	11.6	631
6-8	2.03	22.1	902	59.5	17.7	3.38	11.4	676
6-12	1.09	13.5	753	36.0	16.9	2.14	11.8	674
6-12	1.71	19.2	899	51.5	17.6	2.93	11.4	676
6-23	1.01	13.1	689	35.5	17.5	2.04	11.6	639
7-6	0.38	9.3	559	25.0	17.8	1.51	11.3	637

Averages

Number of Points Averaged	kW_e	kW_t	psig	lb/h	lb/SHP-h[a]	Efficiency[b] %
2	0.49	10.6	565	28.0	18.7	10.7
3	1.04	13.2	724	35.7	17.3	11.7
1	1.71	19.2	899	51.5	17.6	11.4
1	2.03	22.1	902	59.5	17.7	11.4

[a]SHP = Shaft horsepower.

[b]Shaft power output divided by thermal power input.

Table 2-17. Engine Performance in the Temperature Range 382 to 410°C (720 to 770°F)

Date (1981)	Output, kW_e	Input, kW_t	Inlet, psig	Steam, lb/h	lb/SHP-h[a]	Shaft Horsepower	Engine[b] Efficiency,	Inlet Temperature, °F
6-3	1.45	13.2	830	34.5	13.5	2.57	14.5	730
6-3	1.73	16.3	920	42.5	14.4	2.95	13.5	730
6-23	1.44	13.2	835	34.5	13.5	2.55	14.4	730
6-23	1.58	15.4	875	39.5	14.4	2.75	13.3	768
6-29	0.97	12.0	686	31.0	15.6	1.98	12.3	743
6-29	1.06	13.0	716	33.5	16.0	2.09	12.0	741
7-2	0.93	11.4	780	29.5	15.1	1.96	12.8	734
7-2	1.11	13.2	825	34.5	16.1	2.14	12.1	723
7-6	1.50	16.8	888	44.0	16.7	2.63	11.7	727
7-6	2.11	22.6	1132	58.5	16.8	3.48	11.5	766
7-6	2.25	23.2	1129	60.5	16.4	3.70	11.9	757

Averages

Number of Points Averaged	kW_e	kW_t	psig	lb/h	lb/SHP-h[a]	Efficiency %
4	1.02	12.4	752	32.1	15.7	12.3
3	1.46	14.4	851	37.7	14.6	13.5
2	1.66	15.9	898	41.0	14.4	13.4
2	2.18	22.9	1131	59.5	16.6	11.7

[a]SHP = Shaft horsepower.

[b]Shaft power divided by thermal power input.

Table 2-18. Additional Engine Performance Data Points

Date (1981)	Output, kW_e	Input, kW_t	Inlet, psig	Steam, lb/h	lb/SHP-h[a]	Shaft Horsepower	Engine[b] Efficiency,	Inlet Temperature, °F
6-3	1.38	13.3	850	35.0	14.2	2.48	13.9	700
6-29	2.06	20.4	1019	51.5	15.1	3.42	12.5	815
7-2	1.39	15.0	889	38.0	15.3	2.49	12.4	800
7-2	1.64	17.2	963	43.5	15.5	2.81	12.2	809

[a]SHP = Shaft horsepower.

[b]Shaft power divided by thermal power input.

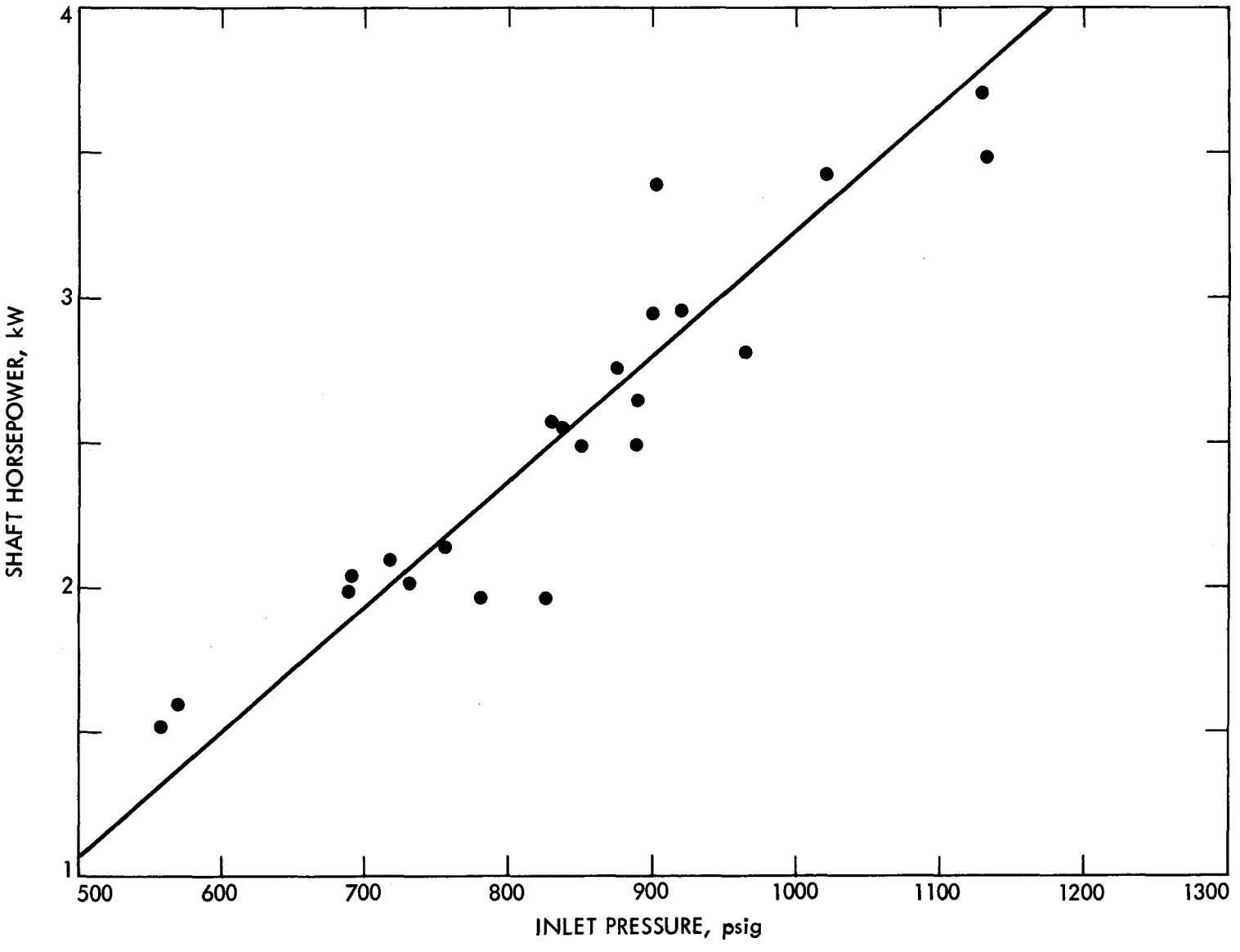

Figure 2-55. Carter Steam Engine, Shaft Horsepower versus Inlet Pressure

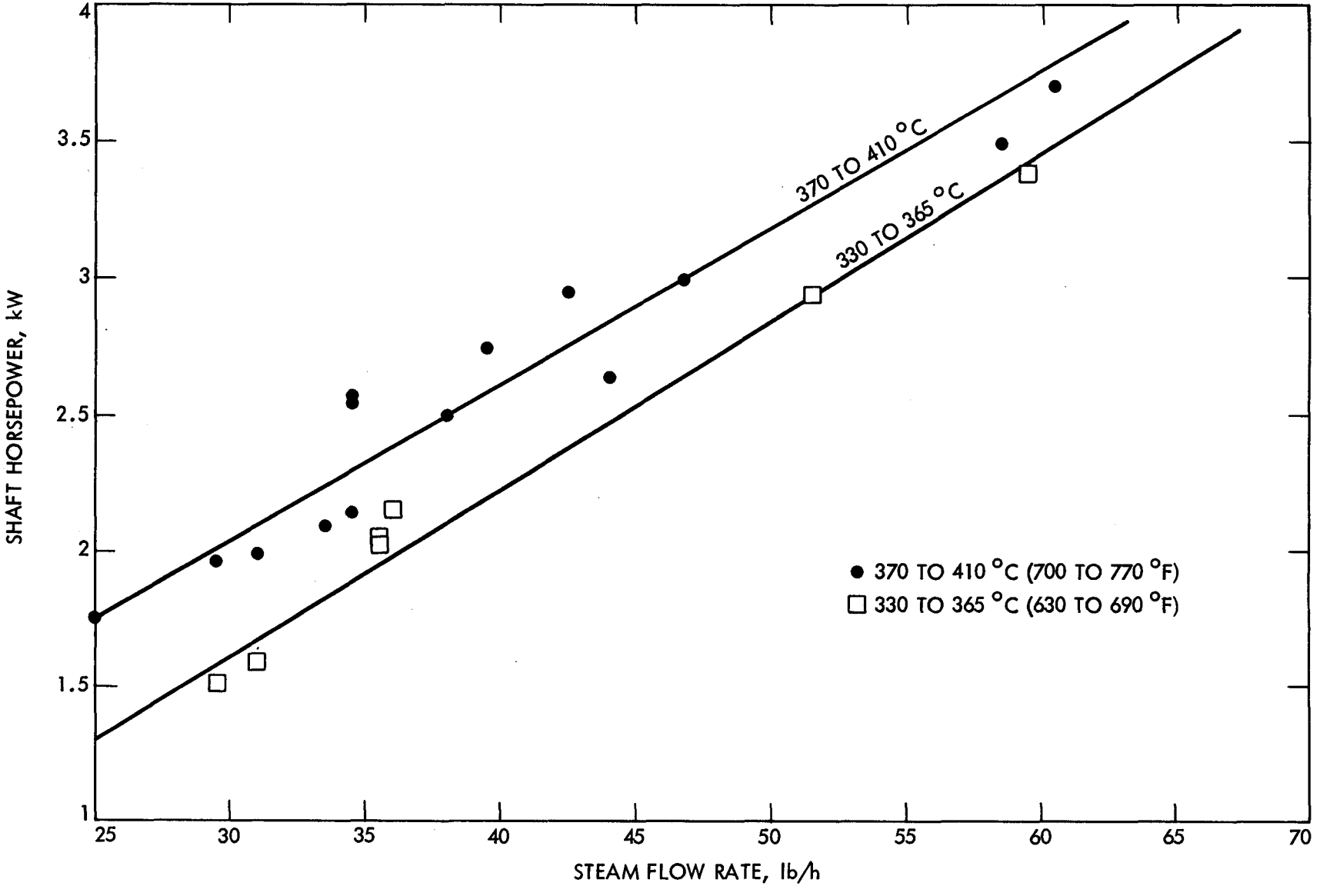

Figure 2-56. Carter Steam Engine, Steam Flow Rate versus Shaft Horsepower

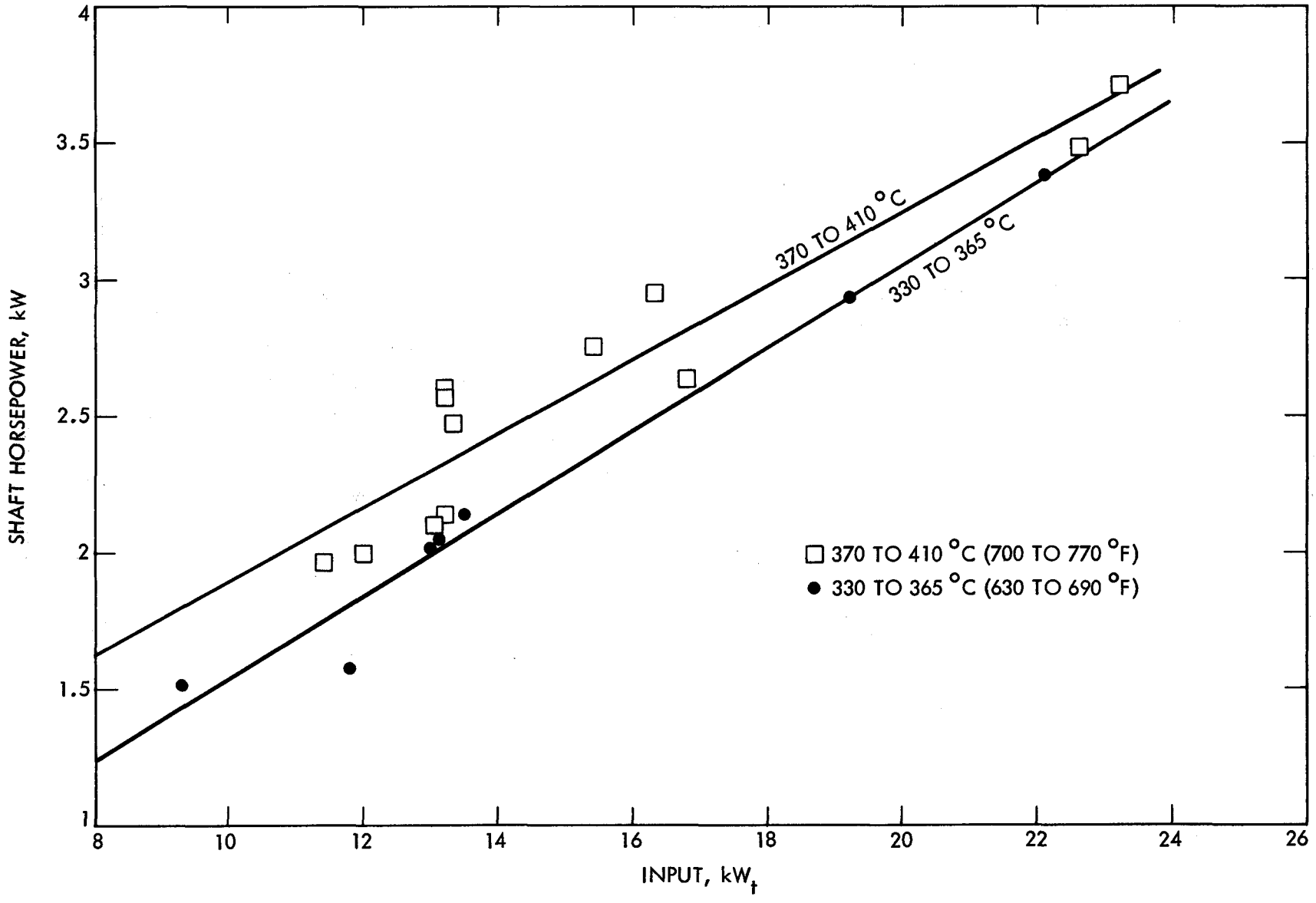

Figure 2-57. Carter Steam Engine, Thermal Input versus Shaft Horsepower

Problems. It was difficult to determine the steam flow rate to the engine. This could not be done by measuring the exhaust condensate for two reasons. First, a substantial amount of steam to "blow-by" the piston rings, which would not show up in the exhaust, was expected. Second, the exhaust condensate is mixed with a large amount of engine oil. Therefore, the engine steam flow rate was calculated by subtracting the bypass flow from the feedwater flow. The problem is that a small number is derived by taking the difference between two large numbers. The steam receiver requires at least 0.27 gal/min of feedwater to avoid overheating. The engine requires a steam flow equivalent to about 0.07 gal/min of feedwater; therefore, 0.20 was subtracted from 0.27 to get 0.07.

The problem was exacerbated by the use of two flow meters in series to measure the bypass condensate flow. One flow meter had a nominal range of 0 to 0.2 gal/min; the other had a nominal range of 0 to 0.5 gal/min. It was expected that the meter with the smaller range would yield more accurate readings at low bypass flow rates. Because the bypass was generally very near 0.2 gal/min and there was about a 6% discrepancy between the two flow-meter readings, it was difficult to decide which reading to use. Most of the later data points were determined using the "smaller" flow meter, which read slightly higher. The engine performance estimates might, therefore, be somewhat optimistic. On the other hand, on the earlier runs the "large" flow meter was used, and the efficiency values generated on these runs were the highest. It has been noted that the engine performance did seem to deteriorate with the passage of time.

The tests were also hampered by a noisy reading in the power meter. A strip-chart recording of the power level from one run showed a sinusoidal variation of $\pm$50 W in the power, which was certainly acceptable. But an oscilloscope showed a large number of spikes of several hundred watts amplitude, lasting about one millisecond. Unfortunately, the data acquisition system had a rapid enough response to read the spikes, causing the power level shown on the computer printout to fluctuate severely. It was felt, however, that a good estimate of the power level was obtained by averaging a large amount of data.

Engine Condition After Testing. After the testing was terminated, the engine was disassembled and inspected.

The cylinder diameter was measured at various heights before and after testing. No change was noted. However, three scoring marks in the cylinder wall were noticeably deeper at the end of the testing program.

The measured clearance between the crankshaft journal and its bearing was 0.0015 in., which was close to the value of 0.001 in. measured at the start of testing. There were, however, several noticeable scratches on the journal.

Wear on the Satellite valve seat on the mating surface with the intake valve was observed. However, the valve and the lifter, both made of Hastellow, showed no wear.

The Inconel "O" ring, which formed a seal between the cylinder and head, was split, and a small segment was missing. This alone may explain the decline in efficiency.

The top of the cylinder head, where the valve seat was pressed in, was bulging downward into the cylinder.

Additional Remarks. The engine emitted about a quart of oil in the exhaust every five minutes. This oil was recovered from the condensate in a simple gravity separator and reused.

An exhaust condenser was designed and built. It consisted of two shell-and-tube exchangers, each with six tubes. The tubes were of 0.5 in. outside diameter, 0.035-in.-thick wall, and 6 ft long. Cooling water flowed over the outsides of the tubes, at a total flow rate of 10 gal/min. The condensate had the appearance of salad dressing.

Conclusions. The small Carter steam engine appears to have adequate efficiency to generate at least 1 kW_e of net power (electric power generated minus system parasitics) if the concentrator used delivers 15 kW_t to a ground-mounted power system. The performance can be improved if a heat exchanger is used to transfer some of the exhaust steam enthalpy to the feedwater.

However, the level of confidence in these conclusions is low. It was mentioned earlier that there was a lot of scatter in the data and that the performance seemed to degrade with time. To obtain better data would require a more careful job of overhauling the engine, as well as a more controllable experimental setup. In particular, the acceptable range of mass flow rates in the steam generator should match the steam demand of the engine.

If the engine is to be used in the future, it needs to be reworked. A caged roller bearing should be installed on the crankshaft journal. The cylinder should be machined and refinished (or a new one built) and a new, stronger cylinder head must be designed and built.

c. Omnium-G Steam Engine Testing.[14] The basic objective of the tests was to characterize the performance of the redesigned Omnium-G power conversion system.

Scope of Testing. The primary purpose of these tests was to determine the steady-state performance characteristics of this Omnium-G power conversion cart and, in particular, the thermal efficiency of the steam engine. Tests were limited to a few representative steam temperatures and to pressures and thermal inputs representative of operating conditions of the

---

[14]Computer programs used to process these test data are described in Appendix B.

Omnium-G concentrator/receiver thermal output. Transient information on start-up, shutdown, and power changes were of secondary importance in this series of tests.

Test Configuration. The general test configuration is as indicated in Figure 2-58. The subsystems requirements include the following test equipment:

(1) Steam Source: Garrett AiResearch steam receiver was used as the steam source.

(2) TBC-1 Concentrator/Receiver/Transport Line:[15] Appropriate steam conditions for the engine system tests were provided by manual control using standard steam supply subsystems.

Omnium-G Power Conversion System. The Omnium-G power cart was located beside the Carter power conversion assembly to permit the use of either the TBC or Carter steam generator steam source. The electrical power outlet of the engine generator unit was tied into the JPL test facility (load bank or power grid). Also, the power conversion system requirements for auxiliaries including condenser cooling, water, and electricity, etc., were provided by JPL.

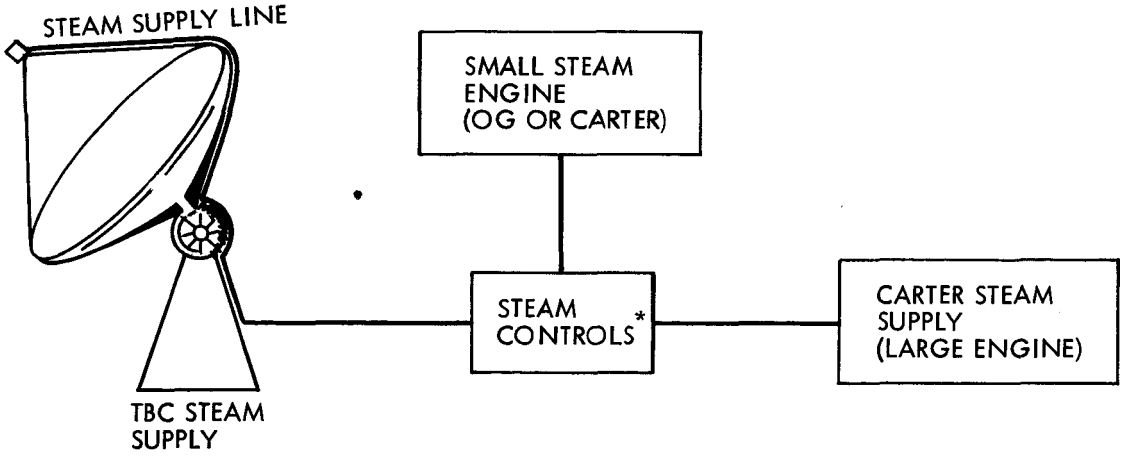

*THE MOST ADAPTABLE OF THE TWO STEAM SUPPLIES CAN BE SELECTED FOR EACH TEST.

Figure 2-58. Small Steam Engine Test (Schematic)

[15]Refers to the TBC-1 transport line to the Carter steam engine test assembly.

Additional Steam Control Devices. In the absence of an automatic steam control system, the approach was to use manual controls to maintain the steady-state steam conditions required for each engine test condition. Because the minimum thermal output of either the Garrett steam receiver on the TBC or the steam generator supplied by Carter might have been somewhat in excess of the Omnium-G power conversion system test requirement (which is 4 kW_t), it was necessary to provide additional steam controls to further reduce the thermal input to the Omnium-G engine.

The steam supplier, steam receiver capabilities on the TBC, and Omnium-G input requirements are given in Table 2-19.

Testing Outline. The testing program consisted of (1) preliminary proof tests, (2) preliminary subsystem operational tests, and (3) final total system performance tests.

Preliminary subsystem proof and operational tests consisted of the following:

(1) Steam Supply Subsystems: The fossil-fuel steam supply subsystem was proofed and operationally tested as indicated in item (2).

Table 2-19. Omnium-G Steam Engine Test Parameters

Steam Conditions	TBC-1/Receiver (Capability)	Omnium-G System Input (Requirements)
Thermal Output		
Maximum	70 to 80 kW_t	12 kW_e (approximate)
Minimum	20 kW_t	4 kW_e (?)[a]
Steam Temperature		
Maximum	565°C (1050°F)	315°C (600°F)
Minimum	150°C (300°F)	150°C (300°F)?
Steam Pressure		
Maximum	2000 psi	400 psi
Minimum	150 psi	300 psi

[a]This minimum value provides for testing a minimum power output of 1/3 the peak output that was measured at the Omnium-G mobile aperture by PDTS personnel.

(2) TBC-1 Steam Supply Source Tests: The entire receiver fluid system and steam transport lines were proof pressure tested for leaks. These tests included the Omnium-G special steam control, bypass, or check valves installed ahead of the engine steam inlet attachment. Operational tests included venting the steam outlet to the atmosphere to check manual controls for steam flow to the engine. These tests included flexing of the transport line due to concentrator travel.

Measurements made during these tests were as follows:

(1) Receiver measurements included standard temperatures, pressures, and flow rates. (The external temperatures on the outer shell were deleted if the number of active channels became critical. Receiver temperature limits of 1350°F and pressure limits of 2000 psi were not exceeded.)

(2) Steam transport line measurements included inlet and outlet temperatures and pressures. These measurements were used for the evaluation of transport losses. This loss was a correction to the system test results to establish system performance with a focal-mounted engine design.

Omnium-G power conversion subsystem tests consisted of appropriate proof and operational tests to assure proper installation and general operation prior to performance tests.

Steam control system tests measured steam conditions at the input to the engine (temperature, pressure, and flow rate) to determine the thermal efficiency of the engine. Operational tests of flow control were run to achieve stable engine steam input conditions at appropriate power levels required for the engine test. This test provided a first rough calibration of proper flow control settings for the various engine test conditions.

Omnium-G power conversion system performance tests were made to establish the thermal efficiency curve of the power converter over the power output range available for the Omnium-G system. Available Omnium-G engine design characteristics and performance estimates are:

Characteristic	Design Estimate
Steam inlet temperature (for engine)	315°C (600°F) maximum
Steam inlet pressure (for engine)	350 psi (approximate)
Steam flow rate (for engine)	90 lb/h at peak power
Peak power (output)	2.9 kW_e
Thermal efficiency	15% at 2.9 kW_e
Rev/min	1000

Tests were conducted to establish the thermal efficiency curve of the power conversion system (engine/generator) over an operating power output range of 0.5 to 3.0 kW_e using the following steam input conditions:

(1) Steam temperatures: 315, 230, and 150°C (600, 450, and 300°F)
(2) Steam pressure: 400 psi (maximum)
(3) Flow rate: 90 lb/h (peak)

During tests, consistent temperatures were maintained and the pressure varied to obtain the power output conditions. Early test emphasis was made covering the power output conditions in the low range (0.5 to 1.5 kW_e). The predicted thermal input to the power conversion system was about 8 to 12 kW_t. Expected power output and efficiencies were:

Power In, kW_t	Power Converter Efficiency, %	Power Out, kW_e
8 to 12	15	1.2 to 1.8
8 to 12	10	0.8 to 1.2
8 to 12	5	0.4 to 0.6

Where: (a) Peak engine steam temperature does not exceed 315°C (600°F).

(b) Tests were run for 20 minutes to obtain stable engine conditions.

Test measurements included the following:

(1) Steam input temperature (18 to 370°C) (0 to 700°F).

(2) Steam input pressure (0 to 500 psi).

(3) Steam input flow rate (0 to 50 lb/h).

(4) Steam output (of engine) temperature (18 to 120°C) (0 to 250°F).

(5) Steam output pressure (0 to TBD).

(6) Engine speed (0 to 1500 rev/min).

(7) Power output (0 to 3 kW_e).

(8) Water Inlet.

The results of these tests proved very difficult to assess due to the operational mode of the system. When the engine was coupled with the OG system, the large thermal storage in the mass of the receiver would allow

bursts of steam to the engine at which time it would operate reasonably well. However, this caused constant major oscillations in the power curve of varying time constant. This made data analysis extremely difficult. The results showed, however, that the engine was quite inefficient, perhaps never achieving more than 1-5% efficiency peak. However, after a burst, the receiver capacitance was depleted and the engine would stop until the mass was reheated, thus giving an average power production ranging from well below zero (i.e., not even generating enough for its own parasitic loads) to perhaps just above zero. This testing clearly indicated that the solar steam production system was considerably too small for the steam engine size. And, in addition to this component size mismatch, the steam transport piping needed much improvement to lower thermal losses between the dish and the engine.

An attempt was made to isolate the problems by running the OG engine from a separate steam source. During May and June 1981, the engine was set up in a special test rig with steam supplied by the Garrett receiver on the TBC-1 concentrator. These tests confirmed that the engine efficiency was very low, with many of the test runs showing efficiencies around 1 or 2% and none over 3-1/2%.

Omnium-G personnel were still convinced at this time that they could correct these deficiencies and took the engine back to their shop in Anaheim, California. The engine was returned to the PDTS in early September 1981. However, no data were obtained on the refurbished engine, as on one of its early test runs the piston seized in the cylinder. A decision was made to stop engine testing at this time, as the remainder of the equipment was required for the SNETCO project.

All Omnium-G steam engine testing was constantly plagued with mechanical, electrical, and control problems. From the very first tests in October of 1979 when the piston rods were bent due to ingesting water through the inlet valves until the final tests in September of 1981, the entire OG power production system ran only a few hours before another major difficulty would arise. At least in part, these problems apparently caused the Omnium-G Company to cease operations in 1982.

5. Solar Tests of Materials for Protection from Walk-Off Damage

A test program to evaluate protective materials that can withstand exposure to walk-off conditions without active cooling consisted of exposure to concentrated sunlight at a peak flux of about 7000 kW/m^2 for a time of 15 minutes.

a. Test Setup. For the materials tests, a fixture was designed in the form of "window frame" with outside dimensions of 380 x 330 mm (15 x 13 in.) and an opening 230 mm (9 in.) square. The sample was placed in this opening. The fixture was 114 mm (4.5 in.) thick and made from graphite, Grade 3499. Figure 2-59 is a photograph of the sample holder on TBC-1.

A key aim of the fixture design was to minimize conductive heat transfer from sample to test fixture and from test fixture to adjacent equipment. The

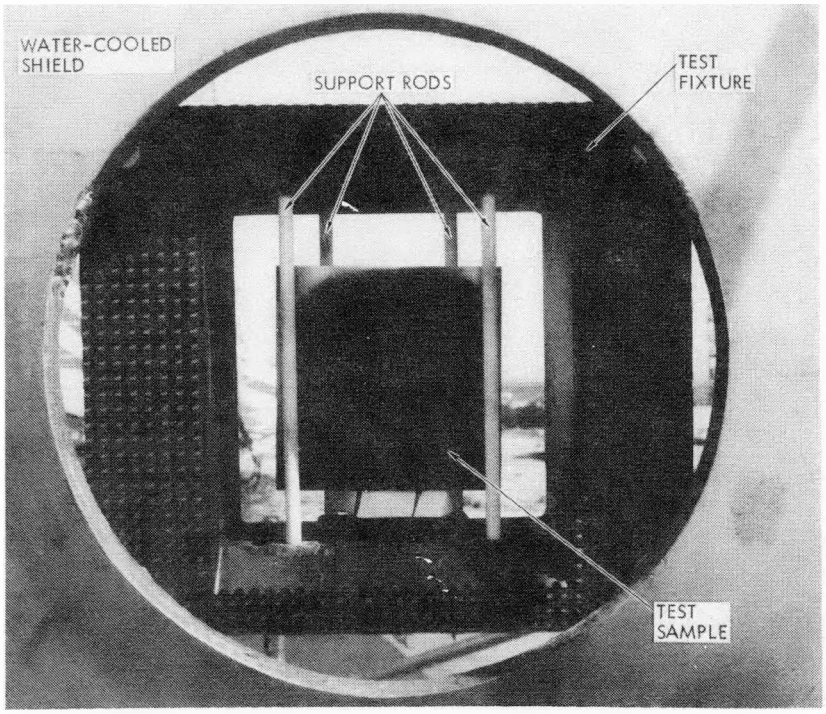

Figure 2-59. Test fixture and sample on concentrator, as set up for walk-off and acquisition tests. Fibrous silica sample mounted in fixture. View looking away from mirrors; photographed after sample was tested. Background landscape is visible through opening between sample and test fixture.

sample was prevented from falling out toward or away from the concentrator mirrors by graphite rods 10 mm (3.75 in.) in diameter, made of graphite, Grade 873S or HC. Rods were used to minimize thermal contact between support and sample. The support rods caused some local blockage of concentrated sunlight; this somewhat increased the thermal gradients and thermal stresses in the samples.

The pointing of individual mirrors on TBC-1 and the distance between the mirrors and the receiver aperture were set to simulate the corresponding distribution of concentrated sunlight expected with PDC-1, a concentrator designed for mass production. The receiver was designed for a flux pattern peaking at 7000 kW/m^2 at an insolation of 1 kW/m^2.

For materials testing, the side of the sample facing the mirrors was positioned 25 mm (1 in.) closer to the mirrors and to the waist of the concentrated pattern of sunlight than the position of the receiver aperture during module test. The distribution of solar flux in this materials test plane was measured with the flux mapper. The peak measured flux in the materials test plane was 7800 kW/m^2 at an insolation of 1 kW/m^2. In the materials tests, the actual insolation was somewhat lower than 1 kW/m^2, and

the peak flux in these tests approximately matched that for the receiver design conditions.

For spillage tests, one edge of the sample was tapered and rounded to form a lip (Figure 2-60). Two chromel-alumel thermocouples, wire diameter 0.25 mm (0.010 in.), were inserted through the back of the 26-mm (1.0-in.)-thick samples, terminating 0.5 mm (0.02 in.) from the lip. The samples were mounted at various radial and axial positions to simulate spillage conditions (such as flux levels) that might be encountered with various solar thermal power modules. Samples were mounted off center so that only the edge of the solar spot struck the sample.

b. Materials and Samples Tested. The general types of materials tested included alumina, zirconia, mullite, silica, silicon carbide, and graphite. Also tested were aluminum and copper with temperature-resistant coatings and graphite with temperature-resistant coatings.

The preferred sample size selected was 200 x 200 x 25 mm (8 x 8 x 1 in.) so that samples were large enough in comparison to the solar spot and were thick enough to provide reasonable protection. A few thicker specimens (about 35 mm, 1.4 in.) were tried to see if greater thickness would improve performance. Because many samples were provided free of charge, they were often smaller than preferred. Some were as thin as 0.4 mm (0.017 in.); these were provided more because of interest in using them for protection during normal acquisition and deacquisition than for walk-off protection.

c. Test Procedures and Rationale. Tests were made at insolation levels of 580 to 960 W/m^2. The concentrator was pointed at the sun with its shutter closed and set to track the sun automatically. The shutter was then opened and the sample observed. Observations were made by two means:

(1) An observer stationed in the shadow of the concentrator watched the sample throughout each test by way of an opening in the center of the mirror array using binoculars and dark glasses.

(2) The concentrator operator observed the sample on television, utilizing a black-and-white television camera mounted on a receiver support leg of the concentrator, and imagery was recorded on a video cassette recorder.

All samples were weighed, measured, observed visually, and photographed in color before and after solar test. Bulk densities prior to testing were calculated from the measured dimensions and weights.

To provide a rough measure of solar absorptivity at minimum cost, sample brightness was measured outdoors, in open shade, with a Pentax-type brightness meter designed for use in photography, and compared with the brightness of Kodak white and gray reflectance standards placed adjacent to the sample. Insolation and weather data were recorded digitally during testing.

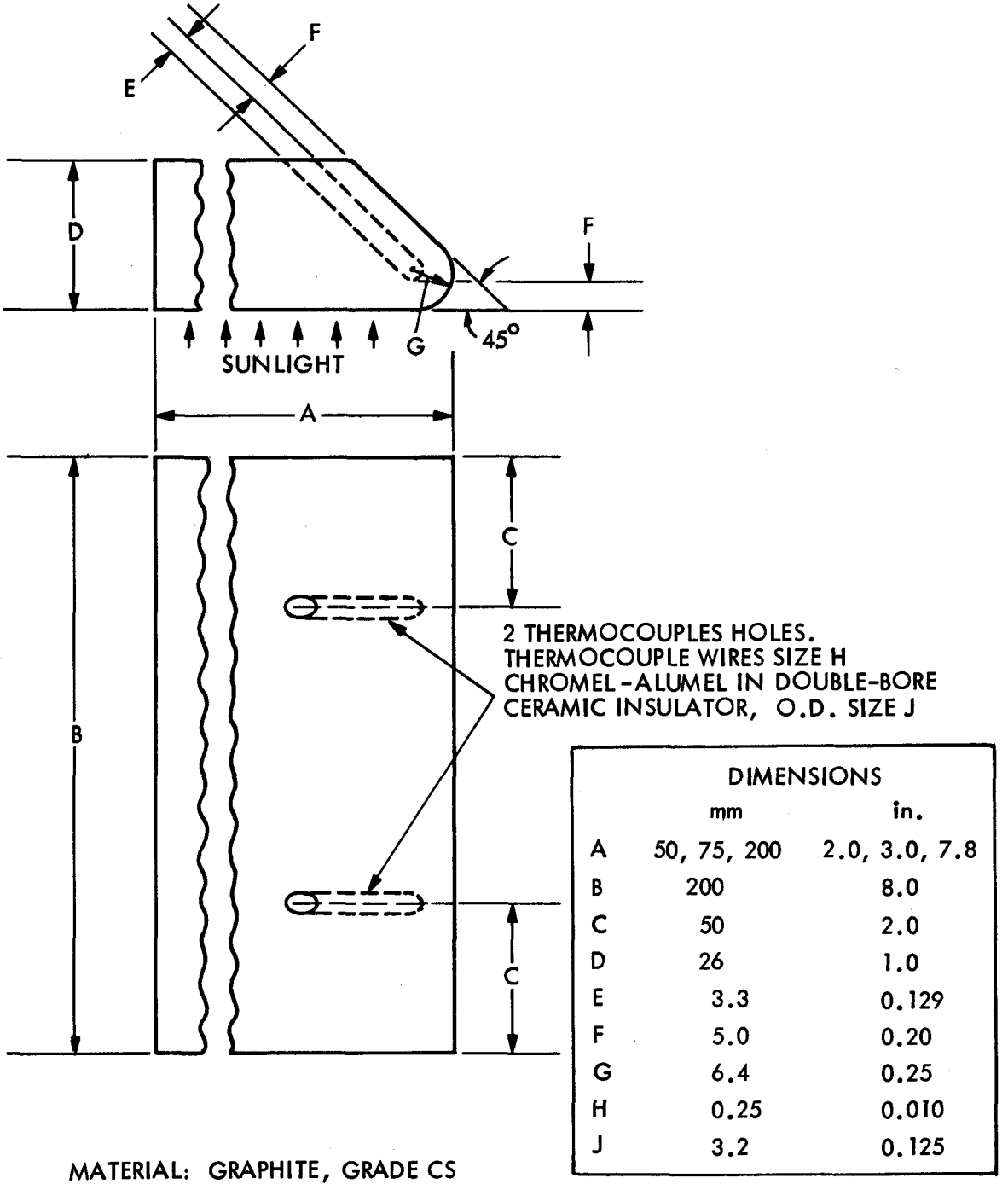

	DIMENSIONS	
	mm	in.
A	50, 75, 200	2.0, 3.0, 7.8
B	200	8.0
C	50	2.0
D	26	1.0
E	3.3	0.129
F	5.0	0.20
G	6.4	0.25
H	0.25	0.010
J	3.2	0.125

Figure 2-60. Sample for Spillage Tests

Walk-Off Tests. All of the materials investigated were tested for their ability to sustain walk-off of the solar beam.

Tests were terminated by closing the shutter 15 min after it was opened, or when the sample failed, whichever occurred first. For this purpose, failure was initially defined as observation of cracking or of melting and dripping. (To reduce the risk of damage to the concentrator mirrors from falling fragments or hot drops, tests were constrained to sun elevations below 45 deg. It was found during testing that some samples cracked part-way, but did not fall apart; the procedure was later changed to continue the test despite such cracking. Also, some samples that survived the test without melting or cracking apart were retested for total exposure times up to 45 min.

Several samples were tested wet to simulate exposure to rain followed by sunlight and walk-off. They were soaked in water to a depth of 15 to 30 cm (6 to 12 in.) prior to solar testing.

Temperature measurements, with minor exceptions, were not made on the samples during test because of cost constraints.

Acquisition Tests. Tests aimed at evaluating behavior under acquisition and deacquisition conditions and under spillage conditions were conducted only on graphite. These tests were run because some grades of graphite appeared promising in the walk-off tests, but there was concern that the rate of loss of graphite by oxidation might be excessive under the long cumulative exposures associated with acquisition/deacquisition and spillage.

Two graphite samples were tested under conditions simulating repeated acquisition and deacquisition. They were mounted in the same way as the samples for walk-off testing. The acquisition/deacquisition tests consisted of multiple cycles of opening and closing the shutter, each approximately 1 s open, 10 to 19 s closed. Maximum exposure was 2000 cycles. Insolation in these tests was 780 to 960 W/m^2; acquisition and deacquisition in service probably would be primarily at low sun elevation, when insolation would be lower.

Spillage Tests. Solar tests to allow estimation of the long-time oxidation rate were made by maintaining the temperature of graphite samples simulating a tapered aperture lip. The lip, with thermocouples inserted, was placed 75 to 175 mm (3 to 7 in.) from the center of the spot of sunlight (representing aperture diameters of 150 to 350 mm, 6 to 14 in.) and at various axial positions. Flux density at the lip position nearest the spot center varied from less than 1 to over 1000 kW/m^2 depending on sample position.

d. Results and Discussion. Results of the solar tests are summarized in Table 2-20. More detailed results of these and other measurements are given in Reference 16. The great majority of these samples melted or shattered in test, many of them within the first few seconds of solar exposure. The only materials tested that appeared promising for walk-off protection were graphite, Grades G-90 and CS, and high-purity slip-cast silica.

Table 2-20. Summary of Results of Walk-Off Tests

Material Type		Thickness, mm	Failure Mode	Time
Graphite	3499	26	Shattered	1 to 8 min
	8826	26	Shattered	1 to 1-1/2 min
	CS	14-50	Cracked halfway (1 of 10 survived)	10 s to 14 min
	HLM	24-26	Shattered	1 to 1-1/2 min
	G-90	24-25	(Survived)	30 min
	Cloth	0.4	Holed	30 s
SiC		6-32	Shattered	1 s
SiO_2	Slip-cast, high purity	18-21	Slumped	1-1/2 to 4 min
	Slip-cast, commercial	20-26	Dripped	10 s
	Fibrous, glazed	41	Dripped	7 s
Silicates	Mullite	32-38	Melted	1 to 4 s
	Processed kaolin	27	Melted	3 s
	Cordierite	25	Melted	2 s
	Alumina-boria-silica	0.5-0.7	Melted	1 s
Al_2O_3	Paper	0.4-1.4	Melted	2 to 6 s
ZrO_2	Cast and sintered	29	Melted	20 s
	Fibrous board	25	Melted	1 min
	Cloth	0.5	Melted	8 s
Copper		26	Melted	1 to 3 min
Aluminum		1.8	Melted	1 s
Steel		2	Melted	2 s
Polytetrafluoroethylene		38	Melted	2 min

Data showing the effect of the wind on mass loss for Grades CS and G-90 graphite is presented in Figure 2-61.

6. Testing of a Special Pyrheliometer Shroud (Reference 17)

Circumsolar radiation manifests itself when the image of the sun is covered by the calorimeter and there is a bright halo around the calorimeter.

Accurate determination of the circumsolar radiation requires an instrument like the one developed by Lawrence Berkeley Laboratories (LBL) of the University of California. Characteristics and performance of the LBL circumsolar telescope is described later in this subsection. The special pyrheliometer shroud is a simple and easy-to-use device to determine circumsolar radiation.

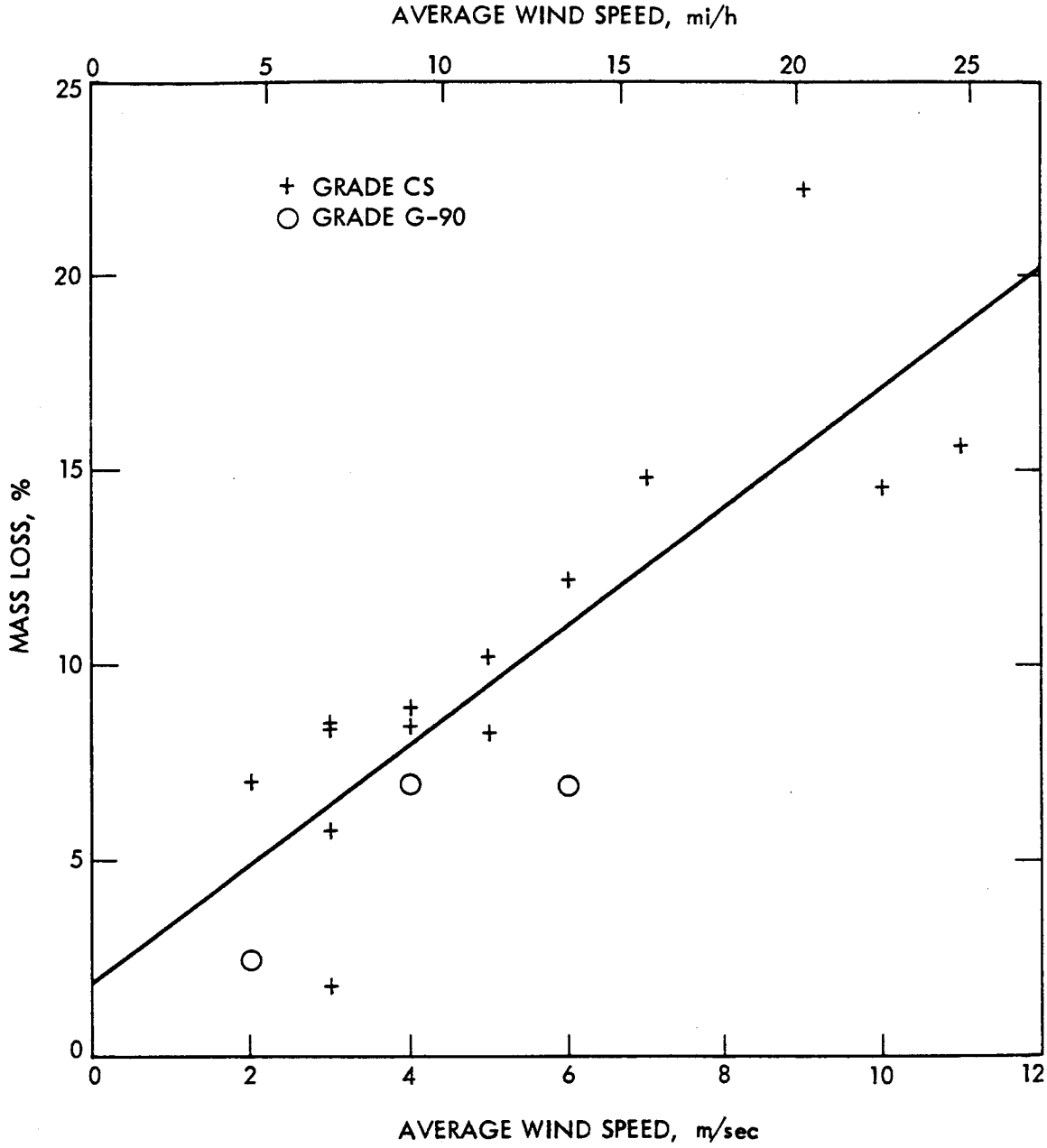

Figure 2-61. Effect of Wind Speed upon Mass Loss by Oxidation for Graphite, Grades CS and G-90, in Walk-Off Tests. (Mass losses normalized to 15 minutes exposure and 25 x 200 x 200 mm (1 x 8 x 8 in.) sample. Line is least-squares fit.)

To ensure that the insolation values accurately represent the input power to a power conversion unit, it is important that the field of view (FOV) of the concentrator aperture and the insolation radiometer are the same. The word "radiometer" is used to refer to both radiometers and pyrheliometers. If the calorimeter and the power conversion unit have the same aperture, the radiometer can be used to normalize all power measurements to a standard insolation value x. (The standard value assumed is 1000 W/m^2 for the JPL data.)

Prior to testing at the PDTS, the pyrheliometer shroud was analyzed and fabricated. Three instruments were used to measure the insolation: an Eppley Normal Incidence Radiometer (NIP) and two versions of the cavity radiometer developed by J. M. Kendal, Sr., at JPL. One of the Kendall radiometers was a Mark VI windowless design used for calibration of radiometers and the other was a Mark III quartz window design used for routine field measurements. The shrouds used to limit the FOV of the radiometers were designed to simulate the FOV of PDC-1 with the cold-water cavity calorimeter (Figure 2-62).

a. Experimental Results. To verify the expected advantages of using an FOV-limiting shroud on an insolation radiometer, a series of calorimeter measurements were made using PDC-1 and the shrouded radiometers. One of the radiometers was an Eppley NIP mounted on the concentrator. The other radiometers were of the Kendall type and were attached to an equatorial mount with a clock drive. The boresight alignment images were checked frequently during the measurement period to ensure that no erroneous data resulted from tracking errors.

The thermal power measured by the calorimeter and the insolation measured by the radiometers were plotted for each measurement period. To test the validity of this technique, the calorimeter values were divided by each of the radiometer values and the results plotted. These ratios gave the net power output of the concentrator normalized to 1000 W/m^2 under sky conditions, which varied from light haze to thin cirrus clouds. No completely clear days occurred during the time these tests were made. There is no reason to believe that the normalized power values would differ from these values for completely clear skies. During the passage of the cirrus clouds, the normalized power values showed a substantial variation over short periods of time as a result of long time constants of the calorimeter relative to the time constants of the radiometers.

Figures 2-63 and 2-64 show the radiometer data plots for two different days, and Figures 2-65 and 2-66 show the corresponding plots of the direct and normalized power measurements. Figure 2-65 demonstrates that the normalized power is relatively constant under a wide range of sky conditions. The value of the normalized power in this figure was too high because of a faulty flow meter. This problem was corrected and the normalized power values shown in Figure 2-66 more accurately represent the performance of PDC-1.

The insolation values measured with these modified radiometers were lower than the values that would have been obtained with standard

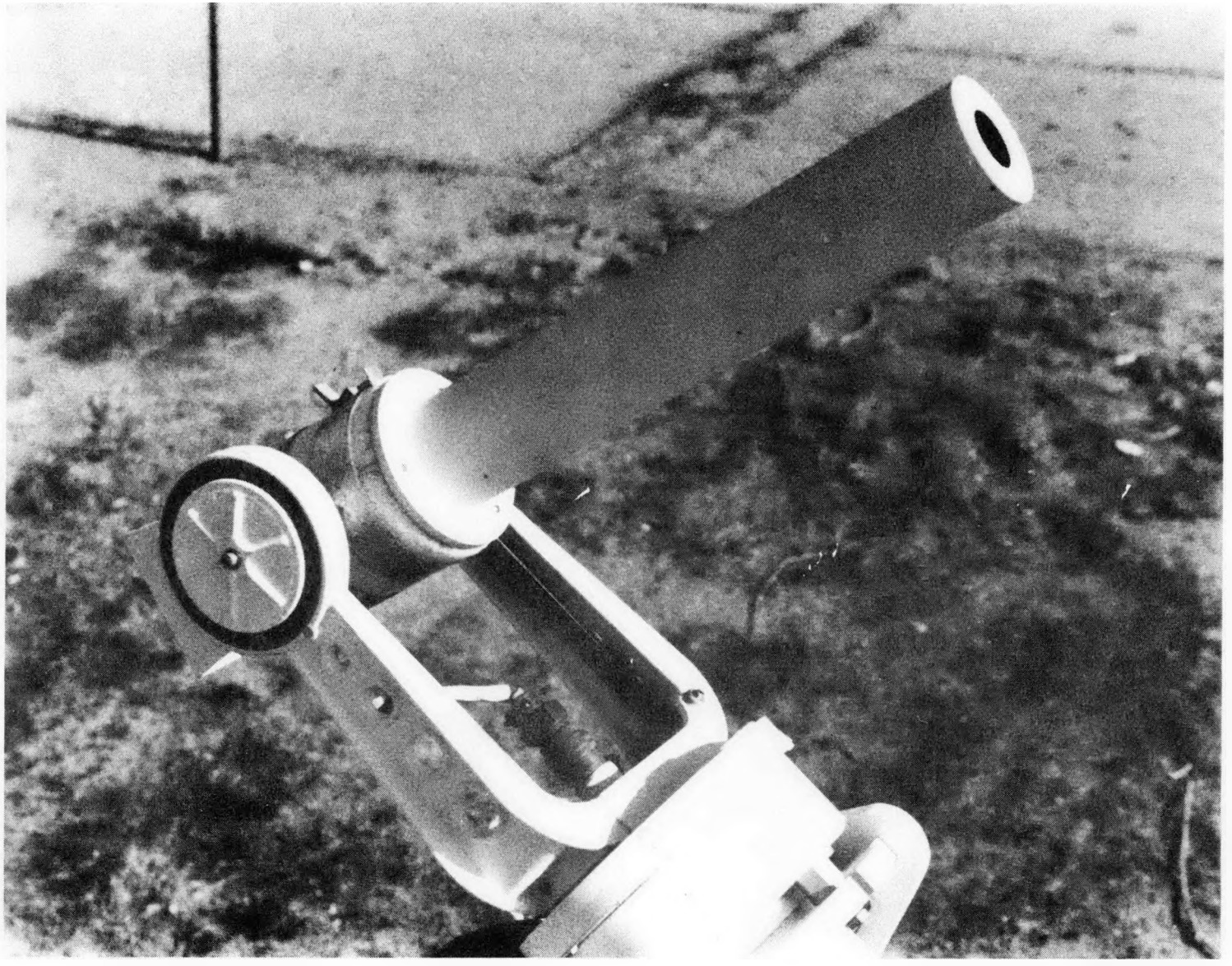

Figure 2-62. Radiometer with Shroud

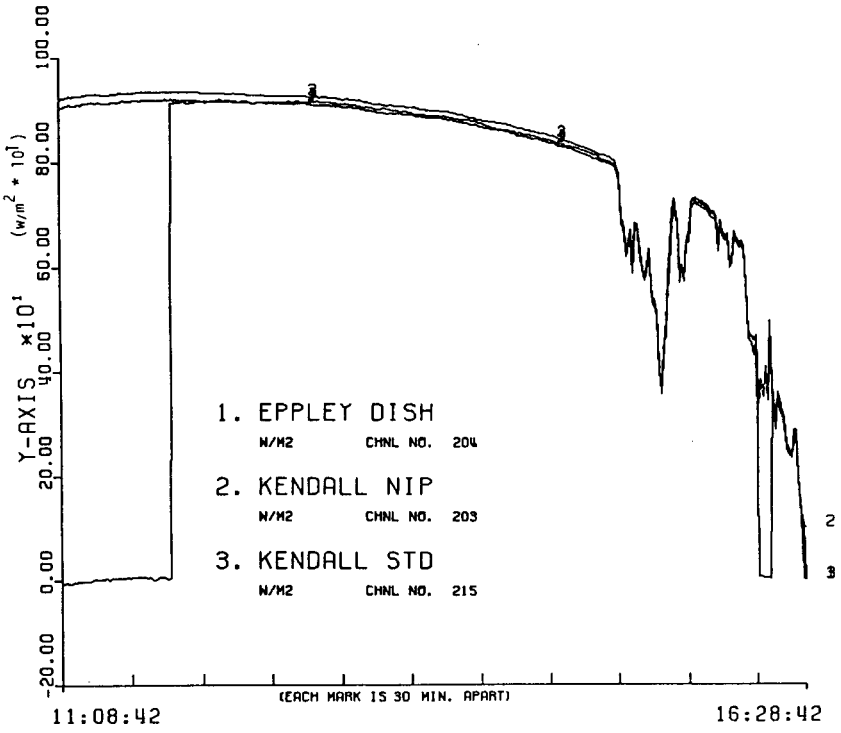

Figure 2-63. Radiometer Plot for February 22, 1983

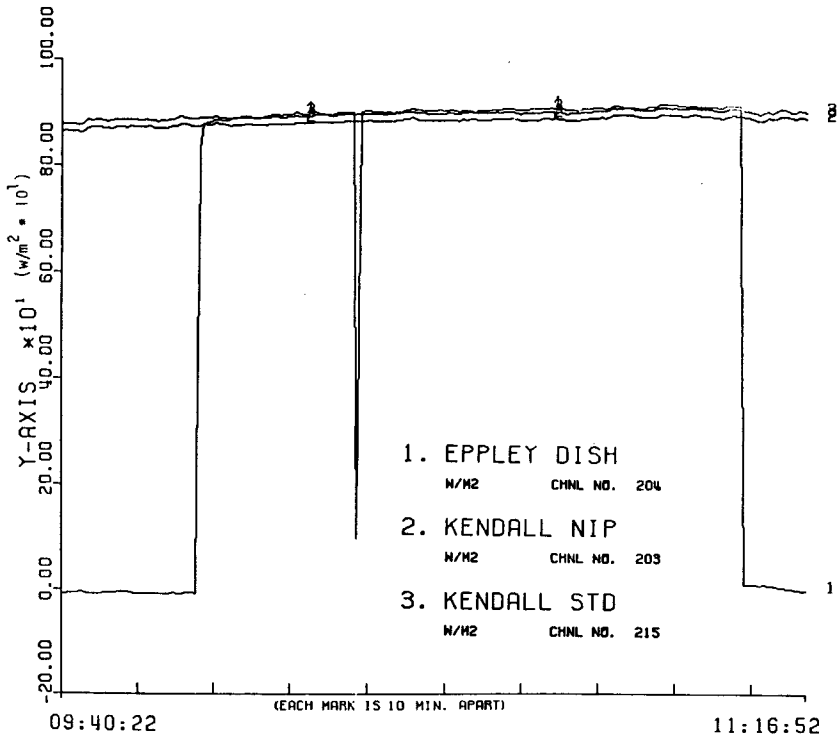

Figure 2-64. Radiometer Plot for July 14, 1983

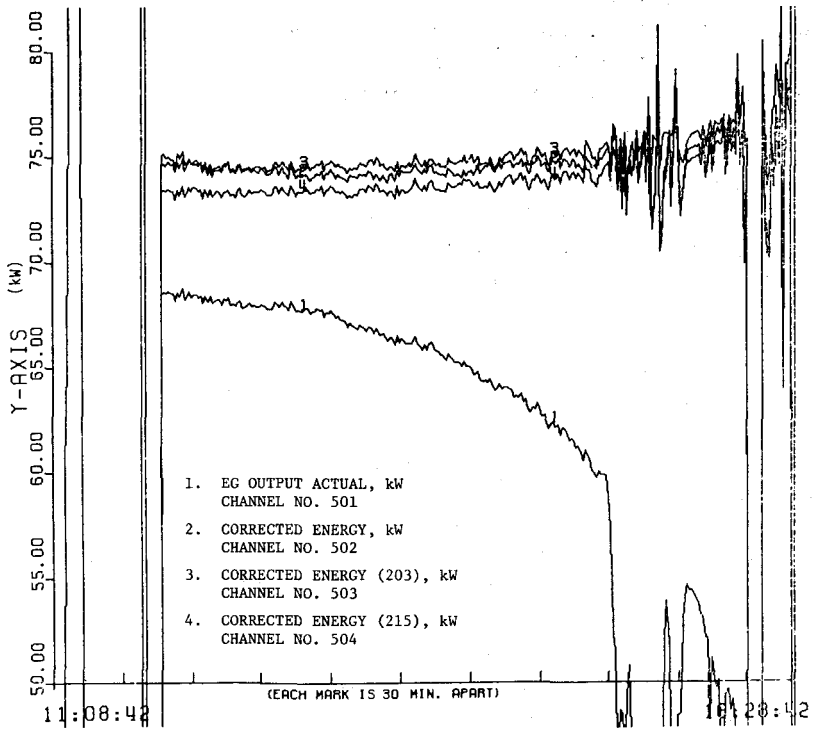

Figure 2-65. Plots of Direct and Normalized Power, February 22, 1983

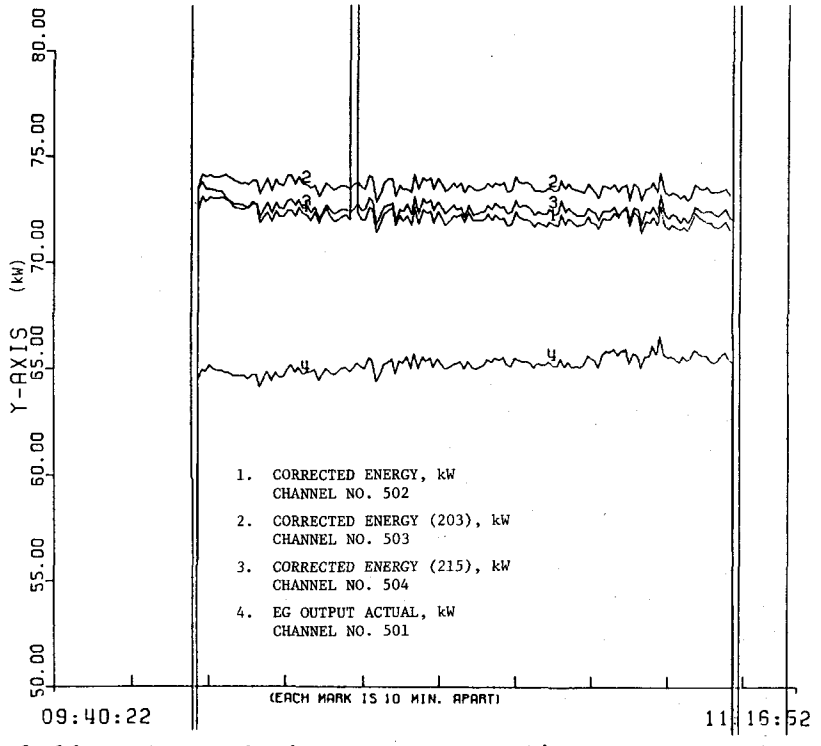

Figure 2-66. Plots of Direct and Normalized Power, July 14, 1983

radiometers. However, the purpose of these measurements was to determine the relationship between the radiometers and the net power throughput of the concentrator with a specific aperture. This calibration would have been used to determine the operating efficiency of the power conversion unit that was to have been used with this concentrator.

During this limited test program, it was not possible to make a direct comparison between these shrouded radiometers and standard radiometers. However, this test program did demonstrate that the normalized power output of PDC-1 was constant under a wide range of sky conditions.

b. Lawrence Berkeley Laboratories Circumsolar Telescope Tests. The circumsolar telescope was developed by LBL in order to obtain solar radiation measurements that could be used for accurate prediction of the performance of solar thermal conversion systems utilizing focusing collectors. The instrument is designed to measure the effects of atmospheric conditions on the direct and circumsolar components of the solar flux. It also incorporates the measurement of total hemispherical insolation in the horizontal plane and in a plane normal to the direction of the sun.

The operation of the instrument is almost completely automatic with only routine servicing required. Once set up and operating, it will track the sun, record data for an entire day, move back during the night so as to acquire the sun and continue the process the following day. Routine checking and date setting each morning are the only daily requirements. Once a week, the magnetic tape must be changed and routine maintenance performed. The telescope incorporates several provisions to protect itself from rain, dust, and dew. However, it should be covered (a weather-proof bag is supplied) in severe storms or during extended periods of inclement weather.

The main components of the system are the solar tracking platform, the scanning telescope, the pyrheliometer, two pyranometers, and the instrument rack. The instrument rack consists of signal conditioner modules, a multiplexer, an A/D converter, a master controller, an incremental digital tape recorder, a digital clock, and power supplies. The telescope is equipped with a device for determining true north, leveling screws, latitude scale, and wheels to facilitate relocation.

In operation, the solar guider accurately aligns the instrument platform at the center of the sun. The telescope body scans back and forth across the image of the sun and circumsolar region to an angle of ± 3 deg (the solar diameter is about 32 minutes of arc). A small aperture located in the image plane restricts the angular view of the telescope to a fraction of the size of the solar disk. The light passing through this aperture is chopped, filtered, detected, digitized, and written on a magnetic tape as a function of the angular position. Two sets of optical filters, stepped synchronously, enable determination of the spectral dependence of the light for both the scanning telescope and the normally incident flux determined by the pyrheliometer. The output from the pyrheliometer, pyranometers, and auxiliary equipment is also digitized and recorded on tape once each scan.

This instrument was used to acquire data at the PDTS but, unfortunately, processing of raw data was not done at the PDTS. Instead, magnetic tapes were sent to LBL. Therefore, little can be said about the variation of circumsolar radiation at the PDTS because almost two years of data was not processed there; neither has LBL's processed data been made available to JPL.

D. TESTING OF SOLAR POWER MODULES

1. Organic Rankine-Cycle Module

Testing was conducted on an organic Rankine-cycle (ORC) power module and its ancillary equipment by the Ford Aerospace and Communications Corporation (FACC), Newport Beach, California, with management and test support from JPL. Extensive reports of the test experience have been issued by FACC and JPL (References 3 and 18). This section is primarily adapted from those reports.

The power module consists of an air-cooled, regenerative 20-kW_e turbo-alternator system coupled to a cavity-type receiver (boiler), all mounted at the focus of a parabolic dish concentrator. The ancillary equipment includes a complete computer-based plant control subsystem and an electrical transport/conditioning subsystem with voltage control and grid interface capability.

Developmental testing of individual components and qualification testing of major subsystems began in 1981. Full-up system testing "on the sun" was conducted in February and March of 1982 at the PDTS utilizing the 11-m diameter TBC.

a. System Description. The solar concentrator and the receiver/engine located at its focus is defined as the "power module." Ancillary equipment consists of a switchboard, inverter, power cabling, and computer and is designed to be centrally located in order to interface with multiple modules that would comprise a typical power plant.

The receiver/engine/alternator is called the power conversion assembly (PCA) and performs the task of converting concentrated sunlight into electrical energy. It does this by boiling the toluene working fluid in a cavity-type receiver and using the 399°C (750°F) vapor to drive a single-stage, axial-flow turbine directly coupled to a permanent magnet alternator. The turbo-alternator, shown in Figure 2-67, operates at speeds up to 60,000 rev/min. The toluene circulates in a closed loop system and is pumped back to the receiver as a liquid after passing through a regenerator in an air-cooled condenser (Figure 2-68).

The high-frequency ac power from the alternator is first rectified to dc so that it may be combined with outputs of other power modules. The dc electrical power is inverted to grid-compatible 3-phase ac. Unattended plant operation is made possible by a computer-based control subsystem that provides dynamic control of all PCA functions, monitors safety functions, and records performance data.

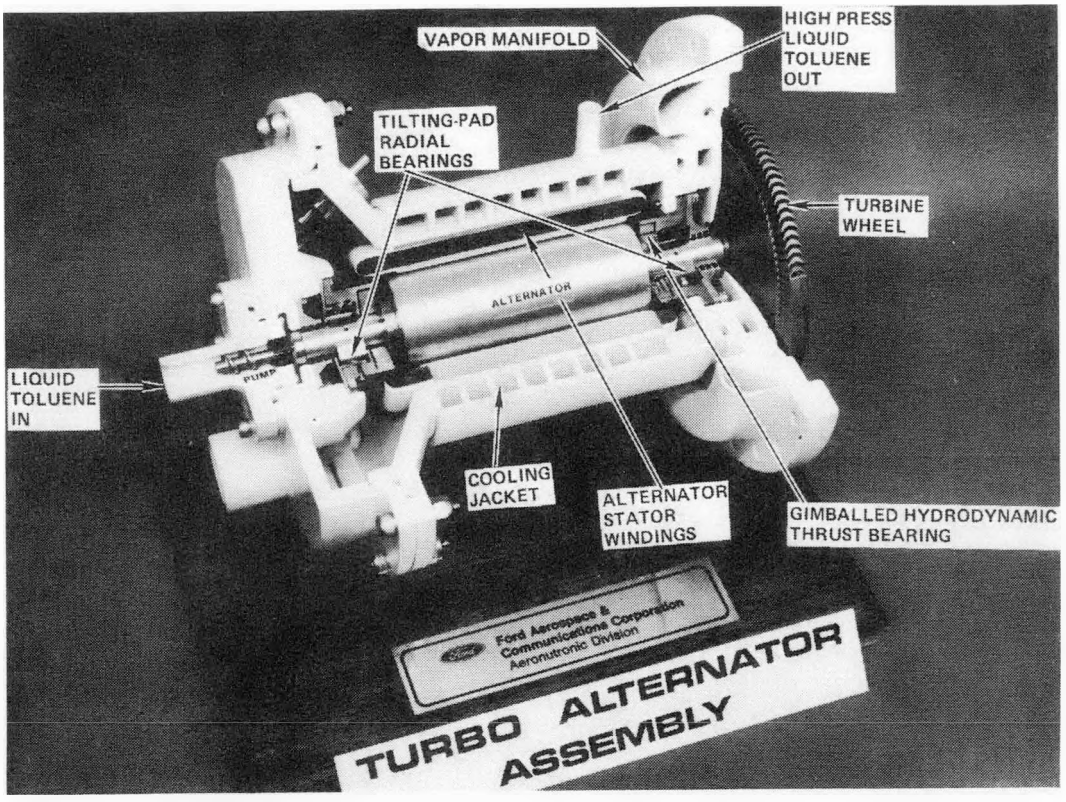

Figure 2-67. ORC Turbo-Alternator Assembly

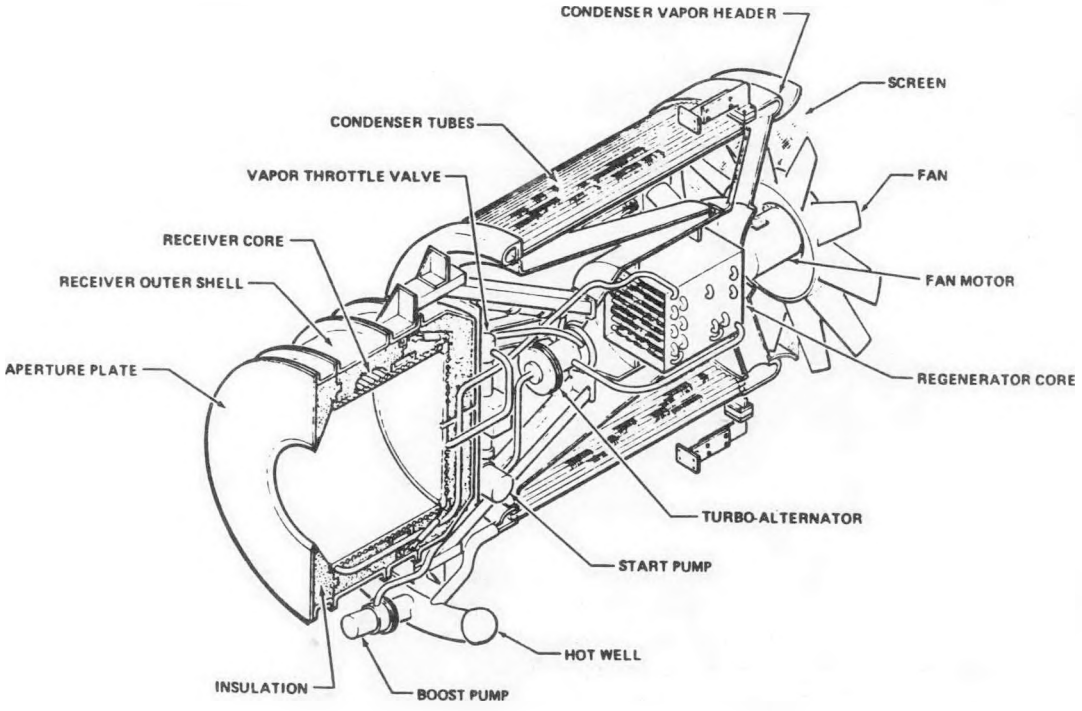

Figure 2-68. ORC Power Conversion Subsystem

b. ORC Test Program. The PCA and associated system components were subjected to a series of development and qualification "ground" tests prior to installation and test on a test bed concentrator at the PDTS. These tests included:

(1) Full functioning of the receiver and vapor control valve at FACC facilities using simulated solar flux provided by a 100 kW electrical radiant heater and a toluene test loop.

(2) Operation of the two types of computers used in the system was verified by means of a hardware-in-loop simulator.

(3) The ORC engine was tested at Barber-Nichols (Arvada, Colorado) on a tilting test rig to map the performance at various attitudes.

(4) Key electrical components were tested at the vendors' laboratories: The dc-ac inverter was tested by Nova Electrical Manufacturing Corp.; the permanent magnet alternator by Simmonds Precision.

(5) The PCA (engine/alternator plus receiver) was assembled at FACC and tested with the 100 kW electrical heater. The inverter was also used in these tests; it performs the key control function of maintaining a constant dc voltage, which is equivalent to PCA load control.

c. Test Setup. The PCA was installed on TBC-1 at the PDTS in January 1982. As shown in Figure 2-69, a water-cooled sliding plate and shield were used to protect the receiver face plate from solar flux during the slow acquisition and detrack rate of the TBC. The sliding plate was also used to simulate dynamic events such as cloud passage and to block the flux to the receiver in the event of an emergency condition.

The test setup included the complete power module with local microprocessor, the central computer, the inverter, switchboard, uninterruptible power supply, load bank, and grid interface protective devices. Weather permitting, on-sun testing was performed between February 8 and March 26, 1982. A total of 33.5 hours of test time was accumulated; 16 test runs were obtained, ranging from 5 minutes to 7 hours duration under all levels of solar insolation and cloud conditions. A portion of the tests were conducted with some of the TBC mirror panels covered in order to obtain low-power data. The emphasis for the early runs was placed on transient operation to permit evaluation of the control subsystem. This was accomplished by opening and closing the sliding plate for predetermined intervals.

d. Data Collection. The data collection technique used for the ORC solar tests utilizes the central computer for real-time processing and recording of performance and test data, and post-test printing or plotting of selected data channels. It is capable of recording, printing, and plotting

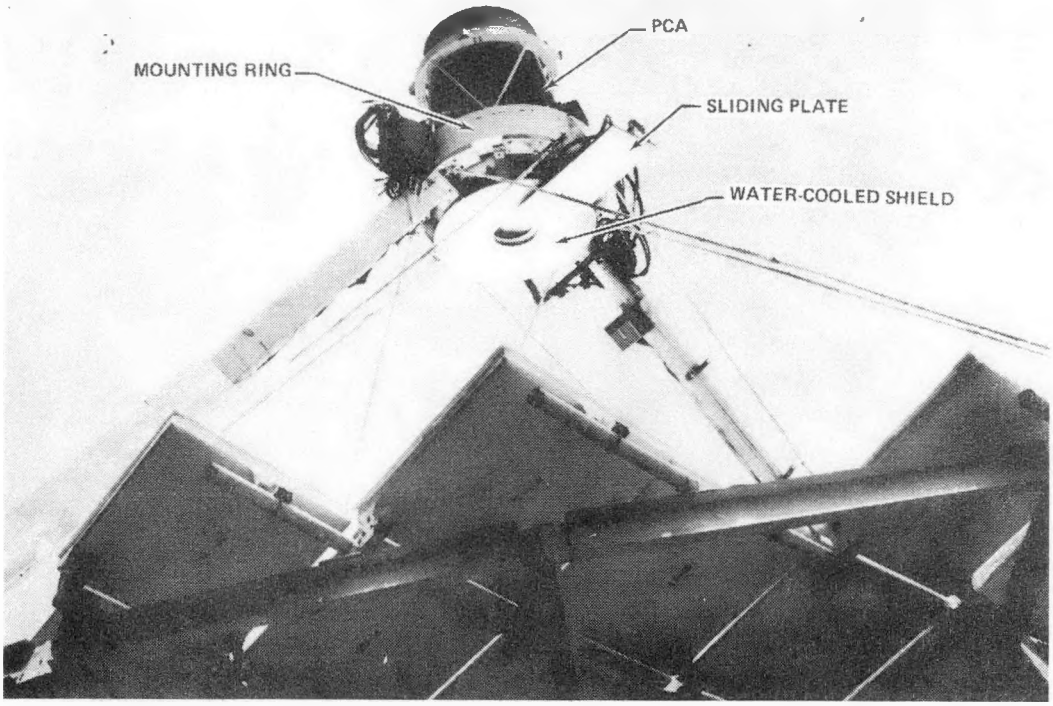

Figure 2-69. View of Aperture End of ORC Unit During Operation On-Sun

103 test parameters per second (93 were used for the tests in February-March, 1983), and proved to be invaluable in presenting test results. The data that are permanently filed on magnetic tape for later printing or plotting by the computer include:

(1) Key temperatures and pressures.

(2) Voltage and current, both ac and dc.

(3) Turbine speed.

(4) Liquid reservoir level.

(5) Vapor control valve position and commanded position.

(6) Status of discrete events/commands.

(7) Weather data, solar flux, and wind speed.

(8) Power, energy, and efficiencies (calculated from data inputs).

Table 2-21 is a sample page of PCA performance data recorded on Run 13 of March 3, 1982. This is only one of 14 pages of printout available; the complete list is documented in Reference 3.

Table 2-21. Typical ORC PCA Performance Data (March 3, 1982; Run 13)

PRINT 02R

TIME			CONDENSATE EXIT TEMP	REGEN LIQUID INLET TEMP	REGEN LIQUID EXIT TEMP	ALTERNATOR TEMP	RECEIVER OUTLET PRESS	TURBINE INLET PRESSURE	TURBINE EXIT PRESSURE	CONDENSER EXIT PRESS	SYSTEM PUMP INLET PRESS	SYSTEM PUMP OUTLET PRESS
			DEG. F	DEG. F	DEG. F	DEG. F	PSIA	PSIA	PSIA	PSIA	PSIA	PSIA
12:00:00	0	0	0082.8	0091.6	0380.4	0056.6	0494.0	0410.8	0001.5	0001.1	0027.8	0527.6
12:00:01	0	0	0082.8	0091.7	0378.4	0056.6	0494.0	0416.0	0001.5	0001.1	0027.4	0528.4
12:00:02	0	0	0082.6	0091.7	0378.4	0056.5	0493.6	0410.0	0001.5	0001.1	0027.8	0528.0
12:00:03	0	0	0082.7	0091.7	0378.8	0056.5	0494.4	0410.4	0001.5	0001.1	0027.7	0528.0
12:00:04	0	0	0082.6	0091.7	0377.6	0056.5	0494.4	0409.6	0001.5	0001.1	0027.8	0527.2
12:00:05	0	0	0082.7	0091.7	0378.4	0056.5	0494.4	0413.2	0001.5	0001.1	0027.4	0528.8
12:00:06	0	0	0082.6	0091.4	0378.4	0056.6	0494.4	0410.8	0001.5	0001.1	0027.6	0528.8
12:00:07	0	0	0082.6	0091.7	0376.8	0056.4	0494.4	0410.8	0001.5	0001.1	0027.7	0528.8
12:00:08	0	0	0082.6	0091.5	0378.0	0056.6	0494.4	0410.8	0001.5	0001.1	0027.8	0528.4
12:00:09	0	0	0082.6	0091.5	0378.8	0056.4	0494.4	0411.2	0001.5	0001.1	0027.5	0528.4
12:00:10	0	0	0082.6	0091.5	0378.8	0056.2	0493.6	0414.4	0001.5	0001.1	0027.5	0529.2
12:00:11	0	0	0082.5	0091.4	0378.4	0056.5	0493.6	0412.8	0001.5	0001.1	0027.6	0528.0
12:00:12	0	0	0082.5	0091.4	0378.4	0056.7	0494.0	0417.6	0001.5	0001.1	0027.7	0528.8
12:00:13	0	0	0082.4	0091.0	0378.4	0056.6	0494.8	0411.6	0001.5	0001.1	0027.9	0528.4
12:00:14	0	0	0082.4	0091.4	0378.4	0056.4	0494.8	0410.8	0001.5	0001.1	0027.7	0528.0
12:00:15	0	0	0082.5	0091.5	0378.4	0056.6	0494.4	0410.4	0001.5	0001.1	0027.8	0528.0
12:00:16	0	0	0082.7	0091.3	0378.4	0056.2	0494.8	0409.6	0001.5	0001.1	0027.8	0528.0
12:00:17	0	0	0082.4	0091.4	0379.2	0056.7	0494.0	0414.0	0001.5	0001.1	0027.7	0527.6
12:00:18	0	0	0082.2	0091.3	0378.4	0056.6	0492.0	0410.4	0001.5	0001.1	0027.8	0528.4
12:00:19	0	0	0082.3	0091.3	0378.4	0056.6	0495.6	0410.8	0001.5	0001.1	0027.8	0527.6
12:00:20	0	0	0082.3	0091.2	0378.4	0056.7	0495.2	0402.8	0001.5	0001.1	0028.0	0527.6
12:00:21	0	0	0082.3	0091.3	0379.2	0056.6	0495.6	0415.6	0001.5	0001.1	0027.7	0528.4
12:00:22	0	0	0082.1	0091.2	0378.4	0056.7	0494.4	0410.4	0001.5	0001.1	0027.8	0527.6
12:00:23	0	0	0082.1	0091.1	0378.4	0056.7	0494.0	0414.4	0001.5	0001.1	0027.6	0529.2
12:00:24	0	0	0082.2	0091.1	0379.6	0056.6	0494.4	0410.8	0001.5	0001.1	0027.6	0528.4
12:00:25	0	0	0082.3	0091.0	0378.4	0056.6	0494.4	0415.6	0001.5	0001.1	0027.8	0528.4
12:00:26	0	0	0082.1	0091.0	0378.0	0056.7	0494.4	0410.8	0001.5	0001.1	0027.8	0528.4
12:00:27	0	0	0082.1	0091.0	0378.4	0056.6	0494.4	0406.0	0001.5	0001.1	0027.8	0527.2
12:00:28	0	0	0082.0	0091.0	0379.2	0056.6	0494.4	0412.4	0001.5	0001.1	0027.7	0528.4
12:00:29	0	0	0082.1	0091.0	0378.4	0056.8	0494.4	0410.8	0001.5	0001.1	0027.7	0528.0
12:00:30	0	0	0082.1	0091.1	0376.8	0056.6	0495.6	0406.0	0001.5	0001.1	0027.8	0527.2

Figures 2-70 through 2-75 are a representative sample of the actual computer printouts of test data for a time period of 08:30 to 15:30 recorded on March 3, 1982 (Run 13). These test results provide typical performance characteristics of the ORC PCA during a 7-h run under automatic computer control. Figure 2-70 shows normal, clear-sky operation interrupted by only one early cloud passage and five intentional closures of the water-cooled plate. Figure 2-70 shows the position of the vapor valve (controlled by the local microprocessor) to maintain the desired 400°C (750°F) receiver outlet temperature. The first engine start and subsequent restarts were under the control of the microprocessor, which senses temperature and pressure in the receiver and commands start-up (or other modes such as shutdown or idle) based on predetermined criteria. At noon, the measured insolation was 983 W/m^2 after correction for estimated circumsolar effects.

Figure 2-71 shows that dc voltage out of the rectifier is controlled by the inverter to a preset value of 500 $\pm$5 V except during periods of very low power output ("idle mode") while the output current varies directly with power level. As shown in the figure, turbine speed is also virtually constant at 48,000 rev/min (indirectly controlled by the voltage set-point) except during periods of idle mode when the speed is ~35,000 rev/min.

Figure 2-72 is a plot of the relative power levels into and out of the receiver and the engine/alternator. Note that for each sliding plate re-opening, there is a momentary overshoot in receiver output power; this is due to a short period surge in toluene flow rate (from the valve opening response) coupled with removal of stored energy in the copper core of the receiver. At noon, the receiver input power[16] was 74.4 kW_t, receiver output power was 70.8 kW_t, and engine power (dc) output was measured at 16.2 kW_e.

Figure 2-73 shows receiver efficiency and corresponding measured wind speed and insolation. For the aforementioned noon data point, receiver efficiency is not a strong function of wind speed, despite gusts up to 13 to 14 m/s (30 mi/h).

Figure 2-74 shows key pressure data for Run 13. The pressure drop between the inlet to the receiver (approximately the same as pump outlet pressure) and the outlet is about 30 psi. The pressure drop between the receiver outlet and turbine inlet is primarily caused by the vapor valve.

e. Engine Performance. The gross engine/alternator power output is 16.2 kW_e, and the corresponding gross efficiency is 22.9% for the noon time period of Run 13 (Figure 2-75). Parasitic power consumption was measured at 688 W at high fan speed and is the grid power consumed in running the electrically driven condenser fan, boost pump, and valves. Net power output is therefore 15.5 kW_e and net efficiency is 21.9%. Engine

[16]Receiver input power is a computed value and is based on insolation data and prior measurements that determine the ratio of reflected to incident energy for TBC-1. Normalized input at 1000 W/m^2 is 75.68 kW_t.

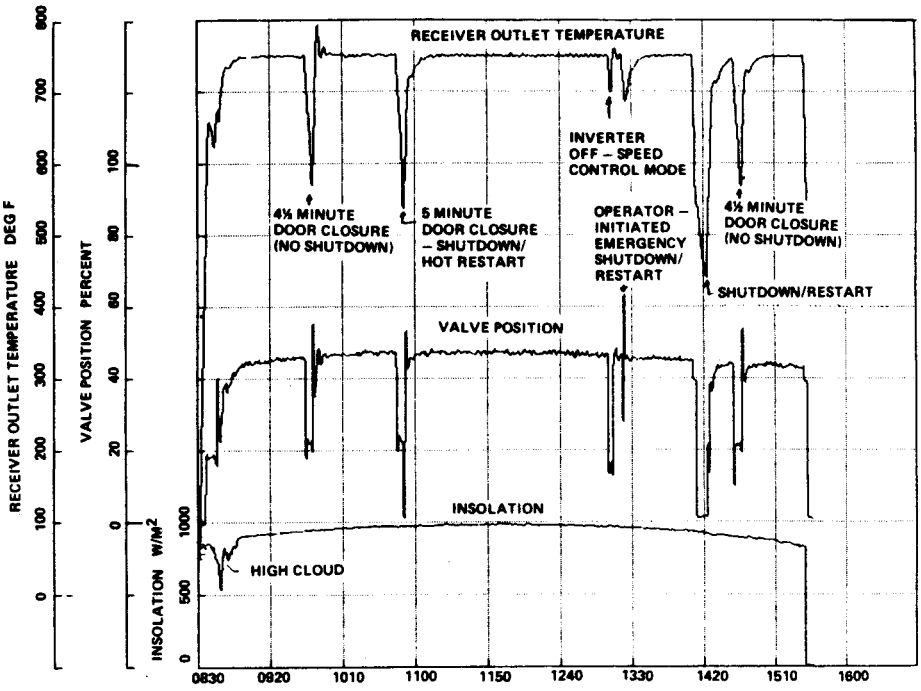

Figure 2-70. ORC Receiver Fluid Outlet Temperature versus Valve Position

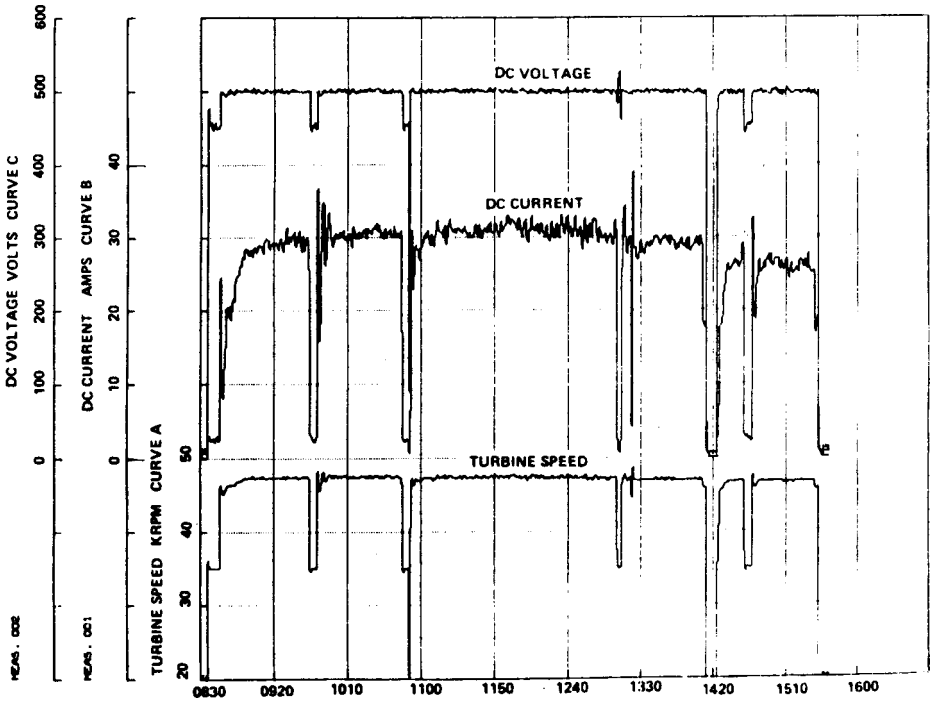

Figure 2-71. Inverter Voltage and Current versus Turbine Speed

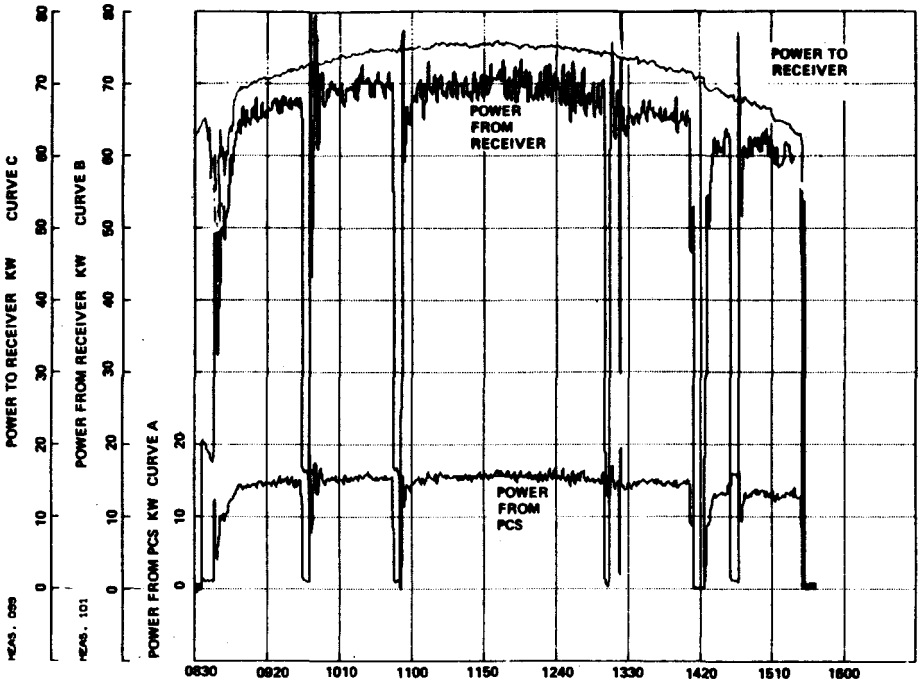

Figure 2-72. Power Levels of ORC Module at Receiver Inlet and Outlet and Engine/Alternator Output

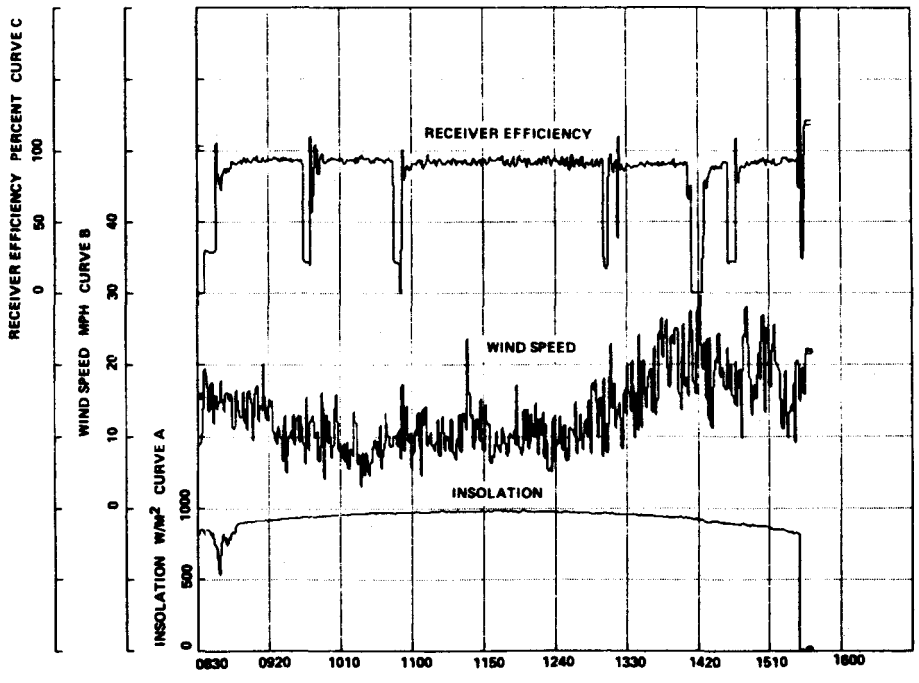

Figure 2-73. ORC Receiver Efficiency versus Wind Speed and Insolation

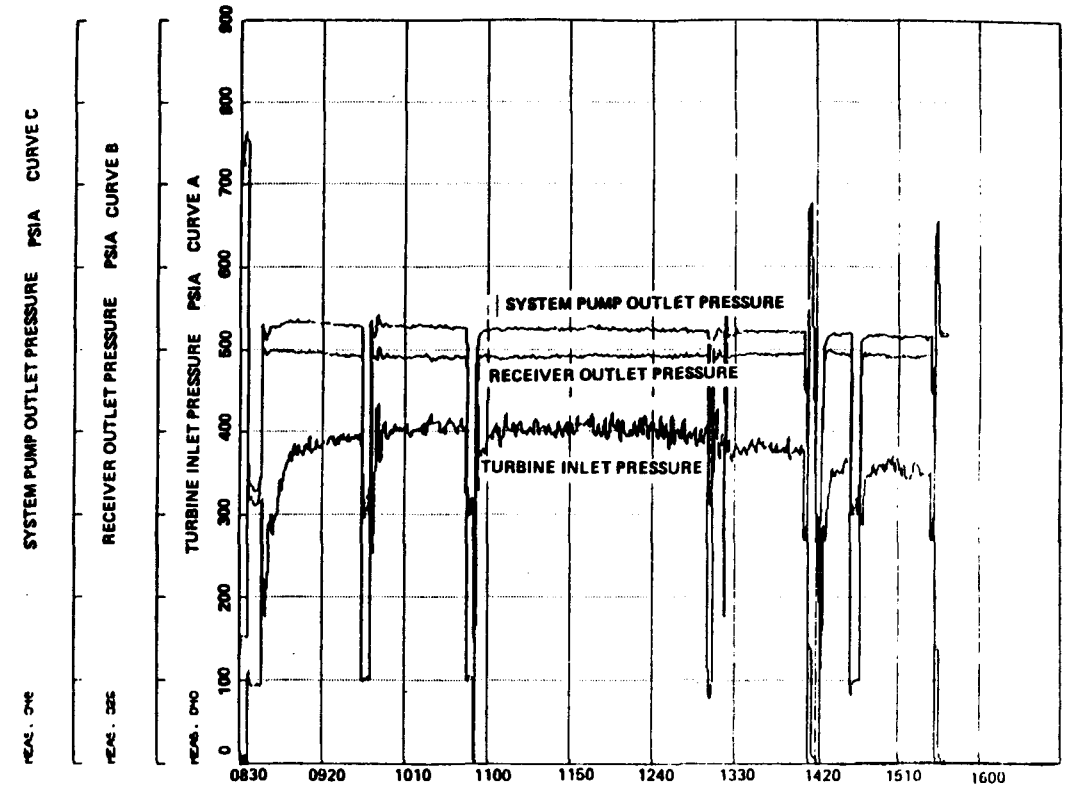

Figure 2-74. ORC Pressure History at Key Points

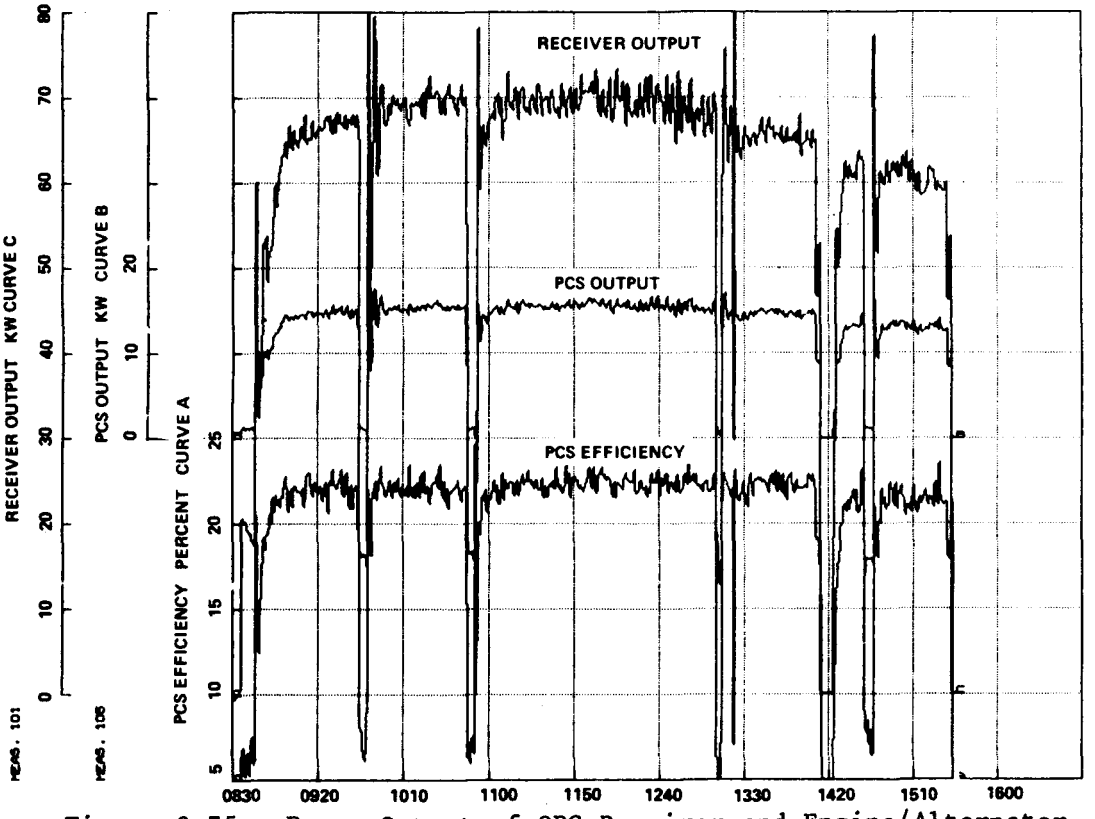

Figure 2-75. Power Output of ORC Receiver and Engine/Alternator

performance over a wide power operating range is shown in Figure 2-76, and represents the results of testing carried out to date. Operation at low fan speed (corresponding to lower input power levels) results in better performance than with the high fan speed because parasitic power is only 373 W.

In general, the engine performed smoothly and was quiet and easily controllable. The vapor control valve and the emergency shutdown system worked as planned under all modes of operation. After teardown of the system, some damage was detected with the axial thrust bearing. Barber-Nichols conducted a bearing evaluation test program using the actual turbine/alternator/pump assembly on a well-instrumented laboratory test rig.

f. Receiver Performance. Figure 2-77 presents receiver wall temperature data for two steady-state runs compared to the original design predictions. Receiver performance was obtained by using the measured fluid pressure and temperature data and a correlation of mass flow. It should be noted that (1) the assumed fluid inlet temperature for the prediction was 20°F higher than for the tests, (2) the predictions were based on supercritical flow (600 psi fluid pressure) whereas all the tests at the PDTS were conducted at subcritical conditions (480 to 550 psi fluid pressure), and (3) uncertainty in the flux distribution from the TBC. Note that the data for the two runs are very close even though the input power to the receiver for Run 13 was 20% higher than for Run 17.

During solar tests at the PDTS, boiling and/or flow instabilities and local "hot spots" were not observed during any of these or previous tests, including the subcritical, two-phase flow regime (which was not the original design condition) in which the unit operated most of the time.

g. Inverter Performance. A unique requirement for the inverter is to control the input voltage, which is equivalent to controlling the load on the engine. As shown in Figure 2-77, voltage control is excellent with a variation of only about ±1% from the nominal input voltage during normal power output, i.e., above idle conditions. The efficiency of the unit was measured at 83.3% for the conditions at noon for Run 13. This value is characteristic of the efficiency for units rated in the 30-kVA range. The fact that the unit was operating only at 16.2 kW for this test and had an input voltage of 500 V compared to a design value of 600 V contributed to the loss in efficiency.

h. Control System Performance. The automatic or computer-controlled subsystem was used for the control of all the solar-powered tests. A brief description of the control subsystem and typical results are given in Reference 18.

i. Conclusions. A number of problems were detected and addressed, primarily related to excessive wear of the bearings in the turbine/alternator/pump unit. The bearings were subsequently redesigned along with changes to the toluene feed system used to lubricate the bearings. Measured engine efficiency over the complete load range was a few points below

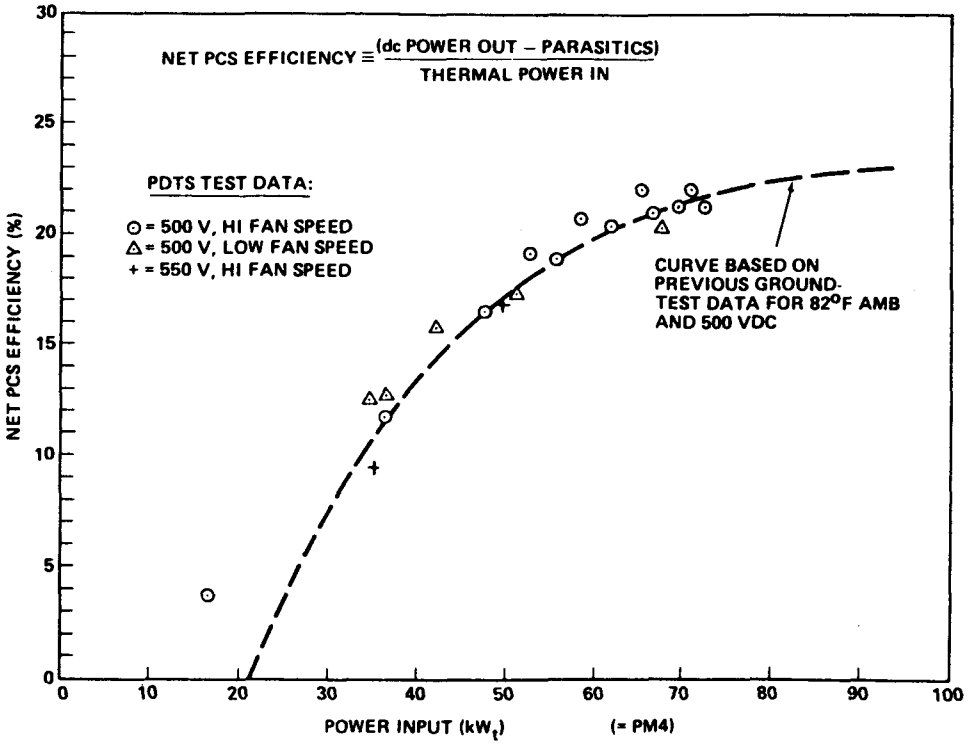

Figure 2-76. ORC Engine Net Efficiency

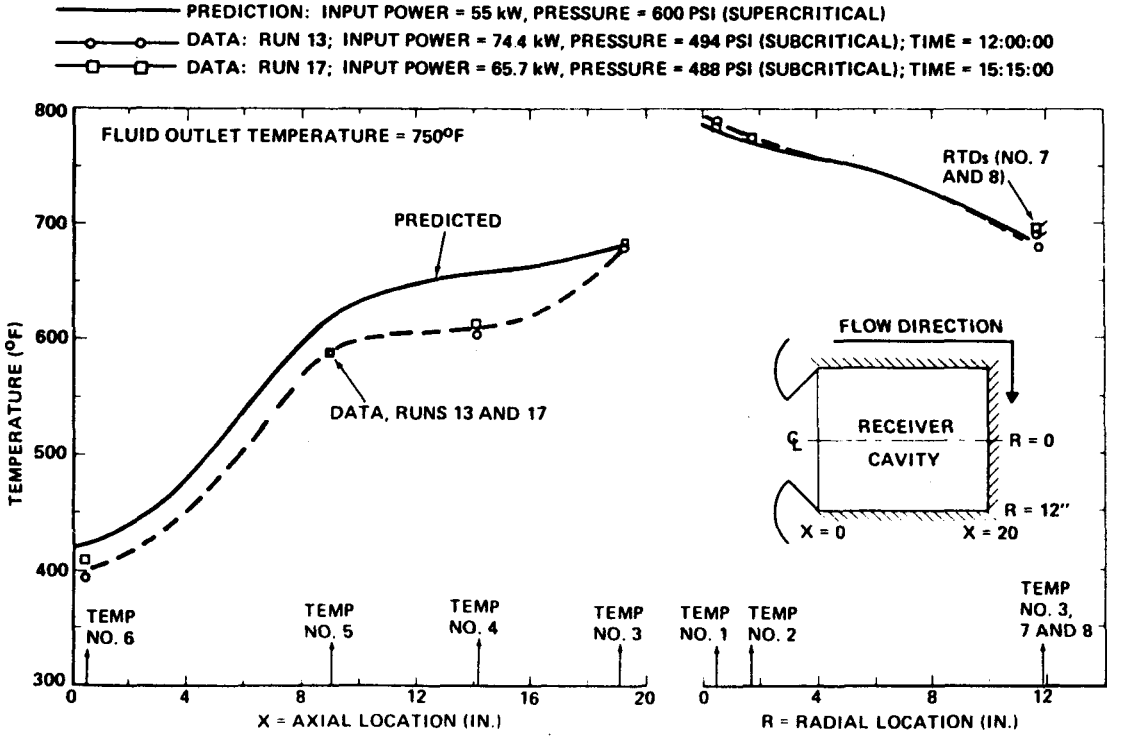

Figure 2-77. Comparison of Predicted and Measured ORC Receiver Temperatures

analytical predictions, primarily attributable to excessive pressure drop in the regenerator, feed pump losses, and permanent-magnet-alternator losses. Component efficiency and performance values are discussed in further detail in References 3 and 18.

2. Hybrid Stirling Module[17,18]

The hybrid-Stirling power module test is also identified as the Dish Stirling System Experiment (DSSE). The receiver is referred to as the dish/Stirling solar receiver (DSSR).

The module operates with a combination of heat inputs from the sun and fuel; therefore, it is considered a hybrid system. Hybrid operation is provided by fossil-fuel combustion augmentation, which enables the Stirling engine to operate continuously at constant speed and power, regardless of insolation level, thus providing the capability to operate on cloudy days and at night.

The DSSE was run on the precursor concentrator pad with gasoline-air mixture only as fuel and at the focus of TBC-2 using natural gas as fuel and solar heat. A 25-kW_e direct-driven induction-type alternator was mounted directly to the Model 4-95 engine built by United Stirling of Sweden AB (USAB) to produce a 60-Hz, 460- to 480-V output.

a. Design Features of the Hybrid Stirling Module. The hybrid Stirling module has a cavity-type receiver, as illustrated in Figure 2-78. The primary receiver surface is a conical plate with integral passages for the helium working fluid. The passages are formed by Inconel 617 tubes imbedded in a copper matrix, which in turn is encapsulated in an Inconel 617 sheet. The cone is heated by solar insolation on the surface exposed to the receiver cavity and by combustion gas on the back surface and the regenerator tubes. The receiver is attached directly to the Stirling engine cylinders and regenerator housings.

The combustion system design is based on heavy-duty industrial burner technology, scaled to the size and configuration required to assure reliable cold start, stable combustion over the full operating range, and uniform heating of the heater tubes extending from the underside of the cone to the engine regenerator manifolds. The combustion air, provided by an electric motor-driven constant-speed blower, is directed through a preheater into the combustion chamber, which contains eight integrally cast venturis, oriented to produce a swirling flow field inside the combustion chamber, providing sufficient residence time to complete combustion and uniform combustion gas temperature upstream of the heater tubes. Fuel is introduced through a jet

---

[17]Development of this module is covered in Reference 2.

[18]Computer programs used to process these test data are described in Appendix B.

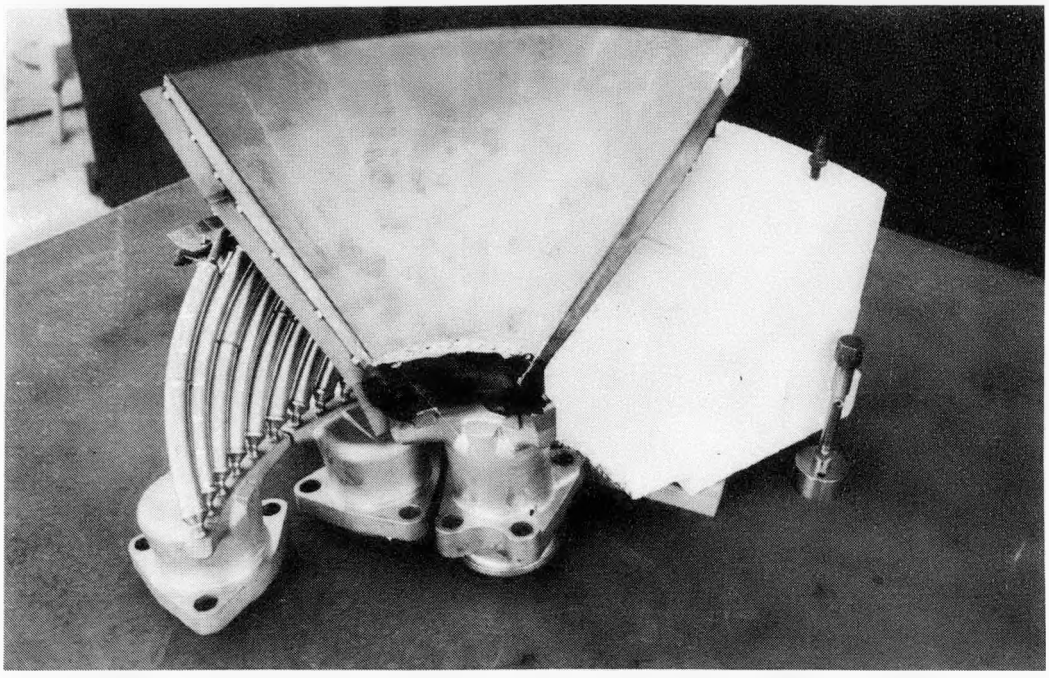

Figure 2-78. Dish/Stirling Solar Receiver Quadrant and Burner

located inside each venturi. Direct electric spark ignition and flame sensing is provided. The flame-sensing subsystem causes the main fuel valve to close automatically in the event of flame-out. Automatic restart is provided.

b. Performance Goals and Test Objectives. The following performance goals were identified during the design phase for the hybrid Stirling module:

(1) Concentrator diameter (active), 10 m.

(2) Geometric concentration ratio, 3000.

(3) Heat input for peak insolation (1 kW/m^2), 76.5 kW_t.

(4) Concentrator efficiency (clean), 0.926%.

(5) Total error (slope plus pointing), 3 mrad.

(6) Fossil-fuel combustor peak heat input to helium, 70.0 kW_t.

(7) Combustor turndown ratio, 10:1.

(8) Working fluid temperature (helium), 650 to 815°C (1200 to 1500°F).

(9) Peak engine pressure (helium), 17 to 20 MPa (2500 to 3000 psi).

Test objectives included evaluation and demonstration of cold start, combustion stability, and energy release at various power levels, combustion air preheat, pressure drop, fuel/air ratios, and heat transfer.

Tests performed were in three basic categories:

(1) Functional test that provided for mechanical integration and the initiation of power, start-up, ignition, engine cranking, power generation, solar tracking, safety, and shutdown functions.

(2) Performance test that provided a quantitative measurement of all system parameters over a full range of pressures and temperatures.

(3) Controls test to evaluate steady-state and transient operations from which conceptual designs can be sketched to meet a number of different system applications.

Tests under item (1) above essentially provided operational information and identified problem areas if any. Except for steady operating conditions, test data were not evaluated. Readings of the instrumentation allowed for monitoring the performance of the module and for diagnostic purposes.

Performance data were acquired during that portion of module operation in which physical parameters were stable. Thus, data for start-up, shutdown, and cloud transient periods were not acquired for performance evaluation.

The third item, control tests, aimed first to evaluate the adequacy of the individual components of the dish/Stirling module prior to system test. The following system test assured that the interactions between the several components were documented, and identified how the system could be optimized for various configurations.

A single, low-power (25-kW_e) prototype unit was tested. In a solar electric power plant, several of these units should operate safely and correctly while interfacing with the utility line. The utility power interface unit, operating with the control console, provides this function.

The system is designed for virtually automatic operation. The only operator intervention available is the setting of temperature of heat input to the engine, setting of the air/fuel ratio on the combustor (as a backup control), setting of cooling water flow, and initiating a start or stop sequence. Certain operating parameters such as helium pressure can be reset between tests by having access to the back of the control console.

Arbitrarily, for initial testing, combustor control on the hybrid receiver was provided to maintain the Stirling engine working fluid temperature at its preset value. Engine speed automatically adjusts to the stable power level of operation to maintain 60 Hz output of the induction alternator, synchronized with the utility grid.

c. Test Setup. The hybrid Stirling power module test setup consisted of the parabolic dish concentrator, the power conversion assembly, power processing equipment module, and environmental data acquisition system.

The following major equipment was provided for the testing of the dish/Stirling module:

(1) United Stirling 4-95 Stirling engine.

(2) General Electric 25-kW_e induction generator.

(3) Fairchild/Stratos dish/Stirling solar receiver.

(4) Advanco system control console.

(5) General Electric utility power interface unit.

(6) Young cooling system.

(7) E-Systems test bed concentrator.

(8) JPL instrumentation facility.

d. Data Collection. All data were recorded and certain key data were observable on meters. The control console is sketched in Figure 2-79. The main control panel and status instrument panel are shown in Figures 2-80 and 2-81.

Instrumentation sensors were mounted as necessary to monitor system operation. The majority of the instrumented elements were control functions that interacted in the control console and were brought from there to the data logger as analog signals. A few signals were multiplexed at the remote scanner and then transmitted to the data logger directly.

Command discretes were not instrumented for direct recording, but could be inferred from changes in the data that were being recorded. Various parameters, such as engine pressure and temperature, were defined and set prior to the start of a test run. The preset values and observable discretes of operating anomalies were identified by test personnel on all test charts as they were generated.

Key instrumentation outputs were monitored at the test console as well as at the data logger. Locations of probes used to test the receiver are marked in Figure 2-82. Receiver tube and other surface temperatures, combustion air and combustion product temperatures, and the O_2 percentage in combustion products were measured.

The computer list of measured data are presented in Table 2-22. Further details of the computer program used to process raw data are given in Appendix B.

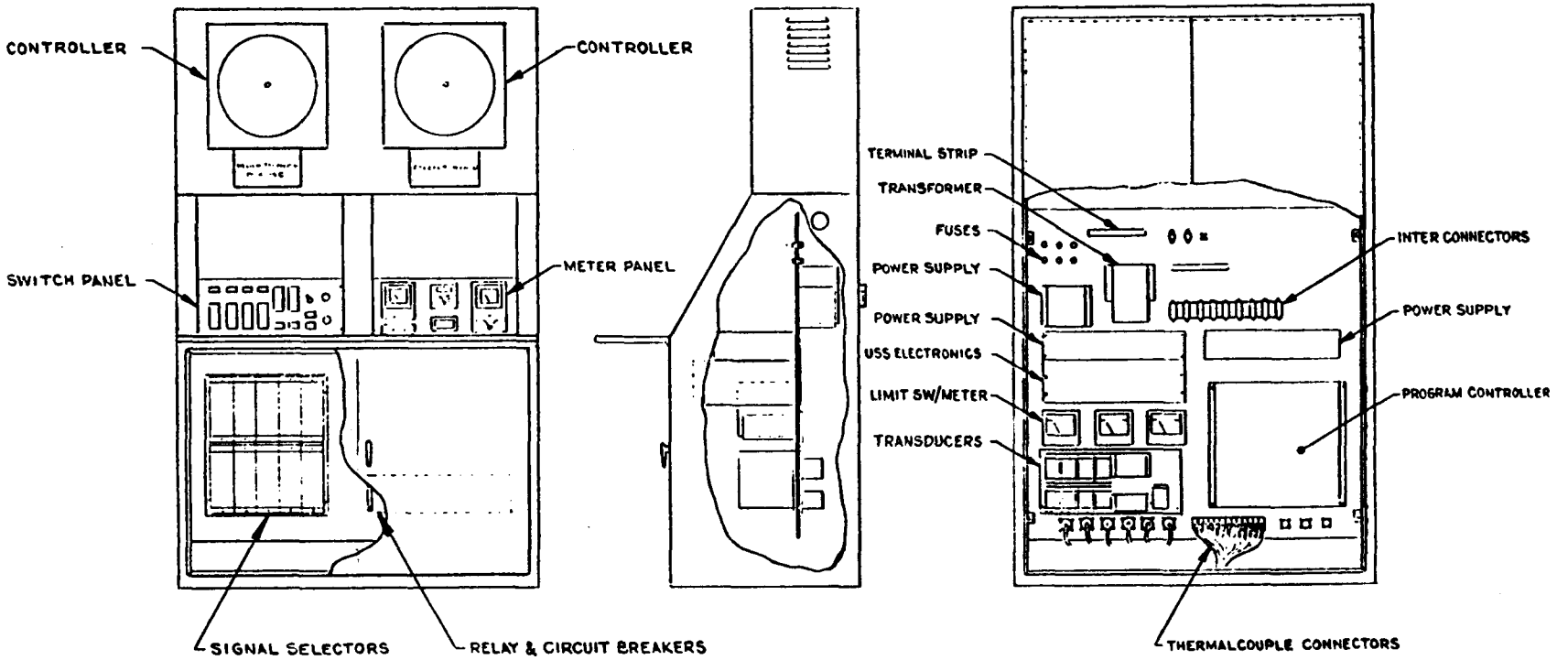

Figure 2-79. Dish/Stirling Module Test Control Console

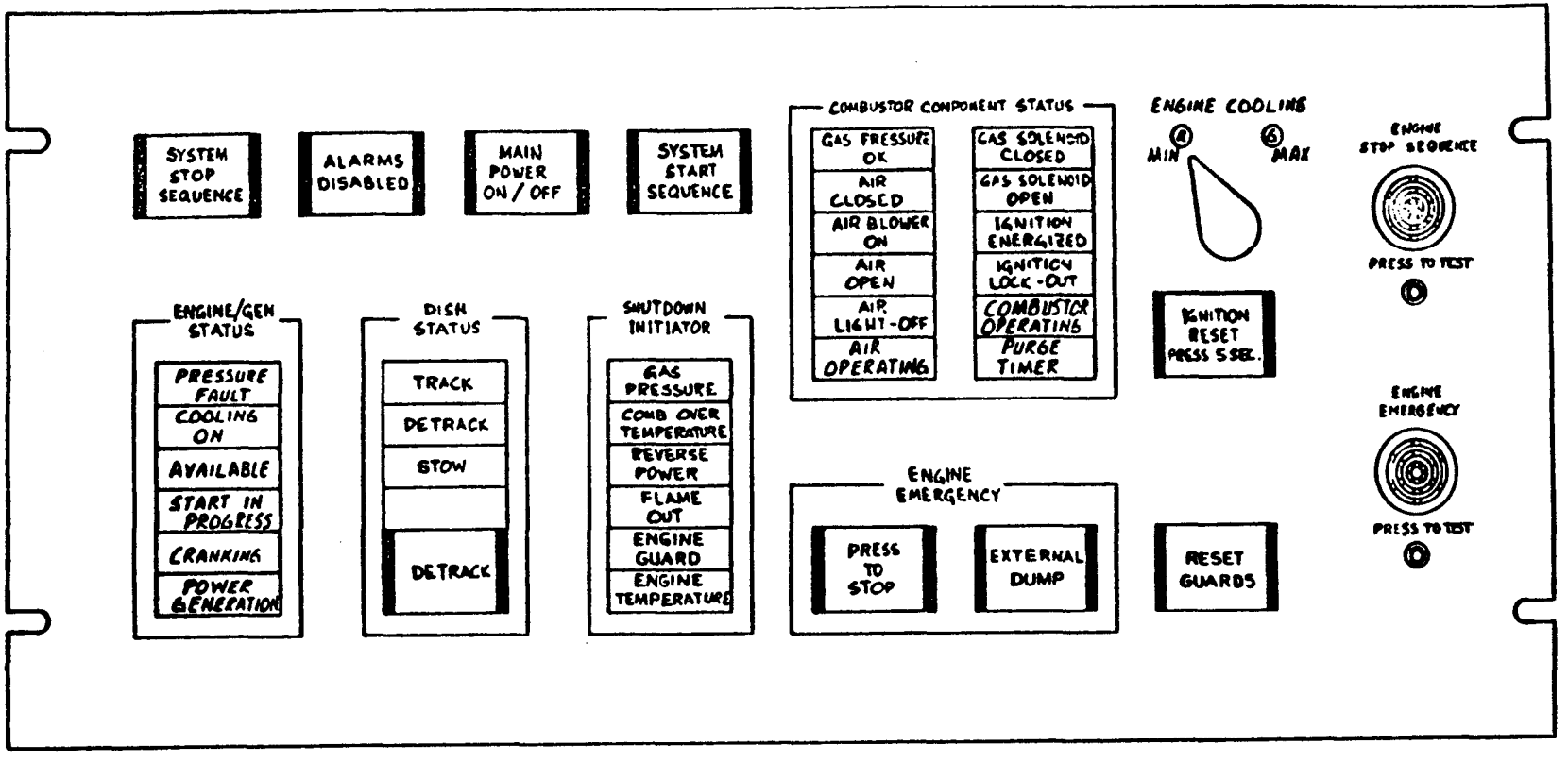

Figure 2-80. Main Control Panel

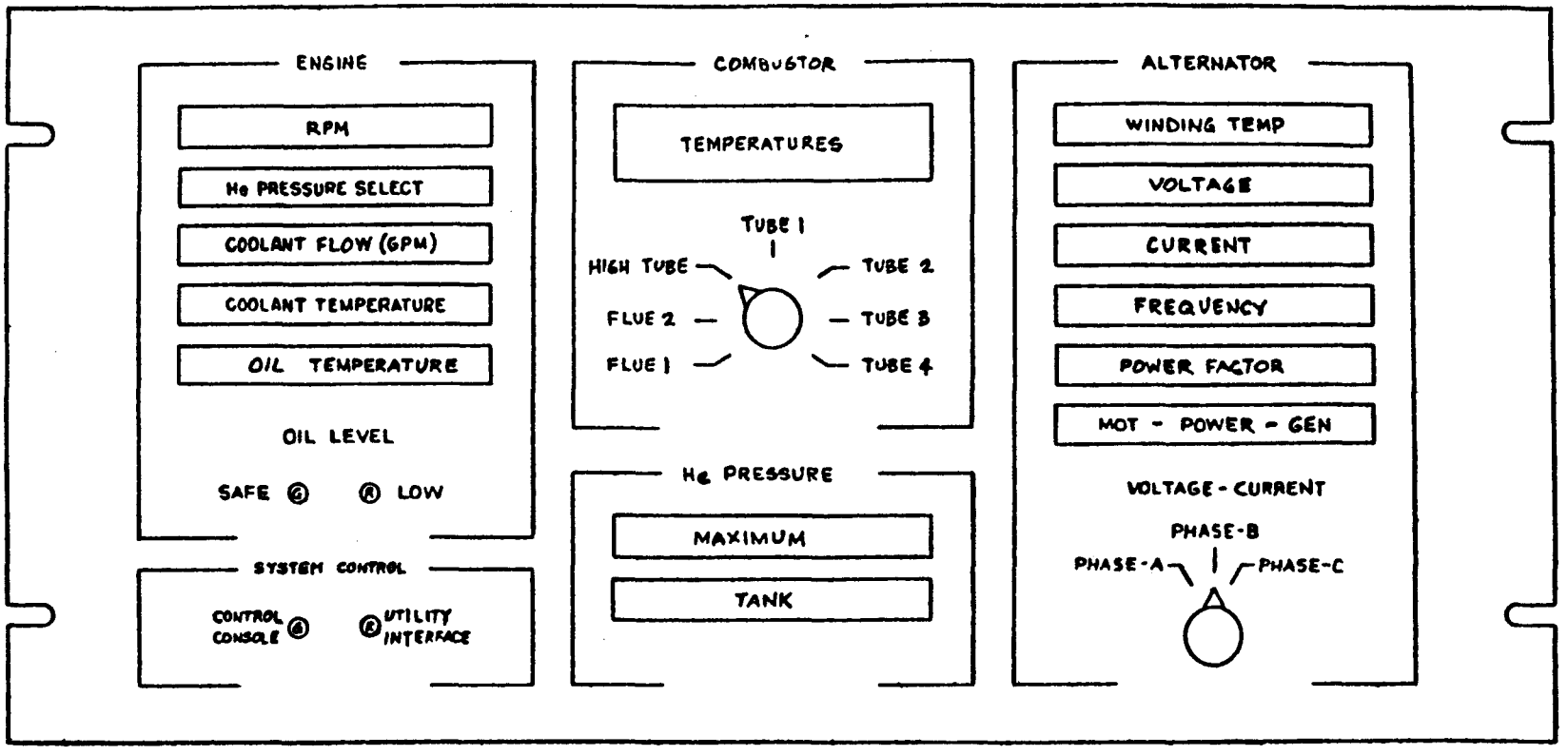

Figure 2-81. Status Instrument Panel

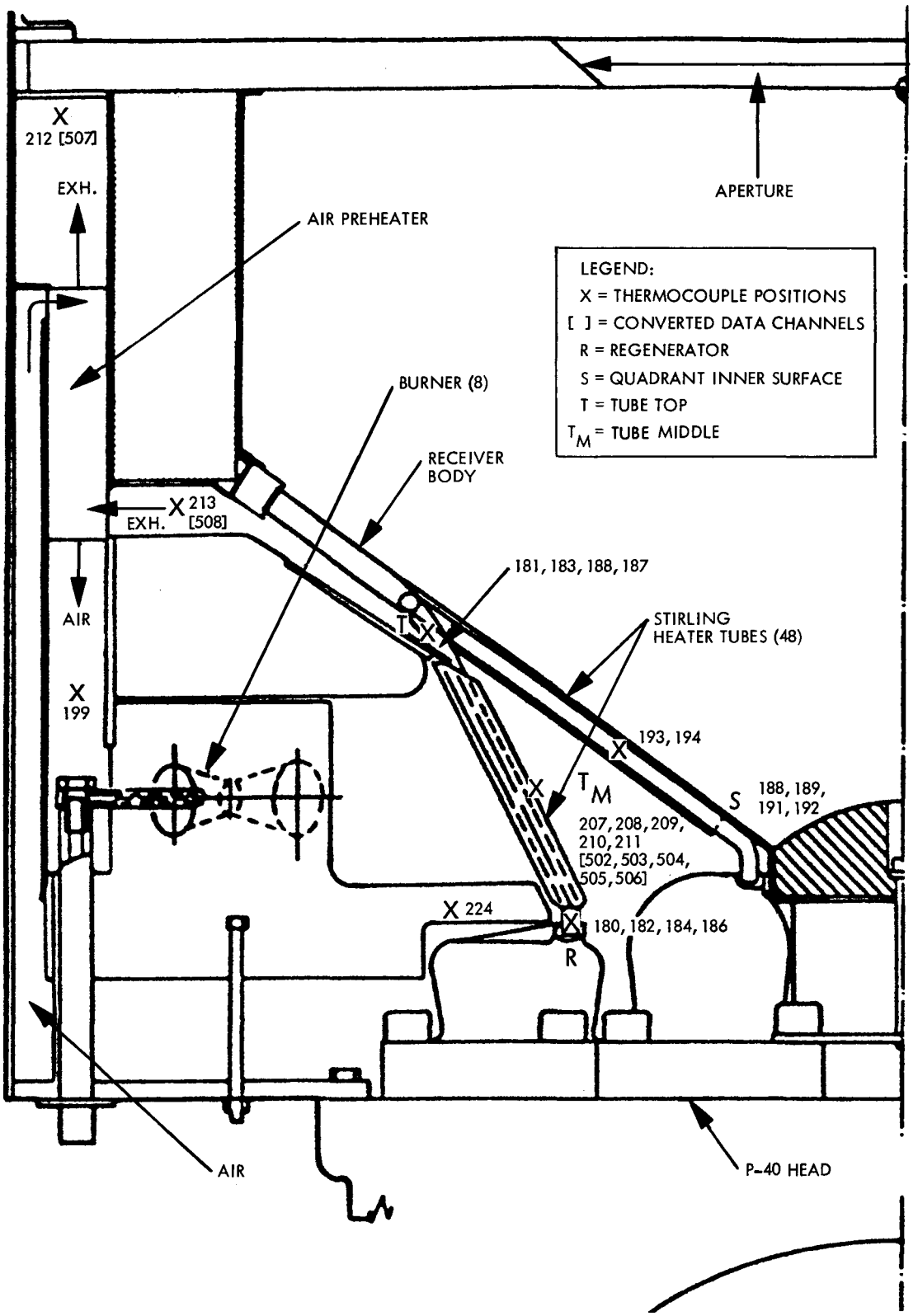

Figure 2-82. DSSR Test Probe Positions

Table 2-22. List of Hybrid Stirling Measurements and Conversions

Channel No.	Factor	Unit	Measurements
180	1.000	°C	R-1 Regenerator Tube
181	1.000	°C	T-1 Top Tube
182	1.000	°C	R-5 Regenerator Tube
183	1.000	°C	T-5 Top Tube
184	1.000	°C	R-7 Regenerator Tube
185	1.000	°C	T-7 Top Tube
186	1.000	°C	R-8 Regenerator Tube
187	1.000	°C	T-8 Top Tube
188	1.000	°C	S-1 Cone Temp
189	1.000	°C	S-8 Cone Temp
190	1.000	°C	Eng Oil Res Temp
191	1.000	°C	Inner Manifold Quad 5
192	1.000	°C	Inner Manifold Quad 7
193	1.000	°C	Back Surface Quad 1
194	1.000	°C	Back Surface Quad 8
195	1.000	°C	Eng Coolant In
196	1.000	°C	Cavity Outer Temp
197	1.000	°C	Orifice Line Temp
198	1.000	°C	Inlet Air Temp
199	1.000	°C	Preheated Air
200	10.00	gal/min	Eng Cool Flow
201	500.0	rev/min	Engine Speed
202	290.0	psig	He Pressure Select
203	10.00	°C	Eng Oil Temp
204	290.0	psig	He Pressure Max
205	290.0	psig	He Pressure Tank
206	1.000	V	Eng Coolant Temp
207	1.000	V	High Temp Select
208	1.000	V	Tube 1 Quad 1
209	1.000	V	Tube 2 Quad 5
210	1.000	V	Tube 3 Quad 7
211	1.000	V	Tube 4 Quad 8
212	1.000	V	Flue (Cone) Temp
213	1.000	V	Preheat Exhaust
214	1.000	V	Alternator Winding Temp
215	50.00	V	Volt Phase A
216	50.00	V	Volt Phase B
217	50.00	V	Volt Phase C
218	5.000	A	Current Phase A
219	5.000	A	Current Phase B
220	5.000	A	Current Phase C
221	1.000	V	Alternator Frequency
222	1.000	V	Power Factor
223	4.000	kW	Alternator Power
224	1.000	V	O_2 Analyzer Thrmox

Table 2-22. List of Hybrid Stirling Measurements and Conversions (Cont'd)

Channel No.	Factor	Unit	Measurements
225	2.000	gal/min	Flt Plt Cool Flo
226	1.667	psig	Orifice Line Pressure
227	0.083	psid	Orifice Delta Pressure
228	10.00	W/m^2	Kendall Pyrheliometer
229	114.9	W/m^2	Eppley Pyrheliometer
230	1.000	(Status)	Slide Plate Status
231	0.006	psid	Manifold Air Pressure
232	4.000	kW	Line Power
233	1.000	V	O_2 Analyzer Corning
501		°C	Eng Coolant Temp
502		°C	High Tube Temp
503		°C	Tube 1 Quad 1
504		°C	Tube 2 Quad 5
505		°C	Tube 3 Quad 7
506		°C	Tube 4 Quad 8
507		°C	Flue (Cone) Temp
508		°C	Preheat Exhaust
509		°C	Alternator Winding Temp
510		Hz	Alternator Frequency
511		pf	Power Factor
512		%	O_2 Analyzer Thrmox

e. Test Procedure. In testing the DSSR, certain steps were followed to start and stop the module. Most of the controls are automatic. Once the engine starts running, load conditions were varied by the operator by adding or removing the load. Data were continuously recorded on magnetic tape. Selected points were later printed in hard copy form or plots showing the time variation of data. The most important data were tabulated, and some sample values are presented in Table 2-22.

When the experiment was terminated, steps were automatically followed to stop the engine without failure to tubes and other components. In case of component failure, the control logic automatically initiated the stop sequence.

f. Tests Performed. The hybrid module was first tested using combustor only on the precursor pad prior to focal-plane testing. The sequence of these functional tests was as follows:

(1) Power.

(2) Start sequence initiate.

(3) Combustor ignition initiate.

(4) Engine start initiate.

(5) Shutdown initiators: engine "guard," gas pressure, over temperature, flame out, and reverse power.

(6) Full power achieved/stable.

Once the functional tests were completed and integrity of the unit was demonstrated, the engine/receiver assembly was installed on the assembly ring located at the focal plane of a TBC. Electrical power and instrumentation cables were installed. Cooling water connections were made to the circulation pump and the alidade-mounted radiator. Instrumentation control console and utility interface unit connections were made, then performance tests were run.

A summary of the performance test plans is presented below:

(1) Minimum power, 7 MPa, 650°C.[19]

(2) Pressure parameter, 7 to 15 MPa.

(3) Helium temperature parameter, 650 to 820°C.

(4) Coolant temperature parameter, 25 to 50°C.

(5) Evaluation of success: receiver at 870°C, 85% (solar only); engine at 820°C, 35%; alternator output at 25 kWe, 93%; and power output constant within 5% with variable cloud cover.

(6) Cloud transient response evaluation.

(7) Air supply evaluation.

(8) Air/fuel ratio evaluation.

(9) Cooling loop optimization.

(10) Multi-unit control parameters identification.

(11) Solar-only operation evaluation.

Tests were run with combustor only and hybrid mode at 25 and 50% solar inputs during the Fall of 1981. Although test data were gathered in accordance with the test plans previously described, some instrument failures did not allow a meaningful interpretation of the test data. Therefore, test logs and sample data as well as their interpretation are not presented in this report. Some additional information on these tests is given in Reference 2. During on-sun tests, some mechanical problems were experienced with the heater head quadrants, resulting in the failure of brazed tube joints. Failed tubes were re-brazed and the system was reassembled during January-February 1982. Hybrid receiver tests, however, were never resumed.

[19] Minimum for operation of O_2 analyzer.

3. Experimental Solar-Only Receiver Tests[20,21]

Under an agreement between JPL and United Stirling of Sweden (USAB), a series of tests was performed at the PDTS beginning in January 1982. Several variations of the experimental solar-only receiver (ESOR) were tested under the cognizance of USAB engineers and technicians. JPL provided the facility but was not involved directly in planning nor in performing of experiments.

Test data from 1982 to 1984 were examined by JPL; a report was published by M. K. Selcuk (Reference 19) that documents this independent examination of ESOR test data. Table 2-23 is a listing of the tests in groups that correspond to the five different receiver configurations tested.

The receiver consists of an aperture cone and a housing that forms the receiver cavity and protects the heater head tubing from wind and other environmental effects. Heater-head tubing configurations varied among the five designs tested.

The Stirling engine under test was the standard USAB Model 4-95 directly coupled to the alternator. Because there was no provision to measure the engine shaft power output, the alternator output was measured. Engine performance was determined on the bases of alternator output, working gas high temperature, cold side temperature, and working gas pressure data.

Each receiver configuration will be briefly described prior to discussion of the test setup and performance of the experiments.

a. ESOR-I Tests. ESOR-I employed the essentially unmodified heater head that was used when the 4-95 engine was operated with a combustor (Figure 2-83). The tube configuration was originally selected for optimum heat transfer from combustion products to the working fluid inside the tubes. Therefore, the diameter of the tube cone formed by the heater tubes is not optimized for solar operation. There are fins on the rear tubes that are not exposed to sunlight. These tubes were originally introduced to enhance the convective heat transfer when the combustor was used. With the solar-only receiver, these finned tubes played a detrimental role. Due to an improperly concentrated flux pattern on the tube bundle, spillage of some concentrated flux onto the receiver inner walls, and non-optimized tube coil dimensions, ESOR-I yielded lower efficiencies than were expected.

---

[20] The context of these tests is reported in Reference 2.

[21] Computer programs used to process these test data are described in Appendix B.

Table 2-23. ESOR Tests

Test Run	Receiver Type	Working Fluid	Test Period
119-124	ESOR I	Helium	Jan 17, 1982
125-138	ESOR IIA	Helium	Feb 2 and 26
139-150	ESOR IIB	Helium	Mar 4-15 and 31
	ESOR IIA	Helium	May 21-27
	ESOR IIB	Helium	Jun 2-17
	ESOR IIB	Helium	Jun 21-23
	ESOR IIA	Helium	Jul 1-13
	ESOR IIA	Hydrogen	Jul 14-15
	ESOR IIA	Helium	Jul 16-20
	ESOR IIA	Helium	Sept 16-Oct 11
201-216	ESOR IIB	Helium	Oct 18-Dec 17
217-218	ESOR IIB	Helium	Jan 17-18, 1983
219-228	ESOR IIA	Helium	Feb 1-24
229-235	ESOR III	Helium	Mar 8-31
236-239-241	ESOR IIA	Helium	Apr 4-8
240-247	ESOR III	Helium	Apr 7-May 2
248-268	ESOR IIA	Helium	May 9-Jun 3
269-283	ESOR III	Helium	Jun 10-Jul 5
284-305	ESOR IIA		
	ESOR III	Helium	Jul 6-27[a]
306-314	ESOR III	Hydrogen	Jul 28-Aug 11
315-316	ESOR III (H_2)		
	ESOR IIA	H_2 & He	Aug 12
317-356	ESOR III (H_2)		
	ESOR IIA	H_2 & He	Aug 18-Oct 13[a]
357-359	ESOR IV	Hydrogen	Oct 21-24
360-362	ESOR III	Hydrogen	Oct 27-Nov 9
362-364	ESOR III	Hydrogen	Nov 9-15
363-365	ESOR IV	Hydrogen	Nov 14-15
366-375	ESOR III	Hydrogen	Nov 17-Dec 8
376-378	ESOR IV	Hydrogen	Dec 19-20
384-385	ESOR IV	Helium	Jan 23-25, 1984

[a] Simultaneous tests of two engines, each installed on one of the two TBCs, were run during this period.

Due to the poor performance of ESOR-I, new generations of receivers were designed and tested. These are ESOR-IIA, ESOR-IIB, ESOR-III, and ESOR-IV. Figure 2-83 illustrates these four ESOR design variations.

b. ESOR-IIA and IIB Test Series. The first series of tests on ESOR-IIA and IIB were run during February and March 1982.

The second series of tests of ESOR-IIA and ESOR-IIB run by USAB commenced on May 21, 1982, and continued until July 20, 1982. The purpose of this test series was to evaluate the experimental receivers, ESOR-IIA and ESOR-IIB, at their optimum positions with respect to the concentrator focal plane. Capability to adjust the power conversion unit position along the Z-axis was therefore provided. From this testing, USAB designed a new receiver having capabilities better than either ESOR-IIA or ESOR-IIB.

By mid-May, the mirrors of TBC-2 had been realigned to a focal plane 22.9 cm (9 in.) inside the face of the mounting ring. "A" mirrors were cross-focused to leave a dark inner circle at the focal plane of approximately 10 cm (4 in.) in diameter to accommodate the Stirling receiver center plug.

ESOR-IIA was installed on the Stirling engine/alternator and mounted on TBC-2 during the week of May 17. A new microprocessor controller was integrated into the system. System operation commenced on May 21, 1982. Water-cooled shutters at the mounting ring were modified to allow their opening to a wider limit. The engine cooling system, supplied by JPL, also fed the water-cooled plates.

Testing commenced with 50% of the mirrors exposed and then continued with 80% exposed. Receiver position was varied to determine its optimum position along the Z-axis of the dish. During this optimization process on May 27, a helium leak developed in one of the heater head tubes. Examination after demounting from TBC-2 showed the leak to be a crack along the seam of the tube. Rolled and welded tubing rather than seamless tubing was used with this receiver. Repair materials were sent from Sweden, and the quadrant was carried to Solar Turbines, Inc., in San Diego on June 3. The braze repair was made, and the unit was returned to JPL on June 7.

On June 2, ESOR-IIB was installed on the Stirling engine/alternator, and the system was mounted on TBC-2. Testing commenced with 80% mirrors and continued through June 7.

On June 8, 1982, the system began operation with 100% mirrors. From that date until June 16, the Z-axis position of the engine was varied over its full range. The search for the optimum heater head position was continued until June 17. On June 18, mirrors were cleaned and the engine was recharged with hydrogen as the working fluid. From June 21 to June 23, the module was run from sunrise to sunset. The engine was programmed over a full range of temperatures and pressures during these tests with hydrogen as the working fluid. These tests were completed, and reinstallation of ESOR-IIA began on July 1, 1982.

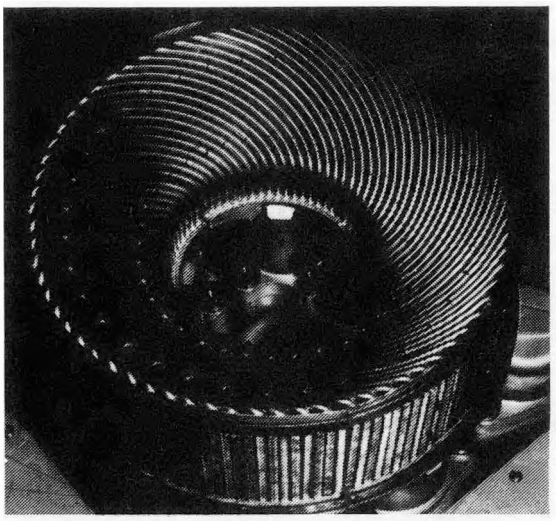

ESOR-I (Involute Heater Head)

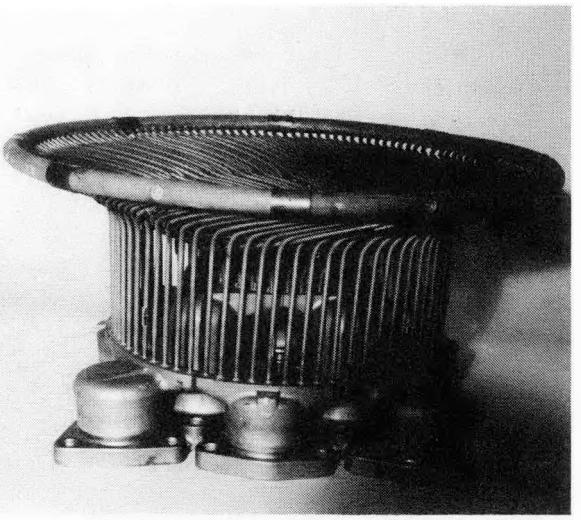

ESOR-IIA

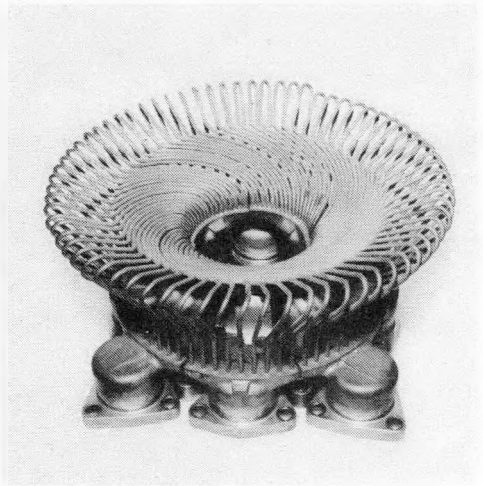

ESOR-IIB

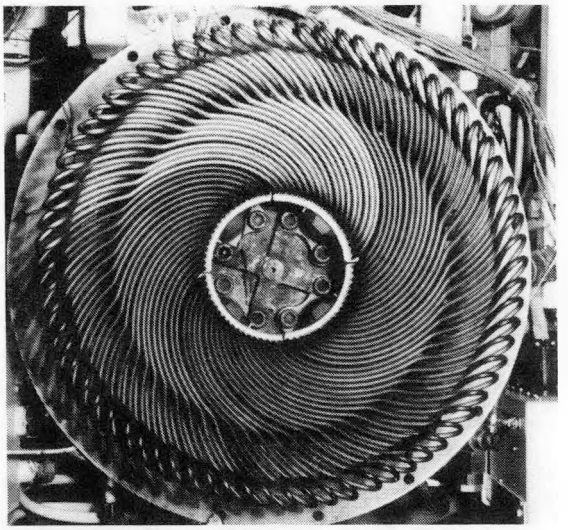

ESOR-III

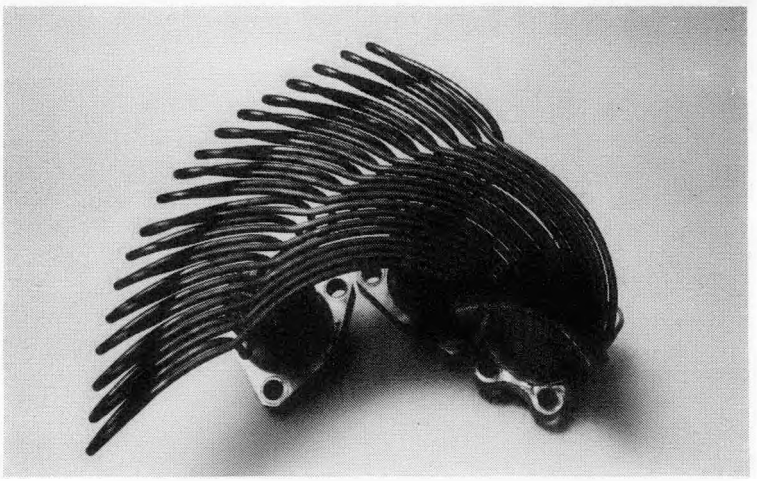

ESOR-IV (Quadrant)

Figure 2-83. ESOR Design Variations

During July 1982, tests with ESOR-IIA at various (Z) positions continued. Except two days (July 14 and 15) when tests were run with hydrogen as the working fluid, all tests were conducted with helium as the working fluid. ESOR-IIA tests with helium were resumed in September. Tests with ESOR-IIA continued during 1983. Tests were performed with helium and hydrogen at various (Z) positions, with and without a quartz window behind the aperture and with a radiator at the focal plane.

c. ESOR-III Tests. Design of this receiver was based upon the experience gained with earlier designs. Its configuration is very similar to that of ESOR-IIB. The tubes were shaped to form a coil at the top of the cone. The space between the front and rear portions of tubes is insulated.

Testing of ESOR-III commenced on March 8, 1983. Helium and hydrogen were used as the working fluids. Testing continued throughout 1983. Various (Z) positions were tested. ESOR-III was also tested with a quartz window installed behind the aperture plane to reduce the convective losses over the heater head tubes.

d. ESOR-IV Tests. ESOR-IV is the latest design based on several years of experience in engine and receiver development. The tube coil configuration is similar to that of ESOR-III. The major difference is the absence of the tube manifold at the regenerator end of the heater tube assembly. Unlike the earlier heater tube assemblies, the regenerator ends of the tubes are directly connected to the regenerator head. Thus, in the ESOR-IV heater tube assembly, tube length is shortened, dead volume is reduced, and better flow distribution is obtained.

A limited number of tests using hydrogen as the working fluid were run during the months of October, November, and December of 1983. Only two significant runs are available with helium as the working fluid from the most recent series of tests performed during January 1984.

e. Test Setup. The experimental arrangement used to evaluate the solar-only Stirling power module consisted of one of the two TBCs, the Stirling power conversion assembly, control and data acquisition system, and utility interface unit. Until the end of June 1983, TBC-2 alone was used to test various ESOR designs. After June 1983, TBC-1 was also used for Stirling module testing. Occasionally, tests with TBC-1 and TBC-2 were run simultaneously.

Unlike the hybrid Stirling module discussed in the previous section, the solar-only Stirling power conversion assembly was installed at the focal plane without fuel line connections. The radiator used to reject the excess heat was connected the same way as the hybrid Stirling module. The radiator and water pump were installed on the alidade of the TBC, and water lines were run to the focal plane and connected to the engine. One exception to this configuration that was common to all ESOR tests was the focal-plane-mounted radiator tests. A specially designed radiator/circulation pump assembly was

tested to examine the effect of radiator position and size on the parasitic power requirements as well as the effect on engine efficiency.

Instrumentation sensors were mounted as necessary to monitor system operation and gather data to evaluate module performance. Receiver tube and cavity surface temperatures, working gas temperatures, engine oil, engine water, and generator winding temperatures were measured. Helium and oil pressures as well as water flow rate were measured. Beam insolation intensity and other environmental data were obtained from the weather station. Electrical parameters such as voltage, current, frequency power factor, alternator, and line power were measured. Other data such as engine rev/min, shutter plate, and coolant flow were acquired. The majority of the instrumented elements are control functions that were interacted in the control console and brought from there to the data logger as analog signals. A few signals were multiplexed at the remote scanner and then transmitted to the data logger directly. Command discretes were not instrumented for direct recording, but can be inferred from changes in the data that were recorded. Various parameters, such as engine pressure and temperature, were defined and set prior to the start of a test run. These preset values and observable discretes of operating anomalies were identified by test personnel on all test charts as they were generated.

Key instrumentation outputs were monitored at the test console as well as at the data logger. These can be seen in Figure 2-81.

A full computer printout, listing instrumentation channel numbers and conversion factors, is presented in Table 2-24.

Thermocouple positions and channel numbers are presented in Figure 2-84 and Table 2-25.

f. Test Procedure. The "solar-only" Stirling tests listed below were run to accomplish the test objectives indicated with each test.

(1) Test No. 1: Initial functional test with ESOR-I, using a cavity with wet felt as the inner reflective surface. Heat input was restricted by covering the concentrator surface. The objective of this test was to demonstrate engine/generator operation and power generation in the solar-only mode.

(2) Test No. 2: Testing of engine/generator at constant heat input levels and at different heat input levels. Power and efficiency were measured. The purpose of this test was to map energy conversion efficiency at different insolation and heat input levels.

(3) Test No. 3: Testing of engine/generator at constant heat input levels and at different temperatures on the receiver. Power, efficiency, and receiver tube temperatures were measured. Analysis of temperature distribution in the receiver and optimization of operating conditions were two test objectives.

Table 2-24. Listing of Instrumentation Channel Numbers and Conversion Factors

```
TBC1 SOLAR STIRLING, ESOR IIA,100% MIRROR
12345678901234567890123456789012345678901234567890123456789012345678901234567890
ST 03 47  050  60  0  001
144   TEMP01   1.0000   DEG. C      FRONT TUBE(INNR) 4 6S 9999. 9999.   45.67
145   TEMP02   1.0000   DEG. C      FRONT TUBE(INNR) 4 6S 9999. 9999.   45.67
146   TEMP03   1.0000   DEG. C      FRONT TUBE(INNR) 4 6S 9999. 9999.   45.67
147   TEMP04   1.0000   DEG. C      FRONT TUBE(INNR) 4 6S 9999. 9999.   45.67
148   TTTTTT   1.0000   DEG. C      REAR TUBE LOWER  4 6S 9999. 850.0   45.67
149   TTTTTT   1.0000   DEG. C      REAR TUBE LOWER  4 6S 9999. 850.0   45.67
150   TTTTTT   100.00   VOLTS       VOLT PHASE A-B   4 3S 9999. 9999.   45.67
151   TTTTTT   100.00   VOLTS       VOLT PHASE C-B   4 3S 9999. 9999.   45.67
152   TTTTTT   100.00   VOLTS       VOLT PHASE C-A   4 3S 9999. 9999.   45.67
153   TTTTTT   1.0000   AMPS        CURRENT PHASE A  4 1S 9999. 9999.   45.67
154   TTTTTT   1.0000   AMPS        CURRENT PHASE B  4 1S 9999. 9999.   45.67
155   TTTTTT   1.0000   AMPS        CURRENT PHASE C  4 1S 9999. 9999.   45.67
156   VAL001   1.0000   VOLTS       ALT FREQUENCY    4 3S 9999. 9999.   45.67
157   VAL005   1.0000   KWATT       POWER-JPL        4 1S 9999. 9999.   45.67
158   VAL002   8.0000   VOLTS       POWER FACTOR     4 1S 9999. 9999.   45.67
160   TTTTTT   1.0000   DEG. C      REAR TUBE(LOWER) 4 6S 9999. 850.0   45.67
161   TTTTTT   1.0000   DEG. C      REAR TUBE(LOWER) 4 6S 9999. 850.0   45.67
162   TTTTTT   1.0000   DEG. C      ENG. COOLANT IN  4 6H 9999. 9999.   45.67
163   TEMP05   1.0000   DEG. C      REAR TUBE OTR    4 6S 9999. 850.0   45.67
164   TEMP06   1.0000   DEG. C      REAR TUBE OTR    4 6S 9999. 850.0   45.67
165   TEMP07   1.0000   DEG. C      REAR TUBE OTR    4 6S 9999. 850.0   45.67
166   TEMP08   1.0000   DEG. C      REAR TUBE OTR    4 6S 9999. 850.0   45.67
167   TTTTTT   1.0000   DEG. C      REAR TUBE OUTER  4 6S 9999. 850.0   45.67
168   TTTTTT   1.0000   DEG. C      REAR TUBE OUTER  4 6S 9999. 850.0   45.67
169   TTTTTT   1.0000   DEG. C      REAR TUBE OUTER  4 6S 9999. 850.0   45.67
170   TTTTTT   1.0000   DEG. C      REAR TUBE OUTER  4 6S 9999. 850.0   45.67
171   TTTTTT   1.0000   DEG. C      FRNT TUBE INNER  4 6S 9999. 850.0   45.67
172   TTTTTT   1.0000   DEG. C      FRNT TUBE INNER  4 6S 9999. 850.0   45.67
173   TTTTTT   1.0000   DEG. C      FRNT TUBE INNER  4 6S 9999. 850.0   45.67
174   TTTTTT   1.0000   DEG. C      FRNT TUBE INNER  4 6S 9999. 850.0   45.67
175   TTTTTT   1.0000   DEG. C      FRONT TUBE OUTER 4 6S 9999. 850.0   45.67
176   TTTTTT   1.0000   DEG. C      FRONT TUBE OUTER 4 6S 9999. 850.0   45.67
178   TTTTTT   1.0000   DEG. C      FRONT TUBE OUTER 4 6S 9999. 850.0   45.67
179   TTTTTT   1.0000   DEG. C      FRONT TUBE OUTER 4 6S 9999. 850.0   45.67
180   TTTTTT   1.0000   DEG. C      ENG.COOLANT.OUT  4 6H 9999. 70.00   45.67
181   TTTTTT   1.0000   DEG. C      CAVITY TEMP TH14 4 6S 9999. 1150.   45.67
182   TTTTTT   1.0000   DEG. C      CAVITY TEMP TH15 4 6S 9999. 1150.   45.67
183   TTTTTT   1.0000   DEG. C      CAVITY TEMP TH16 4 6S 9999. 1150.   45.67
184   TTTTTT   1.0000   DEG. C      CAVITY TEMP TH17 4 6S 9999. 1150.   45.67
185   TEMP09   1.0000   DEG. C      CIRC.CAVITY TH18 4 6S 9999. 1150.   45.67
186   TEMP10   1.0000   DEG. C      CIRC.CAVITY TH19 4 6S 9999. 1150.   45.67
187   TEMP11   1.0000   DEG. C      CIRC.CAVITY TH20 4 6S 9999. 1150.   45.67
188   TEMP12   1.0000   DEG. C      CIRC.CAVITY TH21 4 6S 9999. 1150.   45.67
191   TEMP13   1.0000   DEG. C      WORKING GAS TH9  4 6S 9999. 800.0   45.67
192   TEMP14   1.0000   DEG. C      WORKING GAS TH10 4 6S 9999. 800.0   45.67
193   TEMP15   1.0000   DEG. C      WORKING GAS TH11 4 6S 9999. 800.0   45.67
194   TEMP16   1.0000   DEG. C      WORKING GAS TH12 4 6S 9999. 800.0   45.67
195   TTTTTT   1.0000   DEG. C      CAV.OUT.SUR.TH22 4 6S 9999. 500.0   45.67
196   TTTTTT   1.0000   DEG. C      CAV.OUT.SUR.TH23 4 6S 9999. 300.0   45.67
197   TTTTTT   1.0000   DEG. C      AMBIENT TEMP.    4 6S 9999. 9999.   45.67
200   TTTTTT   10.000   GPM         ENG COOL FLOW    4 3S 2.000 9999.   45.67
```

Table 2-24. Listing of Instrumentation Channel Numbers and Conversion Factors (Cont'd)

```
201   TTTTTT   1000.0   RPM          ENGINE SPEED      4 3S 9999. 2.000   45.67
202   VAL004   4.0000   MPA          PRESSURE DEMAND   4 3S 9999. 9999.   45.67
204   TTTTTT   4.0000   MPA          HE PRESS - MAX    4 3S 9999. 5.000   45.67
205   TTTTTT   4.0000   MPA          HE PRESS - TANK   4 3S 9999. 5.000   45.67
207   TTTTTT   200.00   DEG. C       TEMP CONTROL      4 3S 9999. 4.200   45.67
208   TTTTTT   200.00   DEG. C       TEMP HIGH TUBE    4 3S 9999. 4.200   45.67
209   TTTTTT   20.000   DEG. C       WATER TEMP IN     4 3H 9999. 3.500   45.67
224   VAL003   1.0000   VOLTS        POWER             4 3S 9999. 9999.   45.67
231   TTTTTT   8.0000   KWATTS       LINE POWER        4 3S 9999. 9999.   45.67
232   TTTTTT   2.0000   GPM          FLT.PLT.COOL.FLO  4 3S 4.000 9999.   45.67
233   KENDAL   10.000   W/M2         KENDALL PYRHELIO  4 1H 9999. 9999.   45.67
234   EPPLEY   117.10   W/M2         EPPLEY PYRHELIO   4 1S 9999. 9999.   45.67
235   BARPRE   1.0000   VOLTS        BAROMETRIC PRES.  4 3S 9999. 9999.   45.67
236   DEWPNT   1.0000   VOLTS        DEW POINT         4 3S 9999. 9999.   45.67
237   TTTTTT   6.7056   METER/S.     WIND SPEED        4 3S 9999. 9999.   45.67
238   TTTTTT   108.00   DEGREES      WIND DIRECTION    4 3S 9999. 9999.   45.67
239   TTTTTT   1.0000   MV           100 MV REFERENCE  4 1S 9999. 9999.   45.67
501                      HERTZ        ALT FREQUENCY
502                       P.F.        POWER FACTOR
503                          %        % MIRROR UNCOVRD
504                      PSI          PRESSURE DEMAND
513                      MM HG.       BAROMETRIC PRES.
514                      DEG. C       DEW POINT
PRINTOUT ORDER
207,191,185,202,148,192,186,181,233,193,187,182,237,194,188,183,201,232,195,184,
157,234,204,
REAL TIME PLOTS
157,              0.000    0000.00
233,              0.000    0000.00
207,144,163,      0.000    0000.00
204,              0.000    0000.00
163,164,165,166,400.0      0800.00
144,145,146,147,400.0      0800.00
191,192,193,194,400.0      0800.00
181,182,183,184,000.0      0600.00
185,186,187,188,000.0      0400.00
157,508,          000.0    0000.00
171,172,173,174,400.0      0800.00
148,149,160,161,400.0      0800.00
175,176,178,      400.0    0800.00
195,196,          000.0    0000.00
237,              000.0    0000.00
193,              000.0    0000.00
191,144,163,185,400.0      0800.00
192,145,164,186,400.0      0800.00
193,146,165,187,400.0      0800.00
```

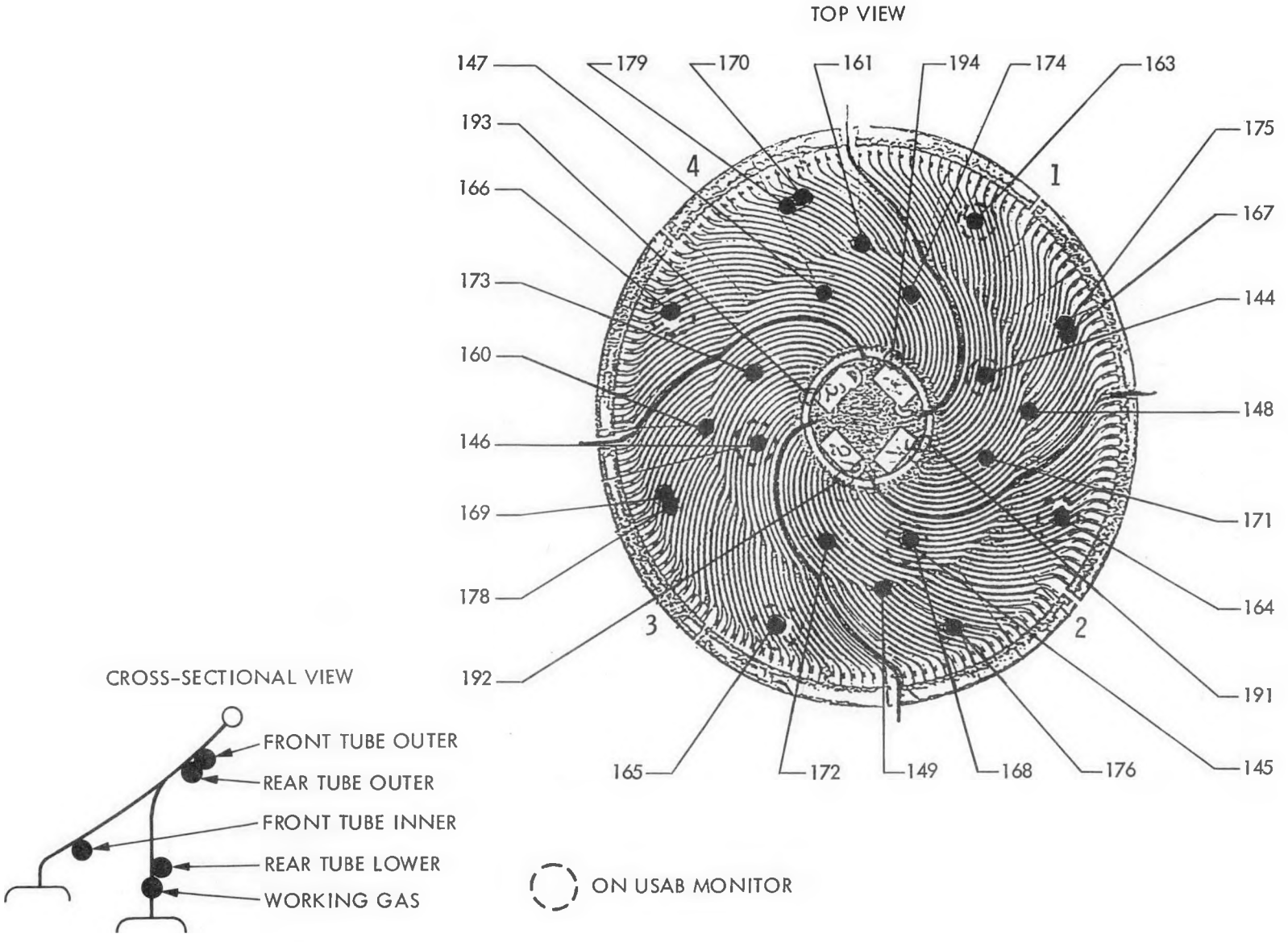

Figure 2-84. ESOR-IIA Thermocouple Positions (on Stirling 4-95, Engine No. 2)

Table 2-25. Thermocouple Positions and Channel Numbers[a]

USAB No.	Standard Channel No.	Data Log Channel	USAB Control Box No.	Location	Quadrant	Tube No.
1	45	144	1	Front Tube Inner	1	5
2	46	145	2	Front Tube Inner	2	5
3	47	146	3	Front Tube Inner	3	5
4	48	147	4	Front Tube Inner	4	5
21	49	148		Rear Tube Lower	1	14
22	50	149		Rear Tube Lower	2	14
23	61	160		Rear Tube Lower	3	14
24	62	161		Rear Tube Lower	4	14
13	64	163	5	Rear Tube Outer	1	5
14	65	164	6	Rear Tube Outer	2	5
15	66	165	7	Rear Tube Outer	3	5
16	67	166	8	Rear Tube Outer	4	5
17	68	167		Rear Tube Outer	1	14
18	69	168		Rear Tube Outer	2	14
19	70	169		Rear Tube Outer	3	14
20	71	170		Rear Tube Outer	4	14
5	72	171		Front Tube Inner	1	14
6	73	172		Front Tube Inner	2	14
7	74	173		Front Tube Inner	3	14
8	75	174		Front Tube Inner	4	14
9	76	175		Front Tube Outer	1	14
10	77	176		Front Tube Outer	2	14
11	79	178		Front Tube Outer	3	14
12	80	179		Front Tube Outer	4	14
25	92	191	9	Working Gas	1	
26	93	192	10	Working Gas	2	
27	94	193	11	Working Gas	3	
28	95	194	12	Working Gas	4	
29	82	181		Cavity Engine, front outer		
30	83	182		high middle		
31	84	183		low middle		
32	85	184		inner		

Table 2-25. Thermocouple Positions and Channel Numbers[a] (Cont'd)

USAB No.	Standard Channel No.	Data Log Channel	USAB Control Box No.	Location
33	86	185	13	Circ. Cavity, engine front
34	87	186		bottom
35	88	187	14	generator
36	89	188	15	top
				Cavity Outer Surf. Temp.
37	96	195		Low
38	97	196		High

[a]All USAB control box thermocouples are presented on USAB monitor.
Front Tube: Tube to/from cylinder. Rear Tube: Tube to/from regenerator.

(4) Test No. 4: Start-up and shutdown sequences to characterize control system parameters for optimization of sequences.

(5) Test No. 5: Control system test. During this test, engine control alternately was obtained by hybrid mode control system and solar-only mode control system to characterize control system operation.

Step-by-step instructions for safety check and operation were prepared by the cognizant engineer and followed in start-up, data acquisition, normal or emergency stop, and hot restart modes.

The control system is designed for autonomous operation after start-up. The control logic takes care of start-up and shutdown, depending upon the cloud cover. The alternator is connected and disconnected to the power line by a breaker.

After system start-up, nothing happens until power is supplied to the engine and the temperature reaches a preset level. The engine is rotated by connecting the alternator to the grid. The engine is operated by supplying the working gas or dumping it out to keep the gas temperature constant at various insolation levels. If the insolation level falls below a preset threshold intensity, the shutdown sequence is started. If the insolation level increases again, the temperature rise initiates the start-up sequence. In a shutdown sequence, the alternator is disconnected from the grid when power from the alternator becomes negative. The system is completely stopped by shutdown of the control system.

Data on parameters related to system monitoring and performance were continually recorded on magnetic tape once every minute, occasionally once every 20 seconds. Accumulated data are made available in hard copy form.

Time variation of selected data points was computer plotted to monitor system behavior and to determine steady performance intervals during which data is meaningful. A sample of such a computer plot is given in Figure 2-85.

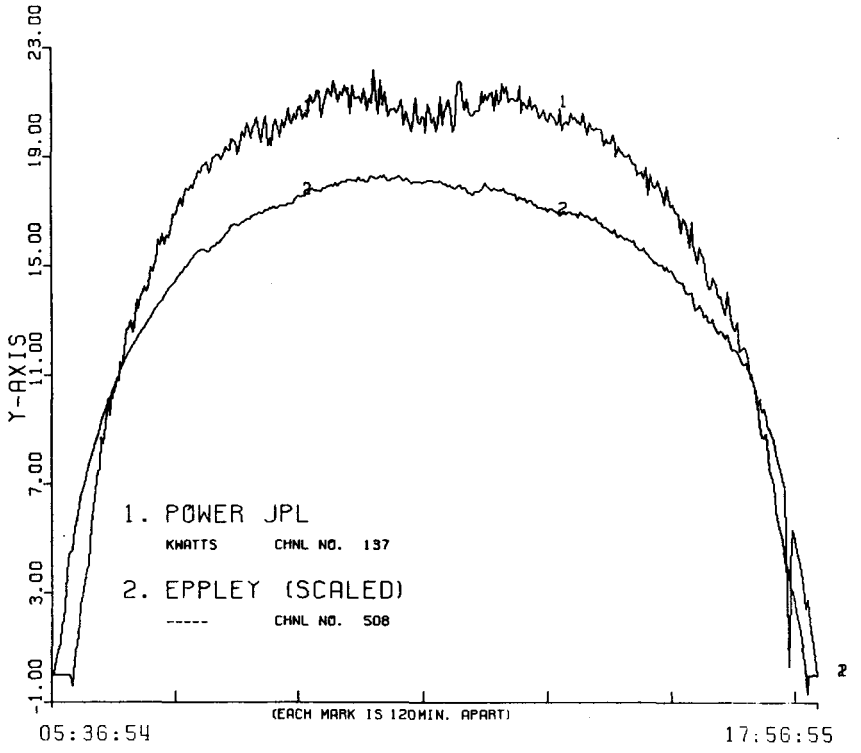

Figure 2-85. Sample Computer Plot of ESOR Test Data (ESOR-III, 100% TBC-2 Mirrors, 742 Scans, 60 s Between Scans, 9-7-83)

SECTION III

LESSONS LEARNED

Every test run at the Parabolic Dish Test Site had certain specific objectives that were reported in a variety of documents mainly as progress reports and final surveys of the JPL thermal power systems work. But beyond these detailed reports, certain common characteristics of all the thermal power systems testing have become evident. While many of these observations may seem obvious, they are noted here to complete the documentation of the PDTS testing experience.

The question has been raised frequently as to whether field testing is a worthwhile technique that justifies the significant expenditures required. JPL's experience strongly supports this type of testing. Not only does it provide the data necessary to positively confirm acceptance criteria but allows for the confirmation and calibration of analytical and computer-based design tools. Often the unexpected problems and unanticipated data lead to new developments of considerable value to the program. And well taken numerical data provide a level of credibility not likely with analysis alone.

Due to the unexpected aspects of any test program, it is here that required resources are most likely to be underestimated. Particularly in the areas of test preparation and instrumentation checkout, both the costs and time scheduled are often seriously overrun. This can and should be avoided by taking as much care with test preparation as with test operations. Two areas that must be considered carefully are the selection of the number of data channels and the amount of data collected. Clearly, enough data sensors and adequate time constants must be used to capture enough data to meet test purposes, but superfluous data not only lead to excess setup costs but put a needless drain on storage and data-reduction resources.

A critical element in the production of unimpeachable test results is well calibrated, reliable, and repeatable test instrumentation. No matter how well designed the experiment may be, if the resulting data are inconsistent, incomplete, or intermittent, test validity will be in doubt. Careful preparation, installation, and calibration including pretest simulations are well worth the effort. This should include a complete end-to-end check of the data acquisition plus data reduction to ensure that no incompatibilities will be found later. "Quick-look" data dumps must be available during testing to allow for instrumentation and data acquisition system verification during real-time testing.

An important part of both preparation and operation is documentation. Carefully thought-through planning of documents, good test procedures, and thorough test data contribute greatly to the success of the test. Documentation is especially important for ensuring the safety of personnel and equipment. Good safety procedures, safety check lists prepared well before the actual test period, and clear emergency operating procedures are an absolutely essential part of a well run test. A regularly kept log book of day-to-day events will often prove invaluable in reconstructing test events if questions arise later and also is a good source for planning new tests.

While knowledgeable, well trained personnel are essential for effective test organization, clearly defined lines of authority and task descriptions must be carefully determined to make effective use of even the best cadre. A clear understanding of each test crew member's responsibilities and duties will ensure successful test data acquisition during normal test periods but, as importantly, will form the essential framework necessary when problems and emergencies arise. It is teamwork that will provide a consistently successful test effort.

SECTION IV

REFERENCES

1. Hagen, T.L., "JPL's Parabolic Dish Test Site," Proceedings of the First Semiannual Receiver Systems Progress Review, JPL Publication 80-10, DOE/JPL-1060-33, pp. 119-123, April 15, 1980.

2. Livingston, F.R., Activity and Accomplishments in Dish/Stirling Electric Power System Development, JPL Publication 85-8, DOE/JPL-1060-82, February 15, 1985.

3. Test Results of an Organic Rankine-Cycle Power Module for a Small Community Solar Thermal Power Experiment, JPL Report No. 9950-995, DOE/JPL-1060-83, Ford Aerospace and Communications Corporation, Newport Beach, California, January 15, 1985.

4. Owen, W.A., The JPL Flux Mapper, JPL Report No. 5105-148, June 15, 1985.

5. Miyazono, C., Software Used with the Flux Mapper at the Solar Parabolic Dish Test Site, JPL Publication 84-76, DOE/JPL-1060-78, September 15, 1984.

6. Patzold, J.D., "Omnium-G Concentrator Test Results," Proceedings of the First Semiannual Distributed Receiver Systems Program Review, JPL Publication 80-10, DOE/JPL-1060-33, pp. 125-131, April 15, 1980.

7. Starkey, D.J., "Initial Test Bed Concentrator Characterization," Proceedings of the First Semiannual Distributed Receiver Systems Program Review, JPL Publication 80-10, DOE/JPL-1060-33, pp. 47-51, April 15, 1980.

8. Starkey, D.J., "Characterization of Point Focusing Test Bed Concentrators at JPL," Parabolic Dish Solar Thermal Power Annual Program Review Proceedings, JPL Publication 81-44, DOE/JPL-1060-46, pp. 135-142, May 1, 1985.

9. Miyazono, C., Overview of Software Development at the Parabolic Dish Test Site, JPL Report No. 5105-155, August 1, 1985.

10. Dennison, E.W., and Thostesen, T.O., Development and Testing of Parabolic Dish Concentrator No. 1, JPL Publication 85-4, DOE/JPL-1060-81, December 15, 1984.

11. Wright, C.C., and Bank, H., "The Development of an 85-kW (Thermal) Steam Rankine Solar Receiver," Parabolic Dish Solar Thermal Power Annual Program Review Proceedings, JPL Publication 81-44, DOE/JPL-1060-46, pp. 67-74, May 1, 1981.

12. Owen, W.A., Design and Testing of Cavity Solar Receivers, JPL Report No. 5105-153, July 15, 1985.

13. Greeven, M., and Owen, W., "The Development of an 85-kW (Thermal) Air Brayton Solar Receiver," Parabolic Dish Solar Thermal Power Annual Program Review Proceedings, JPL Publication 81-44, DOE/JPL-1060-46, pp. 57-65, May 1, 1981.

14. Hanseth, E.J., "Development, Solar Test, and Evaluation of a High-Temperature Air Receiver for Point-Focusing Parabolic Dish Applications," AIAA Meeting, Colorado Springs, Colorado, December 1-3, 1981.

15. Nesmith, B.J., "Jay Carter Enterprises Inc. Steam Engine," Parabolic Dish Solar Thermal Power Annual Program Review Proceedings, JPL Publication 81-44, DOE/JPL-1060-46, pp. 11-15, May 1, 1981.

16. Jaffe, L.D., Solar Tests of Aperture Plate Materials for Solar Thermal Dish Collectors, JPL Publication 83-68, DOE/JPL-1060-62, August 15, 1983.

17. Dennison, E.W., View-Limiting Shrouds for Insolation Radiometers, JPL Report No. 5105-154, March 15, 1985.

18. Kiceniuk, T., Development of an Organic Rankine-Cycle Power Module for a Small Community Solar Thermal Power Experiment, JPL Publication 85-3, DOE/JPL-1060-80, January 15, 1985.

19. Selcuk, M.K., Dish-Stirling Module Performance As Evaluated from Tests of Various Test Bed Concentrator/Stirling Engine Configurations, JPL Report No. 5105-149, June 1, 1985.

SECTION V

BIBLIOGRAPHY

TBC Characterization Tests

Starkey, D.J., and Owen, W.A., "The JPL Flux Mapper and the Characterization of Point Focusing Test Bed Concentrators," International Solar Energy Society Meeting, Philadelphia, Pennsylvania, May 1981.

PDC-1 Characterization

Dennison, E.W., and Argoud, M.J., "Solar Concentrator Panel and Gore Testing in the JPL 25 Foot Space Simulator," AIAA 2nd Terrestrial Energy Systems Conference, Paper No. AIAA-81-2534, Colorado Springs, Colorado, December 1-3, 1981.

Sobczak, I.F., and Thostesen, T., "Parabolic Dish Concentrator (PDC-1) Development," Proceedings Fourth Parabolic Dish Solar Thermal Power Program Review, JPL Publication 83-2, DOE/JPL-1060-58, pp. 161-168, February 1, 1983.

Steam Rankine Solar Receiver Testing

Owen, W., Bank, H., Otth, D., Wright, C., and Hagen, T., "First Results of Steam Receiver Testing at JPL's Parabolic Dish Test Site," Proceedings AS/ISES Meeting, pp. 415-418, Philadelphia, Pennsylvania, May, 1981.

Air Brayton Solar Receiver Testing

Eastwood, J., Greeven, M., and Hall, A., Air Brayton Solar Receiver Design and Performance Evaluation, JPL Contract No. 955136, Garrett AiResearch Report No. 81-17998, June 16, 1981.

Greeven, M., et al, "A Solar Receiver for a 25 kW(e) Gas Turbine," Mech. Engineering, pp. 26-29, January 1981.

Organic Rankine-Cycle Module

Barber, R.E., and Boda, F.P., "Organic Rankine Power Conversion Subsystem Development for the Small Community Solar Thermal Power System," Parabolic Dish Solar Thermal Power Annual Program Review Proceedings, JPL Publication 82-66, DOE/JPL-1060-52, pp. 101-113, July 15, 1982.

Boda, F.P., "The SCSE Organic Rankine Engine," IECEC, Atlanta, Georgia, August 9-14, 1981.

Haskins, H.J., Taylor, R.M., and Osborn, D.B., "Development of the Solar Receiver for an Organic Rankine Cycle Engine," IECEC, Atlanta, Georgia, August 9-14, 1981.

Stirling Module Testing

Nelving, H.G., and Percival, W.H., "Modifications and Testing of a 4-95 Stirling Engine for Solar Applications," Parabolic Dish Solar Thermal Power Annual Program Review Proceedings, JPL Publication 82-66, DOE/JPL-1060-52, July 15, 1982.

APPENDIX A

CHRONOLOGICAL LISTING OF PDTS ACTIVITIES

Oct 77	- Insolation measurements started on strip chart recorders.
Jan 78	- Insolation measurements begun on magnetic tape.
Apr 78	- Started recording insolation, wind, and temperature measurements on magnetic tape.
Jun 78	- Data logger interfaced with digital TV.
Oct 78	- Precursor concentrator test begun; calorimeter built and used.
	- New data logger and magnetic tape for insolation and weather data.
Nov 78	- PDTS manager appointed.
Jan 79	- Initiate Omnium-G testing.
	- First two formal tests run.
	- Weather data instrumentation placed on the standby generator.
Feb 79	- Precursor concentrator tests completed.
	- Omnium-G (OG) calorimeter (flat-plat, cold-water) with and without apertures.
Mar 79	- OG calorimeter test rerun, moonlight alignment tests.
	- Precursor tests with flat-plate calorimeter used in OG testing.
Apr 79	- Old petal OG tests.
May 79	- New OG petals installed -- moonlight alignment.
	- OG flux mapper built.
Jun 79	- OG flat-plate calorimeter tested.
	- New OG receiver installed.
	- Cold-water calorimeter tests with OG receiver.
	- OG cold-water calorimeter tests rerun.
Aug 79	- OG receiver proof test.
	- OG concentrator/receiver high-temperature tests.

Oct 79	- Change name from PFSTS to PDTS (Parabolic Dish Test Site).
Dec 79	- OG system level tests using 10-cm aperture.
	- Flux mapper preparations completed.
Jan 80	- OG flux mapper tests.
	- TBC sensor alignment.
	- Emergency power set installed.
	- 5000-gal tank installed.
Feb 80	- OG flat-plate calorimeter tests (10-in. aperture plate) made.
	- Prepare TBC for flux mapper and cold-water cavity calorimeter (CWCC) testing.
	- Circumsolar telescope failed, then repaired and put back into service.
	- Eppley pyrheliometer added.
	- OG calorimeter tests with 8-in. aperture plate.
	- TBC-1 flux mapping started.
Mar 80	- TBC-1 tests with flux mapper. First, 36 mirror facets uncovered; then 65, 40, and 105 mirrors uncovered.
	- Flux mapper tests on TBC-1.
	- OG calorimeter tests with 8-in. aperture plate.
	- Focal plane fogging tests.
Apr 80	- Flux mapper cooling system redesigned and reinstalled on TBC-1.
	- Three-day automated testing of OG module.
	- Bench test of small Carter steam engine with alternator as a starter.
	- 1-in.-thick zirconia melt-through tests -- 104 mirrors uncovered for a 10-minute exposure on sun.
May 80	- OG high-temperature calorimetry continued.
	- CWCC calibration testing started -- quartz lamps used as heat source.

Jun 80	- Flux mapper radiometer calibration.
	- Mirror alignment using colored disk method on TBC-2.
Jul 80	- CWCC testing with 156, 224, and 104 mirrors uncovered (no aperture).
Aug 80	- TBC-1 and TBC-2 realignment for peak flux reduction.
	- TBC-2 characterization using the flux mapper with 224 mirrors uncovered.
	- TBC-1 CWCC testing, 10-in. aperture, later 8-in. aperture.
Sep 80	- Garrett steam Rankine receiver testing on TBC-1.
Oct 80	- OG flux mapping to see any deterioration of petals.
Nov 80	- Sanders ceramic receiver testing started -- 25% mirrors uncovered on TBC-2.
	- Steam Rankine receiver tests up to 700°C at 7-MPa range.
	- Furfural experiment on TBC-1.
	- TBC-1 flux mapping with 25 and 50% mirrors uncovered.
	- OG flux mapping completed.
Dec 80	- Jay Carter steam engine tests.
	- Sanders ceramic receiver testing with 25, 50, and 100% mirrors uncovered; 1093°C achieved with 100% mirrors.
	- Second furfural experiment on TBC-1 using Garrett steam Rankine receiver.
	- TBC-1 flux mapping to characterize the concentrator at 75 and 100% mirrors uncovered.
Jan 81	- Jay Carter steam engine tests; 15 kW_e delivered.
	- Sanders ceramic receiver tests at 871 to 1427°C.
	- Fairchild/Stratos hybrid Stirling receiver combustor and heat transfer verification. Tests run at partial power.
	- Some Garrett steam receiver tests.
Feb 81	- Sanders receiver tested at full power (1370°C).
Mar 81	- Garrett plate for air Brayton receiver installed, instrumented, and checked.

Mar 81 (cont'd) - Dish/Stirling solar hybrid receiver (DSSR) combustion and heat transfer testing with a larger blower and preheater supplied.

- Testing Garrett steam receiver continued.

Apr 81 - Carter single- and two-cylinder engine tests were set up at PDTS.

- Garrett aperture plate for air receiver tests started at 715°C inlet, 820°C out, 50% mirrors.

- Further preparations for DSSR testing.

- Ground-mounted 0G engine using Garrett steam receiver on TBC-1.

- Two-cylinder Carter steam engine tests completed.

May 81 - Garrett air receiver testing on TBC-2 completed, 100% mirrors at 816°C (1500°F).

- TBC-2 realignment for DSSR testing.

- Single-cylinder Carter engine test.

- 0G steam engine generator tests continued.

Jun 81 - DSSR delivered to PDTS and subsequently mated to a USAB Stirling power conversion unit (engine plus alternator).

- TBC-2 flux mapping for Stirling power conversion assembly (receiver plus PCU) test, 25% mirrors.

- Single-cylinder Carter engine tested at 316-427°C (600 to 800°F).

Jul 81 - 50% mirror configuration flux mapping.

- TV monitor for Stirling power conversion assembly (PCA) testing completed.

- TBC-1 realignment, TBC-2 night optical tests with mock-up receiver.

- CWCC tests were made on TBC-2 with 25, 50, and 80% mirror exposures with 8- and 6-in. aperture plates.

- 100% TBC-2 CWCC tests with 4, 6, 8, and 10-in. apertures.

Aug 81 - TBC-1 realigned for organic Rankine-cycle (ORC) engine testing, and preparations were made for flux mapping.

Aug 81 (cont'd) - Stirling PCA tested on ground pad; ran with fossil fuel up to 15 kW_e.

- OG thermal module testing started.

Sep 81 - Completed ground test of the Stirling PCA and initiated preparation for mounting on TBC-2.

- Completed OG system testing and disassembled and shipped necessary components to Southern New England Telephone Company.

- Reconfigured mirrors on TBC-1 to support ORC test program by reducing the heat intensity at the center of the focal plane.

Oct 81 - Mounted the Stirling PCA and installed associated cooling, fuel, power, and instrumentation on TBC-2 and initiated fossil fuel testing.

- Permanently disconnected the circumsolar telescope after it became inoperative.

- Flux mapped TBC-1 in preparation for ORC PCA testing.

Nov 81 - Initiated "on sun" testing of the solar/hybrid Stirling PCA on TBC-2 with 25% of the mirrors exposed.

- Initiated cavity calorimeter testing on TBC-1 in preparation for testing of the ORC PCA. The test was run with 50% of the mirrors exposed.

Dec 81 - Reinitiated "on-sun" testing of the Stirling PCA on TBC-2 with 50% of the mirrors exposed.

- Completed cavity calorimeter testing on TBC-1 in preparation for testing of the ORC PCA.

Jan 82 - Testing was initiated on the Stirling PCA (ESOR-I and Stirling power conversion unit) and continued throughout the month on TBC-2.

- Mounted the ORC PCA on TBC-1 and completed all mechanical, electrical, and instrumentation connections.

Feb 82 - Videotaped the organic Rankine-cycle and Stirling-cycle PCAs mounted on the TBCs during solar operation.

- Installed orifices in the TBC water return lines to regulate water flow and thus provide freeze protection during cold nights.

- Added a second electrical substation to the PDTS providing greater capacity and sensitive instrumentation isolation. The PDTS computer was connected to this substation.

Feb 82 (cont'd) - Completed testing the first USAB experimental solar-only receiver (ESOR-1) and removed ESOR-1 and the Stirling power conversion unit (PCU) from TBC-2.

- Repositioned the Stirling PCA by removing mounting spacers, thus placing the PCA 0.5 in. closer to the dish to increase power output.

- Completed dry runs on the ORC PCA and initiated testing.

Mar 82 - Completed testing and removed the second USAB experimental solar-only receiver (ESOR-IIA) and Stirling PCU from TBC-2.

- Installed and completed tests of the third USAB solar-only receiver (ESOR-IIB) with the Stirling PCU on TBC-2.

- Completed testing of the ORC PCA.

Apr 82 - Removed the third experimental solar-only receiver (ESOR-IIB) and the Stirling PCU from TBC-2.

- Reassembled the dish/Stirling hybrid solar receiver (DSSR) to the Stirling PCU and installed the assembly on TBC-2. Initial testing was off-sun using the combustor followed by on-sun hybrid testing with 25% exposed mirrors. The hybrid receiver and Stirling PCU were removed from TBC-2.

- Removed ORC PCA from TBC-1 after completion of testing.

- Installed cavity calorimeter at the focal plane of TBC-1 and initiated normal periodic calibration of TBC-1.

- Completed PDC-1 foundation installation.

May 82 - Realigned the mirrors on TBC-2 to increase thermal input for Stirling PCA tests.

- Mated the experimental solar-only receiver (ESOR-IIA) to a second Stirling PCU and then installed the receiver/engine/alternator combination on TBC-2.

- Increased the height and length of travel of the two water-cooled aperture plates (because of the increased size of the sun's image on the water-cooled plate resulting from the mirror realignment).

- Replaced synchronous motor (used for power factor correction) with fixed capacitors, thus reducing parasitics in the Stirling PCU by 2 kW_e.

- Initiated testing of the Stirling PCA first with 50% mirrors exposed and then 80%.

Jun 82

- Mated ESOR-IIB to the Stirling PCU and reinstalled the PCA (receiver/engine/alternator combination) on TBC-2. Initiated testing that continued throughout most of the month.
- Tested the Stirling PCA from sunrise to sunset for three consecutive days as part of the continuing characterization of the engine.

Jul 82

- Resumed testing of ESOR-IIA and the Stirling PCU on TBC-2.
- Executed sunrise-to-sunset testing of ESOR-IIA for two consecutive days.
- Completed the planned series of tests on the ESORs.
- Completed cavity calorimeter testing of TBC-1. This was part of the continuing characterization of TBC-1 in preparation for resuming ORC PCA tests.
- Initiated a series of materials tests on TBC-1.

Aug 82

- Initiated and completed flux mapping test of TBC-2 to assist USAB in the design of a new ESOR to be used in conjunction with followup testing of the Stirling PCU.

Sep 82

- Remounted ESOR-IIA and the Stirling PCU on TBC-2 and resumed testing.
- Initiated and completed cold-water cavity calorimeter testing of TBC-1.

Oct 82

- Completed testing of ESOR-IIA and the Stirling PCU on TBC-2.
- Mounted ESOR-IIB and the Stirling PCU on TBC-2 and initiated testing.
- Completed materials tests on TBC-1.
- Conducted anti-reflection-coated pyrex window transmittance tests.

Nov 82

- Initiated and completed the terminal concentrator tests on TBC-1.
- Completed rework of PDC-1. This was followed by optical tests and preliminary testing using the cold-water cavity calorimeter with no aperture plate.

Dec 82

- Completed installation of the flux mapper on TBC-1.
- Initiated and completed paving around PDC-1.

Jan 83

- Initiated flux mapping tests of TBC-1 in preparation for Brayton testing.

Jan 83 (cont'd) - Initiated and completed cavity calorimeter testing of TBC-2 in preparation for resuming testing of the Stirling PCA.

Feb-Mar 83 - Installed a quartz window in ESOR-IIA and conducted a brief test with the Stirling PCU, providing a direct comparison with all previous ESOR-IIA tests conducted without a window at the PDTS.

- Completed testing of ESOR-IIA and replaced it with ESOR-III on TBC-2 and initiated testing.

- Installed a 380-mm (15-in.) aperture on the CWCC in preparation for further performance testing of PDC-1.

Apr 83 - Completed installation of the early Stirling-cycle PCU with ESOR-IIA on TBC-1. Initiated a series of tests on this new configuration singly and in conjunction with the Stirling PCA on TBC-2.

- Initiated and completed nighttime remote light optical tests to diagnose the uneven heating of the Stirling engine heater heads on TBC-2. Optical tests were also made on TBC-2.

- Initiated performance testing of PDC-1 with a 380-mm (15-in.) aperture on the cold-water cavity calorimeter.

- Initiated a new series of materials tests on TBC-1.

May 83 - Completed a series of materials tests on TBC-1. Fourteen materials were tested at solar fluxes of about 7000 kW/m^2.

- Replaced ESOR-III with ESOR-IIA on TBC-2 and continued testing. Tests were made with and without the quartz window in the newly installed receiver.

- Completed dismantling of the OG unit to make room for the LaJet concentrator, which was to be installed at a later date.

Jun 83 - Completed design drawings detailing necessary modifications to the PDTS to accommodate the LaJet concentrator.

- Full power testing of a USAB Model 4-95 engine with ESOR-III continued without interruption on TBC-2.

- With the aid of T. B. Elfe of the Georgia Tech Research Institute, TBC mirror alignment was accomplished by aligning all mirror images of a remote light at once on a target placed about 30 in. forward or aft of the principal focus.

- The 220 mirror facets on TBC-1 were realigned for the other USAB Model 4-95 engine performance tests.

Jun 83 (cont'd) - Evaluated the amount of oxidation of a graphite aperture plate on TBC-1 because of the concentrated beam spillage.

Jul 83 - Completed installation of the USAB Model 4-95 with ESOR-IIA and TBC-1 and initiated testing.

Aug-Sep 83 - Replaced the broken piston rod in the Stirling engine and reinstalled the PCU and ESOR-IIA on TBC-1 during August. Testing was resumed and continued with no further problems.

- Initiated and completed thermography testing of the Stirling PCA on TBC-2 during August.

- Performed a successful sunrise-to-sunset test with the Stirling PCA on TBC-2 during September.

- Initiated tests during September to determine the feasibility of using PDC-1 for Stirling PCA testing.

Oct-Nov 83 - Performed successful sunrise-to-sunset tests with the Stirling PCA on TBC-2 during October. Hydrogen was used as the working gas during these tests.

- Installed a new receiver (ESOR-IV) on the Stirling PCU and mounted it on TBC-2 during October.

- Reinstalled the Stirling PCU (with ESOR-III) on TBC-2 and resumed testing in November.

- TBC-1 was disassembled by personnel from Sandia National Laboratories-Albuquerque.

Dec 83-Jan 84 - The elevation drive on PDC-1 was modified to preclude slippage of the elevation drive cable on the pulley drives. After modifications with a static imbalance of over 1500 lb, no slippage occurred.

- The ESOR-IV heater heads were repaired by Solar Turbines and returned to the test operations facility and remounted on the Stirling PCU.

- The Stirling PCU (with ESOR-III mated to it) was removed from TBC-2. ESOR-III was then replaced by ESOR-IV and the Stirling PCA was then remounted on TBC-2. Testing was then resumed in December and continued throughout the month of January. The Stirling PCA was removed from TBC-2 at the end of January.

- Two of the three wheels on TBC-2 were moved 1.5 in. toward the center of the concentrator during January to preclude any further propagation of cracks.

APPENDIX B

COMPUTER PROGRAMS EMPLOYED TO PROCESS PDTS TEST DATA

A. INTRODUCTION

After the data acquisition system described in Section II.A of this report became operational, all test data were recorded on magnetic tape and reprocessed for conversion of each signal to engineering units; calculations were then performed to evaluate component or system performance. Data were gathered until January 25, 1984.

A complete list of experiments run during this period is presented in Table B-1. After each test was performed, data were processed by means of a computer program and results made available to cognizant engineers and other users.

In addition to data gathered by the PDTS data acquisition system, data were also recorded at the PDTS by the flux-mapper controller unit, the Lawrence Berkeley Laboratory (LBL) unit, and the FACC computer system:

(1) All flux-mapper data were taken by the flux-mapper controller unit. No flux-mapper data were taken by the PDTS data acquisition system for permanent storage. The data acquisition system was in operation during most flux mappings but only to provide alarms for low water flow. The data were usually erased immediately after the test.

(2) All data for the circumsolar telescope were recorded on magnetic tape on the LBL unit. The data were also analyzed by LBL; some of these results were obtained by JPL personnel.

(3) All data from ORC module testing on a TBC were taken on a computer system installed and maintained by FACC and made available to JPL personnel.

B. COMPUTER PROGRAM DESCRIPTION

Table B-2 is a list of the computer programs utilized at the PDTS. Descriptions of most of the programs follow in which redundant statements dealing with channel numbers, reading, writing, printing page headings, and reformatting are excluded. Instead, only those portions dealing with the calculations used to process raw data are presented.

1. OG Flat-Plate Calorimeter

The program for printing out Omnium-G (OG) flat-plate calorimeter data from magnetic tape and processing it was updated several times.

Table B-1. Log of Tests Run at the PDTS

```
12345678901234567890123456789012345678901234567890123456789012345678901234567890
BR0101 10:13:18  1-APR-81 060   30  XXXX TBC2 ON SUN WITH BRAYTON AIR RECEIVER
OG0101 14:41:53  1-APR-81 043   20  XXXX TBC1 WITH OG STEAM ENGINE
OG0102 10:05:53  3-APR-81 043   20  XXXX TBC1 WITH OG STEAM ENGINE
OG0103 14:28:04  3-APR-81 023   20  XXXX TBC1 WITH OG STEAM ENGINE
BR0103 13:38:34  6-APR-81 046   30  XXXX TBC2 ON SUN WITH BRAYTON AIR RECEIVER
OG0104 10:04:46  7-APR-81 052   20  XXXX TBC1 WITH OG STEAM ENGINE
OG0105 11:07:41  7-APR-81 012   20  XXXX TBC1 WITH OG STEAM ENGINE
OG0106 14:04:17  7-APR-81 060   20  XXXX TBC1 WITH OG STEAM ENGINE
OG0107 10:11:14  8-APR-81 078   20  XXXX TBC1 WITH OG STEAM ENGINE
OG0108 11:18:57  9-APR-81 010   20  XXXX TBC1 WITH OG STEAM ENGINE
OG0109 12:51:38  9-APR-81 070   20  XXXX TBC1 WITH OG STEAM ENGINE
BR0104 10:38:00 13-APR-81 044   30  XXXX TBC2 ON SUN WITH BRAYTON AIR RECEIVER
BR0106 09:55:20 15-APR-81 070   30  XXXX TBC2 ON SUN WITH BRAYTON AIR RECEIVER
BR0107 14:19:24 15-APR-81 072   30  XXXX TBC2 ON SUN WITH BRAYTON AIR RECEIVER
BR0108 09:52:30 16-APR-81 052   30  XXXX TBC2 ON SUN WITH BRAYTON AIR RECEIVER
BR0109 10:09:18 17-APR-81 007   07  XXXX TBC2 ON SUN WITH BRAYTON AIR RECEIVER
OG0110 12:33:09 20-APR-81 102   20  XXXX TBC1 WITH OG STEAM ENGINE
OG0111 09:44:19 21-APR-81 052   20  XXXX TBC1 WITH OG STEAM ENGINE
CR0101 10:31:28 22-APR-81 022   20  XXXX TBC1 WITH OG STEAM ENGINE
CR0102 12:12:08 22-APR-81 020   20  XXXX TBC1 WITH OG STEAM ENGINE
CR0103 13:03:53 22-APR-81 107   20  XXXX TBC1 WITH OG STEAM ENGINE
OG0112 12:01:48 23-APR-81 099   20  XXXX TBC1 WITH OG STEAM ENGINE
BR0110 14:31:40 23-APR-81 014   30  XXXX TBC2 ON SUN WITH BRAYTON AIR RECEIVER
OG0113 11:05:48 24-APR-81 070   20  XXXX TBC1 WITH OG STEAM ENGINE
BR0111 09:52:12 27-APR-81 039   30  XXXX TBC2 ON SUN WITH BRAYTON AIR RECEIVER
BR0112 11:44:09 27-APR-81 023   10  XXXX TBC2 ON SUN WITH BRAYTON AIR RECEIVER
BR0113 13:26:58 27-APR-81 065   30  XXXX TBC2 ON SUN WITH BRAYTON AIR RECEIVER
CR0104 10:18:18 28-APR-81 028   20  XXXX TBC1 WITH OG STEAM ENGINE
CR0105 10:52:24 28-APR-81 158   20  XXXX TBC1 WITH OG STEAM ENGINE
BR0114 09:03:54 29-APR-81 017   10  XXXX TBC2 ON SUN WITH BRAYTON AIR RECEIVER
BR0115 11:19:00 29-APR-81 073   30  XXXX TBC2 ON SUN WITH BRAYTON AIR RECEIVER
BR0116 11:27:35 30-APR-81 091   30  XXXX TBC2 ON SUN WITH BRAYTON AIR RECEIVER
CR0201 12:29:06  1-MAY-81 023   20  XXXX TBC1 WITH CARTER 8 HP ENGINE
CR0202 13:40:56  1-MAY-81 041   20  XXXX TBC1 WITH CARTER 8 HP STEAM ENGINE
CR0203 12:34:00  4-MAY-81 061   20  XXXX TBC1 WITH CARTER 8 HP STEAM ENGINE
BR0117 11:05:22  4-MAY-81 068   30  XXXX TBC2 ON SUN WITH BRAYTON AIR RECEIVER
BR0118 12:33:19  4-MAY-81 063   30  XXXX TBC2 ON SUN WITH BRAYTON AIR RECEIVER
BR0119 07:31:46  5-MAY-81 046   20  XXXX TBC2 ON SUN WITH BRAYTON AIR RECEIVER
BR0120 07:55:56  7-MAY-81 035   30  XXXX TBC2 ON SUN WITH BRAYTON AIR RECEIVER
BR0121 07:55:56  7-MAY-81 015   30  XXXX TBC2 ON SUN WITH BRAYTON AIR RECEIVER
BR0122 09:20:30  7-MAY-81 157   30  XXXX TBC2 ON SUN WITH BRAYTON AIR RECEIVER
OG0114 11:37:29 11-MAY-81 076   20  XXXX TBC1 WITH OG STEAM ENGINE
OG0115 13:01:59 11-MAY-81 026   20  XXXX TBC1 WITH OG STEAM ENGINE
CR0204 12:46:49 12-MAY-81 070   20  XXXX TBC1 WITH CARTER 8HP
OG0116 09:01:18 20-MAY-81 172   20  XXXX TBC1 WITH OG STEAM ENGINE
OG0117 09:25:03 22-MAY-81 012   20  XXXX TBC1 WITH OG STEAM ENGINE
OG0118 11:20:45 22-MAY-81 048   20  XXXX TBC1 WITH OG STEAM ENGINE
OG0119 08:10:33 29-MAY-81 208   20  XXXX TBC1 WITH OG STEAM ENGINE
CR0205 08:44:09  3-JUN-81 115   20  XXXX TBC1 WITH CARTER 8HP
OG0120 11:03:40  5-JUN-81 065   20  XXXX TBC1 WITH OG STEAM ENGINE
OG0121 12:35:03  5-JUN-81 080   20  XXXX TBC1 WITH OG STEAM ENGINE
CR0206 11:02:01  8-JUN-81 174   20  XXXX TBC1 WITH CARTER 8HP
CR0208 09:29:58 12-JUN-81 178   20  XXXX TBC1 WITH CARTER 8HP STEAM ENGINE
OG0122 11:03:52 16-JUN-81 030   20  XXXX TBC1 WITH OG STEAM ENGINE
OG0123 12:00:39 16-JUN-81 121   20  XXXX TBC1 WITH OG STEAM ENGINE
OG0201 07:56:27 19-JUN-81 020   20  XXXX TBC1 WITH OG STEAM ENGINE
OG0202 09:22:37 19-JUN-81 069   20  XXXX TBC1 WITH OG STEAM ENGINE
OG0203 12:05:40 19-JUN-81 122   20  XXXX TBC1 WITH OG STEAM ENGINE
CR0209 11:46:15 23-JUN-81 027   20  XXXX TBC1 WITH CARTER 8HP STEAM ENGINE
CR0210 12:35:31 23-JUN-81 047   20  XXXX TBC1 WITH CARTER 8HP STEAM ENGINE
FM0204 09:21:58 24-JUN-81 066   ZZ  FLX2 TBC2 FLUX MAP, Z=+7.0
```

Table B-1. Log of Tests Run at the PDTS (Cont'd)

FM0205	08:09:53	25-JUN-81	039	ZZ	FLX2 TBC2 FLUX MAP, Z=+0.0
FM0206	09:27:09	25-JUN-81	040	ZZ	FLX2 TBC2 FLUX MAP, Z=-2.0
FM0207	11:00:59	25-JUN-81	060	ZZ	FLX2 TBC2 FLUX MAP, Z=-4.0, TIME ERROR
FM0208	12:15:30	25-JUN-81	055	ZZ	FLX2 TBC2 FLUX MAP, Z=-6.0
FM0230	14:04:16	25-JUN-81	060	ZZ	FLX2 TBC2 FLUX MAP, Z=-7.5, TIME ERROR
CR0211	09:54:19	26-JUN-81	131	20	ARC8 TBC1 WITH CARTER 8HP STEAM ENGINE
FM0210	10:44:24	29-JUN-81	078	ZZ	FLX2 TBC2 FLUX MAP, Z=+7.0
FM0211	12:20:04	29-JUN-81	061	ZZ	FLX1 TBC2 FLUX MAP, Z=+6.0
FM0212	13:33:00	29-JUN-81	070	ZZ	FLX2 TBC2 FLUX MAP
CR0212	12:44:55	29-JUN-81	056	20	ARC9 TBC1 WITH CARTER 8HP STEAM ENGINE
FM0293	10:09:40	30-JUN-81	045	ZZ	FLX1 TBC2 FLUX MAP, Z=+2.0
FM0214	11:37:48	30-JUN-81	039	ZZ	FLX2 TBC2 FLUX MAP, Z=+0.0
FM0295	12:38:26	30-JUN-81	039	ZZ	FLX1 TBC2 FLUX MAP, Z=-2.0
FM0216	13:23:30	30-JUN-81	044	ZZ	FLX1 TBC2 FLUX MAP, Z=-4.0
CR0213	11:17:37	2-JUL-81	100	20	ARC9 TBC1 WITH CARTER 8HP STEAM ENGINE
CR0214	11:24:39	6-JUL-81	068	20	ARC9 TBC1 WITH CARTER 8HP STEAM ENGINE
FM0227	12:30:12	6-JUL-81	038	ZZ	FLX2 TBC2 FLUX MAP, Z=-1.0
FM0217	11:44:40	8-JUL-81	073	ZZ	FLX1 TBC2 FLUX MAP, Z=+7.0
FM0218	13:08:05	8-JUL-81	072	ZZ	FLX2 TBC2 FLUX MAP, Z=+6.0
FM0299	07:33:32	9-JUL-81	039	ZZ	FLX1 TBC2 FLUX MAP, Z=+0.0
FM0220	08:30:14	9-JUL-81	038	ZZ	FLX2 TBC2 FLUX MAP, Z=-1.0
FM0221	09:19:21	9-JUL-81	016	ZZ	FLX2 TBC2 FLUX MAP, Z=-2.0, SHORT SCAN
FM0222	12:44:28	9-JUL-81	014	ZZ	FLX2 TBC2 FLUX MAP, Z=-1.0, SHORT SCAN
FM0223	13:09:49	9-JUL-81	065	ZZ	FLX1 TBC2 FLUX MAP, Z=+7.0
FM0224	09:05:43	10-JUL-81	064	ZZ	FLX2 TBC2 FLUX MAP, Z=+6.0
FM0225	11:34:17	10-JUL-81	015	ZZ	FLX2 TBC2 FLUX MAP, Z=-1.0, SHORT SCAN
FM0226	13:07:35	10-JUL-81	072	ZZ	FLX2 TBC2 FLUX MAP, Z=+7.0
FM0229	12:47:47	13-JUL-81	072	ZZ	FLX1 TBC2 FLUX MAP, Z=+6.0
CW0101	13:19:31	22-JUL-81	064	20	ARC9 TBC2, COLD-WATER CALORIMETER TEST
CW0102	08:54:53	23-JUL-81	082	20	ARC9 TBC2, COLD-WATER CALORIMETER TEST
CW0103	08:43:04	24-JUL-81	094	20	ARC9 TBC2, COLD-WATER CALORIMETER TEST
CW0104	11:52:59	24-JUL-81	080	20	ARC9 TBC2, COLD-WATER CALORIMETER TEST
CW0105	09:01:57	27-JUL-81	074	20	ARC9 TBC2, COLD-WATER CALORIMETER TEST
CW0106	12:15:04	27-JUL-81	074	20	ARC9 TBC2, COLD-WATER CALORIMETER TEST
CW0107	08:39:27	28-JUL-81	076	20	ARC9 TBC2, COLD-WATER CALORIMETER TEST
CW0108	08:31:08	29-JUL-81	065	20	ARC9 TBC2, COLD-WATER CALORIMETER TEST
CW0109	11:13:05	29-JUL-81	066	20	ARC9 TBC2, COLD-WATER CALORIMETER TEST
CW0110	07:29:20	30-JUL-81	030	20	ARC10 TBC2, COLD WATER CALORIMETER TEST
CW0111	08:42:30	30-JUL-81	157	20	ARC10 TBC2, COLD WATER CALORIMETER TEST
CW0112	08:19:24	5-AUG-81	075	20	ARC10 TBC2, COLD-WATER CALORIMETER TEST
ST0102	08:36:39	21-AUG-81	057	20	ARC10 PRECURSOR STIRLING ENGINE TEST
ST0103	11:37:57	21-AUG-81	027	20	ARC10 PRECURSOR STIRLING ENGINE TEST
OG0301	16:13:04	27-AUG-81	037	20	ARC10 OG RETROFIT TESTS
OG0302	09:50:56	28-AUG-81	034	20	ARC10 OG RETROFIT TESTS
OG0304	12:12:04	28-AUG-81	077	20	ARC10 OG RETROFIT TESTS
OG0305	13:40:58	31-AUG-81	056	20	ARC10 OG RETROFIT TESTS
ST0104	10:12:04	31-AUG-81	020	20	ARC10 PRECURSOR STIRLING ENGINE TEST
ST0105	11:28:38	1-SEP-81	025	20	ARC10 PRECURSOR STIRLING ENGINE TEST
ST0106	12:28:09	1-SEP-81	047	20	ARC10 PRECURSOR STIRLING ENGINE TEST
OG0306	09:58:18	15-SEP-81	040	20	ARC11 OG RETROFIT SYSTEM TESTS
OG0307	12:05:17	15-SEP-81	061	20	ARC11 OG RETROFIT SYSTEM TESTS
OG0308	09:47:53	16-SEP-81	109	20	ARC11 OG RETROFIT SYSTEM TESTS
OG0309	12:36:30	16-SEP-81	040	20	ARC11 OG RETROFIT SYSTEM TESTS
ST0107	14:16:00	21-SEP-81	030	20	ARC11 PRECURSOR STIRLING ENGINE TEST
ST0108	09:04:36	22-SEP-81	070	20	ARC11 PRECURSOR STIRLING ENGINE TEST
ST0109	10:30:00	23-SEP-81	141	20	ARC11 PRECURSOR STIRLING ENGINE TEST
FL0301	09:20:21	22-OCT-81	146	20	ARC11 TBC I FLUX MAPPER RUN FOR FORD PROJECT
ST0110	09:30:35	23-OCT-81	035	20	ARC12 TBC1 STIRLING ENGINE TEST, MOUNTED
FL0302	12:41:02	29-OCT-81	094	20	ARC12 TBC I FLUX MAPPER RUN FOR FORD PROJECT
FL0303	09:21:33	30-OCT-81	279	20	ARC12 TBC 1 FLUX MAPPER RUN FOR FORD PROJECT
FL0304	10:41:07	2-NOV-81	183	20	ARC12 TBC I FLUX MAPPER RUN FOR FORD PROJECT
ST0111	14:31:25	3-NOV-81	047	20	ARC12 TBC1 STIRLING ENGINE TEST, MOUNTED
ST0112	09:38:11	4-NOV-81	340	20	ARC13 TBC1 STIRLING ENGINE TEST, MOUNTED
ST0113	10:29:13	9-NOV-81	263	20	ARC13 TBC1 STIRLING ENGINE TEST, MOUNTED
CW0113	13:11:34	18-NOV-81	058	20	ARC13 TBC1, COLD-WATER CAL.; ODD 50% MIRRORS
CW0114	08:58:14	19-NOV-81	080	20	ARC14 TBC1, COLD-WATER CAL.; ODD 50% MIRRORS

Table B-1. Log of Tests Run at the PDTS (Cont'd)

ST0114	12:12:40	20-NOV-81	087	20	ARC14 TBC2 STIRLING ENGINE TEST, MOUNTED
CW0115	09:43:27	23-NOV-81	077	20	ARC14 TBC1, COLD-WATER CAL.; EVEN 50% MIRRORS
CW0116	13:43:42	23-NOV-81	042	20	ARC14 TBC1, COLD-WATER CAL.; 100% MIRRORS
CW0118	12:57:02	24-NOV-81	062	20	ARC14 TBC1, COLD-WATER CAL.; 100% MIRRORS
CW0117	12:27:22	24-NOV-81	300	20	ARC14 TBC1, COLD-WATER CAL.; 100% MIRRORS
ST0115	12:21:19	30-NOV-81	066	20	ARC14 TBC2 STIRLING ENGINE TEST, MOUNTED
ST0116	10:39:48	2-DEC-81	269	20	ARC14 TBC2 STIRLING ENGINE TEST, MOUNTED
ST0117	12:12:13	7-DEC-81	131	20	ARC14 TBC2 STIRLING ENGINE TEST, MOUNTED
CW0119	07:46:35	8-DEC-81	322	20	ARC15 TBC1, COLD-WATER CAL.; 100% MIRRORS
CW0120	09:36:44	9-DEC-81	058	20	ARC15 TBC1, COLD-WATER CAL.; 100% MIRRORS
PY0101	09:27:45	10-DEC-81	125	60	ARC15 PYRHELIOMETER STANDARD COMPARISON TEST
PY0102	08:14:10	11-DEC-81	344	60	ARC15 PYRHELIOMETER STANDARD COMPARISON TEST
PY0103	08:11:16	14-DEC-81	198	60	ARC16 PYRHELIOMETER STANDARD COMPARISON TEST
PY0104	13:28:10	14-DEC-81	096	60	ARC16 PYRHELIOMETER STANDARD COMPARISON TEST
PY0105	08:03:02	15-DEC-81	188	60	ARC16 PYRHELIOMETER STANDARD COMPARISON TEST
PY0106	07:59:11	16-DEC-81	386	60	ARC16 PYRHELIOMETER STANDARD COMPARISON TEST
PY0107	08:26:57	17-DEC-81	359	60	ARC16 PYRHELIOMETER STANDARD COMPARISON TEST
PY0108	09:03:44	28-DEC-81	194	60	ARC16 PYRHELIOMETER STANDARD COMPARISON TEST
PY0109	08:19:19	29-DEC-81	364	60	ARC17 PYRHELIOMETER STANDARD COMPARISON TEST
PY0110	08:12:14	31-DEC-81	231	60	ARC17 PYRHELIOMETER STANDARD COMPARISON TEST
PY0111	10:13:04	8-JAN-82	247	60	ARC17 PYRHELIOMETER STANDARD COMPARISON TEST
PY0112	09:41:10	11-JAN-82	281	60	ARC17 PYRHELIOMETER STANDARD COMPARISON TEST
PY0113	08:02:05	12-JAN-82	387	60	ARC17 PYRHELIOMETER STANDARD COMPARISON TEST
ST0118	10:55:51	19-JAN-82	040	20	ARC17 TBC2 SOLAR ONLY STIRLING, MOUNTED
ST0119	13:25:23	19-JAN-82	072	20	ARC17 TBC2 SOLAR ONLY STIRLING, MOUNTED
ST0120	12:29:08	21-JAN-82	138	20	ARC18 TBC2 SOLAR ONLY STIRLING, MOUNTED, 80% M
ST0121	12:34:29	26-JAN-82	108	20	ARC18 TBC2 SOLAR ONLY STIRLING, MOUNTED, 80% M
ST0122	09:29:38	27-JAN-82	149	20	ARC18 TBC2 SOLAR ONLY STIRLING, MOUNTED, 80% M
ST0123	10:08:29	28-JAN-82	153	20	ARC19 TBC2 SOLAR ONLY STIRLING, MOUNTED, 80% M
ST0124	12:53:15	29-JAN-82	126	20	ARC20 TBC2 SOLAR ONLY STIRLING, MOUNTED, 80% M
ST0125	11:28:47	2-FEB-82	206	20	ARC20 TBC2 SOLAR ONLY STIRLING, MOUNTED, 100%
ST0126	09:48:50	3-FEB-82	314	20	ARC21 TBC2 SOLAR ONLY STIRLING, MOUNTED, 100%
ST0127	09:28:26	5-FEB-82	300	20	ARC22 TBC2 SOLAR ONLY STIRLING, MOUNTED, 100%
ST0128	12:43:29	8-FEB-82	117	20	ARC23 TBC2 SOLAR ONLY STIRLING, MOUNTED, 100%
ST0129	12:53:52	11-FEB-82	097	20	ARC24 TBC2 SOLAR ONLY STIRLING, MOUNTED, 100%
ST0131	12:59:14	16-FEB-82	103	20	ARC24 TBC2 SOLAR ONLY STIRLING, MOUNTED, 80% M
ST0130	09:49:57	16-FEB-82	045	20	ARC25 TBC2 SOLAR ONLY STIRLING, MOUNTED, 80% M
ST0132	13:03:37	17-FEB-82	106	60	ARC25 TBC2 SOLAR ONLY STIRLING, MOUNTED, 80% M
ST0133	12:17:08	18-FEB-82	293	60	ARC26 TBC2 SOLAR ONLY STIRLING, MOUNTED,100% M
ST0134	09:39:45	19-FEB-82	294	60	ARC26 TBC2 SOLAR ONLY STIRLING, MOUNTED, 80% M
ST0135	10:36:27	22-FEB-82	215	60	ARC26 TBC2 SOLAR ONLY STIRLING, MOUNTED, 65% M
ST0136	11:43:08	23-FEB-82	191	60	ARC27 TBC2 SOLAR ONLY STIRLING, MOUNTED, 50% M
ST0137	14:53:21	25-FEB-82	011	60	ARC27 TBC2 SOLAR ONLY STIRLING, MOUNTED,100% M
ST0138	09:53:25	26-FEB-82	229	60	ARC27 TBC2 SOLAR ONLY STIRLING, MOUNTED,100% M
PY0114	08:30:25	3-MAR-82	380	60	ARC27 PYRHELIOMETER STANDARD COMPARISON TEST
ST0139	12:27:56	4-MAR-82	151	60	ARC27 TBC2 SOLAR ONLY STIRLING, MOUNTED, 50% M
ST0140	10:16:02	5-MAR-82	146	60	ARC28 TBC2 SOLAR ONLY STIRLING, MOUNTED, 50% M
ST0141	10:04:11	8-MAR-82	189	60	ARC28 TBC2 SOLAR ONLY STIRLING, MOUNTED, 50% M
ST0142	09:22:30	9-MAR-82	322	60	ARC28 TBC2 SOLAR ONLY STIRLING, MOUNTED, 50% M
ST0143	09:26:36	15-MAR-82	343	60	ARC28 TBC2 SOLAR ONLY STIRLING, MOUNTED, 65% M
ST0144	08:37:14	18-MAR-82	108	60	ARC29 TBC2 SOLAR ONLY STIRLING, MOUNTED, 80% M
ST0145	08:38:29	19-MAR-82	336	60	ARC29 TBC2 SOLAR ONLY STIRLING, MOUNTED, 80% M
ST0146	09:37:18	22-MAR-82	264	60	ARC29 TBC2 SOLAR ONLY STIRLING, MOUNTED,100% M
ST0147	08:24:41	23-MAR-82	318	60	ARC30 TBC2 SOLAR ONLY STIRLING, MOUNTED,100% M
ST0148	09:28:33	29-MAR-82	288	60	ARC30 TBC2 SOLAR ONLY STIRLING, MOUNTED,100% M
ST0149	10:19:25	30-MAR-82	289	60	ARC30 TBC2 SOLAR ONLY STIRLING,HYDROGEN, 80% M
ST0150	09:00:10	31-MAR-82	288	60	ARC30 TBC2 SOLAR ONLY STIRLING,HYDROGEN,100% M
CW0121	13:58:05	7-APR-82	056	20	ARC30 TBC1, CWCC TEST; FLOW MEAS. NO SUN
CW0122	10:20:27	12-APR-82	194	30	ARC31 TBC1, CWCC TEST; 100% MIRR. ON SUN
CW0123	10:18:23	14-APR-82	076	20	ARC31 TBC1, CWCC TEST; 100% MIRR. ON SUN
CW0124	13:14:10	15-APR-82	107	20	ARC31 TBC1, CWCC TEST; 100% MIRR. ON SUN
CW0125	10:17:42	16-APR-82	057	20	ARC31 TBC1, CWCC TEST; 100% MIRR. ON SUN
ST0151	12:05:07	21-APR-82	057	30	ARC31 TBC2 STIRLING HYBRID 25% MIRRORS
CW0126	13:38:49	21-APR-82	051	20	ARC31 TBC1, CWCC TEST; 100% MIRR. ON SUN
ST0152	14:26:15	22-APR-82	036	30	ARC31 TBC2 STIRLING HYBRID 25% MIRRORS
ST0153	08:54:07	23-APR-82	214	30	ARC31 TBC2 STIRLING HYBRID 25% MIRRORS

Table B-1. Log of Tests Run at the PDTS (Cont'd)

```
ST0154 09:55:31 26-APR-82 226  30 ARC31 TBC2 STIRLING HYBRID 25% MIRRORS
ST0155 10:16:17 27-APR-82 167  30 ARC31 TBC2 STIRLING HYBRID 25% MIRRORS
ST0156 08:24:18 28-APR-82 233  30 ARC32 TBC2 STIRLING HYBRID 25% MIRRORS
CW0127 12:05:58 30-APR-82 057  20 ARC32 TBC1, CWCC TEST; 100% MIRR. ON SUN
CW0128 09:58:18  3-MAY-82 134  20 ARC32 TBC1, CWCC TEST; 100% MIRR. ON SUN
CW0129 11:02:37  5-MAY-82 053  20 ARC32 TBC1, CWCC TEST; 100% MIRR. ON SUN
CW0130 09:45:47 13-MAY-82 068  20 ARC32 TBC1, CWCC TEST; 100% MIRR. ON SUN
CW0131 09:51:21 20-MAY-82 058  20 ARC32 TBC1, CWCC TEST; 100% MIRR. ON SUN
ST0157 13:59:54 21-MAY-82 037  20 ARC32 TBC2 SOLAR STIRLING, ESOR II, 50% MIRROR
ST0158 10:08:52 24-MAY-82 240  20 ARC32 TBC2 SOLAR STIRLING, ESOR II, 80% MIRROR
CW0132 12:03:33 25-MAY-82 017  20 ARC33 TBC1, CWCC TEST; 100% MIRR. ON SUN
ST0159 10:08:53 25-MAY-82 239  20 ARC33 TBC2 SOLAR STIRLING, ESOR II, 80% MIRROR
ST0160 08:45:12 27-MAY-82 281  60 ARC33 TBC2 SOLAR STIRLING, ESOR II, 80% MIRROR
CW0133 09:08:13  1-JUN-82 043  20 ARC33 TBC1, CWCC TEST; 100% MIRR. ON SUN
CW0134 11:47:59  1-JUN-82 108  20 ARC33 TBC1, CWCC TEST; 100% MIRR. ON SUN
ST0161 12:40:51  2-JUN-82 300  60 ARC33 TBC2 SOLAR STIRLING, ESOR II, 80% MIRROR
CW0135 10:13:45  3-JUN-82 034  20 ARC33 TBC1, CWCC TEST; 100% MIRR. ON SUN
ST0162 10:05:25  3-JUN-82 163  60 ARC33 TBC2 SOLAR STIRLING, ESOR II, 80% MIRROR
CW0136 12:00:57  4-JUN-82 037  20 ARC33 TBC1, CWCC TEST; 100% MIRR. ON SUN
ST0163 09:50:37  4-JUN-82 230  60 ARC33 TBC2 SOLAR STIRLING, ESOR II, 80% MIRROR
CW0137 09:27:46  7-JUN-82 031  20 ARC34 TBC1, CWCC TEST; 100% MIRR. ON SUN
ST0164 09:42:40  7-JUN-82 264  60 ARC34 TBC2 SOLAR STIRLING, ESOR II, 80% MIRROR
ST0165 08:46:53  8-JUN-82 290  60 ARC34 TBC2 SOLAR STIRLING, ESOR II,100% MIRROR
CW0139 09:23:10  8-JUN-82 029  20 ARC34 TBC1, CWCC TEST; 100% MIRR. ON SUN
ST0165 08:46:53  8-JUN-82 290  60 ARC34 TBC2 SOLAR STIRLING, ESOR II,100% MIRROR
CW0140 13:43:53  8-JUN-82 038  20 ARC34 TBC1, CWCC TEST; 100% MIRR. ON SUN
CW0141 11:46:36  9-JUN-82 042  20 ARC34 TBC1, CWCC TEST; 100% MIRR. ON SUN
CW0142 12:31:46 10-JUN-82 023  20 ARC34 TBC1, CWCC TEST; 100% MIRR. ON SUN
ST0166 07:34:10 10-JUN-82 387  60 ARC34 TBC2 SOLAR STIRLING, ESOR II,100% MIRROR
CW0143 09:41:08 11-JUN-82 030  20 ARC34 TBC1, CWCC TEST; 100% MIRR. ON SUN
ST0167 09:19:38 11-JUN-82 079  60 ARC34 TBC2 SOLAR STIRLING, ESOR II,100% MIRROR
CW0145 09:27:06 14-JUN-82 033  20 ARC34 TBC1, CWCC TEST; 100% MIRR. ON SUN
CW0146 13:49:07 14-JUN-82 029  20 ARC34 TBC1, CWCC TEST; 100% MIRR. ON SUN
ST0168 07:45:46 14-JUN-82 385  60 ARC34 TBC2 SOLAR STIRLING, ESOR II,100% MIRROR
CW0144 09:34:15 15-JUN-82 030  20 ARC35 TBC1, CWCC TEST; 100% MIRR. ON SUN
CW0147 13:41:16 15-JUN-82 029  20 ARC35 TBC1, CWCC TEST; 100% MIRR. ON SUN
ST0169 08:55:56 15-JUN-82 300  60 ARC35 TBC2 SOLAR STIRLING, ESOR II,100% MIRROR
CW0148 11:45:01 16-JUN-82 037  20 ARC35 TBC1, CWCC TEST; 100% MIRR. ON SUN
ST0170 08:37:40 16-JUN-82 298  60 ARC35 TBC2 SOLAR STIRLING, ESOR II,100% MIRROR
ST0171 10:29:24 17-JUN-82 183  60 ARC35 TBC2 SOLAR STIRLING, ESOR II,100% MIRROR
ST0172 07:25:23 21-JUN-82 166  60 ARC35 TBC2 SOLAR STIRLING, ESOR II,100% MIRROR
ST0173 07:49:32 21-JUN-82 644  60 ARC35 TBC2 SOLAR STIRLING, ESOR II,100% MIRROR
CW0149 10:34:58 22-JUN-82 138  20 ARC36 TBC1, CWCC TEST; 100% MIRR. ON SUN
ST0175 10:09:42 22-JUN-82 211  60 ARC36 TBC2 SOLAR STIRLING, ESOR II,100% MIRROR
ST0174 05:16:24 22-JUN-82 225  60 ARC36 TBC2 SOLAR STIRLING, ESOR II,100% MIRROR
ST0173 05:16:24 22-JUN-82 644  60 ARC36 TBC2 SOLAR STIRLING, ESOR II,100% MIRROR
ST0176 04:38:59 23-JUN-82 810  60 ARC36 TBC2 SOLAR STIRLING, ESOR II,100% MIRROR
ST0177 10:19:32  1-JUL-82 223  60 ARC37 TBC2 SOLAR STIRLING, ESOR II,100% MIRROR
ST0178 10:06:59  6-JUL-82 226  60 ARC37 TBC2 SOLAR STIRLING, ESOR II,100% MIRROR
ST0179 09:13:54  7-JUL-82 291  60 ARC37 TBC2 SOLAR STIRLING, ESOR II, 80% MIRROR
ST0180 10:19:21  8-JUL-82 120  60 ARC37 TBC2 SOLAR STIRLING, ESOR II, 80% MIRROR
ST0181 07:26:59  9-JUL-82 369  60 ARC37 TBC2 SOLAR STIRLING, ESOR II, 80% MIRROR
ST0182 08:05:33 12-JUL-82 347  60 ARC37 TBC2 SOLAR STIRLING, ESOR II, 80% MIRROR
ST0183 08:53:47 13-JUL-82 229  60 ARC37 TBC2 SOLAR STIRLING, ESOR II, 80% MIRROR
ST0184 04:49:43 14-JUL-82 850  60 ARC38 TBC2 SOLAR STIRLING, ESOR II,100% MIRROR
ST0185 04:52:55 15-JUL-82 826  60 ARC38 TBC2 SOLAR STIRLING, ESOR II,100% MIRROR
ST0186 09:59:50 16-JUL-82 235  60 ARC38 TBC2 SOLAR STIRLING, ESOR II,80% MIRROR
ST0187 04:56:13 20-JUL-82 548  60 ARC38 TBC2 SOLAR STIRLING, ESOR II,80% MIRROR
MA0101 07:04:33 23-JUL-82 076  20 ARC38 TBC1 MATERIALS TESTING, 100% MIRRORS
MA0102 07:32:33 27-JUL-82 074  20 ARC39 TBC1 MATERIALS TESTING, 100% MIRRORS
MA0103 07:21:50 28-JUL-82 114  20 ARC39 TBC1 MATERIALS TESTING, 100% MIRRORS
MA0104 07:08:18 29-JUL-82 112  20 ARC39 TBC1 MATERIALS TESTING, 100% MIRRORS
MA0105 07:14:48 30-JUL-82 082  20 ARC39 TBC1 MATERIALS TESTING, 100% MIRRORS
MA0106 07:09:10  2-AUG-82 113  20 ARC39 TBC1 MATERIALS TESTING, 100% MIRRORS
MA0107 07:49:48  3-AUG-82 000  20 ARC39 TBC1 MATERIALS, LOG PROB.-NO DATA
MA0108 07:26:18  9-AUG-82 064  20 ARC39 TBC1 MATERIALS TESTING, 100% MIRRORS
```

Table B-1. Log of Tests Run at the PDTS (Cont'd)

MA0109	07:03:13	10-AUG-82	114	20	ARC39 TBC1 MATERIALS TESTING, 100% MIRRORS
FL0305	12:04:03	10-AUG-82	137	60	ARC39 TBC2 FLUX MAPPER,STIRLING MIRROR CONFIG.
MA0110	07:27:13	11-AUG-82	079	20	ARC39 TBC1 MATERIALS TESTING, 100% MIRRORS
FL0306	07:35:19	11-AUG-82	414	60	ARC39 TBC2 FLUX MAPPER,STIRLING MIRROR CONFIG.
MA0111	07:47:36	12-AUG-82	067	20	ARC40 TBC1 MATERIALS TESTING, 100% MIRRORS
FL0307	07:50:23	12-AUG-82	418	60	ARC40 TBC2 FLUX MAPPER,STIRLING MIRROR CONFIG.
MA0112	07:34:17	13-AUG-82	062	20	ARC40 TBC1 MATERIALS TESTING, 100% MIRRORS
FL0308	07:38:24	13-AUG-82	401	60	ARC40 TBC2 FLUX MAPPER,STIRLING MIRROR CONFIG.
FL0309	08:06:23	16-AUG-82	346	60	ARC40 TBC2 FLUX MAPPER,STIRLING MIRROR CONFIG.
FL0310	09:32:49	18-AUG-82	266	60	ARC40 TBC2 FLUX MAPPER,STIRLING MIRROR CONFIG.
FL0311	07:23:19	19-AUG-82	268	60	ARC40 TBC2 FLUX MAPPER,STIRLING MIRROR CONFIG.
FL0312	09:59:30	20-AUG-82	272	60	ARC40 TBC2 FLUX MAPPER,STIRLING MIRROR CONFIG.
FL0313	10:05:58	23-AUG-82	279	60	ARC40 TBC2 FLUX MAPPER,STIRLING MIRROR CONFIG.
FL0314	09:35:16	25-AUG-82	273	60	ARC41 TBC2 FLUX MAPPER,STIRLING MIRROR CONFIG.
CW0150	11:38:44	30-AUG-82	106	20	ARC41 TBC1, CWCC TEST; 100% MIRR. ON SUN
CW0151	08:33:23	1-SEP-82	047	20	ARC41 TBC1, CWCC TEST; 100% MIRR. ON SUN
CW0152	08:42:03	2-SEP-82	229	20	ARC41 TBC1, CWCC TEST; 100% MIRR. ON SUN
CW0153	08:34:46	3-SEP-82	097	20	ARC41 TBC1, CWCC TEST; 100% MIRR. ON SUN
MA0113	06:56:05	10-SEP-82	134	20	ARC41 TBC1 MATERIALS TESTING, 100% MIRRORS
MA0114	14:06:34	10-SEP-82	014	20	ARC41 TBC1 MATERIALS TESTING, 100% MIRRORS
MA0115	07:41:38	13-SEP-82	104	20	ARC41 TBC1 MATERIALS TESTING, 100% MIRRORS
MA0116	14:08:57	13-SEP-82	037	20	ARC41 TBC1 MATERIALS TESTING, 100% MIRRORS
MA0117	07:16:29	15-SEP-82	088	20	ARC41 TBC1 MATERIALS TESTING, 100% MIRRORS
ST0188	10:22:12	17-SEP-82	112	60	ARC42 TBC2 SOLAR STIRLING, ESOR IIA,80% MIRROR
ST0189	07:30:43	21-SEP-82	284	60	ARC42 TBC2 SOLAR STIRLING, ESOR IIA,80% MIRROR
ST0190	09:25:25	22-SEP-82	221	60	ARC42 TBC2 SOLAR STIRLING, ESOR IIA,80% MIRROR
MA0118	07:46:11	22-SEP-82	015	20	ARC42 TBC1 MATERIALS TESTING, 100% MIRRORS
ST0191	08:46:48	23-SEP-82	087	60	ARC42 TBC2 SOLAR STIRLING, ESOR IIA,80% MIRROR
ST0192	08:23:59	28-SEP-82	257	60	ARC42 TBC2 SOLAR STIRLING, ESOR IIA,80% MIRROR
ST0193	11:55:18	29-SEP-82	129	60	ARC42 TBC2 SOLAR STIRLING, ESOR IIA,80% MIRROR
ST0194	08:32:20	30-SEP-82	296	60	ARC42 TBC2 SOLAR STIRLING, ESOR IIA,80% MIRROR
ST0195	08:00:05	4-OCT-82	287	60	ARC42 TBC2 SOLAR STIRLING, ESOR IIA,80% MIRROR
ST0196	11:23:21	5-OCT-82	171	60	ARC42 TBC2 SOLAR STIRLING, ESOR IIA,80% MIRROR
ST0197	07:47:41	6-OCT-82	342	60	ARC42 TBC2 SOLAR STIRLING, ESOR IIA,80% MIRROR
ST0198	06:13:13	7-OCT-82	363	60	ARC42 TBC2 SOLAR STIRLING, ESOR IIA,100% MIRRO
ST0199	09:27:12	8-OCT-82	252	60	ARC43 TBC2 SOLAR STIRLING, ESOR IIA,80% MIRROR
ST0200	08:18:21	11-OCT-82	338	60	ARC43 TBC2 SOLAR STIRLING, ESOR IIA,80% MIRROR
MA0119	08:03:03	11-OCT-82	276	20	ARC43 TBC1 MATERIALS TESTING, 100% MIRRORS
MA0120	13:26:07	11-OCT-82	073	20	ARC43 TBC1 MATERIALS TESTING, 100% MIRRORS
ST0201	12:36:55	18-OCT-82	070	60	ARC43 TBC2 SOLAR STIRLING, ESOR IIB,80% MIRROR
ST0202	09:38:01	19-OCT-82	231	60	ARC43 TBC2 SOLAR STIRLING, ESOR IIB,80% MIRROR
ST0203	09:51:36	20-OCT-82	242	60	ARC43 TBC2 SOLAR STIRLING, ESOR IIB,80% MIRROR
ST0204	08:10:30	28-OCT-82	318	60	ARC43 TBC2 SOLAR STIRLING, ESOR IIB,80% MIRROR
ST0205	09:39:54	1-NOV-82	276	60	ARC44 TBC2 SOLAR STIRLING, ESOR IIB,80% MIRROR
CW0154	10:56:10	2-NOV-82	017	20	ARC44 TBC-1;CWCC WITH TERMINAL CONC;100% MIRR.
CW0155	13:45:45	2-NOV-82	009	20	ARC44 TBC-1;CWCC WITH TERMINAL CONC;100% MIRR.
ST0206	09:12:42	3-NOV-82	203	60	ARC44 TBC2 SOLAR STIRLING, ESOR IIB,80% MIRROR
CW0156	14:59:40	3-NOV-82	026	20	ARC44 TBC-1;CWCC WITH TERMINAL CONC;100% MIRR.
CW0157	09:10:31	4-NOV-82	060	20	ARC44 TBC-1;CWCC WITH TERMINAL CONC;100% MIRR.
CW0158	11:28:16	4-NOV-82	025	20	ARC44 TBC-1;CWCC WITH TERMINAL CONC;100% MIRR.
CW0159	08:50:24	5-NOV-82	036	20	ARC44 TBC-1;CWCC WITH TERMINAL CONC;100% MIRR.
CW0160	12:25:19	5-NOV-82	119	20	ARC44 TBC-1;CWCC WITH TERMINAL CONC;100% MIRR.
ST0207	09:54:27	11-NOV-82	250	60	ARC44 TBC2 SOLAR STIRLING, ESOR IIB,80% MIRROR
CW0161	15:06:54	12-NOV-82	024	20	ARC44 PDC1; CWCC 100% MIRR.
ST0209	13:38:22	17-NOV-82	075	60	ARC44 TBC2 SOLAR STIRLING, ESOR IIB,80% MIRROR
CW0162	12:38:22	17-NOV-82	103	20	ARC44 PDC1; CWCC 100% MIRR.
ST0208	08:36:25	17-NOV-82	209	20	ARC44 TBC2 SOLAR STIRLING, ESOR IIB,80% MIRROR
ST0210	11:26:31	24-NOV-82	199	60	ARC45 TBC2 SOLAR STIRLING, ESOR IIB,80% MIRROR
ST0211	11:02:47	29-NOV-82	192	60	ARC45 TBC2 SOLAR STIRLING, ESOR IIB,80% MIRROR
CW0163	10:46:19	29-NOV-82	043	20	ARC45 PDC1; CWCC 100% MIRR.
ST0212	09:49:20	2-DEC-82	301	60	ARC45 TBC2 SOLAR STIRLING, ESOR IIB,80% MIRROR
ST0213	10:10:58	3-DEC-82	213	60	ARC45 TBC2 SOLAR STIRLING, ESOR IIB,80% MIRROR
ST0214	11:13:16	6-DEC-82	062	60	ARC45 TBC2 SOLAR STIRLING, ESOR IIB,80% MIRROR
ST0215	08:36:11	7-DEC-82	089	60	ARC45 TBC2 SOLAR STIRLING, ESOR IIB,80% MIRROR
ST0216	10:20:58	17-DEC-82	092	60	ARC45 TBC2 SOLAR STIRLING, ESOR IIB,80% MIRROR
ST0216	10:20:58	17-DEC-82	092	60	ARC46 TBC2 SOLAR STIRLING, ESOR IIB,80% MIRROR

Table B-1. Log of Tests Run at the PDTS (Cont'd)

CW0164	10:30:43	28-DEC-82	057	20	ARC45 PDC1; CWCC 100% MIRR.
CW0166	12:42:06	3-JAN-83	104	20	ARC45 PDC1; CWCC 100% MIRR.
CW0165	10:48:48	3-JAN-83	080	20	ARC46 PDC1; CWCC 100% MIRR.
CW0167	10:24:10	4-JAN-83	285	20	ARC45 PDC1; CWCC 100% MIRR.
CW0168	11:37:53	10-JAN-83	176	20	ARC46 TBC-2; CWCC 100% MIRR.
CW0169	09:54:12	11-JAN-83	164	20	ARC46 TBC-2; CWCC 100% MIRR.
CW0170	10:03:01	12-JAN-83	240	20	ARC46 TBC-2; CWCC 100% MIRR.
ST0217	14:36:46	17-JAN-83	038	60	ARC46 TBC2 SOLAR STIRLING, ESOR IIB,80% MIRROR
ST0218	10:55:17	18-JAN-83	014	60	ARC46 TBC2 SOLAR STIRLING, ESOR IIB,80% MIRROR
CW0172	12:43:08	25-JAN-83	071	30	ARC46 PDC1; CWCC 100% MIRR.
ST0219	13:19:53	1-FEB-83	113	60	ARC47 TBC2 SOLAR STIRLING, ESOR IIA,80% MIRROR
CW0173	09:19:27	1-FEB-83	347	30	ARC47 PDC1; CWCC 100% MIRR.
ST0220	14:39:41	4-FEB-83	037	60	ARC47 TBC2 SOLAR STIRLING, ESOR IIA,80% MIRROR
CW0174	12:30:52	4-FEB-83	131	30	ARC47 PDC1; CWCC 100% MIRR.
ST0221	14:43:47	8-FEB-83	042	60	ARC47 TBC2 SOLAR STIRLING, ESOR IIA,80% MIRROR
ST0222	13:03:35	10-FEB-83	111	60	ARC47 TBC2 SOLAR STIRLING, ESOR IIA,80% MIRROR
ST0223	10:36:47	11-FEB-83	039	60	ARC47 TBC2 SOLAR STIRLING, ESOR IIA,80% MIRROR
ST0224	10:15:00	14-FEB-83	218	60	ARC47 TBC2 SOLAR STIRLING, ESOR IIA,80% MIRROR
CW0175	12:50:52	14-FEB-83	102	30	ARC47 PDC1; CWCC 100% MIRR.
CW0176	09:54:41	16-FEB-83	230	30	ARC47 PDC1; CWCC 100% MIRR.
ST0225	09:34:47	16-FEB-83	285	60	ARC47 TBC2 SOLAR STIRLING, ESOR IIA,80% MIRROR
ST0226	10:01:26	17-FEB-83	249	60	ARC48 TBC2 SOLAR STIRLING, ESOR IIA,80% MIRROR
CW0177	10:59:20	17-FEB-83	206	30	ARC48 PDC1; CWCC 100% MIRR.
ST0227	08:45:23	22-FEB-83	379	60	ARC48 TBC2 SOLAR STIRLING, ESOR IIA,80% MIRROR
CW0178	11:08:42	22-FEB-83	321	30	ARC48 PDC1; CWCC 100% MIRR.
ST0228	10:35:42	24-FEB-83	045	60	ARC48 TBC2 SOLAR STIRLING, ESOR IIA,80% MIRROR
CW0179	10:34:35	8-MAR-83	084	30	ARC48 PDC1; CWCC 100% MIRR.
ST0229	14:17:11	8-MAR-83	050	60	ARC48 TBC2 SOLAR STIRLING, ESOR III,80% MIRROR
CW0180	09:35:35	9-MAR-83	262	30	ARC48 PDC1; CWCC 100% MIRR.
ST0230	10:24:20	9-MAR-83	288	60	ARC48 TBC2 SOLAR STIRLING, ESOR III,80% MIRROR
ST0231	08:48:21	24-MAR-83	032	60	ARC48 TBC2 SOLAR STIRLING, ESOR III,80% MIRROR
ST0232	11:11:33	25-MAR-83	170	60	ARC49 TBC2 SOLAR STIRLING, ESOR III,80% MIRROR
ST0233	10:45:03	29-MAR-83	209	60	ARC49 TBC2 SOLAR STIRLING, ESOR III,80% MIRROR
CW0181	10:26:23	30-MAR-83	058	30	ARC49 PDC1; CWCC 100% MIRR.
ST0234	13:38:32	30-MAR-83	095	60	ARC49 TBC2 SOLAR STIRLING, ESOR III,80% MIRROR
ST0235	13:05:56	31-MAR-83	141	60	XXXX TBC2 SOLAR STIRLING, ESOR III,80% MIRROR
ST0236	14:41:07	4-APR-83	030	60	XXXX TBC1 SOLAR STIRLING, ESOR IIA,80% MIRROR
ST0237	14:04:53	5-APR-83	045	60	XXXX TBC1 SOLAR STIRLING, ESOR IIA,80% MIRROR
ST0238	13:36:20	6-APR-83	101	60	XXXX TBC1 SOLAR STIRLING, ESOR IIA,80% MIRROR
ST0239	13:23:16	7-APR-83	078	60	XXXX TBC1 SOLAR STIRLING, ESOR IIA,80% MIRROR
ST0240	09:49:02	7-APR-83	320	60	XXXX TBC2 SOLAR STIRLING, ESOR III,80% MIRROR
ST0241	08:47:36	8-APR-83	095	60	XXXX TBC1 SOLAR STIRLING, ESOR IIA,80% MIRROR
ST0242	08:24:22	8-APR-83	180	60	XXXX TBC2 SOLAR STIRLING, ESOR III,80% MIRROR
MA0121	09:34:34	13-APR-83	014	60	XXXX TBC-1; MATERIALS TEST
MA0122	14:42:38	13-APR-83	048	60	XXXX TBC-1; MATERIALS TEST
ST0244	10:19:46	14-APR-83	312	60	XXXX TBC2 SOLAR STIRLING, ESOR III,80% MIRROR
CW0183	12:37:20	14-APR-83	099	30	XXXX PDC1; CWCC 100% MIRR.
ST0245	11:10:43	15-APR-83	223	60	XXXX TBC2 SOLAR STIRLING, ESOR III,80% MIRROR
CW0184	12:51:17	15-APR-83	071	30	XXXX PDC1; CWCC 100% MIRR.
MA0123	08:00:00	19-APR-83	027	20	XXXX TBC-1; MATERIALS TEST
MA0124	14:00:00	19-APR-83	023	20	XXXX TBC-1; MATERIALS TEST
MA0125	13:20:07	21-APR-83	122	60	XXXX TBC-1; MATERIALS TEST
MA0126	08:12:28	22-APR-83	398	20	XXXX TBC-1; MATERIALS TEST
ST0246	09:30:22	25-APR-83	236	60	XXXX TBC2 SOLAR STIRLING, ESOR III,80% MIRROR
MA0127	07:40:46	25-APR-83	317	20	XXXX TBC-1; MATERIALS TEST

Table B-1. Log of Tests Run at the PDTS (Cont'd)

```
12345678901234567890123456789012345678901234567890123456789012345678901234567890
CW0166 12:42:06  3-JAN-83 104  20 ARC45 PDC1; CWCC 100% MIRR.
CW0165 10:48:48  3-JAN-83 080  20 ARC46 PDC1; CWCC 100% MIRR.
CW0167 10:24:10  4-JAN-83 285  20 ARC45 PDC1; CWCC 100% MIRR.
CW0168 11:37:53 10-JAN-83 176  20 ARC46 TBC-2; CWCC 100% MIRR.
CW0169 09:54:12 11-JAN-83 164  20 ARC46 TBC-2; CWCC 100% MIRR.
CW0170 10:03:01 12-JAN-83 240  20 ARC46 TBC-2; CWCC 100% MIRR.
ST0217 14:36:46 17-JAN-83 038  60 ARC46 TBC2 SOLAR STIRLING, ESOR IIB,80% MIRROR
ST0218 10:55:17 18-JAN-83 014  60 ARC46 TBC2 SOLAR STIRLING, ESOR IIB,80% MIRROR
CW0172 12:43:08 25-JAN-83 071  30 ARC46 PDC1; CWCC 100% MIRR.
ST0219 13:19:53  1-FEB-83 113  60 ARC47 TBC2 SOLAR STIRLING, ESOR IIA,80% MIRROR
CW0173 09:19:27  1-FEB-83 347  30 ARC47 PDC1; CWCC 100% MIRR.
ST0220 14:39:41  4-FEB-83 037  60 ARC47 TBC2 SOLAR STIRLING, ESOR IIA,80% MIRROR
CW0174 12:30:52  4-FEB-83 131  30 ARC47 PDC1; CWCC 100% MIRR.
ST0221 14:43:47  8-FEB-83 042  60 ARC47 TBC2 SOLAR STIRLING, ESOR IIA,80% MIRROR
ST0222 13:03:35 10-FEB-83 111  60 ARC47 TBC2 SOLAR STIRLING, ESOR IIA,80% MIRROR
ST0223 10:36:47 11-FEB-83 039  60 ARC47 TBC2 SOLAR STIRLING, ESOR IIA,80% MIRROR
ST0224 10:15:00 14-FEB-83 218  60 ARC47 TBC2 SOLAR STIRLING, ESOR IIA,80% MIRROR
CW0175 12:50:52 14-FEB-83 102  30 ARC47 PDC1; CWCC 100% MIRR.
CW0176 09:54:41 16-FEB-83 230  30 ARC47 PDC1; CWCC 100% MIRR.
ST0225 09:34:47 16-FEB-83 285  60 ARC47 TBC2 SOLAR STIRLING, ESOR IIA,80% MIRROR
ST0226 10:01:26 17-FEB-83 249  60 ARC48 TBC2 SOLAR STIRLING, ESOR IIA,80% MIRROR
CW0177 10:59:20 17-FEB-83 206  30 ARC48 PDC1; CWCC 100% MIRR.
ST0227 08:45:23 22-FEB-83 379  60 ARC48 TBC2 SOLAR STIRLING, ESOR IIA,80% MIRROR
CW0178 11:08:42 22-FEB-83 321  30 ARC48 PDC1; CWCC 100% MIRR.
ST0228 10:35:42 24-FEB-83 045  60 ARC48 TBC2 SOLAR STIRLING, ESOR IIA,80% MIRROR
CW0179 10:34:35  8-MAR-83 084  30 ARC48 PDC1; CWCC 100% MIRR.
ST0229 14:17:11  8-MAR-83 050  60 ARC48 TBC2 SOLAR STIRLING, ESOR III,80% MIRROR
CW0180 09:35:35  9-MAR-83 262  30 ARC48 PDC1; CWCC 100% MIRR.
ST0230 10:24:20  9-MAR-83 288  60 ARC48 TBC2 SOLAR STIRLING, ESOR III,80% MIRROR
ST0231 08:48:21 24-MAR-83 032  60 ARC48 TBC2 SOLAR STIRLING, ESOR III,80% MIRROR
ST0232 11:11:33 25-MAR-83 170  60 ARC49 TBC2 SOLAR STIRLING, ESOR III,80% MIRROR
ST0233 10:45:03 29-MAR-83 209  60 ARC49 TBC2 SOLAR STIRLING, ESOR III,80% MIRROR
CW0181 10:26:23 30-MAR-83 058  30 ARC49 PDC1; CWCC 100% MIRR.
ST0234 13:38:32 30-MAR-83 095  60 ARC49 TBC2 SOLAR STIRLING, ESOR III,80% MIRROR
ST0235 13:05:56 31-MAR-83 141  60 ARC49 TBC2 SOLAR STIRLING, ESOR III,80% MIRROR
ST0236 14:41:07  4-APR-83 030  60 ARC49 TBC1 SOLAR STIRLING, ESOR IIA,80% MIRROR
ST0237 14:04:53  5-APR-83 045  60 ARC49 TBC1 SOLAR STIRLING, ESOR IIA,80% MIRROR
ST0238 13:36:20  6-APR-83 101  60 ARC49 TBC1 SOLAR STIRLING, ESOR IIA,80% MIRROR
ST0239 13:23:16  7-APR-83 078  60 ARC49 TBC1 SOLAR STIRLING, ESOR IIA,80% MIRROR
ST0240 09:49:02  7-APR-83 320  60 ARC49 TBC2 SOLAR STIRLING, ESOR III,80% MIRROR
ST0241 08:47:36  8-APR-83 095  60 ARC49 TBC1 SOLAR STIRLING, ESOR IIA,80% MIRROR
ST0242 08:24:22  8-APR-83 180  60 ARC49 TBC2 SOLAR STIRLING, ESOR III,80% MIRROR
MA0121 09:34:34 13-APR-83 014  60 ARC49 TBC-1; MATERIALS TEST
MA0122 14:42:38 13-APR-83 048  60 ARC49 TBC-1; MATERIALS TEST
CW0182 00:00:00 13-APR-83 072  30 ARC50 PDC1; CWCC 100% MIRRORS
ST0243 00:00:00 13-APR-83 079  60 ARC50 TBC2 ESOR-III, HELIUM, NO APER. 80% MIR
ST0244 10:19:46 14-APR-83 312  60 ARC50 TBC2 SOLAR STIRLING, ESOR III,80% MIRROR
CW0183 12:37:20 14-APR-83 099  30 ARC50 PDC1; CWCC 100% MIRR.
ST0245 11:10:43 15-APR-83 223  60 ARC50 TBC2 SOLAR STIRLING, ESOR III,80% MIRROR
CW0184 12:51:17 15-APR-83 071  30 ARC50 PDC1; CWCC 100% MIRR.
MA0123 08:00:00 19-APR-83 027  20 ARC50 TBC-1; MATERIALS TEST
MA0124 14:00:00 19-APR-83 023  20 ARC50 TBC-1; MATERIALS TEST
MA0125 13:20:07 21-APR-83 122  60 ARC50 TBC-1; MATERIALS TEST
MA0126 08:12:28 22-APR-83 398  20 ARC50 TBC-1; MATERIALS TEST
ST0246 09:30:22 25-APR-83 236  60 ARC51 TBC2 SOLAR STIRLING, ESOR III,80% MIRROR
MA0127 07:40:46 25-APR-83 317  20 ARC51 TBC-1; MATERIALS TEST
ST0247 08:02:45  2-MAY-83 009  60 ARC51 TBC2 SOLAR STIRLING, ESOR III,80% MIRROR
MA0128 07:55:26  1-JUN-83 056  20 ARC51 TBC-1; MATERIALS TEST
CW0185 12:28:50  2-MAY-83 092  30 ARC51 PDC1; CWCC 100% MIRR.
MA0129 09:04:09  2-JUN-83 024  20 ARC51 TBC-1; MATERIALS TEST
MA0130 10:19:50  2-JUN-83 018  20 ARC51 TBC-1; MATERIALS TEST
```

Table B-1. Log of Tests Run at the PDTS (Cont'd)

MA0131	07:38:31	9-MAY-83	011	20	ARC51 TBC-1; MATERIALS TEST
ST0249	12:12:16	9-MAY-83	150	60	ARC51 TBC2 SOLAR STIRLING, ESOR IIA,80% MIRROR
CW0186	09:13:40	9-MAY-83	093	30	ARC51 PDC1; CWCC 100% MIRR.
ST0248	08:58:47	9-MAY-83	167	60	ARC51 TBC2 SOLAR STIRLING, ESOR IIA,80% MIRROR
ST0250	09:20:39	11-MAY-83	323	60	ARC51 TBC2 SOLAR STIRLING, ESOR IIA,80% MIRROR
ST0251	09:22:09	12-MAY-83	176	60	ARC52 TBC2 SOLAR STIRLING, ESOR IIA,80% MIRROR
ST0252	09:29:06	16-MAY-83	296	60	ARC52 TBC2 SOLAR STIRLING, ESOR IIA,80% MIRROR
ST0253	08:03:30	17-MAY-83	372	60	ARC52 TBC2 SOLAR STIRLING, ESOR IIA,80% MIRROR
ST0254	09:20:47	18-MAY-83	073	60	ARC52 TBC2 SOLAR STIRLING, ESOR IIA,80% MIRROR
ST0255	08:34:54	19-MAY-83	339	60	ARC52 TBC2 SOLAR STIRLING, ESOR IIA,80% MIRROR
ST0256	08:56:22	20-MAY-83	172	60	ARC52 TBC2 SOLAR STIRLING, ESOR IIA,80% MIRROR
ST0258	11:12:54	23-MAY-83	199	60	ARC52 TBC2 SOLAR STIRLING, ESOR IIA,80% MIRROR
CW0187	11:06:14	23-MAY-83	126	30	ARC52 PDC1; CWCC 100% MIRR.
ST0257	08:58:09	23-MAY-83	076	60	ARC52 TBC2 SOLAR STIRLING, ESOR IIA,80% MIRROR
ST0259	00:00:00	24-MAY-83	000	60	ZZZZZ TBC2 SOFTWARE TEST -- NO DATA
ST0260	08:46:04	24-MAY-83	254	60	ARC52 TBC2 SOLAR STIRLING, ESOR IIA,80% MIRROR
ST0261	06:56:51	25-MAY-83	469	60	ARC52 TBC2 SOLAR STIRLING, ESOR IIA,100% MIRRO
CW0188	12:12:11	26-MAY-83	049	30	ARC52 PDC1; CWCC 100% MIRR.
ST0262	11:14:53	26-MAY-83	079	60	ARC52 TBC2 SOLAR STIRLING, ESOR IIA,100% MIRRO
ST0263	07:40:31	27-MAY-83	091	60	ARC53 TBC2 SOLAR STIRLING, ESOR IIA,100% MIRRO
ST0264	07:57:01	31-MAY-83	118	60	ARC53 TBC2 SOLAR STIRLING, ESOR IIA,100% MIRRO
ST0265	07:44:01	1-JUN-83	408	60	ARC53 TBC2 SOLAR STIRLING, ESOR IIA,100% MIRRO
ST0266	07:28:48	2-JUN-83	428	60	ARC53 TBC2 SOLAR STIRLING, ESOR IIA,100% MIRRO
ST0268	11:37:12	3-JUN-83	070	60	ARC53 TBC2 SOLAR STIRLING, ESOR IIA,100% MIRRO
ST0267	07:28:52	3-JUN-83	245	60	ARC53 TBC2 SOLAR STIRLING, ESOR IIA,100% MIRRO
CW0189	09:04:04	6-JUN-83	111	30	ARC53 PDC1; CWCC 100% MIRR.
ST0269	07:58:53	10-JUN-83	371	60	ARC53 TBC2 SOLAR STIRLING, ESOR III,80% MIRROR
CW0190	09:33:37	10-JUN-83	096	30	ARC53 PDC1; CWCC 100% MIRR.
CW0191	12:55:52	13-JUN-83	097	30	ARC53 PDC1; CWCC 100% MIRR.
ST0270	08:55:40	13-JUN-83	292	60	ARC53 TBC2 SOLAR STIRLING, ESOR III,80% MIRROR
ST0271	08:23:02	14-JUN-83	377	60	ARC54 TBC2 SOLAR STIRLING, ESOR III,80% MIRROR
ST0272	08:26:24	15-JUN-83	131	60	ARC54 TBC2 SOLAR STIRLING, ESOR III,80% MIRROR
ST0273	08:15:49	16-JUN-83	321	60	ARC54 TBC2 SOLAR STIRLING, ESOR III,80% MIRROR
MA0132	10:25:07	16-JUN-83	194	20	ARC54 TBC-1; MATERIALS TEST
ST0274	10:34:16	17-JUN-83	226	60	ARC54 TBC2 SOLAR STIRLING, ESOR III,80% MIRROR
MA0133	08:09:01	17-JUN-83	371	20	ARC54 TBC-1; MATERIALS TEST
ST0275	08:35:34	20-JUN-83	307	60	ARC55 TBC2 SOLAR STIRLING, ESOR III,80% MIRROR
ST0276	10:27:52	21-JUN-83	247	60	ARC55 TBC2 SOLAR STIRLING, ESOR III,100% MIRRO
ST0277	07:33:31	22-JUN-83	427	60	ARC55 TBC2 SOLAR STIRLING, ESOR III,100% MIRRO
ST0279	09:33:13	23-JUN-83	273	60	ARC55 TBC2 SOLAR STIRLING, ESOR III,100% MIRRO
ST0280	08:26:48	24-JUN-83	197	60	ARC55 TBC2 SOLAR STIRLING, ESOR III,100% MIRRO
ST0281	09:35:13	27-JUN-83	010	60	ARC55 TBC2 SOLAR STIRLING, ESOR III,100% MIRRO
ST0282	07:29:50	28-JUN-83	422	60	ARC55 TBC2 SOLAR STIRLING, ESOR III,100% MIRRO
ST0283	07:27:46	5-JUL-83	430	60	ARC55 TBC2 SOLAR STIRLING, ESOR III,100% MIRRO
ST0285	10:04:29	6-JUL-83	267	60	ARC55 TBC2 SOLAR STIRLING, ESOR III,100% MIRRO
ST0284	09:36:03	6-JUL-83	250	60	ARC55 TBC1 SOLAR STIRLING, ESOR IIA,80% MIRROR
ST0287	10:13:51	7-JUL-83	134	60	ARC55 TBC2 SOLAR STIRLING, ESOR III,100% MIRRO
ST0286	08:14:31	8-JUL-83	143	60	ARC55 TBC1 SOLAR STIRLING, ESOR IIA,100% MIRRO
ST0288	07:23:05	12-JUL-83	408	60	ARC55 TBC1 SOLAR STIRLING, ESOR IIA,80% MIRROR
ST0289	09:12:17	13-JUL-83	319	60	ARC56 TBC1 SOLAR STIRLING, ESOR IIA,80% MIRROR
ST0290	11:36:41	14-JUL-83	054	60	ARC56 TBC2 SOLAR STIRLING, ESOR III,100% MIRRO
CW0192	09:40:22	14-JUL-83	097	30	ARC56 PDC1; CWCC 100% MIRR.
CW0192	09:40:22	14-JUL-83	097	30	ARC56 PDC1; CWCC 100% MIRR.
ST0291	09:46:49	15-JUL-83	269	60	ARC56 TBC2 SOLAR STIRLING, ESOR III,100% MIRRO
ST0292	09:00:55	18-JUL-83	280	60	ARC56 TBC1 SOLAR STIRLING, ESOR IIA,100% MIRRO
ST0293	08:40:37	18-JUL-83	303	60	ARC56 TBC2 SOLAR STIRLING, ESOR III,100% MIRRO
ST0295	10:32:49	19-JUL-83	250	60	ARC56 TBC2 SOLAR STIRLING, ESOR III,100% MIRRO
ST0294	10:06:32	19-JUL-83	274	60	ARC56 TBC1 SOLAR STIRLING, ESOR IIA,100% MIRRO
ST0297	09:01:25	20-JUL-83	323	60	ARC56 TBC2 SOLAR STIRLING, ESOR III,100% MIRRO
ST0296	08:47:08	20-JUL-83	333	60	ARC56 TBC1 SOLAR STIRLING, ESOR IIA,100% MIRRO
ST0299	08:19:05	21-JUL-83	364	60	ARC56 TBC2 SOLAR STIRLING, ESOR III,100% MIRRO
ST0298	08:08:12	21-JUL-83	371	60	ARC56 TBC1 SOLAR STIRLING, ESOR IIA,100% MIRRO
ST0302	08:57:54	22-JUL-83	317	60	ARC57 TBC2 SOLAR STIRLING, ESOR III,100% MIRRO
ST0301	08:11:01	22-JUL-83	360	60	ARC57 TBC1 SOLAR STIRLING, ESOR IIA,100% MIRRO
ST0304	10:13:43	25-JUL-83	186	60	ARC57 TBC2 SOLAR STIRLING, ESOR III,100% MIRRO
ST0305	09:02:46	27-JUL-83	146	60	ARC57 TBC2 SOLAR STIRLING, ESOR III,100% MIRRO

Table B-1. Log of Tests Run at the PDTS (Cont'd)

ST0303	09:37:46	27-JUL-83	041	60	ARC57	TBC1 SOLAR STIRLING, ESOR IIA,80% MIRROR
ST0306	05:55:43	28-JUL-83	167	60	ARC57	TBC2 SOLAR STIRLING, ESOR III,100% MIRRO
ST0307	05:49:09	29-JUL-83	392	60	ARC57	TBC2 SOLAR STIRLING, ESOR III,100% MIRRO
ST0308	11:18:59	1-AUG-83	117	60	ARC57	TBC2 SOLAR STIRLING, ESOR III,100% MIRRO
ST0309	08:53:57	2-AUG-83	405	60	ARC57	TBC2 SOLAR STIRLING, ESOR III,100% MIRRO
ST0310	10:09:28	3-AUG-83	315	60	ARC57	TBC2 SOLAR STIRLING, ESOR III,100% MIRRO
ST0311	10:00:55	4-AUG-83	257	60	ARC57	TBC2 SOLAR STIRLING, ESOR III,100% MIRRO
ST0312	07:48:20	8-AUG-83	203	60	ARC58	TBC2 SOLAR STIRLING, ESOR III,100% MIRRO
ST0313	07:20:57	10-AUG-83	133	60	ARC58	TBC2 SOLAR STIRLING, ESOR III,100% MIRRO
ST0314	13:25:48	11-AUG-83	076	60	ARC58	TBC2 SOLAR STIRLING, ESOR III,100% MIRRO
ST0316	09:46:59	12-AUG-83	092	60	ARC58	TBC1 SOLAR STIRLING, ESOR IIA,80% MIRROR
ST0315	07:54:22	12-AUG-83	357	60	ARC58	TBC2 SOLAR STIRLING, ESOR III,100% MIRRO
ST0317	08:05:39	18-AUG-83	382	60	ARC58	TBC1 SOLAR STIRLING, ESOR IIA,80% MIRROR
ST0318	07:17:00	22-AUG-83	415	60	ARC58	TBC1 SOLAR STIRLING, ESOR IIA,80% MIRROR
ST0320	08:54:13	24-AUG-83	122	60	ARC58	TBC2 SOLAR STIRLING, ESOR III,100% MIRRO
ST0321	13:21:22	24-AUG-83	079	60	ARC58	TBC2 SOLAR STIRLING, ESOR III,100% MIRRO
ST0322	08:51:50	25-AUG-83	126	60	ARC58	TBC2 SOLAR STIRLING, ESOR III,100% MIRRO
ST0323	08:30:41	26-AUG-83	306	60	ARC58	TBC1 SOLAR STIRLING, ESOR IIA,80% MIRROR
ST0325	07:48:45	31-AUG-83	226	60	ARC59	TBC2 SOLAR STIRLING, ESOR III,100% MIRRO
ST0324	08:24:03	31-AUG-83	180	20	ARC59	TBC1 SOLAR STIRLING, ESOR IIA,100% MIRRO
ST0326	08:21:12	1-SEP-83	219	60	ARC59	TBC1 SOLAR STIRLING, ESOR IIA,100% MIRRO
ST0327	05:08:54	1-SEP-83	547	60	ARC59	TBC2 SOLAR STIRLING, ESOR III,100% MIRRO
ST0328	09:38:05	2-SEP-83	220	60	ARC59	TBC1 SOLAR STIRLING, ESOR IIA,100% MIRRO
ST0329	10:10:16	6-SEP-83	226	60	ARC59	TBC1 SOLAR STIRLING, ESOR IIA,100% MIRRO
ST0330	05:36:54	7-SEP-83	742	60	ARC59	TBC2 SOLAR STIRLING, ESOR III,100% MIRRO
ST0331	12:45:53	8-SEP-83	065	60	ARC60	TBC1 SOLAR STIRLING, ESOR IIA,100% MIRRO
ST0332	11:45:48	14-SEP-83	149	60	ARC60	TBC1 SOLAR STIRLING, ESOR IIA,100% MIRRO
ST0333	12:09:29	14-SEP-83	084	60	ARC60	TBC2 SOLAR STIRLING, ESOR III,80% MIRROR
ST0335	08:10:50	15-SEP-83	381	60	ARC60	TBC2 SOLAR STIRLING, ESOR III,80% MIRROR
ST0335	08:10:50	15-SEP-83	381	60	ARC60	TBC2 SOLAR STIRLING, ESOR III,80% MIRROR
ST0334	09:30:39	15-SEP-83	283	60	ARC60	TBC1 SOLAR STIRLING, ESOR IIA,100% MIRRO
ST0337	09:51:48	16-SEP-83	254	60	ARC60	TBC2 SOLAR STIRLING, ESOR III,80% MIRROR
ST0336	10:08:08	16-SEP-83	216	60	ARC60	TBC1 SOLAR STIRLING, ESOR IIA,100% MIRRO
ST0339	07:23:45	21-SEP-83	124	60	ARC60	TBC2 SOLAR STIRLING, ESOR III,80% MIRROR
ST0338	10:30:09	21-SEP-83	135	60	ARC60	TBC1 SOLAR STIRLING, ESOR IIA,100% MIRRO
ST0340	10:40:09	21-SEP-83	112	60	ARC60	TBC2 SOLAR STIRLING, ESOR III,80% MIRROR
ST0341	09:56:46	22-SEP-83	183	60	ARC60	TBC1 SOLAR STIRLING, ESOR IIA,100% MIRRO
ST0342	08:55:10	22-SEP-83	232	60	ARC60	TBC2 SOLAR STIRLING, ESOR III,80% MIRROR
ST0344	08:25:08	23-SEP-83	263	60	ARC60	TBC2 SOLAR STIRLING, ESOR III,80% MIRROR
ST0343	09:31:44	23-SEP-83	124	60	ARC60	TBC1 SOLAR STIRLING, ESOR IIA,100% MIRRO
ST0345	09:59:11	27-SEP-83	214	60	ARC61	TBC1 SOLAR STIRLING, ESOR IIA,100% MIRRO
ST0346	09:15:43	28-SEP-83	157	60	ARC61	TBC2 SOLAR STIRLING, ESOR III,100% MIRRO
ST0347	10:55:29	28-SEP-83	050	60	ARC61	TBC1 SOLAR STIRLING, ESOR IIA,100% MIRRO
ST0348	08:59:24	3-OCT-83	333	60	ARC61	TBC1 SOLAR STIRLING, ESOR IIA,100% MIRRO
ST0349	08:34:48	3-OCT-83	132	60	ARC61	TBC2 SOLAR STIRLING, ESOR III,100% MIRRO
ST0351	10:41:53	6-OCT-83	205	60	ARC61	TBC1 SOLAR STIRLING, ESOR IIA,100% MIRRO
ST0350	09:03:11	10-OCT-83	272	60	ARC61	TBC1 SOLAR STIRLING, ESOR IIA,100% MIRRO
ST0352	09:15:59	10-OCT-83	252	60	ARC61	TBC2 SOLAR STIRLING, ESOR III,100% MIRRO
ST0354	05:54:55	11-OCT-83	697	60	ARC62	TBC2 SOLAR STIRLING, ESOR III,100% MIRRO
ST0353	09:03:44	11-OCT-83	211	60	ARC61	TBC1 SOLAR STIRLING, ESOR IIA,100% MIRRO
ST0355	05:59:38	12-OCT-83	637	60	ARC61	TBC2 SOLAR STIRLING, ESOR III,100% MIRRO
ST0356	06:00:07	13-OCT-83	457	60	ARC61	TBC2 SOLAR STIRLING, ESOR III,100% MIRRO
ST0357	09:26:21	21-OCT-83	029	60	ARC62	TBC2 SOLAR STIRLING, ESOR IV,100% MIRROR
ST0358	11:38:31	21-OCT-83	179	60	ARC62	TBC2 SOLAR STIRLING, ESOR IV,100% MIRROR
ST0359	09:02:46	24-OCT-83	017	60	ARC62	TBC2 SOLAR STIRLING, ESOR IV,100% MIRROR
ST0360	09:20:07	27-OCT-83	283	60	ARC62	TBC2 SOLAR STIRLING, ESOR IV,100% MIRROR
ST0361	09:44:16	8-NOV-83	298	60	XXXX	TBC2 SOLAR STIRLING, ESOR IV,100% MIRROR
ST0362	09:58:31	9-NOV-83	099	60	XXXX	TBC2 SOLAR STIRLING, ESOR IV,100% MIRROR
ST0363	08:58:27	14-NOV-83	323	60	XXXX	TBC2 SOLAR STIRLING, ESOR IV,100% MIRROR
ST0364	09:40:22	15-NOV-83	309	60	XXXX	TBC2 SOLAR STIRLING, ESOR IV,100% MIRROR
ST0365	08:54:17	16-NOV-83	160	60	XXXX	TBC2 SOLAR STIRLING, ESOR IV,100% MIRROR
ST0366	11:09:31	17-NOV-83	039	60	XXXX	TBC2 SOLAR STIRLING, ESOR IV,100% MIRROR
ST0367	12:32:30	17-NOV-83	157	60	XXXX	TBC2 SOLAR STIRLING, ESOR IV,100% MIRROR
ST0368	06:31:44	18-NOV-83	490	60	XXXX	TBC2 SOLAR STIRLING, ESOR III,100% MIRRO
ST0369	08:48:28	23-NOV-83	133	60	XXXX	TBC2 SOLAR STIRLING, ESOR III,100% MIRRO
ST0370	10:04:19	28-NOV-83	224	60	XXXX	TBC2 SOLAR STIRLING, ESOR III,100% MIRRO

Table B-1. Log of Tests Run at the PDTS (Cont'd)

```
ST0371 08:29:38 29-NOV-83 423  60 XXXX  TBC2 SOLAR STIRLING, ESOR III,100% MIRRO
ST0372 10:53:59  2-DEC-83 022  60 XXXX  TBC2 SOLAR STIRLING, ESOR III,100% MIRRO
ST0373 12:25:53  2-DEC-83 096  20 XXXX  TBC2 SOLAR STIRLING, ESOR III,100% MIRRO
ST0374 12:21:39  5-DEC-83 077  20 XXXX  TBC2 SOLAR STIRLING, ESOR III,100% MIRRO
ST0375 13:05:57  8-DEC-83 023  20 XXXX  TBC2 SOLAR STIRLING, ESOR III,100% MIRRO
ST0376 13:17:59 19-DEC-83 096  20 XXXX  TBC2 SOLAR STIRLING, ESOR III,100% MIRRO
ST0377 10:39:14 20-DEC-83 040  20 XXXX  TBC2 SOLAR STIRLING, ESOR III,100% MIRRO
ST0378 12:43:13 20-DEC-83 053  20 XXXX  TBC2 SOLAR STIRLING, ESOR III,100% MIRRO
ST0379 12:24:20 11-JAN-84 192  60 XXXX  TBC2 SOLAR STIRLING, ESOR III,100% MIRRO
ST0380 09:22:08 12-JAN-84 289  60 XXXX  TBC2 SOLAR STIRLING, ESOR III,100% MIRRO
ST0381 09:23:22 13-JAN-84 337  60 XXXX  TBC2 SOLAR STIRLING, ESOR III,100% MIRRO
ST0382 XX:XX:XX 20-JAN-84 021  60 ARC64 DATA SYSTEM TEST
ST0383 XX:XX:XX 20-JAN-84 268  60 ARC64 TBC2 SOLAR STIRLING, ESOR IV,100% MIRROR
ST0384 XX:XX:XX 23-JAN-84 254  60 ARC64 TBC2 SOLAR STIRLING, ESOR IV,100% MIRROR
ST0385 XX:XX:XX 25-JAN-84 270  60 ARC64 TBC2 SOLAR STIRLING, ESOR IV,100% MIRROR
********LAST TEST AT PDTS**********
```

Table B-2. List of Computer Programs Employed to Process PDTS Test Data

Experiment	Described in this Appendix	Remarks
OG Flat-Plate Calorimeter	x	
Cold-Water Cavity Calorimeter		
a) Original	x	
b) Modified	x	
Flux Mapper		
Steam Rankine Receiver	x	
Air Brayton Solar Receiver	x	Last test run on May 7, 1981.
Ceramic Receiver	x	
OG Steam Engine	x	
J. Carter Steam Engine	x	
Face Plate Material		Only signal conversion to engineering units; no calculations.
Pyrheliometer Shroud		Only signal conversion to engineering units; no calculations.
LBL Circumsolar Telescope		
Organic Rankine Module		
Hybrid Stirling Module	x	
Solar-Only Stirling Module	x	

Table B-3. OG Calorimeter Program Versions (Prints)

Print No.	Date	Description
.001	3 Apr 79	Version for OG thermal test; only one logger used, no other input devices; no calculations in the program.
.002	23 May 79	Version for OG calorimeter test; only one logger, no other input devices; two limited calculations in the program.
.003	29 Jun 79	Similar to .002 version except additional calculation of delta temperature included (using channels 198 & 199).
.004	18 Jul 79	IBID, postamble display included, processing of warnings included also.
.005	1 Aug 79	IBID, updated postamble display, included list of channels printed.
.006	17 Aug 79	IBID, updated to include calculations for OG system tests.
.007	10 Jan 80	IBID, includes multiple time intervals and channel assignments for calorimeter tests.
.008	25 Apr 80	IBID, includes calculation of delta temperature using channels 198 & 199.

Table B-3 presents eight versions of the program. (Print 8 is the most recent version.) Table B-4 describes the portion of the program that deals with processing of test data.

Data acquisition system channel numbers used were the following:

C VALUE (1).....CHNL 198 .....T_2

C VALUE (2).....CHNL 199 .....T_1

C VALUE (3).....CHNL 200 V

C VALUE (4).....CHNL 201 .....I_b

Table B-4. Portion of OG Calorimeter Print 8 Providing Calculations

Fortran Notation	Formulas
DIFFER = (CVALUE(2)-CVALUE(1))	$\Delta T = T_2 - T_1$
D = (0.1468)*DIFFER*(9./5.)*CVALUE(3)	$Q = (0.1468)* \Delta T*(9/5)*V$
COP = (D*1000.)/(25.9*CVALUE(4))	$\eta = 1000\ Q/(25.9*I_b)$

In Table B-4, T_2 is the water outlet and T_1 is the water inlet temperatures, both measured in ^{o}C. Q is the heat in kW_t picked up by the water circulated. The volumetric flow rate, V, is measured in gallons per minute. η is the optical efficiency of the OG concentrator under test for the given aperture. The net projected concentrator area is 25.9 m^2. The beam insolation, I_b, is measured in W/m^2.

2. Cold-Water Cavity Calorimeter

a. Original Calculations. The cavity-type cold-water cavity calorimeter (CWCC) was used to characterize the TBCs and PDC-1. During earlier runs, prior to April 5, 1982, algorithms used will be called "original" algorithms. Table B-5 gives the original algorithms of the CWCC tests.

b. Modified Calculations. The cold-water calorimeter test data evaluation algorithm was modified after April 5, 1982. The weather data were included on October 12, 1982, PDC-1 calculations were added on November 15, 1982, and Kendall standard and regular Kendall pyrheliometers were included on February 4, 1983.

The modified CWCC algorithm is presented in Table B-6. This code was used to characterize the PDC-1 concentrator by means of the CWCC. The polynominal fit to steam tables (saturated) are identical to the subroutine PROP, which was presented for the original CWCC calculations.

3. Steam Rankine Solar Receiver

The steam Rankine solar receiver test data evaluation code consists of a main program and the subroutine STEAM. The main program, PRIN12, calculates steam properties for both the primary boiler/superheater and the reheat sections. The subroutine calculates the enthalpy of the steam

Table B-5. CWCC Original Calculation Routines
(Last Update November 20, 1981)

Routine	Explanation
For the Cavity Colorimeter	
TINF=(TINCAL+273.16)*1.8-459.69	T_{in}, conversion of ^{o}C to ^{o}F absolute
CALL PROP(TINF,P,V,H)	Properties at inlet conditions
HIN=H+V*(PATM+PINCAL-P)*(144./778.16)	H = U + PV/J
DELTAT=7.5*(DTCALL-1.00268)	ΔT, conversion
TOUT=TINF+DELTAT	$T_{out} = T_{in} + \Delta T$
MDOT=FMCALL*.13368*(60./V)	$\dot{m}$: conversion gal/min to lb/h
CALL PROP(TOUT,P,V,H)	Properties at outlet conditions (Btu/h)
HOUT=H+V*(PATM+PINCAL-P)*(144./778.16)	$H = H_o + PV/J$
EINCAL=MDOT*(HOUT-HIN)/3413.	$Q = \dot{m}\ \Delta H/3413$, kW
ECOR=EINCAL*1000./EPPLEY	$\eta = Q/I$
For the Aperture Plate	
TINAPF=(TINAPR+273.16)*1.8-459.69	$T_{in,ap.f.}$ = (^{o}C to ^{o}F)
CALL PROP(TINAPF,P,V,H)	Properties at outlet conditions
HINAPR=H+V*(PATM+PINAPR-P)*(144./778.16)	H = U + PV/J
TEXAPR=TINAPF+DTAPRR	$T_{ex,ap.f} = T_{in,ap.f} + \Delta T$
MDOTAP=FMAPRR*.13368*(60./V)	$\dot{m}$: conversion gal/min to lb/h
CALL PROP(TEXAPR,P,V,H)	
HEXAPR=H+V*(PATM+PEXAPR-P)*(144./778.16)	H = U + PV/J
EINAPR=MDOTAP*(HEXAPR-HINAPR)/3413.	$Q = \dot{m}\ \Delta H/3413$, kW
ECORAP=EINAPR*1000./EPPLEY	$\eta = Q/I_b$

Continued

Table B-5. CWCC Original Calculation Routines (Cont'd)

Routine	Explanation
DTCALL=DELTAT/1.8	^{o}F to ^{o}C
DTAPRR=DTAPRR/1.8	^{o}F to ^{o}C
MDOT = MDOT*(.000125998)	lb/h to kg/sec
MDOTAP=MDOTAP*(.000125998)	lb/h to kg/sec

Subroutine	Explanation
PROP (T,P,V,H)	Determines the properties of water as a function of temperature and pressure.

```
U = (T-75.)/25.
P = .42936+.3585*U+.13416*U**2+.02705*U**3
V = .016068+.00005*U+.00001116*U**2
H = 43.0297+24.9479*U-.0100444*U**2
```

Fortran Notation	Units	Variable	Channel Number
TINAPR	^{o}C	Aperture Plate Water Inlet Temperature	198
TINCAL	^{o}C	Calorimeter Water Inlet Temperature	199
TINF	^{o}F	Calorimeter Water Inlet Temperature	
FMCAL	gal/min	Calorimeter Flow Rate	200
DTCALL	^{o}C	Differential Thermocouple Reading	201
FMAPR	gal/min	Aperture Water Flow Rate	202
EPPLEY	W/m^2	Beam Insolation	204
PINCAL	psi	Calorimeter Inlet Pressure	205
PEXCAL	psi	Calorimeter Exit Pressure	206
PINAPR	psi	Aperture Plate Inlet Pressure	207
PEXAPR	psi	Aperture Plate Exit Pressure	208
DTAPR	psi	Differential Pressure	209

Table B-6. CWCC Modified Calculation Routines

Routine	Explanation
TINF=(TINCAL*1.8) + 32.	^{o}C to ^{o}F ($T_{f,in}$)
DELTAT=DTC1 * (DTCALL-DTC2)	ΔT
TEXF=TINF + DELTAT	$T_{f,ex} = T_{f,in} + \Delta T$
CALL PROP (TINF,PINC,VINC,HINC)	Water properties at $T_{f,in}$
CALL PROP (TEXF,PEXC,VEXC,HEXC)	Water properties at $T_{f,exit}$
MDOT=FMCALL * C2/VINC	$\dot{m}$: gal/min to lb/h
PINCAL=PEXCAL + DELTAP	$P_{in} = P_{ex} + \Delta P$
HIN=HINC + VINC * (PINCAL-PINC)*C3	$H_{in} = U_{in} + PV/J$
HEX=HEXC + VEXC * (PEXCAL-PEXC)*C3	$H_{ex} = U_{ex} + PV/J$
EINCAL=MDOT * (HEX-HIN)/C1	$Q = \dot{m}\ \Delta H$
EU(163)=EINCAL	
ECOR=EINCAL*1000./EPPLEY	$\eta = Q/I_b$, Eppley
EU(164)=ECOR	
EU(165)=EINCAL*1000./KENDEL	$\eta = Q/I_b$, Kendall (Regular)
EU(166)=EINCAL*1000./KENSTD	$\eta = Q/I_b$, Kendall (Standard)
EU(167)=DELTAT	
EU(168)=((BARPRE*1.3) + 24.6) * 25.4	$P_{barometric}$
EU(169)=(DEWPNT*16.) - 30.	$P_{dew\ point}$

Subroutine	Explanation
PROP	
ADDITIONAL CONSTANTS PLACED HERE	

Continued

Table B-6. CWCC Modified Calculation Routines (Cont'd)

Subroutine	Explanation
PROP (Cont'd)	
BTU/(kW*HR)	Conversion factor Btu to kWh
C1 = 3413.	
(CUFT/GAL)*(MIN/HR)	$(ft^3/gal)(min/h)$, gal/min to ft^3/h
C2 = 0.13368 * 60.	
(SQ. IN/SQ. FT)/((FT*LB)/BTU)	psi to lb/ft^2, ft-lb to Btu
C3 = 144./778.16	
DELTAT CONSTANTS	
DTC1 = 7.4970	
DTC2 = 1.001411	

Fortran Notation	Units	Variable
TINCAL	^oC	Calorimeter Input Temperature
DTCAL	V	Temperature Differential
TINF	^oF	Calorimeter Input Temperature
TOUT	^oF	Calorimeter Output Temperature
PINCAL	psig	Calorimeter Input Pressure
PEXCAL	psig	Calorimeter Output Pressure
PATM	psia	Atmospheric Pressure
EINCAL	kW_t	Calorimeter Net Input Power

at a given temperature and pressure. It consists mainly of standard steam tables adapted from Thermodynamic Properties of Steam by J.H. Keenan and F.G. Keyes, published by John Wiley and Sons, Inc., New York.

Table B-7 presents the calculation routines of the main program as well as the subroutine calculations.

4. Air Brayton Solar Receiver

The air Brayton solar receiver (ABSR) test data evaluation code consists of a main program and a subroutine AIRENT (T,H) that calculates the properties of the air. (AIRENT is also part of the ceramic honeycomb solar receiver test data evaluation code.) The main program, run during April and May 1981, is presented in Table B-8.

5. Ceramic Honeycomb Solar Receiver

The test setup and data evaluation program (PRIN13) for the Sanders Associates' ceramic honeycomb solar receiver is similar to the ABSR code. The main program processes data; the subroutine AIRENT (T,H) calculates the air enthalpy.

The main program (PRIN13) and subroutine calculations are presented in Table B-9. An instrumentation listing (which includes channel numbers, conversion factors, units being measured, and variables) is given in Table B-10.

6. Omnium-G Steam Engine

The Omnium-G steam engine was tested using steam generated by the steam Rankine solar receiver mounted at the focal point of TBC-1. The computer code consists of a main program (CALC2) that uses two subroutines. The first subroutine, STEAM, determines the steam properties (enthalpy) at a given temperature and pressure. The other subroutine, INTERP, performs second-order interpolations. Both subroutines were described earlier in this Appendix (Table B-7).

Highlights of the algorithms and their mathematical representation are given in Table B-11. An instrumentation listing and calculated quantities are given in Table B-12.

7. J. Carter Steam Engine

The algorithms used to analyze the J. Carter steam engine (operating on steam from the Rankine receiver mounted at the focal plane of a TBC) are very similar to those used for analyzing the Omnium-G engine. A list of algorithms and equations used in data analysis are presented in Table B-13. Table B-14 gives the instrumentation listing.

Table B-7. Calculation Routines for the Steam Rankine Solar Receiver[a]

Routine	Explanation
For the Boiler/Superheater	
POW = CVALUE(3)	Pressure of water
TI = (CVALUE(1)*9./5.) + 32.	T_{in} , ^{o}C to ^{o}F
TO = (CVALUE(2)*9./5.) + 32.	T_{out} , ^{o}C to ^{o}F
IF = (TO.LT.60.) GO TO 586 !MINIMUM TOUT IS 60 F IF = (POW.GT.2500.) GO TO 586 !MAX PRESS IS 2500 LB/SQ.IN.	Check minimum T_{out} and maximum pressure
Call Steam1(TI,TO,POW,ENTH)	Steam properties
IF (ENTH(2).NE.0.) GO TO 568 !WATER-STEAM MIXTURE	
ISIGN = 0 !FLAG FOR TWO LINES = ZERO	
DIFFER = ENTH(1)	ΔH = change of enthalpy (Btu/lb^{o}F)
D = (0.14614)*CVALUE(4)*DIFFER	$Q = 0.14614\ \dot{m}\ \Delta H$
IF (ISIGN.EQ.1) D1=(0.14614*CVALUE(4)*DIFF1	$Q_1 = 0.14614\ \dot{m}\ \Delta H$
COP = (D*1000.)/(AREA*CVALUE(5))	$\eta = Q/AI_b$
IF (ISIGN.EQ.1) COP1=(D1*1000.)/AREA*CVALUE(5)	First loop $\eta = Q_1/AI_b$
For the Reheat Section	
Repeat calculations above	

[a]Program updated on September 22, 1980 (Print .010) to include calculations for TBC steam receiver tests using delta temperatures calculated from channels 198 and 196, asks number of uncovered mirrors, and uses effective area of 80. Print .011 (November 5, 1980) used in Sanders receiver tests. All calculations and special barometric pressure entries from the log program are included. The final print (.012) was updated on November 10, 1980, to include steam tables for enthalpy calculations, link with STEAM1, STEAM2, and INTERP (uses channel numbers 192, 212, 200, 204, and 208 in calculations).

Table B-7. Calculation Routines for the Steam Rankine Solar Receiver (Cont'd)

Subroutine[b]

```
SUBROUTINE STEAM(TI,TO,P,ENTH)

STEAM.001

SUBROUTINE TO COMPUTE THE ENTHALPY INCREASE FOR CONSTANT PRESSUR
WATER. WATER ENTERS THE SYSTEM AT TEMPERATURE TI AND LEAVES
AT TEMPERATURE TO.  P IS THE PRESSURE OF THE WATER IN THE SYSTEM
ENTH IS THE ENTHALPY INCREASE CALCULATED BY THE SUBROUTINE.  IF
THE OUTPUT TEMPERATURE IS AT THE SATURATION TEMPERATURE THEN TWO
ENTHALPY VALUES ARE RETURNED, ONE FOR WATER, THE OTHER FOR STEAMC
THE INLET TEMPERATURE CAN BE AS LOW AS 32 DEG F.  THE MINIMUM
OUTLET TEMPERATURE CAN BE 60 DEG F.  THE SUBROUTINE YIELDS
RESULTS WITHIN .75% OF THE STEAM TABLE VALUES.

LINK: CALLS INTERP TO DO SECOND ORDER INTERPOLATION

DIMENSION ENTH(2), T(64), PP(64), EV(64)

T IS THE TEMPERATURE FOR SATURATED WATER FROM 32 TO 670 DEGREES
FAHRENHEIT, PP IS CORRESPONDING PRESSURE IN POUNDS PER SQUARE
INCH, EV IS THE ENTHALPY FOR SATURATED STEAM.  THE ENTHALPY FOR
SATURATED WATER AND SUPERHEATED STEAM ARE APPROXIMATED BY
EMPERICAL EXPRESSIONS.  THE MAXIMUM ERROR FOR THE APPROXIMATIONS
IS .75 PERCENT.
```

(64 values of temperature data are input from 40 to 670°F, and 64 values of pressure from 0.12166 to 2529 psia are input. Similarly, 64 values of the enthalpy of the saturated steam are input.)

[b]The subroutine calculates the enthalpy in the following sequence:

(1) Compute input enthalpy.
(2) Check for compressed fluid.
(3) Compute saturation temperature.
(4) Check to see if outlet is saturated steam.
(5) Check to see if outlet is saturated water and steam.
(6) Compute outlet water enthalpy.
(7) Compute saturated steam enthalpy.
(8) Superheated steam calculations.
(9) Calculation of the enthalpy increase.

Table B-8. ABSR Calculation Routines[a]

Routine	Explanation
D=1.25	Orifice diameter, d
BAROM=13.48	Barometric pressure
TEMP22 = (TEMP22+273.16)*1.8	Temperature conversion to ^{o}F absolute
PRES11=PRES11+BAROM	P_1: absolute pressure (PRESS 11), ΔP_1: pressure differential (PRESS 22)
ANUM=(PRES11*PRES22) ANUM=ANUM/((1.-(D/2.067)**4)*TEMP22) ANUM=ANUM**.5	$N = \sqrt{P_1(\Delta P_1)/(1-\beta^4)T}$
MPRIME=.51*D**2*ANUM	$\dot{m} = 0.51d^2N$
RED=(1175298.*MPRIME)/(D*1000.)	$R_e = (1175298\dot{m})/(1000d)$
CD=(.6152*D**.042834)/(RED**0.0035085)	$C_d = 0.6152 * d\ exp(0.042834)/R_e\ exp(0.0035085)$
WRITE(5,400) Y=(0.41 +.0192*D**4) P=PRES22/(PRES11*1.4) WRITE(5,400) Y=1.-Y*P	$Y = 1 - [0.041 + 0.0192d^4] \times \Delta P/(P \times 1.4)$
MDOT=.863*CD*Y*D**2*ANUM	$\dot{m} = 0.863 \times C_d \times Y \times d^2 \times N$, lb/sec
TINPUT=(TINPUT+273.)*1.8	

[a]Code reference: Fortran IV, V02.2-1, April 28, 1981, TT5:=CALC1.FTN.

Continued

Table B-8. ABSR Calculation Routines (Cont'd)

Routine	Explanation
TOUTPT=(TOUTPT+273.)*1.8	
CALL AIRENT (TINPUT,HINPUT)	H_i: Enthalpy of air function of inlet temperature
CALL AIRENT(TOUTPT,HOUTPT)	H_o: Enthalpy of air function of outlet temperature
DELTAH=(HOUTPT-HINPUT)	Change of enthalpy: $\Delta H = H_o - H_i$
EOUT=MDOT*DELTAH*3600./3413.	$E_{out} = \dot{m}\ \Delta H \times 3600/3413$-energy out, kW
IMIR = 224	Active mirror panel number (all assumed working!): Energy input 80 kW_t for 100% mirrors, kW
EIN=(80.*EPPLEY*IMIR)/224000.	$E_{in} = 80 \times I_b \times I_m/224000$, I_b: W/m^2 Eppley, I_m: active mirror panel number
CDP=(EOUT/EIN)*100.	$\eta = E_{out}/E_{in}$, EF

Table B-9. Ceramic Receiver Calculation Routines[a]

Routine	Explanation
PGC = 48.*(CVALUE(1)/CVALUE(2)) - 6.0	$P_{GC} = 48(C_1/C_2) - 6$, gauge pressure
PAC = PGC + PATM	$P_{ac} = P_{GC} + P_{atm}$, absolute pressure
DPC = 8.032*(CVALUE(4)/CVALUE(2)) - 0.9588	$\Delta P_c = 8.032(C_4/C_2) - 0.9588$, differential pressure
XX = ((DPC*PAC)/(CVALUE(5)+273.)) CFLOW = 0.399 * 0.0801 * (XX)**0.5	$C_f = (0.399)(0.0801) \times \sqrt{D_{pc} \cdot P_{ac}/(C_5+273)}$
PGM = 48.*(CVALUE(6)/CVALUE(7)) - 6.0	$P_{GM} = 48(C_6/C_7) - 6$, gauge pressure conversion
PAM = PGM + PATM	$P_{am} = P_{GM} + P_{atm}$, absolute pressure
DPM = 8.076*(CVALUE(9)/CVALUE(7)) - 0.9732	$\Delta P_c = 8.076(C_9/C_7) - 0.972$
DIAM = 0.95	d = 0.95
TEMP22 = (TEMP22+273.16)*1.8	T_{22}: conversion to °F absolute (°R)
ANUM = (PAM*DPM)/((1.-(DIAM/1.375)**4.) *TEMP22)	N
ANUM = SQRT(ANUM)	$N = \sqrt{P_{am}\ \Delta P_c}$, flow factor
XX = 0.51 * DIAM**2 * ANUM	$XX = 0.51d^2N$
RED = (1175298.*XX)/(DIAM*1000.)	$R_e = 1175298(XX)/(1000d)$, Reynolds Number
CD = 0.58909 * Exp(RED * 1.08098E-4)	C_d: 0.58989 exp(0.000108098 Re), discharge coefficient

[a]Print .013 (dated June 26, 1981) to be used in Sanders receiver tests. Print .014 (dated March 17) allows printing of postamble to line printer.

Continued

Table B-9. Ceramic Receiver Calculation Routines (Cont'd)

Routine	Explanation
YY = (0.41 + 0.0979*DIAM**4) PP = DPM/(PAM*1.4) YY = 1. - YY*PP	$Y = 1 - (0.41 + 0.0979d^4)[\Delta P_m/(1.4P_{am})]$
AMDOT = 0.872 * CD * YY * DIAM**2 * ANUM	$\dot{m} = 0.872\ C_d Y d^2 N$, mass flow rate
PGF = 63.974*(CVALUE(11)/CVALUE(12))-8.1247	$P_{gf} = 63.974\ (C_{11}/C_{12})-8.1247$
PAF = PGF + PATM	$P_{af} = P_{gf} + P_{at}$, absolute pressure
DPF = 7.9856*(CVALUE(14)/CVALUE(12))-1.0022	$\Delta P_f = 7.9856(C_{14}/C_{12})-1.0022$
XX = ((DPF*PAF)/(CVALUE(15) + 273.)) FFLOW = 0.493 * 0.130 * (XX)**0.5	$F_f = (0.493)(0.130)\sqrt{\Delta P_f P_{af}/(C_{15} + 273)}$
	Pressure Conversions:
PIN = 8.0305*(CVALUE(16)/CVALUE(17))-0.9747	$P_{in} = 8.0305(C_{16}/C_{17}) - 0.9747$
PCAV = 8.1081*(CVALUE(18)/CVALUE(17))-0.9400	$P_{c,av} = 8.1081(C_{18}/C_{17}) - 0.9400$
PMATR = 8.0305*(CVALUE(19)/CVALUE(17))-9747	$P_{matrix} = 8.0305(C_{19}/C_{17}) - 0.9747$
PRCVR = 8.0048*(CVALUE(20)/CVALUE(17))-0.99059	$P_{rec} = 8.0048(C_{20}/C_{17}) - 0.99059$
TIN = (CVALUE(21)+CVALUE(22)+CVALUE(23))/3.	Average inlet temperature in ^oF
TIN = (TIN + 273.) * 1.8	$T_{in} = [((C_{21}+C_{22}+C_{23})/3)+273] \times 1.8$
TOUT = (CVALUE(25)+CVALUE(24))/2.	Average outlet temperature in ^oF

Continued

Table B-9. Ceramic Receiver Calculation Routines (Cont'd)

Routine	Explanation
TOUT = (TOUT + 273.) * 1.8	$T_{out} = [((C_{25}+C_{24})/2)+273] \times 1.8$
CALL AIRENT(TIN,HIN)	H_{in}: inlet enthalpy calculated
CALL AIRENT(TOUT,HOUT)	H_{out}: outlet enthalpy calculated
DELTAH = (HOUT-HIN)	E $\Delta H = H_o - H_{in}$, enthalpy rise
EOUT = AMDOT * DELTAH * 3600./3413.	$E_{out} = \dot{m}$ (ΔH) 3600/3413, heat collected in kW
EIN = (80. * CVALUE(26) * ZMIRRO)/224000.	$E_{in} = 80\ C_{26}Z_m/224000$, Z_m: number of active mirror panels; C_{26}: pyrheliometer reading in W/m^2; Nominal heat input to receiver at 1000 W/m^2
COP = (EOUT/EIN)*100.	$\eta = (E_{out}/E_{in})100$, efficiency in percent
PATM = 0.48977 * ((ATM*1.38) + 24.6) !ATM in volts, PATM in PSI	Conversion of pressure transducer in volts to psi

Subroutine	Explanation
AIRENT	
U = (T-2010.)/1050.	T: temperature in ^oF
H = 507.459+291.272*U+12.226*U**2-2.705*U**3	H: enthalpy in Btu/lb^oF

Table B-10. Instrumentation Listing for Ceramic Receiver Testing

CHANNEL	MNEMONIC	FACTOR	ENG.UNIT	SCALE	SIG.DIG
0	REF	1.0000	1000MV	100	4
108	PSOT	1.0000	DEG. C	2000	4
109	PEFT	1.0000	DEG. C	1990	4
110	CAVTY.WALL	1.0000	DEG. C	1400	4
111	R73,Z24	1.0000	DEG. C	1400	4
115	R116,Z87	1.0000	DEG. C	1400	4
116	R116,Z46	1.0000	DEG. C	1400	4
117	R114,Z06	1.0000	DEG. C	1400	4
118	R130,Z-20	1.0000	DEG. C	1400	4
119	R105,Z-17	1.0000	DEG. C	1400	4
120	AMTEMP	1.0000	DEG. C	50	4
121	RXRLET	1.0000	DEG. C	100	4
122	RERET-1	1.0000	DEG. C	100	4
123	RERET-2	1.0000	DEG. C	100	4
124	RERET-3	1.0000	DEG. C	100	4
125	RERET-4	1.0000	DEG. C	100	4
126	BPTC-1	1.0000	DEG. C	100	4
127	BPTC-3	1.0000	DEG. C	100	4
128	BPTC-4	1.0000	DEG. C	100	4
134	SIPMAT	1.0000	DEG. C	1400	4
135	SIPAT	1.0000	DEG. C	1400	4
136	SIPMIT	1.0000	DEG. C	1400	4
137	SOPMAT	1.0000	DEG. C	1400	4
139	SOPMIT	1.0000	DEG. C	1400	4
142	RIRT-1	1.0000	DEG. C	1400	4
144	RIRT-2	1.0000	DEG. C	1400	4
145	RIRCT	1.0000	DEG. C	1400	4
146	RORT-1	1.0000	DEG. C	1400	4
148	RORT-2	1.0000	DEG. C	1400	4
149	RORCT	1.0000	DEG. C	1400	4
154	WISFT	1.0000	DEG. C	1400	4
155	VESNET	1.0000	DEG. C	1400	4
156	FOVEWT	1.0000	DEG. C	1400	4
157	VEFLAT	1.0000	DEG. C	1400	4
158	OUNWT	1.0000	DEG. C	1400	4
159	EXFLT	1.0000	DEG. C	1400	4
160	WICOAT	1.0000	DEG. C	1400	4
178	BORCT	1.0000	DEG. C	1400	4
180	BOR75T	1.0000	DEG. C	1400	4
182	BIRNT	1.0000	DEG. C	1400	4
183	BIRT	1.0000	DEG. C	1400	4
184	BURIT	1.0000	DEG. C	1400	4
185	BVIST	1.0000	DEG. C	1400	4
186	BPEFT	1.0000	DEG. C	1400	4
187	BPCFT	1.0000	DEG. C	1400	4
188	BPIFT	1.0000	DEG. C	1400	4
189	BPCFT	1.0000	DEG. C	1400	4
190	BPI.FAR.T	1.0000	DEG. C	1400	4
193	BCMFT	1.0000	DEG. C	1400	4
195	MAPT	1.0000	DEG. C	1400	4
196	BEFT	1.0000	DEG. C	1400	4
200	FP.FLOW	3.0000	GPM	1	3
202	APFLO-1	2.0000	GPM	1	3
205	PYRHEL	1.0000	W/SQ.M	1200	5
207	MFPSIG	1.0000	PSIG	30	3
208	CAPSID	1.0000	PSID	5	4
209	MFPSID	1.0000	PSID	5	4
210	FUPSID	1.0000	PSID	5	4
211	FUPSIG	1.0000	PSIG	40	3
212	REDP1-2	1.0000	PSID	5	4
213	REDP1-3	1.0000	PSID	5	4
214	RECPSIG	1.0000	PSIG	30	4
215	REDP1-5	1.0000	PSID	5	4
216	IFVOS	1.0000	VOLTS	12	4
217	REVOS	1.0000	VOLTS	12	4
218	FLADET	1.0000	VOLTS	12	4
219	INSOLKEN	10.0000	W/SQ.M	1200	4
220	INSOLEP	117.1000	W/SQ.M	1200	4
221	INCONS	1.0000	VOLTS	12	4
222	EXCONS	1.0000	VOLTS	12	4
223	MANCOS	1.0000	VOLTS	12	4
224	WINPSIG	3.3333	PSIG	100	4
225	GASPSIG	3.3333	PSIG	100	4
229	100 MV REF	1.0000	MV	120	4
232	IFCAFT	1.0000	DEG. C	100	4
233	IFCOFFT	1.0000	DEG. C	100	4
234	IFMAFT	1.0000	DEG. C	100	4

Table B-11. Omnium-G Steam Engine Calculation Routines (Subroutine CALC2(NPOTS,CALNUM,CALC,EU); last update on May 28, 1981)

Routine	Explanation
OG ENGINE: RECEIVER OUTPUT IN kW_t	
DEGF = (RTEMPO*1.8) + 32.	Conversion from ^oC to ^oF ($T_{r,o}$)
CALL STEAM(32., DEGF,RPRESO,ENTH)	Steam enthalpy at $T_{r,o}$
ROKWTH = ENTH(1)*RECFLO*0.14614	$Q_{rec,o} = h \cdot \dot{m}_r$ (0.14614), receiver outlet energy
OG ENGINE: ENGINE INPUT IN kW_t	
DEGF = (ETEMPI*1.8) + 32.	Conversion of ^oC to ^oF ($T_{eng,i}$)
CALL STEAM(32.,DEGF,EPRESI,ENTH)	h_i: enthalpy of steam at $T_{eng,i}$
FLOREL = RELFL2	Relief valve flow
IF (RELFL2.LT.0.2) FLOREL=RELFLO !BYPASS CH 216 IF LOW PRES	
EIKWTH = ENTH(1)*(RECFLO-FLOREL)*0.14614	$Q_{eng,i} = h_i \dot{m}_{net}(0.14614)$
OG ENGINE: LINE LOSSES	
EU(165) = ROKWTH - EIKWTH	$Q_{rec,o} - Q_{eng,i}$
OG ENGINE: ENGINE EXHAUST OUTPUT IN kW_t	
DEGF = (ETEMPO*1.8) + 32.	Conversion of ^oC to ^oF ($T_{eng,o}$)
CALL STEAM (32.,DEGF,EPRESO,ENTH)	h_i: enthalpy at engine exhaust
EOKWTH = ENTH(1)*(RECFLO-FLOREL)*0.14614	$Q_{eng,o} = h_o \dot{m}_{net}(0.14614)$
EU(166) = EOKWTH	

Continued

Table B-11. Omnium-G Steam Engine Calculation Routines (Cont'd)

Routine	Explanation
OG ENGINE: THERMAL ENERGY USED BY ENGINE	
EU(167) = EIKWTH - EOKWTH	$Q_{net} = Q_{eng,i} - Q_{eng,o}$
OG ENGINE: OVERALL ENERGY EFFICIENCY (THERMAL TO ELECTRIC)	
EFFENG=((ALTWAT/1000.)/EIKWTH)*100.	$\eta_{eng} = [(P_{alt}/1000)/Q_{eng,i}]\ 100$, in percent
OG ENGINE: ENGINE EFFICIENCY BASED ON THERMAL ENERGY USED	
OENGEF=((ALTWAT/1000.)/(EIKWTH-EOKWTH))*100.	$\eta_{eng} = [(P_{alt}/1000)/Q_{net}]\ 100$, in percent
OG ENGINE: RECEIVER EFFICIENCY	
RECEFF = (ROKWTH/82.)*(1000./EPPLEY))*100.	$\eta_{rec} = (Q_{rec,o}/82)(1000/I_b)100$, efficiency based upon 82 kW_t nominal TBC concentrator output at I_b = 1000 W/m^2 insolation.

Table B-12. Instrumentation Listing for Omnium-G Steam Engine Testing

```
TEST BED CONCENTRATOR I WITH OG STEAM ENGINE
12345678901234567890123456789012345678901234567890123456789012345678901234567890
OG 01 23  121   20  0  000
021    TEM13C    01.000    DEG.C        REC. CAVTC 13C    4 6S 0000. 0000.    45.67
022    TEM14C    01.000    DEG.C        REC. CAVTC 14C    4 6S 0000. 0000.    45.67
023    TEM15C    01.000    DEG.C        REC. CAVTC 15C    4 6S 0000. 0000.    45.67
024    TEMY-Z    01.000    DEG.C        BACKPLATE Y-Z     4 6S 9999. 1149.    45.67
025    TEMP      01.000    DEG.C        BACKPLATE -ZOUT   4 6S 9999. 1149.    45.67
026    TEMP      01.000    DEG.C        BACKPLATE-ZCNT    4 6S 9999. 1149.    45.67
027    TEMP      01.000    DEG.C        BACKPLATE CENT    4 6S 9999. 1149.    45.67
028    TEMP      01.000    DEG.C        REFLECTOR +YT     4 6S 9999. 1149.    45.67
029    TEMP      01.000    DEG.C        REFLECTOR -ZT     4 6S 9999. 1149.    45.67
030    TEMP      01.000    DEG.C        RX TNG LD EDG     4 6S 0000. 0000.    45.67
031    TEMP      01.000    DEG.C        BI-PD TC-3        4 6S 0000. 0000.    45.67
032    TEMP      01.000    DEG.C        AB WRP ARND       4 6S 0000. 0000.    45.67
033    TEMP      01.000    DEG.C        BL WRP ARND       4 6S 0000. 0000.    45.67
034    TEMP      01.000    DEG.C        IN ALDAD TR       4 6S 0000. 0000.    45.67
035    TEMP      01.000    DEG.C        OUT ALDAD TR      4 6S 0000. 0000.    45.67
036    TEMP      01.000    DEG.C        BI-PD TC-1        4 6S 0000. 0000.    45.67
037    TEMP      01.000    DEG.C        BI-PD TC-4        4 6S 0000. 0000.    45.67
038    TEMP      01.000    DEG.C        REC.CAV TC 10D    4 6S 0000. 0000.    45.67
039    TEMP      01.000    DEG.C        REC.CAV TC 10E    4 6S 0000. 0000.    45.67
040    TEMP      01.000    DEG.C        REC.CAV TC 10F    4 6S 0000. 0000.    45.67
041    TEMP      01.000    DEG.C        REC. EX TC 13A    4 6S 9999. 538.0    45.67
042    TEMP      01.000    DEG.C        REC. EX TC 15A    4 6S 9999. 538.0    45.67
043    TEMP      01.000    DEG.C        REC. EX TC 17A    4 6S 9999. 538.0    45.67
044    TEMP      01.000    DEG.C        REC. EX TC 19A    4 6S 9999. 538.0    45.67
045    TEMP      01.000    DEG.C        REC. EX TC 20A    4 6S 9999. 538.0    45.67
046    TEMP      01.000    DEG.C        REC. EX TC 21A    4 6S 9999. 538.0    45.67
047    TEMP      01.000    DEG.C        REC.CAV TC 2C     4 6S 9999. 732.0    45.67
048    TEMP      01.000    DEG.C        REC.CAV TC 3C     4 6S 9999. 732.0    45.67
049    TEMP      01.000    DEG.C        REC.CAV TC 4C     4 6S 9999. 732.0    45.67
050    TEMP      01.000    DEG.C        REC.CAV TC 5C     4 6S 9999. 732.0    45.67
051    TEMP      01.000    DEG.C        REC.CAV TC 6C     4 6S 9999. 732.0    45.67
052    TEMP      01.000    DEG.C        REC.CAV TC 7C     4 6S 9999. 732.0    45.67
053    TENP      01.000    DEG.C        REC.CAV TC 8C     4 6S 9999. 732.0    45.67
054    TEMP      01.000    DEG.C        REC.CAV TC 9C     4 6S 9999. 732.0    45.67
055    TEMP      01.000    DEG.C        REC.CAV TC 10C    4 6S 9999. 732.0    45.67
056    TEMP      01.000    DEG.C        REC.CAV TC 11C    4 6S 9999. 732.0    45.67
057    TEMP      01.000    DEG.C        REC. EX TC 20B    4 6S 9999. 538.0    45.67
058    TEMP      01.000    DEG.C        REC. EX TC 21B    4 6S 9999. 538.0    45.67
059    TEMP      01.000    DEG.C        REC. EX TC 22     4 6S 9999. 538.0    45.67
060    TEMP      01.000    DEG.C        REC. EX TC 23     4 6S 9999. 538.0    45.67
061    TEMP      01.000    DEG.C        REC. EX TC 24     4 6S 9999. 538.0    45.67
062    TEMP      01.000    DEG.C        REC. EX TC 25     4 6S 9999. 538.0    45.67
063    TEMP      01.000    DEG.C        REC. EX TC 26     4 6S 9999. 538.0    45.67
064    TEMP      01.000    DEG.C        REC. EX TC 27     4 6S 9999. 538.0    45.67
065    TEMP      01.000    DEG.C        REC. EX TC 28     4 6S 9999. 538.0    45.67
066    TEMP      01.000    DEG.C        REC. CAV TC 1     4 6S 9999. 732.0    45.67
067    TEMP      01.000    DEG.C        REC. CAV TC 2     4 6S 9999. 732.0    45.67
069    TEMP      01.000    DEG.C        REC. CAV TC 4     4 6S 9999. 732.0    45.67
070    TEMP      01.000    DEG.C        REC. CAV TC 5     4 6S 9999. 732.0    45.67
071    TEMP      01.000    DEG.C        REC. CAV TC 6     4 6S 9999. 732.0    45.67
072    TEMP      01.000    DEG.C        REC. CAV TC 8     4 6S 9999. 732.0    45.67
074    TEMP      01.000    DEG.C        REC. CAV TC 9     4 6S 9999. 732.0    45.67
076    TEMP      01.000    DEG.C        REC. CAV TC 11    4 6S 9999. 732.0    45.67
077    TEMP      01.000    DEG.C        REC. CAV TC 12    4 6S 9999. 732.0    45.67
078    TEMP      01.000    DEG.C        REC. CAV TC 1A    4 6S 9999. 732.0    45.67
079    TEMP      01.000    DEG.C        REC. CAV TC 2A    4 6S 9999. 732.0    45.67
080    TEMP      01.000    DEG.C        REC. CAV TC 3A    4 6S 9999. 732.0    45.67
081    TEMP      01.000    DEG.C        REC. CAV TC 4A    4 6S 9999. 732.0    45.67
082    TEMP      01.000    DEG.C        REC. CAV TC 5A    4 6S 9999. 732.0    45.67
083    TEMP      01.000    DEG.C        REC. CAV TC 6A    4 6S 9999. 732.0    45.67
```

Table B-12. Instrumentation Listing for Omnium-G Steam Engine Testing (Cont'd)

```
084   TEMP     01.000   DEG.C      REC. CAV TC 7A    4 6S 9999. 732.0   45.67
085   TEMP     01.000   DEG.C      REC. CAV TC 8A    4 6S 9999. 732.0   45.67
086   TEMP     01.000   DEG.C      REC. CAV TC 9A    4 6S 9999. 732.0   45.67
087   TEMP     01.000   DEG.C      REC. CAV TC10A    4 6S 9999. 732.0   45.67
088   TEMP     01.000   DEG.C      REC. CAV TC11A    4 6S 9999. 732.0   45.67
089   TEMP     01.000   DEG.C      REC. CAV TC12A    4 6S 9999. 732.0   45.67
090   TEMP     01.000   DEG.C      U TUBE INPUT      4 6S 9999. 732.0   45.67
091   TEMP     01.000   DEG.C      U TUBE OUTPUT     4 6S 9999. 732.0   45.67
092   TEMP     01.000   DEG.C      REC. INPUT TMP    4 6S 9999. 40.00   45.67
183   TEM      01.000   DEG.C      STM DNR LN TEM    4 6S 9999. 9999.   45.67
186   ETEMPI   01.000   DEG.C      O.G. EN INLET     4 6S 9999. 315.0   45.67
187   ETEMPO   01.000   DEG.C      O.G. EN OUTLET    4 6S 0000. 0000.   45.67
188   TEMP     01.000   DEG.C      COND OULET TEM    4 6S 9999. 90.00   45.67
189   TEMP     01.000   DEG.C      STM DMP LINE      4 6S 0000. 0000.   45.67
190   AMPS     010.00   AMPS       O.G. ALTOR AC     4 3S 0000. 0000.   45.67
191   VOLTS    100.00   VOLTS      O.G. ALTOR VC     4 3S 0000. 0000.   45.67
192   AMPS     10.000   AMPS       O.G. ALTOR AB     4 3S 0000. 0000.   45.67
193   VOLTS    100.00   VOLTS      O.G. ALTOR VB     4 3S 0000. 0000.   45.67
194   AMPS     010.00   AMPS       O.G. ALTOR AA     4 3S 0000. 0000.   45.67
195   VOLTS    100.00   VOLTS      O.G. ALTOR VA     4 3S 0000. 0000.   45.67
196   VOLTS    100.00   VOLTS      O.G. STNR VOLT    4 3S 0000. 0000.   45.67
197   AMPS     100.00   AMPS       O.G. STNR AMPS    4 2S 0000. 0000.   45.67
200   RECFLO   00.100   GPM        REC. H2O FLO      4 3S 0000. 0000.   45.67
201   RELFLO   00.040   GPM        REL. H2O FLO      4 3S 0000. 0000.   45.67
202   EPRESI   33.333   PSIG       O.G. ENG. IN      4 1S 9999. 12.00   45.67
203   PRES     100.00   PSIG       REC. INPUT        4 1S 0000. 0000.   45.67
204   RPRESO   100.00   PSIG       REC. OUTPUT       4 1S 0000. 0000.   45.67
205   FREQ     10.000   HZ         O.G. ALTNR FREQ   4 3S 9999. 7.000   45.67
206   ALTWAT   10000.   WATTS      O.G. ALTNR POWR   4 2S 0000. 0000.   45.67
207   INS      10.000   W/M2       KENDALL NIP       4 1H 0000. 0000.   45.67
208   EPPLEY   117.10   W/M2       EPPLEY NIP        4 1H 0000. 0000.   45.67
209   REF      01.000   MVOLT      REFERENCE         4 1S 0000. 0000.   45.67
210   FLOW     02.000   GPM        APERATURE         4 3S 04.00 9999.   45.67
211   FLOW     02.000   GPM        FLAT PLT COOL     4 3S 04.00 9999.   45.67
212   RTEMPO   1000.0   DEG.C      REC. OUTPUT       4 2S 0000. 0000.   45.67
216   RELFL2   00.100   GPM        REL. H2O FLO      4 3S 0000. 0000.   45.67
217   FLOW     01.000   GPM        REL. CON FLO      4 3S 01.00 9999.   45.67
219   EPRESO   1.6666   PSIA       O.G ENG OUT PRES  4 1S 0000. 0000.   45.67
220   TEMP     01.000   DEG.C      REC. CAV TC-3     4 6S 0000. 0000.   45.67
221   TEMP     01.000   DEG.C      REC. CAV TC-7     4 6S 0000. 0000.   45.67
222   TEMP     01.000   DEG.C      REC. CAVTC-10     4 6S 0000. 0000.   45.67
501                     KWATTS     RECVR OUTPUT-TH
502                     KWATTS     ENGINE INPUT-TH
503                     KWATTS     LINE LOSSES -TH
504                     KWATTS     ENG EX OUTPT-TH
505                     KWATTS     TH ENRGY-IN ENG
506                     %(TH)EL)   OVERALL ENG EFF
507                       %        EFF-TH ENRGY USE
508                       %        RECEIVER EFF.
PRINTOUT ORDER
86,200,204,205,206,213,212,
REAL TIME PLOTS
186,187,        0.        0.
196,197,198,    0.        0.
190,192,194,    0.        0.
191,193,195,    0.        0.
205,206,        0.        0.

206,            0.        0.
200,212,186,    0.        0.
200,215,216,    0.        0.
END
```

Table B-13. Carter Steam Engine Calculation Routines (Subroutine CALC2(NPTRS,CALNUM,CALC,EU); last update on June 4, 1981)

Routine	Explanation
ETEMPI=EU(CALNUM(1)+12) !ENGINE INLET TEMP	
ETEMPO=EU(CALNUM(2)=12) !ENGINE OUTLET TEMP	
RPRESO=EU(CALNUM(3)+12) !RECEIVER OUTPUT PRESSURE	
ALTWAT=EU(CALNUM(4)+12) !ALTERNATOR WATTS	
EPPLEY=EU(CALNUM(5)+12) !INSOLATION	
EPRESI=EU(CALNUM(6)+12) !ENGINE INLET PRESSURE	
EPRESO=EU(CALNUM(7)+12) !ENGINE OUTLET PRESSURE	
RTEMPO=EU(CALNUM(8)+12) !RECEIVER OUTLET TEMP	
RECFLO=EU(CALNUM(9)+12) !RECEIVER WATER FLOW	
RELFL2=EU(CALNUM(10)+12) !RELIEF VALVE WATER FLOW, CH. 216	
RELFLO=EU(CALNUM(11)+12) !RELIEF VALVE WATER FLOW, CH. 201	
CARTER ENGINE; RECEIVER OUTPUT IN kW_t	
DEGF=(RTEMPO*1.8)+32.	Conversion ^oC to ^oF
RPRESO=RPRESO+13.5 !CHANGE PSIG TO PSIA	
CALL STEAM(DEL,DEGF,RPRESO,ENTH)	Steam properties

Continued

Table B-13. Carter Steam Engine Calculation Routines (Cont'd)

Routine	Explanation
ROKWTH=ENTH(1)*RECFLO*0.14614	$Q_{rec,o}$, outlet energy in kW_t
CARTER ENGINE: ENGINE INPUT IN kW_t	
DEGF=(ETEMPI*1.8)+32.	Conversion ^oC to ^oF
EPRESI=EPRESI+13.5 !CHANGE PSIG TO PSIA	
CALL STEAM(DEL,DEGF,EPRESI,ENTH)	
FLOW=RELFL2	
IF(RELFL2.LT.0.2)FLOW=RELFLO !BYPASS CH 216 IF LOW PRESS	
EIKWTH=ENTH(1)*(RECFLO-FLOW)*0.14614	Inlet energy in kW_t
CARTER ENGINE: LINE LOSSES	
EU(165)=ROKWTH-(ENTH(1)*RECFLO*0.14614)	Net energy in kW_t
CARTER ENGINE: ENGINE EXHAUST OUTPUT IN kW_t	
DEGF=(ETEMPO*1.8)+32.	Conversion ^oC to ^oF
ENTH(1)=0.	
CALL STEAM(DEL,DEGF,EPRESO,ENTH)	Steam properties
EOKWTH=ENTH(1)*(RECFLO-FLOW)*0.14614	Outlet energy in kW_t

Continued

Table B-13. Carter Steam Engine Calculation Routines (Cont'd)

Routine	Explanation
CARTER ENGINE: THERMAL ENERGY USED BY ENGINE	
EU(167)=EIKWTH-EOKWTH	Net energy used
CARTER ENGINE: OVERALL ENGINE EFFICIENCY (THERMAL TO ELECTRIC)	
EFFENG=((ALTWAT/1000.)/EIKWTH)*-100.	$\eta = (P_{alt}/E_{in})100$
CARTER ENGINE: RECEIVER EFFICIENCY BASED ON THERMAL ENERGY USED	
OENGEF=((ALTWAT/1000.)/(EIKWTH-EOKWTH))*-100.	$\eta = (P_{alt}/E_{net})1000$
CARTER ENGINE: RECEIVER EFFICIENCY	
RECEFF=((ROKWTH/82.*(1000./EPPLEY))*100.	$\eta_{rec} = (Q_{rec,o}/I_b 1000)100$, I_b in W/m^2

Table B-14. Instrumentation Listing for Carter Steam Engine Testing

```
TBC I WITH CARTER 8HP STEAM ENGINE
12345678901234567890123456789012345678901234567890123456789012345678901234567890
CR 02 11  131  20  0  000
021   TEM13C   01.000   DEG.C     REC. CAVTC 13C   4 6S 9999. 9999.   45.67
022   TEM14C   01.000   DEG.C     REC. CAVTC 14C   4 6S 9999. 9999.   45.67
023   TEM15C   01.000   DEG.C     REC. CAVTC 15C   4 6S 9999. 9999.   45.67
024   TEMY-Z   01.000   DEG.C     BACKPLATE Y-Z    4 6S 9999. 1149.   45.67
025   TEMP     01.000   DEG.C     BACKPLATE -ZOUT  4 6S 9999. 1149.   45.67
026   TEMP     01.000   DEG.C     BACKPLATE-ZCNT   4 6S 9999. 1149.   45.67
027   TEMP     01.000   DEG.C     BACKPLATE CENT   4 6S 9999. 1149.   45.67
028   TEMP     01.000   DEG.C     REFLECTOR +YT    4 6S 9999. 1149.   45.67
029   TEMP     01.000   DEG.C     REFLECTOR -ZT    4 6S 9999. 1149.   45.67
030   TEMP     01.000   DEG.C     RX RNG LD EDG    4 6S 9999. 9999.   45.67
031   TEMP     01.000   DEG.C     BI-PD TC-3       4 6S 9999. 9999.   45.67
032   TEMP     01.000   DEG.C     AB WRP ARND      4 6S 0000. 0000.   45.67
033   TEMP     01.000   DEG.C     BL WRP ARND      4 6S 0000. 0000.   45.67
034   TEMP     01.000   DEG.C     IN ALDAD TR      4 6S 0000. 0000.   45.67
035   TEMP     01.000   DEG.C     OUT ALDAD TR     4 6S 0000. 0000.   45.67
036   TEMP     01.000   DEG.C     BI-PD TC-1       4 6S 9999. 9999.   45.67
037   TEMP     01.000   DEG.C     BI-PD TC-4       4 6S 9999. 9999.   45.67
038   TEMP     01.000   DEG.C     REC.CAV TC 10D   4 6S 9999. 9999.   45.67
039   TEMP     01.000   DEG.C     REC.CAV TC 10E   4 6S 9999. 9999.   45.67
040   TEMP     01.000   DEG.C     REC.CAV TC 10F   4 6S 9999. 9999.   45.67
041   TEMP     01.000   DEG.C     REC. EX TC 13A   4 6S 9999. 538.0   45.67
042   TEMP     01.000   DEG.C     REC. EX TC 15A   4 6S 9999. 538.0   45.67
043   TEMP     01.000   DEG.C     REC. EX TC 17A   4 6S 9999. 538.0   45.67
044   TEMP     01.000   DEG.C     REC. EX TC 19A   4 6S 9999. 538.0   45.67
045   TEMP     01.000   DEG.C     REC. EX TC 20A   4 6S 9999. 538.0   45.67
046   TEMP     01.000   DEG.C     REC. EX TC 21A   4 6S 9999. 538.0   45.67
047   TEMP     01.000   DEG.C     REC.CAV TC 2C    4 6S 9999. 732.0   45.67
048   TEMP     01.000   DEG.C     REC.CAV TC 3C    4 6S 9999. 732.0   45.67
049   TEMP     01.000   DEG.C     REC.CAV TC 4C    4 6S 9999. 732.0   45.67
050   TEMP     01.000   DEG.C     REC.CAV TC 5C    4 6S 9999. 732.0   45.67
051   TEMP     01.000   DEG.C     REC.CAV TC 6C    4 6S 9999. 732.0   45.67
052   TEMP     01.000   DEG.C     REC.CAV TC 7C    4 6S 9999. 732.0   45.67
053   TEMP     01.000   DEG.C     REC.CAV TC 8C    4 6S 9999. 732.0   45.67
054   TEMP     01.000   DEG.C     REC.CAV TC 9C    4 6S 9999. 732.0   45.67
055   TEMP     01.000   DEG.C     REC.CAV TC 10C   4 6S 9999. 732.0   45.67
056   TEMP     01.000   DEG.C     REC.CAV TC 11C   4 6S 9999. 732.0   45.67
057   TEMP     01.000   DEG.C     REC. EX TC 20B   4 6S 9999. 538.0   45.67
058   TEMP     01.000   DEG.C     REC. EX TC 21B   4 6S 9999. 538.0   45.67
059   TEMP     01.000   DEG.C     REC. EX TC 22    4 6S 9999. 538.0   45.67
060   TEMP     01.000   DEG.C     REC. EX TC 23    4 6S 9999. 538.0   45.67
061   TEMP     01.000   DEG.C     REC. EX TC 24    4 6S 9999. 538.0   45.67
062   TEMP     01.000   DEG.C     REC. EX TC 25    4 6S 9999. 538.0   45.67
063   TEMP     01.000   DEG.C     REC. EX TC 26    4 6S 9999. 538.0   45.67
064   TEMP     01.000   DEG.C     REC. EX TC 27    4 6S 9999. 538.0   45.67
065   TEMP     01.000   DEG.C     REC. EX TC 28    4 6S 9999. 538.0   45.67
066   TEMP     01.000   DEG.C     REC. CAV TC 1    4 6S 9999. 732.0   45.67
067   TEMP     01.000   DEG.C     REC. CAV TC 2    4 6S 9999. 732.0   45.67
069   TEMP     01.000   DEG.C     REC. CAV TC 4    4 6S 9999. 732.0   45.67
070   TEMP     01.000   DEG.C     REC. CAV TC 5    4 6S 9999. 732.0   45.67
071   TEMP     01.000   DEG.C     REC. CAV TC 6    4 6S 9999. 732.0   45.67
072   TEMP     01.000   DEG.C     REC. CAV TC 8    4 6S 9999. 732.0   45.67
074   TEMP     01.000   DEG.C     REC. CAV TC 9    4 6S 9999. 732.0   45.67
076   TEMP     01.000   DEG.C     REC. CAV TC 11   4 6S 9999. 732.0   45.67
077   TEMP     01.000   DEG.C     REC. CAV TC 12   4 6S 9999. 732.0   45.67
078   TEMP     01.000   DEG.C     REC. CAV TC 1A   4 6S 9999. 732.0   45.67
079   TEMP     01.000   DEG.C     REC. CAV TC 2A   4 6S 9999. 732.0   45.67
080   TEMP     01.000   DEG.C     REC. CAV TC 3A   4 6S 9999. 732.0   45.67
081   TEMP     01.000   DEG.C     REC. CAV TC 4A   4 6S 9999. 732.0   45.67
082   TEMP     01.000   DEG.C     REC. CAV TC 5A   4 6S 9999. 732.0   45.67
083   TEMP     01.000   DEG.C     REC. CAV TC 6A   4 6S 9999. 732.0   45.67
084   TEMP     01.000   DEG.C     REC. CAV TC 7A   4 6S 9999. 732.0   45.67
085   TEMP     01.000   DEG.C     REC. CAV TC 8A   4 6S 9999. 732.0   45.67
```

Table B-14. Instrumentation Listing for Carter Steam Engine Testing (Cont'd)

```
086   TEMP     01.000   DEG.C      REC. CAV TC 9A    4 6S 9999. 732.0   45.67
087   TEMP     01.000   DEG.C      REC. CAV TC10A    4 6S 9999. 732.0   45.67
088   TEMP     01.000   DEG.C      REC. CAV TC11A    4 6S 9999. 732.0   45.67
089   TEMP     01.000   DEG.C      REC. CAV TC12A    4 6S 9999. 732.0   45.67
090   TEMP     01.000   DEG.C      U TUBE INPUT      4 6S 9999. 732.0   45.67
091   TEMP     01.000   DEG.C      U TUBE OUTPUT     4 6S 9999. 732.0   45.67
092   TEMP     01.000   DEG.C      REC. INPUT TMP    4 6S 9999. 60.00   45.67
180   ETEMPI   01.000   DEG.C      CRT8 IN TMP       4 6S 9999. 9999.   45.67
181   ETEMPO   01.000   DEG.C      CRT8 OUT TMP      4 6S 9999. 9999.   45.67
182   TEMP     01.000   DEG.C      CRT8 HED TMP      4 6S 9999. 9999.   45.67
183   TEM      01.000   DEG.C      STM DNR LN TEM    4 6S 9999. 9999.   45.67
188   TEMP     01.000   DEG.C      COND OULET TEM    4 6S 9999. 90.00   45.67
189   TEMP     01.000   DEG.C      STM DMP LINE      4 6S 9999. 9999.   45.67
198   ALTWAT   100.00   WATTS      CRTR 8  HP MTR    4 1S 9999. 9999.   45.67
200   RECFLO   00.100   GPM        REC. H20 FLO      4 3S 9999. 9999.   45.67
201   RELFLO   00.040   GPM        REL. H20 FLO      4 3S 9999. 9999.   45.67
202   PRES     03.333   PSIG       CRT8 OIL PRES     4 1S 006.0 9999.   45.67
203   PRES     100.00   PSIG       REC. INPUT        4 1S 9999. 9999.   45.67
204   RPRESO   100.00   PSIG       REC. OUTPUT       4 1S 9999. 9999.   45.67
207   INS      10.000   W/M2       KENDALL NIP       4 1H 9999. 9999.   45.67
208   EPPLEY   117.10   W/M2       EPPLEY NIP        4 1H 9999. 9999.   45.67
209   REF      01.000   100MV      REFERENCE         4 1S 9999. 9999.   45.67
210   FLOW     02.000   GPM        APERATURE         4 3S 03.50 9999.   45.67
211   FLOW     02.000   GPM        FLAT PLT COOL     4 3S 04.00 9999.   45.67
212   RTEMPO   1000.0   DEG.C      REC. OUTPUT       4 2S 9999. 9999.   45.67
213   EPRESI   100.00   PSIG       CRT8 IN PRES      4 1S 9999. 9999.   45.67
214   EPRESO   03.333   PSIA       CRT8 OU PRES      4 1S 9999. 9999.   45.67
215   REVS     500.00   RPM        CRT8  RPM         4 3S 9999. 05.00   45.67
216   RELFL2   00.100   GPM        REL. H20 FLO      4 3S 9999. 9999.   45.67
217   FLOW     01.000   GPM        REL. CON FLO      4 3S 01.00 9999.   45.67
218   FLOW     02.000   GPM        CRT8  CON CL FLO  4 3S 9999. 9999.   45.67
220   TEMP     01.000   DEG.C      REC. CAV TC-3     4 6S 9999. 9999.   45.67
221   TEMP     01.000   DEG.C      REC. CAV TC-7     4 6S 9999. 9999.   45.67
222   TEMP     01.000   DEG.C      REC. CAVTC-10     4 6S 9999. 9999.   45.67
501                     KWATTS     RECVR OUTPUT-TH
502                     KWATTS     ENGINE INPUT-TH
503                     KWATTS     LINE LOSSES -TH
504                     KWATTS     ENG EX OUTPT-TH
505                     KWATTS     TH ENRGY-IN ENG
506                     %(TH)EL)   OVERALL ENG EFF
507                       %        EFF-TH ENRGY USE
508                       %        RECEIVER EFF.
PRINTOUT ORDER
180,181,198,202,207,208,213,214,215,
REAL TIME PLOTS
186,187,      0.      0.
196,197,198,  0.      0.
190,192,194,  0.      0.
191,193,195,  0.      0.
205,206,      0.      0.
206,          0.      0.
200,212,186,  0.      0.
200,215,216,  0.      0.
END
```

8. Hybrid Stirling Module

The test setup and instrumentation for evaluating the performance of the hybrid Stirling module consist of components dealing with both solar and fuel energies. Malfunctioning of some fuel-related instrumentation did not allow an accurate and reliable evaluation of the test data. However, the algorithms and mathematical expressions related to the measurement of fuel and combustion products are presented in Table B-15. (One simplified version of the program does not contain algorithms related to fuel and combustion products. Because the original version is more comprehensive, the simplified version is not presented herein to avoid duplication.) A full list of instrumentation is presented in Table B-16.

9. Stirling Engine with Experimental Solar-Only Receiver (ESOR)

The algorithms for the solar-only Stirling engine test data evaluation program are similar to the hybrid Stirling code. Obviously, there are no relations describing the combustor portion of the solar-only module. Although five varieties of experimental solar-only receivers (ESORs) have been tested, there are no differences among the codes for evaluating each type of receiver.

The algorithms and mathematical expressions needed to evaluate the ESOR-III Stirling module are presented in Table B-17. Table B-18 is a listing of instrumentation used for testing the ESOR-III receiver. Almost identical probes were used with other types of ESORs.

Table B-15. Hybrid Stirling Module Calculation Routines (Subroutine CALC2(NPTS,CALNUM,CALC,EU,LCRT); latest update on May 5, 1982)

Routine	Explanation
VAL011=-.01922*(VAL011*VAL011)-(.004947*VAL011)+1.002104	Power factor
AMPA=VAL013*0.006895	Working gas pressure in MPa
PREH=(VAL002-1.0)*250.	
PWR=VAL014	Alternator power in kW_e
IF(AMPA.LT.3.0. OR .AMPA.GT.15.0) GO TO 1490 !BYPASS IF OUT RANGE	PWR = 0

IF(AMPA.GE.3.0. AND .AMPA.LT.7.0) GO TO 1420
IF(AMPA.GE.7.0. AND .AMPA.LT.11.0) GO TO 1440
IF(AMPA.GE.11.. AND .AMPA.LE.15.0) GO TO 1460
	Engine performance curve ranges

X3=-20.8404255+0.078894325*PREH-0.0000342717*PREH*PREH X7=-40.8660163879+0.189097181*PREH-(0.0001580264 1*PREH*PREH)+0.0000000472*PREH**3. X=((X7-X3)*(AMPA-3.0)/4.0)+X3	Efficiency, function of T_H and P (from 3 MPa to 7 MPa)
CONTINUE X7=-40.8660163879+0.189097181*PREH-(0.0001580264 1*PREH*PREH+0.0000000472*PREH**3. X11=-33.564651489+0.1679228544**PREH-(0.0001268844 1*PREH*PREH)+0.0000000346*PREH**3. X=((X11-X7)*(AMPA-7.0)/4.0)+X7	Efficiency, function of T_H and P (from 7 MPa to 11 MPa)

Continued

Table B-15. Hybrid Stirling Module Calculation Routines (Cont'd)

Routine	Explanation
CONTINUE X11=-33.564651489+0.1679228544*PREH-(0.0001268844 1*PREH*PREH)+0.0000000346*PREH**3. X15=-43.6027030945+0.2080245763*PREH-(0.0001734427 1*PREH*PREH)+0.0000000531*PREH**3. X=((X15-X11)*(AMPA-11.0)/4.0)+X11	Efficiency, function of T_H and P (from 11 MPa to 15 MPa)
ETASTR=X/100.	
ETAALT=-0.000223*VAL014*VAL014+0.00378*VAL014+0.922	ηStirling (electrical power) in percent
X=(X/100.)*ETAALT	ηStirling (shaft power) in percent
PWR=PWR/X	Shaft power, PWR
EU(177)=PERSOL	Input solar percentage
EU(178)=FLEAK	Gas leakage factor
EU(179)=FCON	Conduction loss factor
ETAALT=-0.000223*VAL014*VAL014+0.00378*VAL014+0.922	Alternator efficiency $\eta_{alt}=-0.000223P^2 + 0.00378P + 0.922$
CP GAS CALCULATION	
CPGAS=0.2486+0.0000242*EU(169)	
GASFL=VAL017/0.08333 !TO BE REPLACED WITH AN ALGORITHM LATER	

Continued

Table B-15. Hybrid Stirling Module Calculation Routines (Cont'd)

Routine	Explanation
ROTPER=-0.110452*GASFL*GASFL+1.37149*GASFL+9.58786	
GASFL=-0.00000121*ROTPER*ROTPER+0.00609685*ROTPER	
GASFL=GASFL-0.001451865	
CORGAS=0.00007143*VAL016*VAL016-0.0105237*VAL016	
CORGAS=CORGAS+0.8245105	
GASFL=(GASFL/CORGAS)*60.	
AFR=EU(174)	
RFA=16.038563-0.769173*AFR+1.2398553*AFR*AFR	
RFA=RFA-(0.3437886*AFR**3)+(0.0443899*AFR**4)	
RFA=RFA-(0.0026121*AFR**5)+(0.0000584*AFR**6)	
AFR=RFA	A/F, air/fuel ratio
IF(AFR.LT.16.0) AFR=16.0	
AIRFL=AFR*GASFL	Airflow, $F_a = F_g$ (F/A)
COMPRF=AIRFL+GASFL	Combustion products flow, F_{cg}= Fa+Fg
ETACOM=0.98 !TO BE REPLACED WITH AN ALGORITHM LATER	Combustion efficiency

Continued

Table B-15. Hybrid Stirling Module Calculation Routines (Cont'd)

Routine	Explanation
QSTACK=COMPRF*1.8*(ABS(EU(170)-VAL015))*CPGAS	Stack losses
QBURN=GASFL*21000.*ETACOM	Combustion heat
QLEAK=QBURN*FLEAK	Combustion heat leakage
QCOND=QBURN*FCON	Conduction losses
QNETB=QBURN-QLEAK-QCOND-QSTACK	Net combustion heat in Btu/h
QNETBK=QNETB/3414.	Net combustion heat in kW
QSOL=0.077*(PERSOL/100.)*EPPLEY*SLIDE	Solar heat input; slide = 1.0 or 0.0
QRAD=(18.0E-13)*(PREH+273.)**4.	Radiation losses
QCONVD=(314.0E-7)*(1.3*((PREH-VAL015)**0.33)+30.)*(PREH-VAL015)	Convection losses
QSOLN=QSOL-QRAD-QCONVD	Net solar heat
QSOLN=QSOLN*SLIDE	Solar net heat (shutter open same, closed: 0.0)
QNETTK=QNETBK+QSOLN	Net kW_t heat input
ETASLI=VAL020/QNETTK	$\eta_{line} = P_{line}/Q_{net,k}$
ETASAL=VAL014/QNETTK	$\eta_{alt} = P_{alt}/Q_{net,k}$
PARALS=VAL014-VAL020	$P_{parasitic} = P_{alt} - P_{line}$

Continued

Table B-15. Hybrid Stirling Module Calculation Routines (Cont'd)

Routine	Explanation
WENG=VAL014/ETAALT	$W_{eng} = P_{alt}/\eta_{alt}$, engine work
STRHIN=WENG/ETASTR	$Q_{ST,in} = W_{eng}/\eta_{STIR}$, Stirling heat input
HEINER=STRHIN=QNETTK	$Q_{rejected} = Q_{in} - Q_{net}$, engine heat rejection
QBUACK=STRHIN-QSOLN	Burner heat in kW_t
QBUACB=QBUACK*3414.	Burner heat in Btu
QNBUWC=QBUACB+QSTACK	Net burner heat, $Q_{net,b} = Q_{heat,in} + Q_{stack}$
ETABWC=QNBUWC/QBURN	$\eta_{burner} = Q_{net,b}/Q_{combustor}$

Table B-16. Instrumentation Listing for Hybrid Stirling Module Testing

```
TBC2 STIRLING ENGINE, SELCUK CALCULATIONS
12345678901234567890123456789012345678901234567890123456789012345678901234567890
ST 01 51  057  30  0  002
180   TTTTTT  1.0000   DEG. C    R-1               4 6S 9999. 9999.   45.67
181   TTTTTT  1.0000   DEG. C    T-1               4 6S 9999. 9999.   45.67
182   TTTTTT  1.0000   DEG. C    R-5               4 6S 9999. 9999.   45.67
183   TTTTTT  1.0000   DEG. C    T-5               4 6S 9999. 9999.   45.67
184   TTTTTT  1.0000   DEG. C    R-7               4 6S 9999. 9999.   45.67
185   TTTTTT  1.0000   DEG. C    T-7               4 6S 9999. 9999.   45.67
186   TTTTTT  1.0000   DEG. C    R-8               4 6S 9999. 9999.   45.67
187   TTTTTT  1.0000   DEG. C    T-8               4 6S 9999. 9999.   45.67
188   TTTTTT  1.0000   DEG. C    S-1               4 6S 9999. 9999.   45.67
189   TTTTTT  1.0000   DEG. C    S-8               4 6S 9999. 9999.   45.67
190   TTTTTT  1.0000   DEG. C    ENG.OIL.RES.TEMP  4 6S 9999. 9999.   45.67
191   TTTTTT  1.0000   DEG. C    INR MNFOLD QAD 5  4 6S 9999. 9999.   45.67
192   TTTTTT  1.0000   DEG. C    INR MNFOLD QAD 7  4 6S 9999. 9999.   45.67
193   TTTTTT  1.0000   DEG. C    BACK SURF.QUAD 1  4 6S 9999. 9999.   45.67
194   TTTTTT  1.0000   DEG. C    BACK SURF.QUAD 8  4 6S 9999. 9999.   45.67
195   TTTTTT  1.0000   DEG. C    ENG.COOLANT.IN    4 6S 9999. 9999.   45.67
196   TTTTTT  1.0000   DEG. C    CAVITY OUTER TEM  4 6S 9999. 9999.   45.67
197   VAL015  1.0000   DEG. C    ORIFICE LINE TMP  4 6S 9999. 9999.   45.67
198   TTTTTT  1.0000   DEG. C    PREHEATD AIR PRB  4 6S 9999. 9999.   45.67
199   TTTTTT  1.0000   DEG. C    PREHEATED AIR     4 6S 9999. 9999.   45.67
200   TTTTTT  10.000   GPM       ENG COOL FLOW     4 3S 2.000 9999.   45.67
201   TTTTTT  500.00   RPM       ENGINE SPEED      4 3S 9999. 4.000   45.67
202   TTTTTT  290.00   PSIG      HE PRESS SELECT   4 3S 9999. 10.00   45.67
203   TTTTTT  10.000   DEG.C     ENG  OIL TEMP     4 3S 9999. 8.000   45.67
204   VAL013  290.00   PSIG      HE PRESS MAX      4 3S 9999. 10.00   45.67
205   TTTTTT  290.00   PSIG      HE PRESS  -TANK   4 3S 9999. 10.00   45.67
206   VAL001  1.0000   VOLTS     ENG COOLANT TMP   4 3S 9999. 3.400   45.67
207   VAL002  1.0000   VOLTS     HIGH TUBE TEMP    4 3S 9999. 4.600   45.67
208   VAL003  1.0000   VOLTS     TUBE 1 QUAD1      4 3S 9999. 4.600   45.67
209   VAL004  1.0000   VOLTS     TUBE 2 QUAD5      4 3S 9999. 4.600   45.67
210   VAL005  1.0000   VOLTS     TUBE 3 QUAD7      4 3S 9999. 4.600   45.67
211   VAL006  1.0000   VOLTS     TUBE 4 QUAD8      4 3S 9999. 4.600   45.67
212   VAL007  1.0000   VOLTS     FLUE (CONE) TEMP  4 3S 9999. 5.000   45.67
213   VAL008  1.0000   VOLTS     PREHEAT EXHAUST   4 3S 9999. 5.000   45.67
214   VAL009  1.0000   VOLTS     ALT WINDING TEMP  4 3S 9999. 3.400   45.67
215   TTTTTT  50.000   VOLTS     VOLT PHASE A      4 3S 9999. 9999.   45.67
216   TTTTTT  50.000   VOLTS     VOLT PHASE B      4 3S 9999. 9999.   45.67
217   TTTTTT  50.000   VOLTS     VOLT PHASE C      4 3S 9999. 9999.   45.67
218   TTTTTT  5.0000   AMPS      CURRENT PHASE A   4 3S 9999. 9999.   45.67
219   TTTTTT  5.0000   AMPS      CURRENT PHASE B   4 3S 9999. 9999.   45.67
220   TTTTTT  5.0000   AMPS      CURRENT PHASE C   4 3S 9999. 9999.   45.67
221   VAL010  1.0000   VOLTS     ALT FREQUENCY     4 3S 9999. 9999.   45.67
222   VAL011  1.0000   VOLTS     POWER FACTOR      4 3S 9999. 9999.   45.67
223   VAL014  4.0000   KWATTS    ALTERN POWER      4 3S 9999. 9999.   45.67
224   VAL012  1.0000   VOLTS     OXYGEN ANA. (T)   4 3S 9999. 9999.   45.67
225   TTTTTT  2.0000   GPM       FLT.PLT.COOL.FLO  4 3S 4.000 9999.   45.67
226   VAL016  1.6667   PSIG      ORIFCE LINE PRES  4 1S 9999. 9999.   45.67
227   VAL017  .08333   PSID      ORIFCE DELTA PRS  4 1S 9999. 9999.   45.67
228   KENDAL  10.000   WATT/M2   KENDALL PYRHELIO  4 1S 9999. 9999.   45.67
229   EPPLEY  117.10   WATT/M2   EPPLEY PYRHILIO.  4 1S 9999. 9999.   45.67
230   VAL018  1.0000   (STATUS)  SLIDE PLATE STAT  4 2S 9999. 9999.   45.67
231   VAL019   00567   PSID      MANIFLD AIR PRES  4 1S 9999. 9999.   45.67
232   VAL020  4.0000   KWATT     LINE POWER        4 3S 9999. 9999.   45.67
233   TTTTTT  1.0000   VOLTS     OXYGEN ANA. (C)   4 3S 9999. 9999.   45.67
501                    DEG.C     ENG COOLANT TEMP
502                    DEG.C     HIGH TUBE TEMP
503                    DEG.C     TUBE 1 QUAD1
504                    DEG.C     TUBE 2 QUAD6
505                    DEG.C     TUBE 3 QUAD7
506                    DEG.C     TUBE 4 QUAD8
```

Table B-16. Instrumentation Listing for Hybrid Stirling Module Testing (Cont'd)

```
507                     DEG.C       FLUE(CONE)TEMP
508                     DEG.C       PREHEAT OUT TEMP
509                     DEG.C       ALT WINDING TEMP
510                     HERTZ       ALT FREQUENCY
511                       PF        POWER FACTOR
512                     PERCENT     OXYGEN ANA. (T)
513                     MPA         SCALED CHAN 204
514                     KW(TH.)     ENGNE ENGY INPUT
515                       %         SOLAR PERCENTAGE
516                                 FLEAK
517                                 FCON
518                                 ETAALT
519                     BTU/LB.F    CP GAS
520                     LB/HR       GAS FLOW
521                                 AFR
522                     LB/HR       AIR FLOW
523                     LB/HR       COMPR FLOW
524                                 ETA COM
525                     BTU/HR      QSTACK
526                     BTU/HR      QBURN
527                     BTU/HR      QLEAK
528                     BTU/HR      QCOND
529                     BTU/HR      Q NET B
530                      KW         Q SOL
531                      KW         Q NET TK
532                                 ETASLI
533                                 ETASAL
534                      KW         PARALS
535                                 WENG
536                     KW(TH)      STRHIN
537                                 HEINER
538                      KW         Q SOL N
539                     BTU/HR      Q BUACB
540                     BTU/HR      Q NBUWC
541                                 ETABWC
PRINTOUT ORDER
188,192,200,201,202,203,204,205,215,218,219,220,222,223,228,229,230,232,501,502,
507,510,511,
REAL TIME PLOTS
188,                0.0       0.0
194,                0.0       0.0
199,508,            0.0       0.0
201,                0.0      2500.
223,                0.0       0.0
228,229,            0.0      1200.
503,504,505,506,    0.0       0.0
510,                0.0      100.
512,                0.0       0.0
514,                0.0      100.
END
```

Table B-17. Solar-Only Stirling Calculation Routines (Subroutine CALC2(NPTS,CALNUM,CALC,EU,LCRT); latest update, March 23, 1983)

Routine	Explanation
POWER FACTOR CALCULATION FOR COMBINED SYSTEM	
VAL002=-.01922*(VAL002*VAL002)-(.004947*VAL002)+1.002104	Calculation of the power factor from the meter reading
CALCULATE THERMAL INPUT FROM CONCENTRATOR TO CAVITY	
QTH=(EPPLEY/1000.)*75.*AMIR	$Q_{in} = I_b x 75 x A_m /$ 1000, receiver input in kW_t. Based on nominal 75 kW_t input at 1000 W/m^2.
CALCULATE TOTAL POWER CONVERSION EFFICIENCY	
UNTOT=VAL005/QTH	$\eta = P/Q_{in}$, power reading in kW_e
EU(171)=(TEMP01+TEMP02+TEMP03+TEMP04)/4.	$T_{av,tf}=(T_{t1}+T_{t2}+T_{t3}+T_{t4})/4$, front tubes
EU(172)=(TEMP05+TEMP06+TEMP07+TEMP08)/4.	$T_{av,tr}=(T_{t5}+T_{t6}+T_{t7}+T_{t8})/4$, rear tubes
EU(173)=(TEMP09+TEMP10+TEMP11+TEMP12)/4.	$T_{av,cc}=(T_{C9}+T_{C10}+T_{C11}+T_{C12})/4$, circular cavity
EU(174)=(TEMP13+TEMP14+TEMP15+TEMP16)/4.	$T_{av,wg}=(T_{g13}+T_{g14}+T_{g15}+T_{g16})/4$, working gas
BAROMETRIC PRESSURE MEASUREMENT	
EU(175)=((BARPRE*1.3)+24.6)*25.4	Barometric pressure conversion

Continued

Table B-17. Solar-Only Stirling Calculation Routines (Cont'd)

Routine	Explanation
DEW POINT CALCULATION	
EU(176)=(DEWPNT*16.)-30.	Dew point conversion
POWER FACTOR CALCULATION FOR TBC-2 SYSTEM	
CMBPWF=1.0000176-0.00004807*CMBPWF-0.00021386*CMBPWF*CMBPWF 1-0.000000158*CMBPWF**3+(9.1E-9)*CMBPWF**4	Calculation of the power factor for TBC system. Corrected power factor = $1.0000176 - 0.00004807C - 0.00021386C^2$
	The following calculations are based on tests run in Sweden at USAB:
CALCULATE ENGINE/RECEIVER EFFICIENCY	Calculation of the engine/receiver efficiency
UNG=-0.0002203*VAL012*VAL012+0.0037896*VAL012+0.92192	η_g (generator efficiency) = $0.0002203*K^2+0.0037896K + 0.92192$ K: alternator (generator) power
UNER=UNTOT/UNG	$\eta_{eng/rec} = \eta_{total}/\eta_g$, η_{total}: overall efficiency
CALCULATE CAVITY EFFICIENCY	
GASP=VAL013*0.006895	Working gas pressure, P

Continued

Table B-17. Solar-Only Stirling Calculation Routines (Cont'd)

Routine	Explanation
UNENG=18.8735+(2.0919*GASP)-(0.055596*GASP*GASP) UNENG=UNENG*(1.15965-0.003185*TCOLD) UNENG=UNENG*(-0.656+0.00338*THOT-.0000015*THOT*THOT) UNENG=UNENG*.01	η_e = [18.8735 + (2.0919P) - (0.055596*P^2)]* [1.15965 - 0.03185T_c]* 0.1 [-0.656 + 0.00338T_H - 0.0000015T_H^2]
UNCAV=UNER/UNENG	η_{cavity} = $\eta_{eng/rec}$/ η_e
CALCULATE ENGINE POWER	Engine power
PENG=(1.46529*VAL013*0.006895)-0.91 PENG=PENG*(1.21655-0.004345*TCOLD) PENG=PENG*(-0.698698+0.00302299*THOT-0.00000085*THOT*THOT)	P_{eng} = [1.46529* V*0.006895-0.91]* [1.21655 - 0.004345*T_C]* [-0.0698698 + 0.0302299T_H - 0.00000085T_H^2]
CALCULATE PEL/NG	
EU(181)=PEL/UNG	K/η_g
CALCULATE PEL/NG*PENG	
EU(182)=PEL/UNG*PENG)	(K/η_g)*P_{eng} Comment: If K and P_{eng} readings are correct, (K/η_g)*P_g=1.00 should hold.

Table B-18. Instrumentation Listing for Solar-Only Stirling Testing

```
TBC2 SOLAR STIRLING, ESOR III,80% MIRROR
12345678901234567890123456789012345678901234567890123456789012345678901234567890
ST 03 42  232  60  0  001
130   TTTTTT   100.00   VOLTS      VOLTAGE,PHASE AB 4 3S 9999. 9999.   45.67
131   TTTTTT   100.00   VOLTS      VOLTAGE,PHASE CB 4 3S 9999. 9999.   45.67
132   TTTTTT   100.00   VOLTS      VOLTAGE,PHASE CA 4 3S 9999. 9999.   45.67
133   TTTTTT   1.0000   AMPS       CURRENT, PHASE A 4 1S 9999. 9999.   45.67
134   TTTTTT   1.0000   AMPS       CURRENT, PHASE B 4 1S 9999. 9999.   45.67
135   TTTTTT   1.0000   AMPS       CURRENT, PHASE C 4 1S 9999. 9999.   45.67
136   VAL001   1.0000   VOLTS      ALT. FREQ.       4 3S 9999. 9999.   45.67
137   VAL005   1.0000   KWATTS     POWER JPL        4 1S 9999. 9999.   45.67
138   CMBPWF   1.0000   VOLTS      POWER FACTOR     4 1S 9999. 9999.   45.67
144   TEMP01   1.0000   DEG. C     FRONT*TUBE(INNR) 4 6S 9999. 850.0   45.67
145   TEMP02   1.0000   DEG. C     FRONT*TUBE(INNR) 4 6S 9999. 850.0   45.67
146   TEMP03   1.0000   DEG. C     FRONT*TUBE(INNR) 4 6S 9999. 850.0   45.67
147   TEMP04   1.0000   DEG. C     FRONT*TUBE(INNR) 4 6S 9999. 850.0   45.67
148   TTTTTT   1.0000   DEG. C     REAR TUBE LOWER  4 6S 9999. 850.0   45.67
149   TTTTTT   1.0000   DEG. C     REAR TUBE LOWER  4 6S 9999. 850.0   45.67
150   TTTTTT   1.0000   DEG. C     IR REC REF 1     4 7S 9999. 9999.   45.67
152   TTTTTT   1.0000   DEG. C     IR REC REF 3     4 7S 9999. 9999.   45.67
153   TTTTTT   1.0000   DEG. C     IR REC REF 4     4 7S 9999. 9999.   45.67
154   TTTTTT   1.0000   DEG. C     IR REC REF 5     4 7S 9999. 9999.   45.67
160   TTTTTT   1.0000   DEG. C     REAR TUBE(LOWER) 4 6S 9999. 850.0   45.67
161   TTTTTT   1.0000   DEG. C     REAR TUBE(LOWER) 4 6S 9999. 850.0   45.67
162   TTTTTT   1.0000   DEG. C     ENG. COOLANT IN  4 6S 9999. 9999.   45.67
163   TEMP05   1.0000   DEG. C     REAR*TUBE OTR    4 6S 9999. 850.0   45.67
164   TEMP06   1.0000   DEG. C     REAR*TUBE OTR    4 6S 9999. 850.0   45.67
165   TEMP07   1.0000   DEG. C     REAR*TUBE OTR    4 6S 9999. 850.0   45.67
166   TEMP08   1.0000   DEG. C     REAR*TUBE OTR    4 6S 9999. 850.0   45.67
167   TTTTTT   1.0000   DEG. C     REAR TUBE OTR    4 6S 9999. 850.0   45.67
168   TTTTTT   1.0000   DEG. C     REAR TUBE OTR    4 6S 9999. 850.0   45.67
169   TTTTTT   1.0000   DEG. C     REAR TUBE OTR    4 6S 9999. 850.0   45.67
170   TTTTTT   1.0000   DEG. C     REAR TUBE OTR    4 6S 9999. 850.0   45.67
171   TTTTTT   1.0000   DEG. C     FRNT TUBE INNR   4 6S 9999. 850.0   45.67
172   TTTTTT   1.0000   DEG. C     FRNT TUBE INNR   4 6S 9999. 850.0   45.67
173   TTTTTT   1.0000   DEG. C     FRNT TUBE INNR   4 6S 9999. 850.0   45.67
174   TTTTTT   1.0000   DEG. C     FRNT TUBE INNR   4 6S 9999. 850.0   45.67
175   TTTTTT   1.0000   DEG. C     FRNT TUBE OTR    4 6S 9999. 850.0   45.67
176   TTTTTT   1.0000   DEG. C     FRNT TUBE OTR    4 6S 9999. 850.0   45.67
178   TTTTTT   1.0000   DEG. C     FRNT TUBE OTR    4 6S 9999. 850.0   45.67
179   TTTTTT   1.0000   DEG. C     FRNT TUBE OTR    4 6S 9999. 850.0   45.67
180   TTTTTT   1.0000   DEG. C     ENG.COOLANT.OUT  4 6S 9999. 70.00   45.67
181   TTTTTT   1.0000   DEG. C     CAVITY*TEMP TH14 4 6S 9999. 1200.   45.67
182   TTTTTT   1.0000   DEG. C     CAVITY*TEMP TH15 4 6S 9999. 1150.   45.67
183   TTTTTT   1.0000   DEG. C     CAVITY*TEMP TH16 4 6S 9999. 1150.   45.67
184   TTTTTT   1.0000   DEG. C     CAVITY TEMP TH17 4 6S 9999. 1150.   45.67
185   TEMP09   1.0000   DEG. C     CIRC.CAVITY TH18 4 6S 9999. 1150.   45.67
186   TEMP10   1.0000   DEG. C     CIRC.CAVITY TH19 4 6S 9999. 1150.   45.67
187   TEMP11   1.0000   DEG. C     CIRC.CAVITY TH20 4 6S 9999. 1150.   45.67
188   TEMP12   1.0000   DEG. C     CIRC.CAVITY TH21 4 6S 9999. 1150.   45.67
189   TTTTTT   1.0000   DEG. C     CONE SURF. TEMP. 4 6S 9999. 9999.   45.67
191   TEMP13   1.0000   DEG. C     WORKING*GAS TH9  4 6S 9999. 800.0   45.67
192   TEMP14   1.0000   DEG. C     WORKING*GAS TH10 4 6S 9999. 800.0   45.67
193   TEMP15   1.0000   DEG. C     WORKING*GAS TH11 4 6S 9999. 800.0   45.67
```

Table B-18. Instrumentation Listing for Solar-Only Stirling Testing (Cont'd)

194	TEMP16	1.0000	DEG. C	WORKING*GAS TH12	4	6S	9999.	800.0	45.67
195	TTTTTT	1.0000	DEG. C	CAV.OUT.SUR.TH22	4	6S	9999.	500.0	45.67
196	TTTTTT	1.0000	DEG. C	CAV.OUT.SUR.TH23	4	6S	9999.	500.0	45.67
197	TTTTTT	1.0000	DEG. C	AMBIENT TEMP.	4	6S	9999.	9999.	45.67
200	TTTTTT	10.000	GPM	ENG COOL FLOW	4	3S	2.000	9999.	45.67
201	TTTTTT	1000.0	RPM	ENGINE SPEED	4	3S	9999.	2.000	45.67
202	VAL004	4.0000	MPA	PRESSURE DEMAND	4	3S	9999.	9999.	45.67
204	TTTTTT	4.0000	MPA	HE PRESS - MAX	4	3S	9999.	5.000	45.67
205	TTTTTT	4.0000	MPA	HE PRESS - TANK	4	3S	9999.	5.000	45.67
207	TTTTTT	200.00	DEG. C	TEMP CONTROL	4	3S	9999.	4.200	45.67
208	TTTTTT	200.00	DEG. C	TEMP HIGH TUBE	4	3S	9999.	4.200	45.67
209	TTTTTT	200.00	DEG. C	TEMP.W.G. MEAN	4	3S	9999.	9999.	45.67
215	TTTTTT	50.000	VOLTS	VOLT PHASE A	4	3S	9999.	9999.	45.67
216	TTTTTT	50.000	VOLTS	VOLT PHASE B	4	3S	9999.	9999.	45.67
217	TTTTTT	50.000	VOLTS	VOLT PHASE C	4	3S	9999.	9999.	45.67
218	TTTTTT	10.000	AMPS	CURRENT PHASE A	4	3S	9999.	9999.	45.67
219	TTTTTT	10.000	AMPS	CURRENT PHASE B	4	3S	9999.	9999.	45.67
220	TTTTTT	10.000	AMPS	CURRENT PHASE C	4	3S	9999.	9999.	45.67
221	TTTTTT	1.0000	VOLTS	ALT FREQUENCY	4	3S	9999.	9999.	45.67
222	VAL002	1.0000	VOLTS	POWER FACTOR	4	3S	9999.	9999.	45.67
223	TTTTTT	8.0000	KWATTS	ALTERNATOR POWER	4	3S	9999.	9999.	45.67
224	VAL003	1.0000	VOLTS	POWER-STIRLING	4	3S	9999.	9999.	45.67
230	TTTTTT	1.0000	VOLTS	SLIDE PLT STATUS	4	2S	9999.	9999.	45.67
231	TTTTTT	8.0000	KWATTS	LINE POWER (CMB)	4	3S	9999.	9999.	45.67
232	TTTTTT	2.0000	GPM	FLT.PLT.COOL.FLO	4	3S	4.000	9999.	45.67
233	KENDAL	10.000	W/M2	KENDALL PYRHELIO	4	1H	9999.	9999.	45.67
234	EPPLEY	129.00	W/M2	EPPLEY PYRHELIO	4	1S	9999.	9999.	45.67
235	BARPRE	1.0000	VOLTS	BAROMETRIC PRES.	4	3S	9999.	9999.	45.67
236	DEWPNT	1.0000	VOLTS	DEW POINT	4	3S	9999.	9999.	45.67
237	TTTTTT	6.7056	METER/S.	WIND SPEED	4	3S	9999.	9999.	45.67
238	TTTTTT	108.00	DEGREES	WIND DIRECTION	4	3S	9999.	9999.	45.67
239	TTTTTT	1.0000	MV	100 MV REFERENCE	4	1S	9999.	9999.	45.67
501			HERTZ	ALT FREQUENCY					
502			P.F.	POWER FACTOR-CMB					
503			%	% MIRROR UNCOVRD					
504			PSI	PRESSURE DEMAND					
505			KW (TH)	THERM.IN. (Q TH)					
506			(EFF.)	TOT.PWR.CNV.EFF.					
507			KWATTS	POWER					
508			-----	EPPLEY (SCALED)					
509			DEG. C	INNR FRNT MEAN					
510			DEG. C	OUTR FRNT MEAN					
511			DEG. C	CIR CAVITY MEAN					
512			DEG. C	WORK GAS MEAN					
513			MM HG.	BAROMETRIC PRES.					
514			DEG. C	DEW POINT					
515			P.F.	POWER FACTOR					

Table B-18. Instrumentation Listing for Solar-Only Stirling Testing (Cont'd)

194	TEMP16	1.0000	DEG. C	WORKING*GAS TH12	4	6S	9999.	800.0	45.67
195	TTTTTT	1.0000	DEG. C	CAV.OUT.SUR.TH22	4	6S	9999.	500.0	45.67
196	TTTTTT	1.0000	DEG. C	CAV.OUT.SUR.TH23	4	6S	9999.	500.0	45.67
197	TTTTTT	1.0000	DEG. C	AMBIENT TEMP.	4	6S	9999.	9999.	45.67
200	TTTTTT	10.000	GPM	ENG COOL FLOW	4	3S	2.000	9999.	45.67
201	TTTTTT	1000.0	RPM	ENGINE SPEED	4	3S	9999.	2.000	45.67
202	VAL004	4.0000	MPA	PRESSURE DEMAND	4	3S	9999.	9999.	45.67
204	TTTTTT	4.0000	MPA	HE PRESS - MAX	4	3S	9999.	5.000	45.67
205	TTTTTT	4.0000	MPA	HE PRESS - TANK	4	3S	9999.	5.000	45.67
207	TTTTTT	200.00	DEG. C	TEMP CONTROL	4	3S	9999.	4.200	45.67
208	TTTTTT	200.00	DEG. C	TEMP HIGH TUBE	4	3S	9999.	4.200	45.67
209	TTTTTT	200.00	DEG. C	TEMP.W.G. MEAN	4	3S	9999.	9999.	45.67
215	TTTTTT	50.000	VOLTS	VOLT PHASE A	4	3S	9999.	9999.	45.67
216	TTTTTT	50.000	VOLTS	VOLT PHASE B	4	3S	9999.	9999.	45.67
217	TTTTTT	50.000	VOLTS	VOLT PHASE C	4	3S	9999.	9999.	45.67
218	TTTTTT	10.000	AMPS	CURRENT PHASE A	4	3S	9999.	9999.	45.67
219	TTTTTT	10.000	AMPS	CURRENT PHASE B	4	3S	9999.	9999.	45.67
220	TTTTTT	10.000	AMPS	CURRENT PHASE C	4	3S	9999.	9999.	45.67
221	TTTTTT	1.0000	VOLTS	ALT FREQUENCY	4	3S	9999.	9999.	45.67
222	VAL002	1.0000	VOLTS	POWER FACTOR	4	3S	9999.	9999.	45.67
223	TTTTTT	8.0000	KWATTS	ALTERNATOR POWER	4	3S	9999.	9999.	45.67
224	VAL003	1.0000	VOLTS	POWER-STIRLING	4	3S	9999.	9999.	45.67
230	TTTTTT	1.0000	VOLTS	SLIDE PLT STATUS	4	2S	9999.	9999.	45.67
231	TTTTTT	8.0000	KWATTS	LINE POWER (CMB)	4	3S	9999.	9999.	45.67
232	TTTTTT	2.0000	GPM	FLT.PLT.COOL.FLO	4	3S	4.000	9999.	45.67
233	KENDAL	10.000	W/M2	KENDALL PYRHELIO	4	1H	9999.	9999.	45.67
234	EPPLEY	129.00	W/M2	EPPLEY PYRHELIO	4	1S	9999.	9999.	45.67
235	BARPRE	1.0000	VOLTS	BAROMETRIC PRES.	4	3S	9999.	9999.	45.67
236	DEWPNT	1.0000	VOLTS	DEW POINT	4	3S	9999.	9999.	45.67
237	TTTTTT	6.7056	METER/S.	WIND SPEED	4	3S	9999.	9999.	45.67
238	TTTTTT	108.00	DEGREES	WIND DIRECTION	4	3S	9999.	9999.	45.67
239	TTTTTT	1.0000	MV	100 MV REFERENCE	4	1S	9999.	9999.	45.67
501			HERTZ	ALT FREQUENCY					
502			P.F.	POWER FACTOR-CMB					
503			%	% MIRROR UNCOVRD					
504			PSI	PRESSURE DEMAND					
505			KW (TH)	THERM.IN. (Q TH)					
506			(EFF.)	TOT.PWR.CNV.EFF.					
507			KWATTS	POWER					
508			-----	EPPLEY (SCALED)					
509			DEG. C	INNR FRNT MEAN					
510			DEG. C	OUTR FRNT MEAN					
511			DEG. C	CIR CAVITY MEAN					
512			DEG. C	WORK GAS MEAN					
513			MM HG.	BAROMETRIC PRES.					
514			DEG. C	DEW POINT					
515			P.F.	POWER FACTOR					